



POLITECNICO
MILANO 1863

Politecnico di Milano

Dipartimento di Chimica, Materiali e Ingegneria Chimica “G. Natta”

Doctoral program in Materials Engineering (XXIX)

**Corrosion protection of steel embedded in new
sustainable cementitious materials**

Ph.D. Candidate: Fan Yang

Supervisor: Dr. Maddalena Carsana

Tutor: Prof. Luca Bertolini

Coordinator: Prof. Chiara Castiglioni

2013 - 2017

Dedication

In memory of Prof. Luca Bertolini.

Table of Contents

Dedication	i
Table of Contents.....	ii
Introduction.....	v
Chapter 1 Corrosion protection of steel in sustainable concrete.....	- 1 -
1.1 Corrosion principles.....	- 1 -
1.2 Passivity of steel.....	- 2 -
1.3 Carbonation-induced steel corrosion	- 5 -
1.4 Chloride-induced steel corrosion	- 6 -
1.5 Rusted steel	- 7 -
1.6 Galvanised steel.....	- 11 -
1.7 Sustainable new materials.....	- 15 -
1.7.1 Recycled waste glass	- 15 -
1.7.2 Calcium sulfoaluminate cement	- 20 -
1.7.3 Cement-stabilised rammed earth	- 28 -
Chapter 2 Experimental procedure.....	- 34 -
2.1 Materials.....	- 34 -
2.1.1 Binder type	- 34 -
2.1.2 Aggregates	- 35 -
2.1.3 Reinforcements.....	- 36 -
2.2 Mix proportion.....	- 37 -
2.3 Summary of test specimens and test types	- 39 -
2.4 Experimental methods.....	- 42 -
2.4.1 Materials characterisation methods.....	- 42 -
2.4.2 Tests on mortar and concrete	- 43 -
2.4.3 Electrochemical tests on reinforced mortar	- 48 -
Chapter 3 Results	- 52 -
3.1 Tests on carbon steel bars with different surface conditions	- 52 -
3.1.1 Characterisation of carbon steel bars with different surface conditions	- 52 -
3.1.2 Properties of studied concrete	- 57 -
3.1.3 Corrosion behaviour of pre-rusted steel in concrete	- 58 -
3.2 Tests on mortar with waste glass.....	- 64 -
3.2.1 Fresh and hardened properties of waste glass mortar	- 64 -

3.2.2	Durability properties of waste glass mortar	- 66 -
3.2.3	Corrosion behaviour of carbon steel embedded in waste glass mortar	- 67 -
3.3	Tests on concrete with CSA-based cements	- 68 -
3.3.1	Properties of CSA-based concretes	- 68 -
3.3.2	Corrosion behaviour of steel embedded in CSA-based concretes	- 79 -
3.4	Tests on cement-stabilised rammed earth	- 101 -
3.4.1	Properties of cement-stabilised rammed earth	- 101 -
3.4.2	Corrosion behaviour of carbon steel embedded in cement-stabilised rammed earth	- 101 -
Chapter 4	Discussion	- 104 -
4.1	The factors influencing passivation of steel	- 105 -
4.1.1	pH of new cementitious materials	- 105 -
4.1.2	Steel surface condition.....	- 107 -
4.2	Passivation of carbon steel in alkaline ordinary concrete.....	- 109 -
4.3	Passivation of carbon steel in sustainable cementitious materials	- 112 -
4.3.1	Properties of sustainable cementitious materials	- 112 -
4.3.2	Effect of glass powder on corrosion protection of carbon steel.....	- 121 -
4.3.3	Effect of CSA-based cement on corrosion protection of carbon steel.....	- 122 -
4.3.4	Effect of cement-stabilised rammed earth on corrosion protection of carbon steel.....	- 124 -
4.4	Corrosion behaviour of pre-rusted steel in ordinary concrete.....	- 125 -
4.4.1	In carbonated ordinary concrete	- 125 -
4.4.2	In ordinary concrete subjected to chloride penetration	- 126 -
4.5	Corrosion behaviour of carbon steel in carbonated CSA-based concretes	- 129 -
4.6	Passivation of galvanised steel in CSA-based concretes and its corrosion behaviour in carbonated CSA-based concretes.....	- 132 -
4.6.1	Passivation of galvanised steel in CSA-based concrete.....	- 132 -
4.6.2	Effect of exposure conditions.....	- 133 -
4.6.3	Corrosion behaviour of galvanised steel in carbonated CSA-based concrete.....	- 135 -
Conclusions and future work.....	- 136 -
List of References.....	- 141 -
List of Test Standards	- 151 -
Appendix A	Microstructure observations of reference concrete and CSA-based concretes	- 152 -
A.1	Concrete with CEM II/A-L 42.5R	- 152 -
A.2	Concrete with SL05 NF binder	- 153 -
A.3	Concrete with SL05 NF+CaO binder.....	- 156 -

Table of Contents

A.4 Concrete with SL05+CaO binder.....	- 159 -
A.5 Concrete with SR03 binder	- 162 -
Acknowledgements	- 163 -

Introduction

Concrete is the most widely used construction material in the world because it has excellent performance if properly designed and produced. Indeed, more than 10 billion tonnes of concrete are consumed each year due to the high demand in developing countries, particularly in China and India. As a consequence, concrete has an enormous impact on the environment because it consumes huge amounts of natural resources and energy and produces high CO₂ emission [1], [2]. It has been reported that in 2015 cement industry contributed to about 8% of global CO₂ emission, including the CO₂ emission released in clinker production process and by fuel combustion related to clinker production process [3]. Thus, cement and concrete industry is facing a lot of challenges to find a sustainable solution.

However, if on the one hand the concrete has a significant environmental impact, on the other hand this offers interesting opportunities to be an environmentally friendly material. One could be to replace Portland cement by supplementary cementitious materials (SCMs), especially those are by-products of industrial process such as fly ash, silica fume and ground granulated blast furnace slag; in alternative it could use new type of cement, for instance calcium sulfoaluminate (CSA) cement and alkali-activated cements [4] or recycled materials in place of natural aggregates. Several materials have been suggested in literature as replacement of ordinary ingredients of concrete. Nevertheless, the performance of these new binders or SCMs materials in relation to the durability of reinforced concrete structures is still not clear or it has not yet been studied. For this reason, it's important to investigate the protection provided to embedded steel and the alkalinity of these new sustainable materials in order to guarantee passive conditions. Secondly, the protection offered to the reinforcing steel bars against carbonation and chloride-induced corrosion has to be also studied. There is a need to investigate the actual behaviour of steel embedded in new cementitious materials. Moreover, any improvement of durability and service life of reinforced concrete structures, thanks also to new binders or SCMs materials, could reduce the amount of materials needed for their replacement or restoration, besides to decrease the construction and demolition waste. Advantages in terms of durability of reinforced concrete structures could be obtained from combined use of new sustainable materials and corrosion-resistant steel bars such as epoxy coated steel, stainless steel and galvanised steel.

The aim of this thesis was to study the corrosion protection of steel embedded in new sustainable cementitious materials. Firstly, the thesis focused on the study of the protection of steel bars in ordinary concrete, considering the role of oxide layer on steel surface which may be formed at the production plant (such as the mill scale) or at the construction site (such as the rust caused by atmospheric exposure); also the effect of carbonation and chloride penetration on the corrosion

behaviour of pre-rusted bars was considered. Secondly, the passivation and corrosion behaviour of steel in some new sustainable cementitious materials was studied. In particular, in the first phase, the thesis has investigated the properties of some sustainable cementitious materials such as recycled waste glass mortar, CSA-based concretes and cement-stabilised rammed earth (CSRE).

In order to reach the aim of this thesis, the work has been divided into four subtopics: 1) the study of the passivation of pre-rusted carbon steel bars in ordinary concrete, and the effect of carbonation and chloride on corrosion behavior of pre-rusted carbon steel bars embedded in ordinary concrete; 2) the investigation on the durability-related properties of mortar made with recycled waste glass, including glass powder and expanded glass (respectively used as mineral addition and lightweight aggregate), and the passivation of carbon steel in mortar made with glass powder; 3) the study of passivation and corrosion behavior of both carbon steel and galvanized steel in concrete made with CSA-based cements (blends of CSA cement with ordinary cement); 4) the study of passivation of carbon steel in cement-stabilised rammed earth. In addition, the durability-related properties were also investigated on CSA-based concretes and CSRE.

The oxide layer (mill scale and rust) on steel surface due to production process or atmospheric corrosion was characterised by visual examination, microstructure investigation and composition analysis. The durability-related properties of waste glass mortar made with glass powder or expanded glass have been studied in terms of electrical resistivity, alkali silica reaction (ASR) and alkali attack. A series of tests were carried out on CSA-based concretes such as electrical resistivity, capillary absorption and water absorption, pH, scanning electron microscope (SEM) observations and carbonation and chloride penetration resistance. Moreover, the electrical resistivity and carbonation resistance of cement-stabilised rammed earth were also investigated. Several types of electrochemical tests including corrosion potential measurements, linear polarisation resistance (LPR) and potentiostatic polarisation, were performed on reinforced specimens made with these new sustainable cementitious materials in order to study their passivation and corrosion behaviour, considering also the effect of environmental conditions with different relative humidity and temperature. The experimental work was carried out at Cement-based Materials and Durability (mCD) Laboratory, Department of Chemistry, Materials and Chemical Engineering “Giulio Natta” (Politecnico di Milano).

The thesis has been broken down into 4 chapters. **Chapter 1** focuses on the literature review regarding to the corrosion protection of steel in sustainable concrete. **Chapter 2** illustrates the experimental procedures followed in this research. **Chapter 3** presents the experimental results about the durability-related properties of the sustainable cementitious materials, and the passivation and corrosion behaviour of steel embedded in these sustainable cementitious materials. **Chapter 4** is devoted to discuss the obtained results. Finally, the main conclusions and future work are presented.

Chapter 1

Corrosion protection of steel in sustainable concrete

This chapter targets aim to review the background and literature regarding to corrosion protection of steel in sustainable concrete.

1.1 Corrosion principles

The corrosion of metal is an electrochemical process, as shown in **Figure 1.1**. The whole process is broke down into four partial processes [5]:

- Anodic process: the oxidation of metal that results in the formation of metal ions (cations) and electrons;
- Cathodic process: the reduction of oxygen that consumes the electrons produced by anodic reaction and then forms anions;
- Transport of current in electrolyte: ions produced by anodic and cathodic reactions move in electrolyte;
- Transport of current in metal: electrons produced by anodic reaction travel in metal.

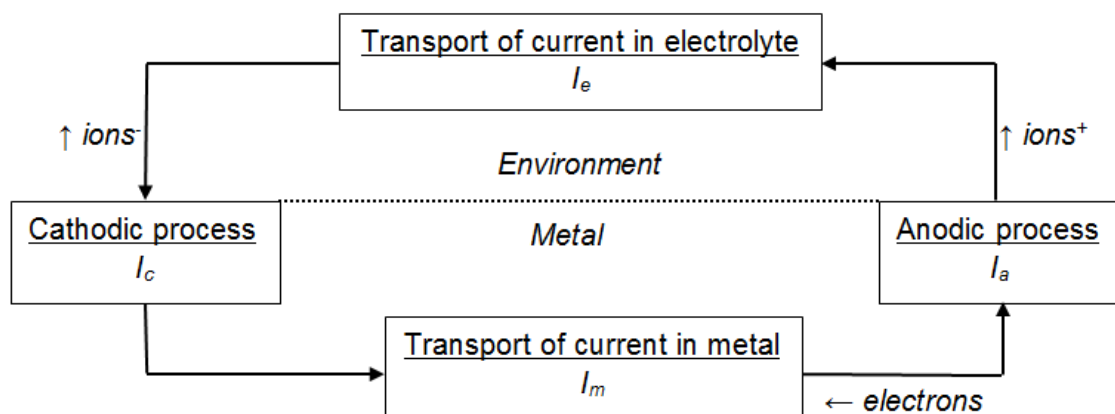


Figure 1.1 Schematic of electrochemical process of corrosion of metal, adapted from [5].

I_a , I_e , I_c and I_m represent respectively anodic current, the current that flows in electrolyte from anode to cathode, cathodic current and the current that flows in metal from cathode to anode. These currents form a closed current loop, therefore $I_a = I_e = I_c = I_m$. As a matter of fact, the common value of these currents is termed as corrosion current (I_{corr}). Instead of I_{corr} , corrosion current density (i_{corr}) that means corrosion current per unit area, is more often used.

In particular, the corrosion of steel can happen in an aqueous environment that is near neutral pH value in the presence of dissolved oxygen. The mechanism is illustrated by **Figure 1.2**. The dissolved products, such as Fe^{2+} and OH^- ions due to anodic and cathodic reactions, can be transported in the aqueous solution and, further react with water and oxygen to form a loosely adhere rust layer on the surface of steel, with a composition of oxyhydroxides (FeOOH) [6]. The rusting of steel can also simply occur when it is exposed to the common atmosphere environment.

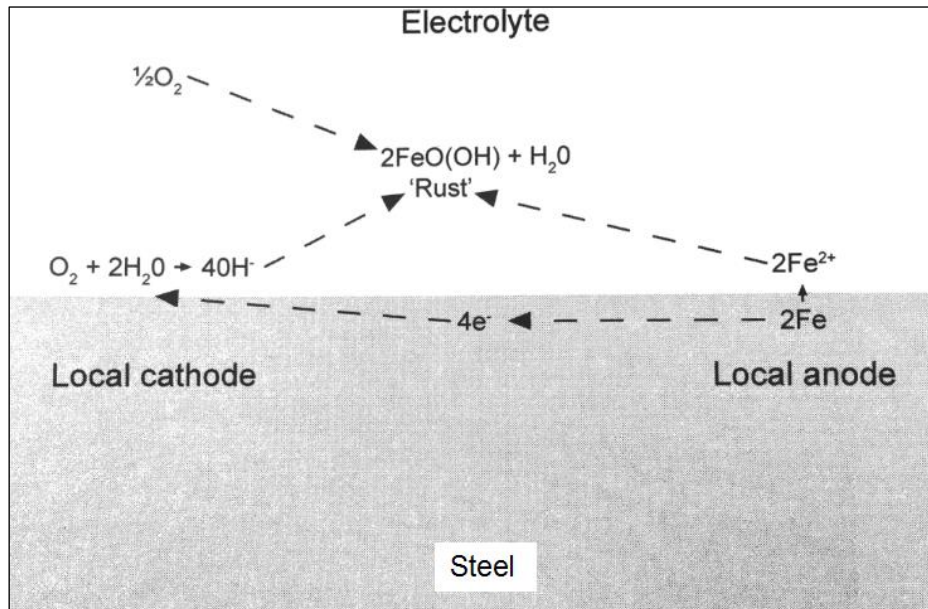
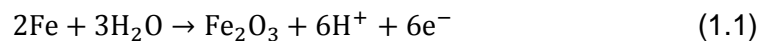


Figure 1.2 Electrochemical mechanism of rusting of steel [6].

1.2 Passivity of steel

Although rusting of steel could occur in atmospheric environment or a near neutral aqueous solution, that does not happen when steel is placed in dense concrete. **Figure 1.3** shows the Pourbaix diagram of iron that is the plot of redox (reversible) potential in terms of pH; it is clear that there is a zone of potential and pH where iron stays in passive state preventing from corrosion. When steel is exposed into an aqueous solution with $\text{pH} > 11.5$ in the presence of dissolved oxygen, an oxide layer of some nanometres thick is formed on the surface of steel [6]:



The thin Fe_2O_3 layer formed on the surface of steel is called passive film. It can effectively reduce the anodic iron dissolution, therefore lower I_{corr} to a very low level, corresponding to an average thickness loss less than $1 \mu\text{m}$ per year.

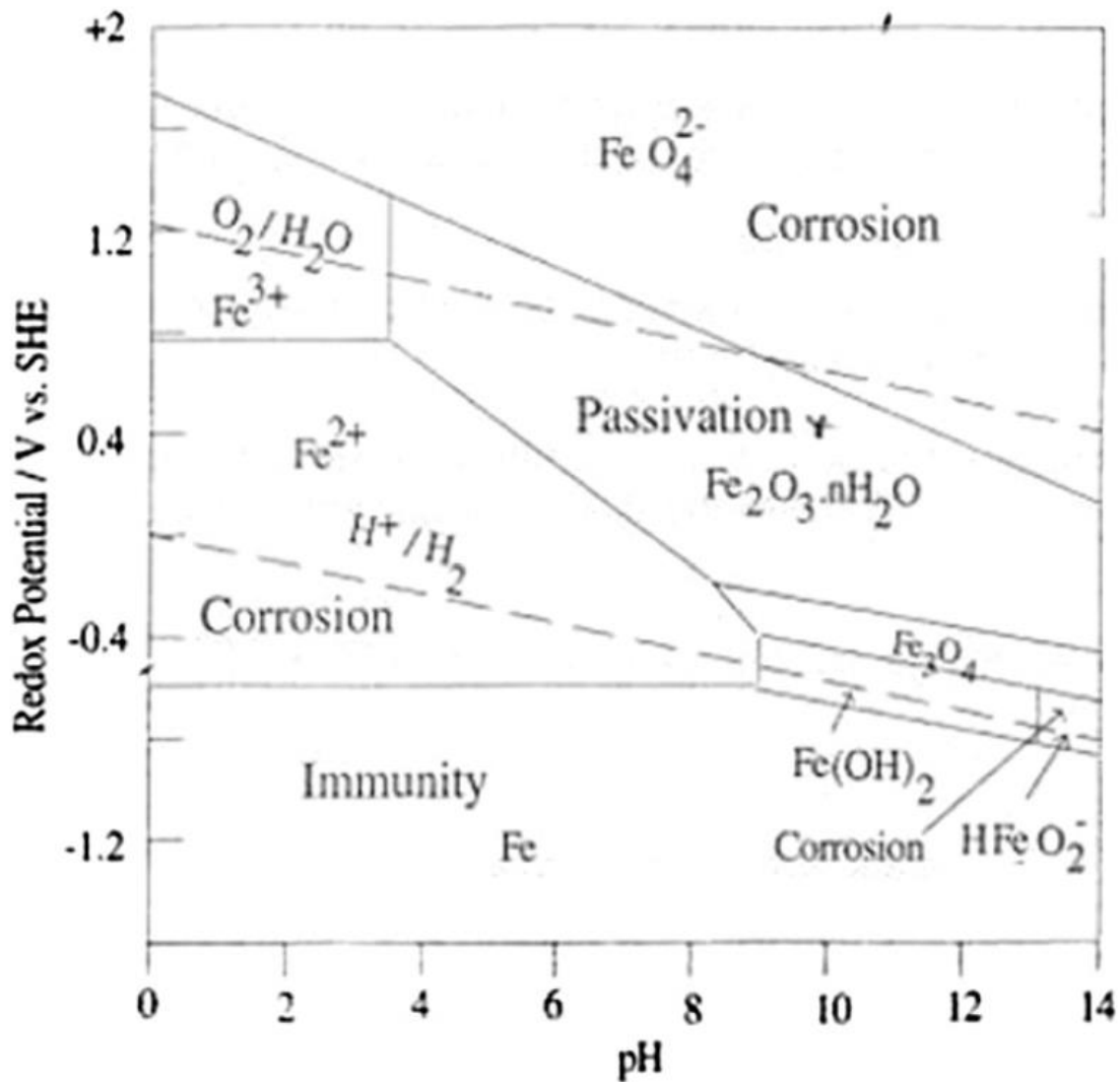


Figure 1.3 Potential-pH (Pourbaix) diagram for iron [7]. SHE: Standard Hydrogen Electrode.

The effectiveness of passive film may be illustrated through anodic polarisation curve that is the relationship between applied potential and current density. As shown in **Figure 1.4**, in saturated Ca(OH)₂ solution without chloride addition (0% Cl⁻), the onset of formation of a passive film is marked by a sharp fall in the anodic current density when the potential is raised above a critical value (around -700 mV vs SCE¹). As the passive film merely thickens very slowly, very little change in the anodic current density with the further increase in the steel potential is observed, until another critical potential is reached at which oxygen gas starts to be produced by electrolytic decomposition of water.

¹ SCE: Saturated Calomel Electrode

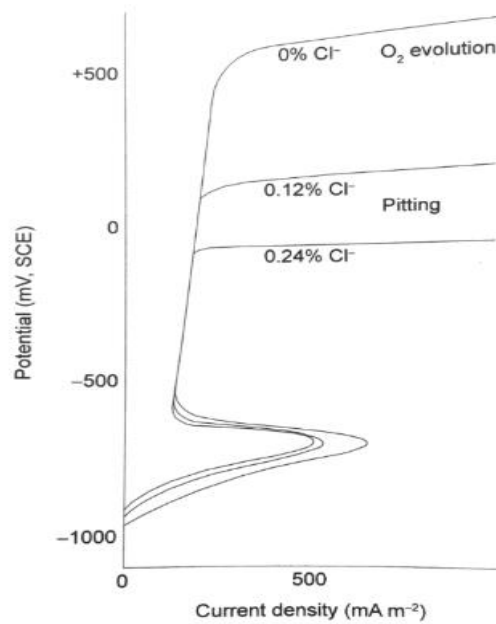


Figure 1.4 Typical potentiodynamic anodic polarisation curves for mild steel in saturated calcium hydroxide solution without and with chloride [6].

The passivity of steel can also be obtained in hardened concrete as shown in **Figure 1.5**. That is because cement hydration results in the pH of concrete pore solution more than 12.6 owing to the dissolved $\text{Ca}(\text{OH})_2$, NaOH and KOH. Thereby, alkaline concrete can offer corrosion protection to steel by the formation of passive film. However, once the passive film is broken, the corrosion protection would fail. The common actions that can damage the passive film of steel embedded in concrete include carbonation and chloride penetration. Carbonation can lead to the depletion of alkalinity in concrete and further dissolve the passive film. The presence of a certain concentration of chloride ions in the alkaline electrolyte adjacent to the steel tends to cause localised breakdown of the passive film on steel, a phenomenon termed pitting, as shown in **Figure 1.4** [6]. Also depletion of oxygen could cause the failure of passivation film. In addition, the presence of rust layer of steel surface might hinder the passivation of steel in alkaline concrete .

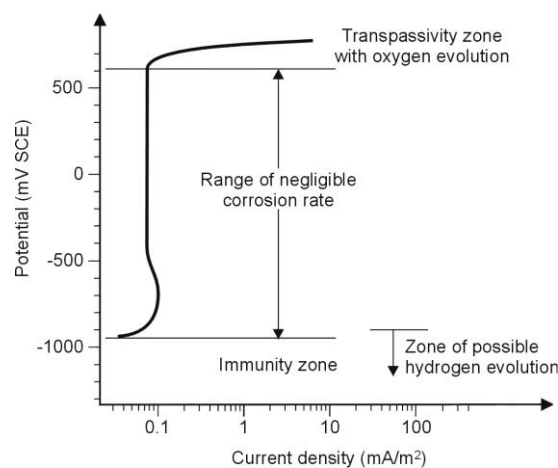
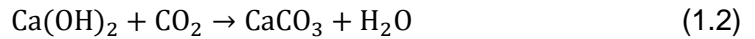


Figure 1.5 Schematic of anodic polarisation curve of steel in alkaline concrete [5].

1.3 Carbonation-induced steel corrosion

The carbonation of concrete is the reaction of carbon dioxide (CO₂) in the atmosphere reacts with alkaline components of concrete, for instance Ca(OH)₂, calcium-silicate-hydrates (C-S-H), NaOH and KOH [8]:



The carbonation reactions could reduce the pH of concrete pore solution down around 9. When the carbonation front approaches the surface of steel embedded in concrete, the carbonated concrete with low alkalinity can dissolve quickly the passive film of steel. Once the steel becomes active, if oxygen supply and moisture content are sufficient to maintain the corrosion, steel corrosion would start. The expansive corrosion products can result in the cracking, spalling and delamination of concrete cover layer, leading to the failure of reinforced concrete structure. **Figure 1.6** illustrates the process of carbonation-induced corrosion in reinforced concrete. Due to the fact that the shape of the carbonation front of concrete is even [8], in general, the type of corrosion induced by carbonation is general corrosion.

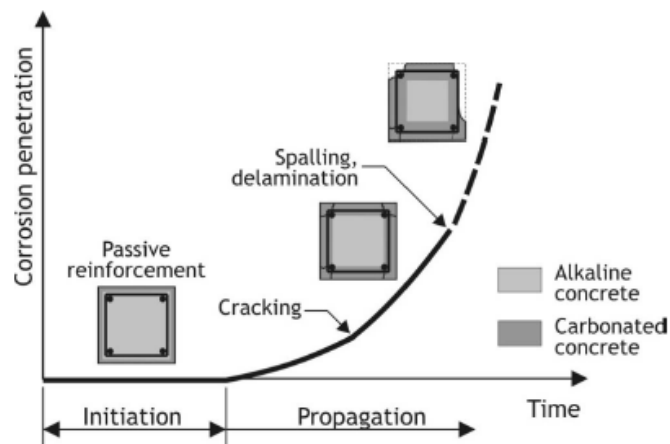


Figure 1.6 Evolution of carbonation in reinforced concrete over time [9].

The relationship between carbonation depth and time can be correlated by the following equation:

$$d = K\sqrt{t} \quad (1.3)$$

where, d is carbonation depth at time t , K is carbonation coefficient.

Apparently, concrete cover depth and carbonation rate characterised by K , are the dominated parameters related to the service life of reinforced concrete structure being subjected to carbonation. The main factors that can affect carbonation rate of concrete include CO₂ concentration in air, cement content of concrete and CaO content of binder, pore characteristics of concrete, relative humidity and temperature [6]. **Figure 1.7** shows the effect of relative humidity (R.H.) on carbonation rate of concrete. The carbonation rate of concrete is low in water saturation

condition due to the difficulty of CO₂ diffusion as well as in dry condition because of absence or insufficiency of water. Since wetting of concrete is faster than drying, more frequent although shorter periods of wetting are more effective in reducing the penetration of carbonation than less frequent and longer periods. Carbonation can only occur while existing a certain amount of water in concrete pores since carbonation reactions require water to uptake CO₂ in order to form carbonic acid (CO₃²⁻) firstly [10].

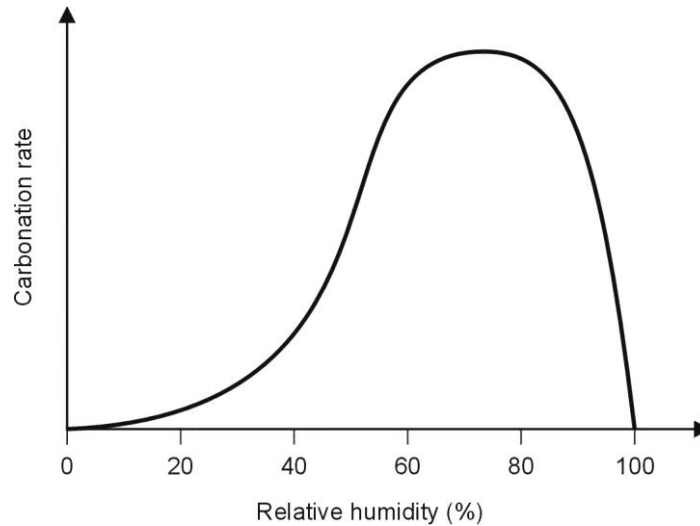


Figure 1.7 Effect of relative humidity of the environment on carbonation rate of concrete [5].

1.4 Chloride-induced steel corrosion

In some particular circumstances, such as those derived from the use of deicing salts or from the exposure to the marine environment, when the chloride content at rebar depth reaches to a certain value that is so-called “chloride threshold value”, corrosion of steel in concrete initiates. The chloride threshold value depends on concrete properties including the presence of macro voids near steel surface [9] the pH of pore solution [11], [12], the composition and microstructure of steel and the potential of steel [13], [14] and environmental parameters such as moisture content and temperature. The corrosion morphology of steel induced by chloride is that typical of pitting corrosion. Due to the stochasticity of occurrence of pitting corrosion, chloride threshold value can only be defined by statistical results [9].

Once pitting corrosion has initiated on the steel surface, a very aggressive micro environment will be created inside the pits that provide places for the subsequent corrosion. Therefore, the corrosion inside the pits is an autocatalytic process, which can maintain high corrosion rate, consuming quickly the cross-section of steel. The corrosion of steel in concrete induced by chloride is illustrated in **Figure 1.8**.

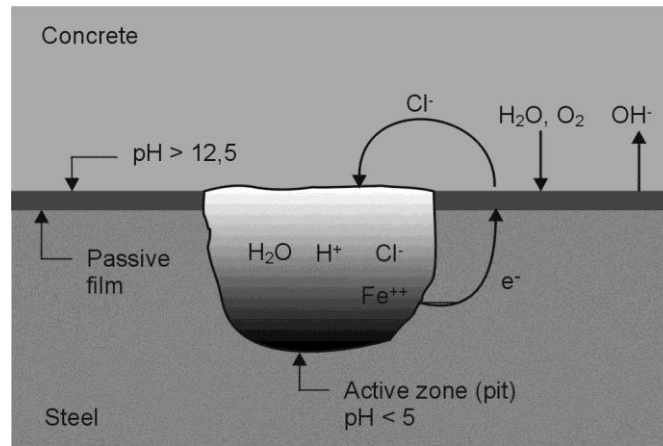


Figure 1.8 An illustration of chloride-induced steel corrosion in concrete [5].

Apparently, such factors as depth of concrete cover, chloride penetration rate and chloride threshold value jointly affect the service life of reinforced concrete structure suffering from chloride-induced corrosion of steel. Among of them, chloride penetration plays the primary role. The mechanism of chloride penetration in concrete can be related to the transport actions such as diffusion, capillary suction, permeation, and migration [5]. In real conditions, the process is often the result of some combinations of these actions. Essentially, they all depend on the microstructure of concrete. The chloride content profile of concrete subjected to chloride penetration could be predicted by the following formula derived from Fick's second law:

$$C(x, t) = C_s \left[1 - \operatorname{erf} \left(\frac{x}{2\sqrt{Dt}} \right) \right] \quad (1.4)$$

where $C(x, t)$ is the chloride concentration (by mass of cement or concrete) at depth x and at exposure time t ; C_s is the surface chloride content (by mass of cement or concrete) that is determined by the regression analysis; D is the apparent diffusion coefficient for chloride (m^2/sec).

1.5 Rusted steel

Steel bars, as a result of manufacturing process, are covered by a layer of the mill scale, i.e. oxides generated at high temperature. The chemical composition, thickness and adherence of mill scale on carbon steel depends on manufacturing method [15], such as water cooling and air cooling. In general, the thickness of the mill scale is about tens of micrometres. Rapid water cooling, when compared with air-cooling, does not allow mill scale to grow easily and therefore results in a thinner mill scale layer [16]. The mill scale of carbon steel bars is not considered harmful and therefore is not removed at the end of manufacturing process.

In the period between the production of steel and casting of concrete, the bars are exposed for a certain time to the atmospheric moisture which can lead to the formation of rust. Atmospheric corrosion can take place when the steel surface is wet or covered by a moisture film (e.g. formed

by condensation). The kinetics of rusting depends on the thickness and chemical composition of the aqueous film, on the time of its permanence on the steel surface, and the presence of contaminants such as sulphur oxides and chlorides.

In general, 70 ~ 80% of relative humidity is considered as a threshold value, beyond which a liquid film forms, which promotes corrosion on the steel surface. When the steel bars are kept in a dry internal environment, normally this threshold is not reached and the effect of rusting is negligible. Instead, outdoor exposure can often promote rusting of steel, even in condition sheltered from rain. When contaminants are present or when the steel surface is already covered by rust, the critical threshold of R.H. can be lower than the values above indicated.

Contaminant type and content in atmosphere vary from region to region, which can affect not only rusting rate but also final rusting products [17], [18]. Moreover, the different surface condition and the initial oxide layer on steel bars due to different production processes, play a critical role in the rusting of steel in atmosphere [15]. However, it seems that the thickness of rust layer does not depend on the size of steel bar for any given environment [19]. However, the rust formed on steel surface is generally coarse, flaky and porous [20], is not of the protective property that passive film provides [21]. The presence of rust is often questioned in the process of quality acceptance, because of the fear that it might compromise the durability and performance of reinforced concrete structure.

In literature, regarding to the passivation of rusted steel embedded in concrete or in mortar, some contradicted results were reported. In reference [22], the corrosion rate of rust-covered steel bars (diameter 12 mm) in 0.5 and 0.7 water/cement (w/c) ratios concrete made with pozzolanic cement was monitored for one year; the passivation of rust-covered bars, namely for corrosion rate less than 1 $\mu\text{m}/\text{year}$, was reached in one year for both w/c ratios. The passivation of rusted steel was also studied in the reference [23]; the authors investigated the corrosion of steel bars with three surface conditions, i.e. polished (mirror finish), mill-scale covered (black oxide) and rusted (red oxide), embedded in 0.5 w/c ratio ordinary mortar; based on their experimental results, all steel bars including rusted steel became passive in mortar during 30 days curing in 100% R.H., as shown in **Figure 1.9**. On the contrary, in the literature reference [24], the passivation of pre-rusted steel bars with three degrees of rusting (253, 239 and 116 g/m^2) was studied in mortar with w/c ratio equal to 0.5; the obtained results suggested that during around 1000 days, none of the pre-rusted bars reached passive state, as shown in **Figure 1.10**; another pre-rusted steel with the rusting degree about 395 g/m^2 was not passivated in saturated $\text{Ca}(\text{OH})_2$ solution in one week. Similarly, in the reference [25], rusted steel bars both in mortar with w/c ratio of 0.5 for about 2 years and in saturated $\text{Ca}(\text{OH})_2$ solution for 30 days showed corrosion rate higher than 0.1 $\mu\text{A}/\text{cm}^2$ (1 mA/m^2). In literature reference [26], the corrosion rate of pre-rusted steel sheets with five

degrees of rusting (0.89, 1.52, 3.41, 7.95 and 12.43 mg/cm²) in saturated Ca(OH)₂ solution was measured for 30 days; the results showed that even the presence of 0.89 mg/cm² of rust on the steel sheet surface can cause it to lose passivity ($i_{corr} > 0.1 \mu\text{A}/\text{cm}^2$); the value of corrosion rate (measured in terms of mass loss) of rusted steel was proportional the grade of rusting, as shown in **Figure 1.11**; the high corrosion rate of rusted steel sheet might be ascribed to the self-reduction of rust ($\text{Fe}^{3+} \rightarrow \text{Fe}^{2+}/\text{Fe}_3\text{O}_4$) in the first phase and rust layer acting as a porous electrode that promotes oxygen reduction reaction in the later phase.

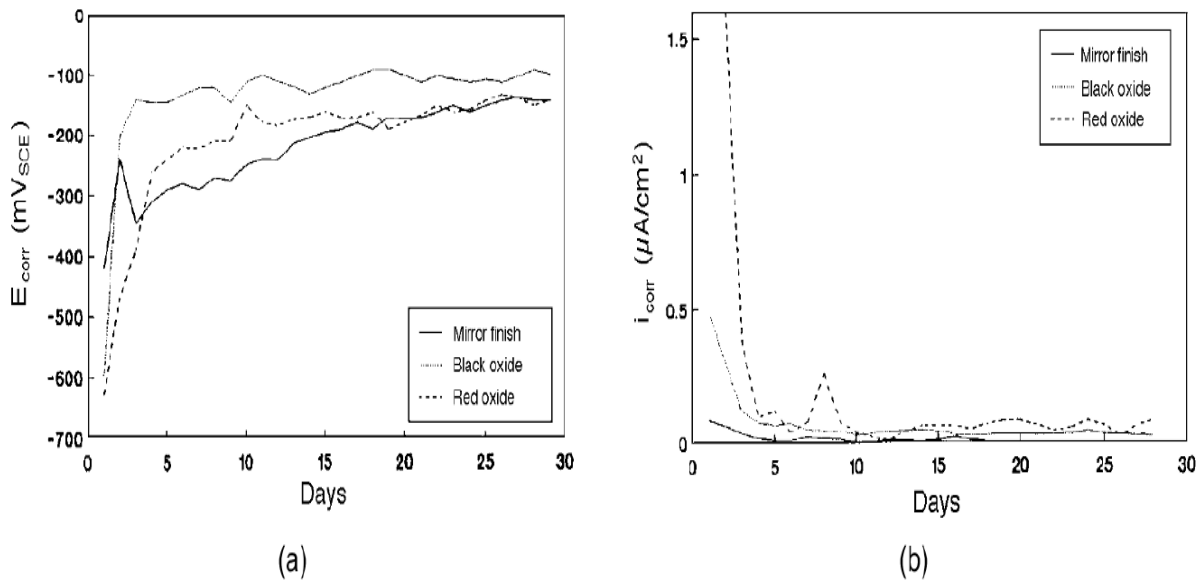


Figure 1.9 Evolution of (a) corrosion potential (E_{corr} vs SCE) and (b) corrosion rate (i_{corr}) of steel bars with different surface conditions (mirror finish, black oxide, red oxide) in mortar over 30 days curing (100% R.H.) [23].

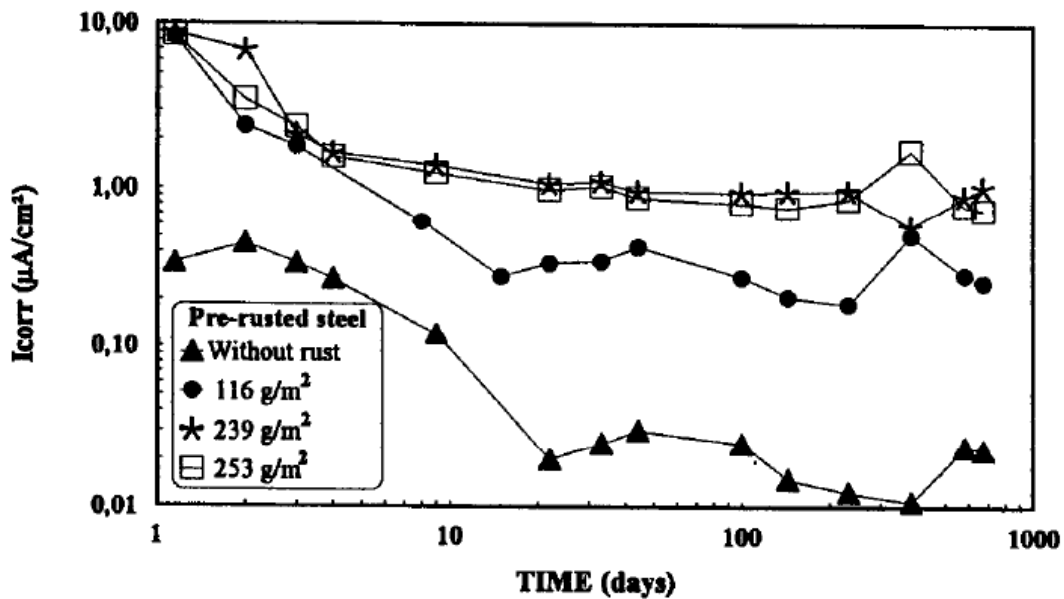


Figure 1.10 Evolution of corrosion rate (i_{corr}) of pre-rusted steels in mortar [24].

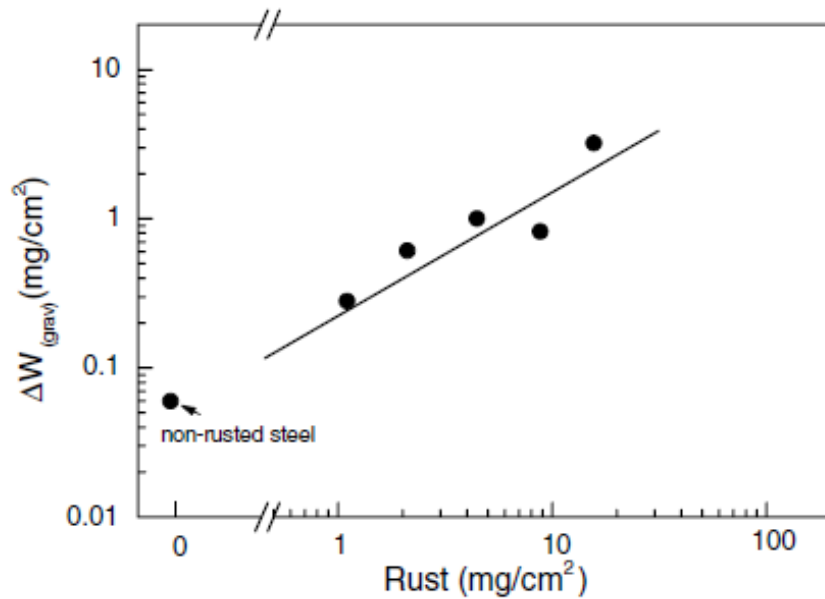


Figure 1.11 Mass loss ($\Delta W_{(grav)}$) of pre-rusted steel sheets with different initial degrees of rusting (mg/cm^2) after 30 days immersion in saturated $\text{Ca}(\text{OH})_2$ solution [26].

In literature reference [27], the authors studied the corrosion behaviour of 10 mm diameter pre-rusted bars (obtained by outdoor exposure half-year) embedded in concrete with different chloride contents (< 0.05%, 0.4% and 2.5% by cement mass), exposed to different R.H. (60%, 80%, 90% and 100%) in course of 4 years; the corrosion rate calculated by mass loss of pre-rusted bars was above $1 \mu\text{m}/\text{year}$, except in the case of 0.4% chloride content and 60% R.H.; in particular, the worst cases were 2.5% chloride content and R.H. between 70% and 90%; the authors ascribed this phenomenon to the composition of rust layer which was contaminated by sulphates during atmospheric exposure, besides to the porous rust which behaved as barrier for alkaline pore solution and as crevice for corrosion stimulating anions. In [23], the authors found that i_{corr} of rusted bar could be more than $0.1 \mu\text{A}/\text{cm}^2$ ($1 \text{mA}/\text{m}^2$) when the reinforced specimens were partially immersed in double-distilled water and chloride solutions (1% and 3% Cl); they have deduced that, apart from oxygen reduction reaction, alternative cathodic reaction may contribute to the high corrosion rate of steel.

The negative effect of the rust present on steel surface on its corrosion behaviour was also reported in reference [20]; 10 mm diameter rusted steels were tested in saturated $\text{Ca}(\text{OH})_2$ solution (without chloride and 3% chloride) in comparison with polished steel; it was observed that, in the presence of rust, i_{corr} of steel has increased but polarisation resistance, pitting potential and total impedance of the steel/electrolyte system have decreased; the authors explained the results by the fact that rust provokes the decrease of the electrolyte resistance at the steel/electrolyte interface and reduces the repassivating ability but also considering that rust layer behaves as a physical barrier, hindering OH^- diffusion toward the surface of steel.

However, in reference [28], the authors investigated chloride threshold value for 13 mm diameter steel bars with five different surface conditions such as polished (*P*), mill-scaled (*M*), brown-rusted (*BR*), black-rusted (*BL*), and pre-passivated (*PP*), all embedded in concrete with w/c ratio of 0.5 and cyclically immersed in seawater (17087 ppm Cl) for 3.5 days at 60°C and 3.5 days in normal atmospheric temperature; based on the obtained results, the ranking of chloride threshold value for the steel bars is sequenced as $PP > BL > P$ (0.8% of cement mass) $> BR$ (0.5% of cement mass) $> M$ (0.4% of cement mass). The slightly higher chloride threshold value for *BR* steel compared with *M* steel is attributed to a weak physical barrier of rust layer between steel and cement hydrates. It was also found in reference [12] that removing rust layer and mill scale by sandblasting can increase chloride threshold value of steel, by testing steels with three surface conditions such as as-received (with mill scale), pre-rusted and sandblasted in saturated $\text{Ca}(\text{OH})_2$ solution and simulated concrete pore solutions (pH=13.3 and 13.6). The positive effect of rust layer to increase chloride threshold value has also been reported in [16], [29].

The work in literature reference [30] revealed that chloride threshold (Cl^-/OH^-) of steel bars that were tested in saturated $\text{Ca}(\text{OH})_2$ solution is no relation with the degree of rusting of steel but the microstructure of steel; they claimed that tempered steels with martensite surface seems to be more susceptible than steels with ferrite-pearlite microstructure.

1.6 Galvanised steel

The service life of reinforced concrete structure depends not only on the properties of concrete, but also on the corrosion resistance of steel. Corrosion resistance of steel can be increased either by modifying chemical composition of steel or by applying a metallic or organic coating on its surface [5]. Three types of corrosion-resistant bar are commonly used in reinforced concrete structure, including stainless steel, epoxy-coated steel and galvanised steel. Stainless steel has a very good performance in concrete, but the biggest disadvantage is its high price that apparently increases the cost of reinforced concrete structure. Due to the damage and debonding of coating of epoxy-coated steel, it is difficult to maintain a defect-free epoxy-coated steel, which weakens the effectiveness of epoxy-coated steel.

Conversely, galvanised steel is the reinforcing bar with a protective zinc coating applied for dipping of a properly prepared bar into a molten bath of zinc at 450 ~ 460°C, also known as hot-dip galvanising [31]. The metallurgical reaction between zinc and iron finally forms a series of thin zinc-iron alloy layers as shown in **Figure 1.12**. A pure zinc layer, also known as η layer, is the outermost layer; inwardly laying several iron-zinc alloy layers (ζ , δ , Γ) [32]; the closer to steel substrate, the higher iron content.

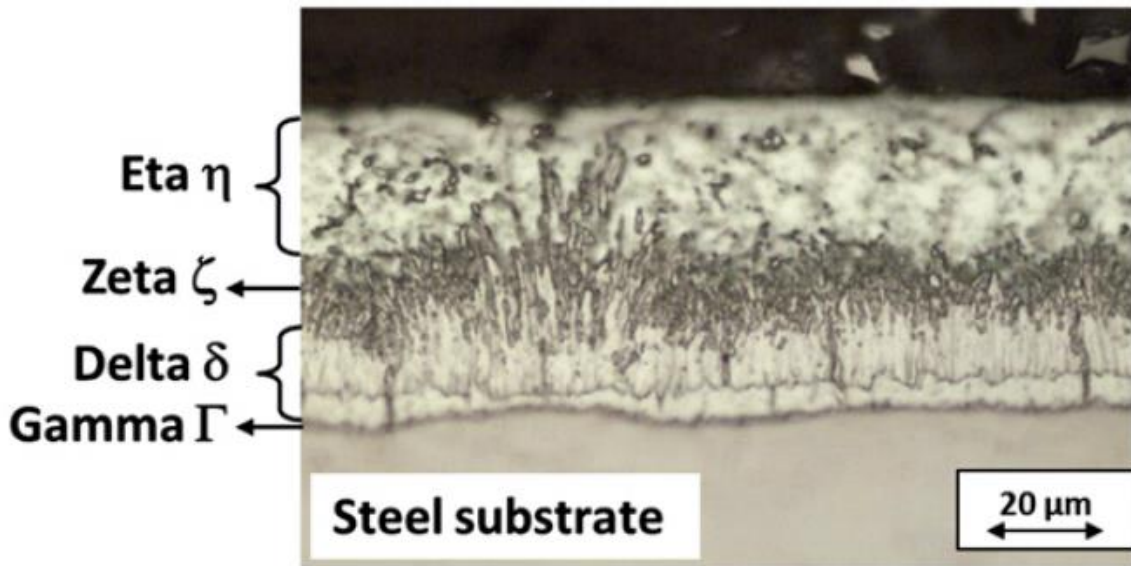


Figure 1.12 Microstructure of coating layer of hot-dip galvanised steel [33].

Zinc is an amphoteric metal that reacts readily in both strong acidic and basic circumstances as shown in **Figure 1.13**. Both neutral and mildly alkaline circumstances are favourable conditions for lowering the corrosion of zinc. This can be explained by the Pourbaix diagram of zinc-water system at 25°C as shown in **Figure 1.14**. In acidic environment, Zn^{2+} is the reaction product of anodic reaction; in neutral and mildly alkaline environments, zinc is passivated by the formation of passive layer consisting of the mixed composition of $\text{Zn}(\text{OH})_2$ and ZnO ; $\text{Zn}(\text{OH})_2$ is more effective to provide protection than ZnO ; with harsh alkaline environment, the passive layer could be decomposed to transform into soluble zincates such as HZnO_2^- and ZnO_2^{2-} [34].

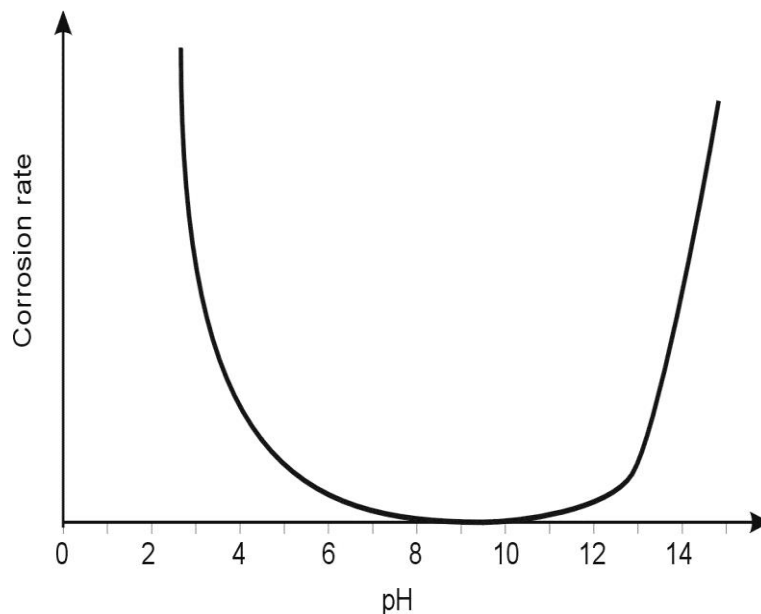


Figure 1.13 Effect of pH on the corrosion rate of zinc [5].

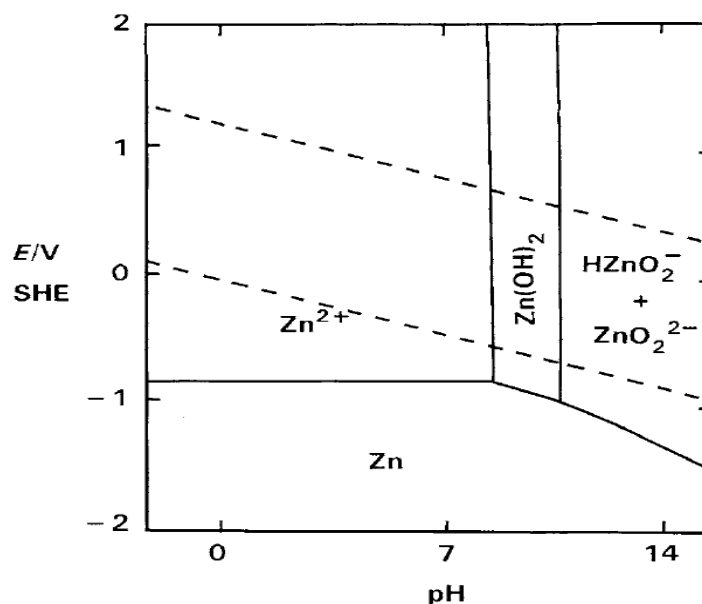


Figure 1.14 Pourbaix diagram for zinc-water system at 25°C [35]. SHE: Standard Hydrogen Electrode.

In fact, in alkaline environment, the corrosion behaviour of galvanised steel depends not only on pH, but also on the absence or presence of calcium cations. Ca(OH)_2 is the dominant component of concrete pore solution that also contains minor alkaline components such as KOH and NaOH. The galvanised steel embedded in alkaline concrete can develop a compact passive layer of calcium hydroxyzincate ($\text{Ca[Zn(OH)}_3\text{]}_2 \cdot 2\text{H}_2\text{O}$) [36], [37], as described by the below reaction:



In fact, the real reaction in alkaline concrete is much more complicated than this reaction. Zinc may form Zn(OH)_2 first, and then transform Zn(OH)_2 to $\text{Ca[Zn(OH)}_3\text{]}_2 \cdot 2\text{H}_2\text{O}$ [34]. Due to the release of hydrogen induced by the reaction between zinc layer with wet concrete, as shown in **Reaction 1.5**, the porosity of cement paste close to steel surface increases at early hydration stage [38]. Nevertheless, passive film is not possible to be formed when pH is beyond 13.3 [39].

Although the formed passive film (calcium hydroxyzincate) in alkaline concrete could be destroyed by carbonation action, it seems that galvanised steel still can remain in passive state in carbonated concrete [37]. A study published in reference [40] revealed that carbonation changed the passive film $\text{Ca[Zn(OH)}_3\text{]}_2 \cdot 2\text{H}_2\text{O}$ into the new amorphous products ZnCO_3 and $\text{Zn}_5(\text{CO}_3)_2(\text{OH})_6$, with a prevailing presence of the former, which both are protective as well. The results of corrosion rates of galvanised steel and carbon steel embedded in concrete that were exposed in accelerated carbonation chamber confirmed that galvanised steel is under protected with increasing exposure time but carbon steel is corroded, as shown in **Figure 1.15**.

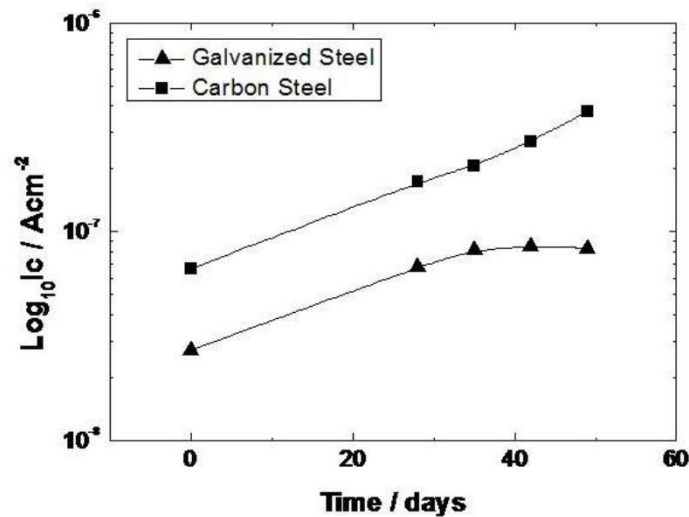


Figure 1.15 Time evolution of corrosion current density of galvanised steel and carbon steel embedded in concrete exposed in accelerated carbonation chamber [41].

Once the outermost zinc layer (η) dissolves completely, the underlying Zn-Fe layer will be exposed, i.e. ζ layer. Corrosion resistance of Zn-Fe layer is lower than that of pure zinc layer. Due to the reduction of zinc content in this layer, it takes longer time to form passive film for Zn-Fe layer [34]. If galvanised steel is active, zinc would dissolve sacrificially instead of iron. Obviously, the thickness of coating layer, especially the thickness of pure zinc plays an important role to the protection ability of galvanised steel in concrete. The thickness of pure zinc layer should be at least 10 μm . To allow corrosion protection, generally, the total thickness of zinc-based coating layer is around 100 μm , depending on the galvanising process and substrate steel type. **Table 1.1** lists some thickness values reported in literature papers considered in this review.

Table 1.1 Coating layer thickness of galvanised steel considered in some literature studies.

Thickness	[42]	[31]	[43]	[44]	[36]	[37]*	[40]*	[45]	[34]	[46]
μm	110	100	80~100	≈ 100	100**	120 \pm 10	55 \pm 5	140	102	120~280

* Galvanised steel sheet.

** Including 20 μm thick pure zinc layer.

In practical, the thickness of coating layer is totally uneven; the variation of coating thickness certainly has an effect on the extent of corrosion, as confirmed through a study on the corrosion mechanism of galvanised steel in artificial cracked concrete in [32]. Besides, in construction site, the coating layer of galvanised steel embedded in concrete is often discontinuous due to cutting bar-end, bending and welding of the bars; the discontinuous coating layer can lead to the quicker corrosion, especially in the presence of chloride ions [47]. Although zinc sacrificially protects adjacent areas of exposed steel, the range/distance protected is limited. It's reported that the distance protected is as large as 4 cm in the presence of chloride in reference [47].

Galvanised steel can significantly delay the onset of chloride-induced corrosion [31], [48] due to the sacrificial protection coating layer; however, it seems that galvanised steel was more susceptible to localised corrosion comparing with carbon steel [48]. The coating layer can also help improve chloride penetration resistance in terms of critical chlorides threshold value. In equivalent concrete and exposure conditions, galvanised steel showed to tolerate Cl^- levels at least 2.5 times higher than black steel, and 4 to 5 times longer for the corrosion onset [42]. The initiation time and chloride threshold value of reinforced specimens with galvanised steel embedded in concrete with different w/c ratios (0.4, 0.5, 0.6 and 0.7) exposed in the north coast of the Yucatan Peninsula (Mexico) for 9 years have been studied; the results suggested that the initiation time of galvanised steel corrosion induced by chloride penetration was almost twice as much as black steel; and the chloride threshold value was more than twice [49]. In the case of directly mixing CaCl_2 into concrete, it's found that galvanised steel could tolerate up to 2.5% content so that the corrosion process was not initiated [45]. However, carbonated concrete with galvanised steel exposed in 3.5% NaCl solution resulted in a noticeable decrease of chloride threshold value [40].

1.7 Sustainable new materials

Based on literature survey, it's not found that a relevant number of scientific papers regarding the corrosion protection of steel embedded in new sustainable cementitious materials such as recycled waste glass mortar or concrete, CSA-based concrete and cement-stabilised rammed earth. Instead, it has been found that most of such literature papers were dedicated to the studies of the performance properties of these new cementitious materials. Thus, in this section, the literature review will mainly focus on the properties of concrete made with these materials related to corrosion protection of steel.

1.7.1 Recycled waste glass

Waste glass derives from municipal waste, such as beverage containers, pharmaceutical containers, domestic glass products. It occupies extensive parts of the landfills due to the non-biodegradable nature of glass, which makes landfilling not an environment-friendly solution [50]. Recycling waste glass to produce concrete is a promising way that helps improve the sustainability of concrete industry [51], [52]. In concrete, waste glass can be used either as fine or coarse aggregate [53]–[62] or as mineral addition to replace partially cement [63]–[66]. In recent years, waste glass has also been developed to manufacture expanded glass that can be used as lightweight aggregates, by burning ground glass and by expanding agent together [67]–[69]. Therefore, in this section, the use of glass powder as mineral addition and expanded glass as lightweight aggregates is reviewed. **Table 1.2** summarises all reviewed researches considering in this section and dealing with waste glass used as mineral addition and lightweight aggregate.

Table 1.2 A summary for all reviewed research on the use of waste glass as mineral addition and lightweight aggregate.

Ref.	Glass type	Particle size (μm)	Main compositions (% by weight)				Sample type	Replacement ratio (by weight)	Test type
			SiO ₂	Na ₂ O	K ₂ O	CaO			
[50]	Soda-lime	75~150; 38~75; <38	72.8	16.3	0.3	4.9	Concrete/mortar	30% cement (by volume)	Compressive strength; ASR expansion
[54]	Flint	150~4750	72.17	13.13	0.61	10.92	Mortar	100% aggregate	ASR expansion
	Amber		72.08	13.71	0.16	10.45			
	Green		71.24	13.12	0.63	10.79			
	Blue		72.05	13.02	0.51	10.96			
[57]	Mixed color	75~2360	71.40	13.00	0.73	10.90	Mortar	10, 25, 50, 100% aggregate	ASR expansion
[58]	Mixed color	630~1250; 160~315; >81; <41	69.4	13.6	0.6	12.5	Mortar	10, 20, 30, 40% cement	Compressive strength
[63]	Green	400 and 600m ² /kg	68.67	13.25	1.11	11.35	Mortar	30% cement	Compressive strength; Electrical resistivity; Chloride penetration; Sulphate expansion
[64]	White	<600	70.39	16.66	0.23	6.43	Mortar	10, 20, 30, 40% cement	Compressive strength; ASR expansion
	Green		72.05	14.31	0.52	10.26			
	Amber		70.01	15.35	0.82	10			
[65]	-	< 1000	70	16	0.35	8.7	Mortar	10, 20% cement	Workability; Flexural and compressive strength; ASR expansion; Capillary absorption; Chloride penetration and carbonation resistance; Sulphate attack
[70]	-	< 75	71.4	12.25	0.36	11.2	Concrete	5, 10, 15, 20, 25% cement	Workability; Compressive and Tensile strength; Water absorption; Voids ratio; Hardened density
[71]	-	40~700; 264, 467 and 582 m ² /kg	72.5	13.2	0.12	9.18	Mortar	20% cement	Compressive strength; Expansion
[72]	-	400 and 600m ² /kg	68.67	13.25	1.11	11.35	Mortar	30% cement	Compressive strength; Electrical resistivity; Chloride penetration; Sulphate attack
[73]	-	28.3, 47.9, 88.5, 204*	73.5	12.74	0.69	10.48	Cement paste/mortar	20% cement	Heat of hydration; Stiffening; Flowability
[74]	-	414 m ² /kg	68.2	7.62	0.23	9.90	Mortar	5, 10, 20% cement	Compressive strength; ASR expansion
[75]	-	45*	72.3	13.31	0.52	8.61	Concrete	20% cement	Workability; Wet density;
	Mixed color	<5 mm	72.1	12.40	0.64	10.63		50, 100% aggregate	Compressive, tensile and flexural strength; Water absorption
[76]	Amber	0~45; 45~75; 75~150	73.27	10.37	1.10	11.36	Mortar	10, 20, 25, 30, 40% cement	Workability; Compressive strength; ASR expansion
	Green		72.25	10.54	1.15	12.35			
	Flint		74.07	9.94	1.14	11.53			

Chapter 1

Corrosion protection of steel in sustainable concrete

[77]	Clear		72.42	13.64	0.35	11.50	Concrete	10, 20, 30, 40% cement; 0~100% fine aggregate; 50% coarse aggregate	Workability; Compressive strength; Expansion; Drying shrinkage
	Brown	<10; 150~4750;	72.21	13.75	0.20	11.57			
	Green	4750~12000	72.38	13.52	0.27	11.26			
[78]	Mixed color	8, 11, 120, 238, 473, 940, 1875, 3750*	68.6	13.5	0.6	12.3	Mortar	20, 40% cement	Compressive strength; ASR expansion
[67]	Expanded glass	-	-	-	-	-	Concrete	36~56% aggregate (by volume)	Compressive, tensile and flexural strength; Density
[68]	Expanded glass	150~300;1000~3000	-	-	-	-	Mortar	100% aggregate	Apparent density; Water absorption; ASR expansion
[79]	Expanded glass	500~5600*	-	-	-	-	Concrete	77% aggregate	Compressive strength; ASR expansion
[80]	Expanded glass	370 m ² /kg	71.2	13.5	0.9	10.1	Mortar	100% aggregate	ASR expansion
[81]	Expanded glass	250~500	71.2	13.3	0.9	8.5	Mortar	0.59, 1.77% (by mortar mass)	Workability; Density; Water absorption; Compressive and flexural strength; Pozzolanicity

* Average particle size.

1.7.1.1 Glass powder as mineral addition

The pozzolanic reactivity of glass powder in concrete has been confirmed in [50], [63], [70]–[72]. The pozzolanic reactivity of waste glass increased as its fineness increased [50], [71]. In concrete, silica-rich glass powder can react with the alkalis (mainly $\text{Ca}(\text{OH})_2$) released by cement hydration and form C-S-H. Therefore, glass powder can be used as mineral addition to replace cement.

The workability of concrete with glass powder is quite comparable with that of ordinary concrete, even slightly higher [65], [70]. That is because that glass powder is of the optimizing gradation effect, and filling effect that lower friction between particles through releasing water enclosed in interstices of particles [73]. Although the density of glass powder is slightly lower than that of cement, usually the density of concrete with glass powder is comparable with ordinary concrete when cement replacement ratio is low [66].

Concrete with glass powder showed low compressive strength at early age when compared with ordinary concrete [50], [63]–[65], [70], [71], [74]. That should be due to the fact that pozzolanic reaction of glass powder in concrete occurs in later curing stage [65].

Concrete with glass powder showed comparable water absorption as reported in [65], [75]. The improvement of chloride penetration resistance of concrete with glass powder [63], [65], [66], [72] is the result of the refinement of concrete pore structure due to pozzolanic reaction of glass powder. The densification of pore microstructure was clearly revealed by electrical resistivity measurements [63], [66]. However, both the decrease of carbonation resistance [65] and the improvement of sulphate attack resistance [63], [65], [72] are due to the consumption of $\text{Ca}(\text{OH})_2$ by pozzolanic

reaction of glass powder so that there is less $\text{Ca}(\text{OH})_2$ available to react with CO_2 and sulphates [65].

However, there are two main concerns which can limit the use of glass powder in concrete. One concern is the mingling of different types of waste glass due to the small amounts of additives often added during the production to obtain different colours or specific properties. Anyway, it has been demonstrated that glass colour does not show significant effect on compressive strength of waste glass mortar and its expansion [76]. The other concern is the potential expansion of concrete or mortar containing glass powder. That is because that glass contains large quantities of amorphous silica and high sodium oxide, which might lead to potential ASR when glass powder is incorporated in concrete or mortar. Nevertheless, reducing size of glass efficiently decreased ASR expansion of concrete containing waste glass. In reference [50], the expansion of mortar with 30% cement replaced by 38, 75 and 150 μm glass powder did not exceed the expansion limit 0.1% according to ASTM C1260; the finer the particle size of glass powder, the less the expansion. Based on the results in literature reference in [57], glass mortar did not lead to deleterious ASR expansion when using glass smaller than 600 μm , this results in agreement with observed in reference [77]. It's been shown that no expansion occurred when glass mortar made with 20% glass of particle size less than 1 mm in reference [78]; fine glass powders with surface area ranging between 180 and 540 m^2/kg even decreased the expansion of mortars subjects to ASR. A widely-accepted understanding behind this phenomenon is that finer particles favour pozzolanic reaction, whereas coarser particles are more likely to occur ASR [54], [64]. It has been further found that coarse particles take place in pozzolanic reaction first and ASR later, whereas fine particles only occur pozzolanic reaction; pozzolanic reaction gives rise to C-S-H with high Ca/Si and low alkali content while ASR brings about low Ca/Si and high alkali ASR gel [58].

The pozzolanic property of glass powder is beneficial not only to improve the properties of concrete or mortar made with glass powder, but also to suppress the ASR expansion. In addition to the reduction of glass particle size, another way to suppress ASR expansion is to use the porous lightweight expanded glass, as shown in **Figure 1.16**.

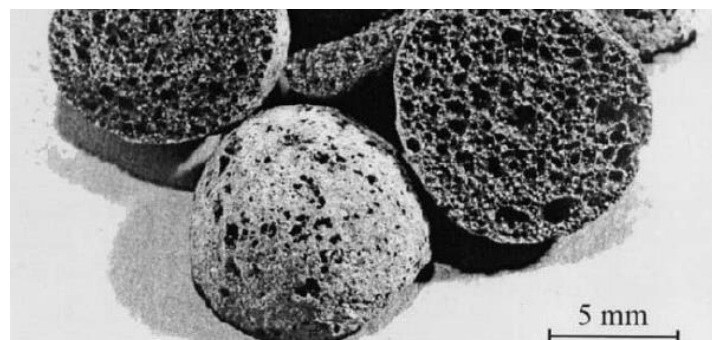


Figure 1.16 An example of cross sections of expanded glass particles [68].

1.7.1.2 Expanded glass as lightweight aggregate

Due to the high porosity, the bulk density of expanded glass is low. Typically, its bulk density varies between 300 and 2000 kg/m³ [67], even as below as 187 ~ 230 kg/m³ reported in [79]. High porosity also leads to its high water absorption [68], [69], [79]–[81]. The water absorption of expanded glass is correlated with its particle density according to [67]. In addition, crushing resistance of expanded glass particle seems to be proportional to particle density as well [67]. However, it has been reported that expanded glass is feasible to produce structural lightweight concrete by adjusting manufacturing process to produce expanded glass with relatively high crushing resistance and low water absorption [67].

Both coarse and fine expanded glass aggregates showed no influence to the initial slump of expanded glass concrete [69]. Fine expanded glass particles (0.25 ~ 0.50 mm) even increased slightly the slump when compared with ordinary aggregates [81]. The quick workability loss after mixing, was observed as the result of water absorption of porous expanded glass particles; the loss accelerated with the increasing proportion of expanded glass in concrete [69].

Up to 15 % fine expanded glass particles in partial replacement of natural fine aggregates, it has been showed a positive influence on concrete strength due to the particle packing effect and the benefits of pozzolanic reaction of fine expanded glass particles; the porous surface texture of expanded glass particles could also be helpful through enhancing bonding strength between cement paste and glass particle. However, the use of coarse expanded glass particles in concrete has caused a noticeable strength loss; the extent of strength loss highly depends on w/c ratio and replacement ratio of coarse expanded glass aggregate [69]. Concrete with 100% replacement ratio of expanded glass aggregates with natural aggregates had very low strength [69], [79]. The strength value of expanded glass concrete has shown a correlation with its density in [67], [81], [82]. Besides, the modulus of elasticity of expanded glass concrete decreased alongside the increasing proportion of expanded glass in concrete due to low elasticity modulus of expanded glass; on the contrary, flexural strength showed a slight improvement [69]. Early-age shrinkage cracking of expanded glass concrete is linear with water absorption capacity of expanded glass particle [82]. It's also found that the high porosity of expanded glass particle increased the pore volume of concrete, therefore weakened the carbonation resistance of expanded glass concrete [69].

Although expanded glass particles showed high reactivity in terms of alkali–silica reactivity tests, no noticeable ASR expansion was observed in mortar with expanded glass [68], [80]. That was ascribed to the accommodation capacity of pores of expanded glass particles to ASR gel produced by ASR [68]. The benefit of high porosity to ASR expansion of expanded glass concrete was also confirmed in [69]. However, the ASR tests in 0.92 w/c ratio mortars with expanded glass (average size 0.5 ~ 5.6 mm) by using eight commercial cements, showed high ASR expansions [79].

1.7.2 Calcium sulfoaluminate cement

In the mid-1970s, CSA cement was firstly produced in an industrial scale in China by burning the mixture of limestone, bauxite and gypsum ($\text{CaSO}_4 \cdot 2\text{H}_2\text{O}$) at $1300 \sim 1350^\circ\text{C}$ [83]. In China, CSA cements are usually treated as a special cement on the basis of its nature which allows rapid setting, shrinkage compensation and high early-age strength, thanks to its main phase of tetracalcium trialuminate sulphate, named ye'elimite ($\text{C}_4\text{A}_3\bar{\text{S}}$)². Ye'elimite is also known as Klein's salt which was patented by Klein in 1966 to manufacture expansive cement. The amount of ye'elimite phase in CSA cement usually varies from 20% to 70% as shown in **Table 1.3**. Apart from ye'elimite, generally belite (C_2S) is another main phase in CSA cement; while the secondary phases may include C_4AF , C_3A , C_{12}A_7 and C_6AF_2 [84].

Table 1.3 Mineralogical composition of CSA cement or clinker reported in some references (wt.%).

Ref.	$\text{C}_4\text{A}_3\bar{\text{S}}$	C_2S	CT	CA	CA_2	C_3A	C_{12}A_7	MA	C_2AS	C_4AF	Calcite	$\text{C}\bar{\text{S}}$
[85]	20.1	47.1	0	0	0	0	0	0	0	13.8	0	19.8
[86]	27.5	56.3	0	0	0	0	0	0	0	7.9	0	4.4
[86]	10	51.5	0	0	0	0	0	0	0	15	0	16.1
[87]	21	44.54	0	0	0	0	0	0	0	15.81	0	19.83
[88]	33.9	53.2	0	0	0	0	0	0	0	7.9	0	4.3
[89]	6.7	67.1	0	0	0	0	0	0	0	19.0	0	7.0
[89]	5.8	59.7	0	0	0	0	0	0	0	19.6	0	7.1
[90]*	53.5	21.2	9.0	0	0	0	0	0	0	16.3	0	0
[91]*	57	0	4	15	0	0	1	0	16	4	0	0.5
[92]*	53.5	21.2	0	0	0	0	0	0	0	16.3	0	9.0
[93]*	68.1	0	3.6	7.8	1.2	3.4	0	0	14.8	0	0	0
[94]*	62.8	0	5.7	8.1	3.1	0	0	1.8	18.3	0	0	0
[95]*	65.3	22.4	0	0	0	0	0	0	0	3.2	0	8.9
[95]*	42.0	44.9	0	0	0	0	0	0	0	6.1	0	6.8
[95]*	15.4	70.8	0	0	0	0	0	0	0	7.2	0	6.6
[96]	42.4	21.7	0	0	0	9.3	0	0	0	3.9	6	16.2**
[97]	52	20	2	0	0	0	0	0	0	0	0	25
[98]*	68.1	1.7	3.9	3.2	0.7	0	1.4	1.1	19.4	0	0	0
[99]*	56.7	25.6	0	0	0	8.0	0	0	0	1.1	0	3.9
[100]*	67.7	20.3	2.5	0	0	0	0	0	0	0	0	7.9
[101]	54.7	26.6	0	0	0	9.0	0	0	3.1	1.1	0	3.9
[101]	70.9	6.0	0	0	0	7.2	0	0	7.6	0	0	6.3
[101]	45.1	20.6	0	0	0	6.7	0	0	1.5	1.4	0	23.2
[102]	53.0	13.2	0	0	0	0	10.3	0	0	0	0	18.6

* CSA clinker.

**Including 11.3% gypsum and 4.9% anhydrite.

CSA cement is a sustainable cement when compared with OPC [95]. Firstly, for its production, since less limestone is required due to the low CaO content in ye'elimite phase [95]; moreover, more gypsum or anhydrite (CaSO_4) is needed to prepare CSA cement in the requirement of

² Cement chemistry notations: C=CaO, A= Al_2O_3 , $\bar{\text{S}}$ = SO_3 , S= SiO_2 , H= H_2O , F= Fe_2O_3 , M= MgO , T= TiO_2 .

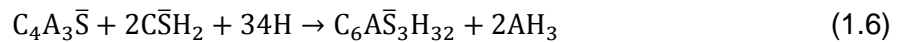
hydration; therefore, the CO₂ released in CSA cement production process is much less than that for OPC production. Secondly, its calcination temperature is 100 ~ 150°C lower than that of OPC, which helps increase clinker output more than 20% and reduce 15% coal consumption with respect to OPC [103]; this certainly slashes CO₂ emission due to less energy consumption. Thirdly, its clinker is porous and friable, which makes it easier to be ground [104]; this further reduces energy consumption.

However, the use of CSA cement to replace OPC 100% might encounter some adversities such as over-short setting time [103], low pH of pore solution [89], even high price [105] and potential expansion risk [95]. Thereby, blending CSA with OPC might combine their advantages and improve properties such as expansion and setting time [106], passivation ability of steel and pore microstructure and porosity [89].

1.7.2.1 Hydration of CSA cement

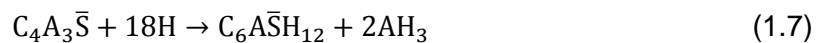
The hydration process of CSA cement has been extensively studied [84], [104], [107], [108]. It has been recognised that the hydration behaviour of CSA cement is significantly different with that of OPC due to its distinct chemical composition.

Once CSA cement is mixed with water, the first hydration reaction in the presence of gypsum (C \bar{S} H₂) will be:



The formation of ettringite (C₆A \bar{S} ₃H₃₂), also called AFt, mainly takes place in the first hours, very fast and numerous [85]. Based on this reaction equation, the theoretical w/c ratio for complete hydration of ye'elimite is 0.64; if anhydrite is used, the w/c ratio would be 0.78. Apparently, the w/c ratio for the complete hydration of CSA cement is higher than that for OPC.

When gypsum is depleted, the following reaction will occur:



This reaction forms monosulphate (C₆A \bar{S} ₃H₁₂), also named as AFm.

AFt and AFm will coexist when gypsum is not enough to react with ye'elimite totally; that is to say, the quantity of gypsum strongly effects the ratio of AFt/AFm [109]. Usually, in order to prepare CSA cement, 16 ~ 25 wt.% of calcium sulphate is grinded with CSA clinker [104]. In practice, three forms of calcium sulphate, namely anhydrite, calcium sulphate hemihydrate (CaSO₄·0.5H₂O) and gypsum, can be used to produce CSA cement; gypsum or anhydrite is more often used. It has been found that calcium sulphate which plays a key role to hydration of ye'elimite [94], [100], [108], [110]. That is due to the fact that the solubility and quantity of calcium sulphate decide the amount of available CaSO₄ that reacts with ye'elimite. For instance, the slower dissolution of anhydrite can

change the kinetics of hydration reactions, even the hydrated phases [94]. Increasing the amount of calcium sulphate is accompanied with the increase of hydration kinetics of ye'elimite [111] due to more available CaSO₄.

Hydration of belite typically occurs at later age due to its low reactivity. Because the hydration products of ye'elimite contain amorphous AH₃, as it's seen in **Reaction 1.6** and **1.7**, the hydration reaction of belite in the presence of AH₃ will form stratlingite (C₂ASH₈) rather than C-S-H [112]:

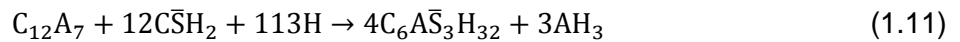
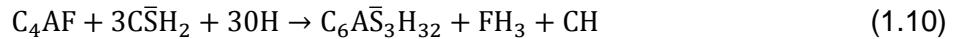


Only if AH₃ is lack, belite will give rise to C-S-H and CH as the below reaction:



Reaction 1.8 may also take place in early age, which in some way contributes to the early-age strength of CSA concrete; **Reaction 1.9** usually takes place in later age [105].

Most of the ye'elimite and gypsum react in first 7 days; while most of belite could be unhydrated even at 90 days [95]. Additionally, the minor phases also take part in hydration process, again their hydration products depend on the sufficiency of calcium sulphate, as detailed below [105]:



The former three reactions represent hydration reaction of minor phases in the presence of gypsum, the later three ones in the absence of gypsum. The titanium-contained phase (CT) and gehlenite (C₂AS) are thought as inert phases [108].

The real hydration process of CSA cement should be much more complicated than the above equations. In particular, unlike OPC, the composition of CSA cement or clinker varies in a wider range as shown in **Table 1.3**, which definitely complexes the hydration of CSA cement.

In case of blended CSA cement made with OPC cement, their hydration products highly depend on the ratio of OPC/CSA. For low OPC/CSA ratio, the hydration of OPC takes place in several days later after casting [93]. Alite (C₃S) in OPC cement can react with AH₃ that is the hydration product of ye'elimite at early stage, to form stratlingite (C₂ASH₈) and portlandite (CH) at early stage [106]:



For high OPC/CSA ratio, alite can bring about C-S-H and portlandite firstly; then the produced portlandite together with gypsum may change the hydration reaction of ye'elimite with the following reaction:



Moreover, at early stage, the aluminate phase (C_3A) can bring about AFm when gypsum is insufficient; when gypsum is absent, unstable calcium aluminate hydrates such as C_4AH_{13} would be formed first and stable hydrogarnet hydrate (C_3AH_6) later. Meanwhile, other secondary phases such as brownmillerite (C_4AF) or mayenite ($C_{12}A_7$) can also influence the hydration process of banded CSA cement [106].

1.7.2.2 General properties of CSA mortar and concrete

Due to the different mineralogical composition of CSA cements when compared to ordinary Portland cement, the hydration of CSA cements differs from that of ordinary Portland cement as described in the previous section. Therefore, CSA mortar or concrete may have different properties from ordinary concrete. Some interesting publications, which have studied the general properties of CSA mortar or concrete, have been considered in this section (**Table 1.4**).

Table 1.4 A summary for all reviewed researches on CSA mortar and concrete.

Ref.	Binder type	Sample type	w/c ratio	Test type
[86]	0~100% CSA (by weight) in place of OPC	Mortar	0.5	Setting time; Compressive and flexural strength; Dynamic modulus of elasticity; Length change; water absorption capacity; pH of pore solution; Potentiodynamic test
[87]	CSA clinker	Mortar	0.45	Weight loss and corrosion potential of steel in CSA mortar; pH of pore solution; porosity
[89]	85% CSA +15%OPC; 100%CSA	Mortar	0.5	Compressive strength; Water absorption capacity; Elasticity modulus; Total porosity; Length change; Potentiodynamic test
[95]	CSA clinker	Mortar	0.30, 0.45, 0.70	Expansion; Hydration products; Microstructure
[97]	CSA clinker	Concrete	0.55	Compressive strength; Electrical resistivity; pH of pore solution; Carbonation; Corrosion test
[102]	CSA clinker	Cement paste/mortar	0.5	Compressive strength; Hydration products; Porosity
[103]	CSA clinker	Concrete	0.563	Workability; Compressive strength; Carbonation; Chloride penetration; Sulphate attack; Expansion
[108]	CSA clinker	Cement paste	0.72, 0.80	Hydration; pH and composition of pore solution
[109]	CSA clinker	Cement paste	0.5	Compressive strength; Hydration; Porosity; Chloride penetration
[111]	CSA clinker	Cement paste/mortar	0.40, 0.525, 0.65	Hydration; Oxygen diffusion; Water absorption; Porosity; Compressive and flexural strength; Expansion; Carbonation
[113]	CSA clinker	Concrete	0.38, 0.44, 0.47, 0.57	Workability; Compressive strength; Chloride penetration resistance; Pore radius and volume
[114]	CSA clinker	Cement paste	0.5	Early age hydration
[115]	CSA clinker	Cement paste	0.5, 0.6, 0.8	pH and composition of pore solution

A w/c ratio of 0.43 for CSA cement paste allowed an initial set at 45 min and final set at 60 min [104]. The short setting time of CSA concrete is due to the quick and large formation of ettringite in the first hours of hydration. As a consequence, **Figure 1.17** evidenced that CSA concrete in different strength grades developed higher early-age strength than OPC concrete, especially in the case of CSA concrete in high strength grades [113]. Considering thin shape of AH_3 gel, early-age strength of CSA concrete might be attributed to the bonding and interlocking among ettringite crystals [114]. Content of anhydrite in CSA concrete can influence early-age compressive and flexural strengths as well; increasing anhydrite content means more ye'elimite phase which reacts at early age and therefore forms more hydration products [111].

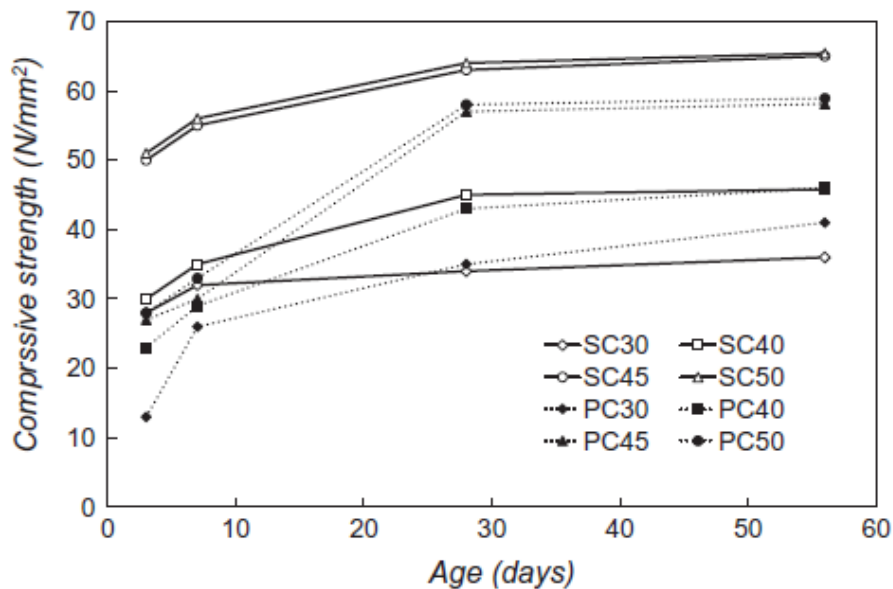


Figure 1.17 Compressive strength development of CSA and OPC concrete at different strength grades over curing age [113]. SC=CSA; PC=OPC.

A w/c ratio of 0.45 for CSA mortar, during the first 8 months exposure in tap water, showed no significant pore volume change with time, but larger average pore diameter than OPC mortar as shown in **Figure 1.18** [87]. Stable pore volume was observed within first 180 days in a w/c ratio of 0.45 for CSA mortar, but the pore volume decreased at 1 year [104]. However, a study performed on a 0.5 w/c ratio CSA cement paste revealed that a bimodal pore distribution was developed since the very early age; lower porosity is dominant, but not connected with higher porosity [102]. The authors found that the average pore size of CSA concrete is smaller than that of OPC. They also noticed that the refinement trend of total porosity almost ceased at later age. The porosity of CSA mortar decreased with the increase of anhydrite content and the decrease of w/c ratio [111].

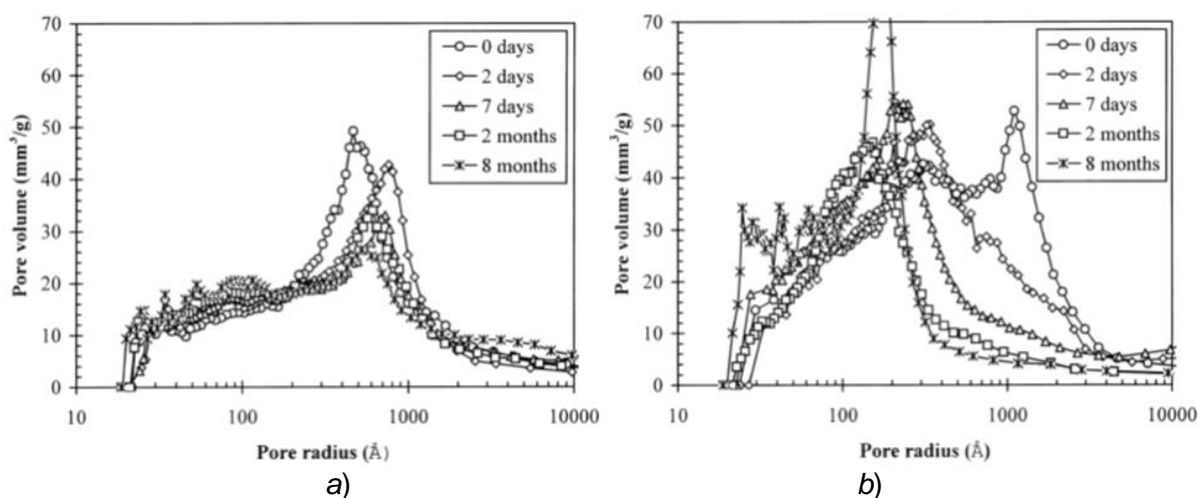


Figure 1.18 Pore size distribution of a) CSA and b) OPC mortars exposed in tap water over time [87].

The water absorption of CSA mortar can be influenced by w/c ratio, but not by anhydrite content; at 0.4 w/c ratio, water absorption of CSA mortar was lower than that of OPC mortar [111]. However, CSA mortar with w/c ratio of 0.5 showed higher water absorption in [86] when compared with OPC mortar, no matter dry or wet curing condition. Due to the higher theoretical w/c ratio for complete hydration, low w/c ratio CSA concrete can undergo self-desiccation and leave unhydrated ye'elimite even at late stage. In reference [104], two CSA concretes with different w/c ratios of 0.30 and 0.44 showed stable internal relative humidity around 60% and 90% respectively after 1.5 year and unhydrated clinkers existed in both concretes after 575 days.

A series of factor can influence the expansion of CSA concrete as summarised in [95]: ye'elimite content, pore structure, w/c ratio, sulphate content, free lime content, alkali hydroxide content, and cement particle fineness; among of them, ye'elimite content plays an important role. When the portion of ye'elimite is more than 50% in CSA cement, expansion, cracking and loss of strength appear at later age; the proper content of ye'elimite seems to range from 30% to 40% [116]. It has been reported that CSA prisms with w/c ratio of 0.563 showed no significant change of length over one year in water storage and a better performance than OPC [103].

The main hydration product of CSA concrete is ettringite that does not provide OH⁻. The pH of two pure CSA concretes with 0.5 w/c ratio were respectively 10.23 and 10.53 after 90 days curing [89]. In [87], w/c ratio of 0.45 CSA mortar showed extreme low pH around 6. However, a high pH around 13, within first 60 days hydration, has been observed in [115] by using a CSA cement paste with high w/c ratio 0.8. An exhaustive investigation on two CSA cement pastes with w/c ratios of 0.72 and 0.8 revealed that: in the case of w/c ratio of 0.72 CSA cement paste, within the first hours of hydration, the pH was as low as 10.3 ~ 10.7 due to the fact that the initial saturated pore solution was dominated by aluminate, calcium and sulphate; after 16 hours, calcium and sulphate

concentrations decreased noticeably due to the depletion of gypsum, thus pH went around 11.8; after 28 days, the pH value could reach 12.7 based on the fact that the ongoing release of alkali ions of CSA clinker and the increase of alkali concentrations caused by the continuous consumption of the pore fluid by the formation of hydrates; while 0.8 w/c ratio CSA cement paste showed the similar trend, but a slight higher pH at each stage [108].

Ettringite is susceptible to carbonation, leading to the concern on the carbonation resistance of CSA concrete [103]–[105]. According to laboratory result, it seems that the carbonation resistance of CSA concrete is weaker than that of OPC concrete [97], [103], [111]. **Figure 1.19** shows the higher carbonation depth of CSA concrete when compared to ordinary concrete under both accelerated and outdoor exposure [97]. However, the investigation on two CSA concrete samples collected from long-term service suggested that the carbonation resistance of normal CSA concrete is comparable with that of OPC concrete; particularly, high-strength CSA concrete is of excellent carbonation resistance [117]. Recently, it was found that the carbonation resistance of CSA mortar increased along with the increase of anhydrite content, as well as the decrease of w/c ratio; meanwhile it was also found that carbonation changed the strength performance of CSA mortar due to the modification of porosity caused by carbonation [111].

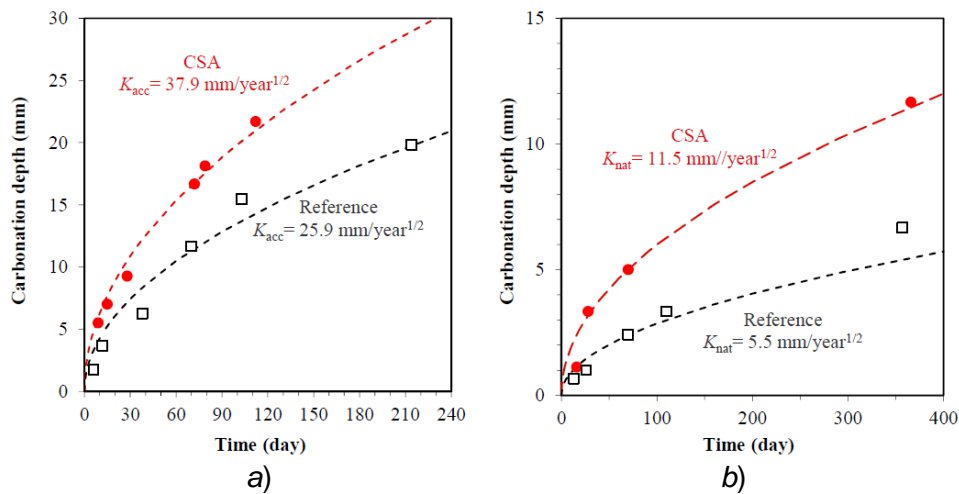


Figure 1.19 Time evolution of carbonation depth of CSA concrete and reference concrete (made with OPC) under a) accelerated test and b) indoor exposure [97].

The lower chloride penetration resistance of CSA concrete when compared to OPC concrete was observed in [103]. Conversely, low chloride diffusion coefficients of CSA concretes with different strength grades when compared with their OPC counterparts were obtained, as shown in **Figure 1.20** [113]. To enhance the chloride penetration resistance of CSA concrete, the mean of modifying AFm/AFt ratio through varying the gypsum content with the hope to let more AFm bind chlorides, was carried out in [109]; the results suggested that binding capacity of CSA concrete is inversely

proportional to the total calcium sulphate content, at the condition of high chloride concentrations. Besides, the good sulphate resistance of CSA concrete was reported in [89], [103], [104].

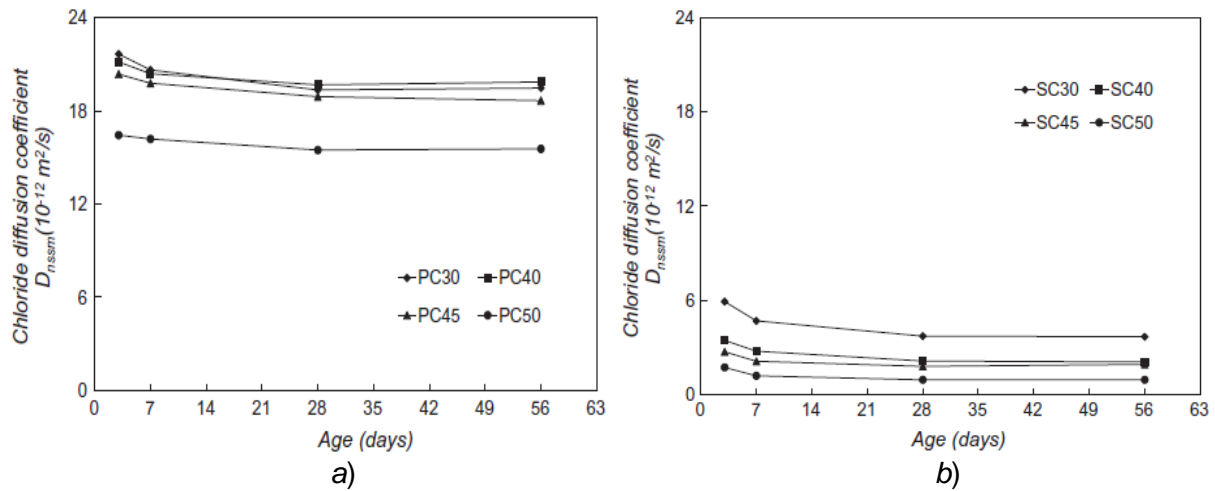


Figure 1.20 Evolution of chloride diffusion coefficients of a) CSA and b) OPC concretes at different strength grades over curing age [113]. SC:CSA; PC:OPC.

In case of blended CSA cement, it was shown that increasing the portion of OPC in blended CSA cement (15%, 55%, 70% and 85%) is possible to delay the setting time, increase strength and dynamic elastic modulus, decrease water absorption, reduce expansion in moist air and shrinkage in dry air, decrease porosity, improve the pH [86].

Currently, there is very few publications dealing with the passivation and corrosion behaviour of steel embedded in CSA concrete. It's been reported that mild steel embedded in 14 years old structure was not yet corroded, however the pH and w/c ratio of concrete were unknown unfortunately [104]. In reference [87], steel in CSA mortar showed a higher corrosion rate than steel in OPC mortar exposed either in continuous or intermittent contact to 3.5% NaCl solution; the corrosion rate was monitored by direct measurement of weight loss of the steel; half-cell potential measurement of the steel showed that steel embedded in CSA mortar was depassivated, showing high corrosion rate either in continuous or intermittent exposure to 3.5% NaCl solution, due to the low pH (around 6) of pore solution of CSA mortar. However, corrosion potential and corrosion rate of steel embedded in 0.55 w/c ratio CSA concrete with a pH value of 11.5 showed the passivation of embedded steel, even in concrete exposed to an environment with 95% R.H. and 40°C or immersed in water [97]. In reference [89], it's found that mortar made with 100% CSA cement was not capable of passivating steel; however, CSA cement blended with 15% OPC was enough to guarantee the passivation of steel as the shown in **Figure 1.21**; it's noted that the pH of CSA mortar extract was 11.32 while pH of extract of mortar made with blended CSA cement (15% OPC) was 11.88.

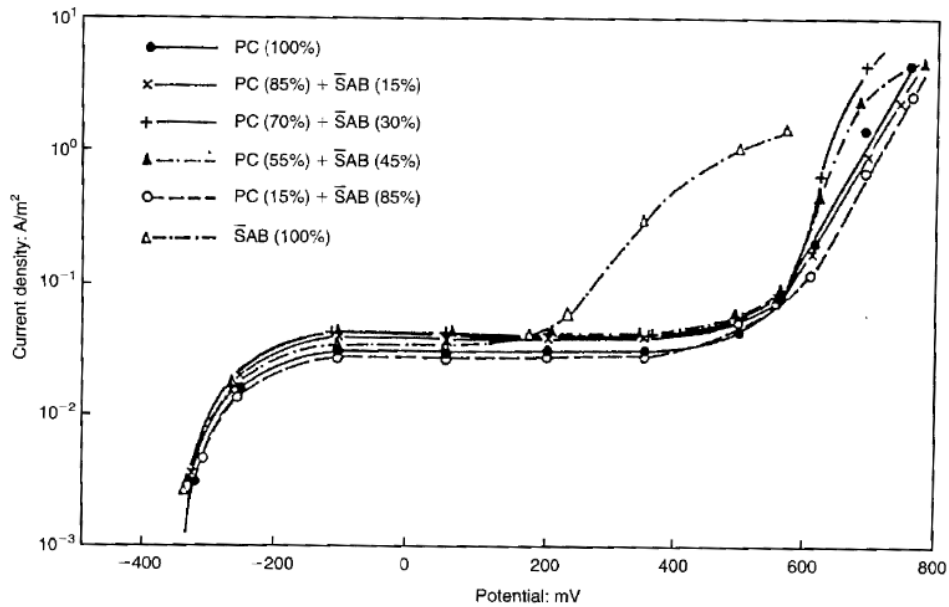


Figure 1.21 Potentiodynamic curves of steel bars in mortar extracts [86]. $\bar{S}AB$:CSA; PC:OPC.

1.7.3 Cement-stabilised rammed earth

Rammed earth is an ancient construction material and technique, being widely used in the past across the dry areas in the world [118]–[120]. A well-known example is the great wall of China which was built more than 2000 years ago by using local materials: rammed earth, stones, baked bricks and wood [121]. Traditional rammed earth can be simply erected by hand through compacting subsoil consisting of sand, silt and/or clay, but lack of organic matter and humus, layer by layer with the support of formwork. Modern rammed earth can be manufactured by mixing sand, gravel and clay/silt together [119], [122], [123], and is compacted by machine for the sake of efficiency and quality control. The components of modern rammed earth are analogous with those of concrete, sand and gravel representing fine and coarse aggregates, and clay/silt used as binder [119]. In some particular regions such as western Australia, the use of crushed limestone in place of natural soil to produce rammed earth is more popular owing to the benefits of improved quality control, aesthetic appeal, and ready availability [124], [125].

The noticeable advantages of rammed earth construction compared to other modern construction forms include: cheap and accessible raw materials, both less energy consumption and waste emissions, good insulation properties [126]. Thereby, in recent decades, it has been increasingly recognized as a sustainable building material, and has received more and more attention in some regions [120], [127]. Nevertheless, unstabilised rammed earth (by using only clay as a stabiliser) showed weak shear strength [122], low compressive strength [123], [128] and poor erosion resistance [129]. Particularly, due to the difficulty of quality control in construction site compared with in laboratory, the in-situ rammed earth could have even more lower strength. The strength and

durability of rammed earth can be improved by using rammed earth stabilisers such as cement [118], [124], [130]–[132], lime [133]–[135], and the combination of them [129], [133]. However, the success of stabilisation also depends on the selection of an appropriate soil [133]. In fact, the most frequently used stabiliser is cement which can not only help enhance compressive strength, durability, but also allow some unsuitable soils to be used [126]. In fact, the use of cement as a stabiliser might provide corrosion protection to steel embedded in cement-stabilised rammed earth (CSRE) as well. Currently, there is no literature works involving in the corrosion of steel embedded in CSRE. The available literature papers related to CSRE mainly focus on the properties of CSRE as summarised in **Table 1.5**.

Table 1.5 A summary of reviewed papers considering the properties of cement-stabilised rammed earth.

Ref.	Materials	Cement content (by soil mass)	Test type
[118]	Clay sandy soil; OPC	0 ~ 20%	Compressive and tensile strength and elasticity; Shrinkage; Water permeability; Conductivity; Water absorption; Accelerated erosion test
[124]	Crushed limestone; laterite	10%	Density; Compressive strength
[125]	Crushed limestone	5%	Optimum water content; Dry density; Compressive strength; Microstructure
[126]	Kaolin clay with sand; natural subsoil	2.5 ~ 10%	Pull-out test
[128]	Crushed limestone	10%	Unconfined compressive strength; Accelerated erosion test; Wire brush test
[129]	Clay; Silt; Sand; Gravel	4.5/5%	Unconfined compressive strength; Accelerated erosion test; Drying shrinkage
[131]	Laterite	6, 8, 10%	Dry/ wet compressive strength; Load-deformation test
[132]	Laterite	6, 8, 10%	Dry/ wet compressive strength; Load-deformation test; Water absorption; Accelerated erosion test; Shrinkage
[136]	Subsoil	0 ~ 10%	Dry density; Dry/ wet compressive strength; Stress-strain test; Porosity; Chloride penetration
[137], [138]	Clayey soil; river sand	5, 8, 12%	Dry density; Dry/ wet compressive strength; Water absorption; Stress-strain test;
[139]	Clay; river sand	7, 10%	Dry density; Compressive strength
[140]	Crushed limestone	10%	Unconfined compressive strength; Density; Load- deformation test

1.7.3.1 Properties of cement-stabilised rammed earth

Compressive strength is the utmost important property of rammed earth because of its fundamental role in terms of bearing load. It's well-known in soil mechanics, earth gains its maximum compressive strength at its optimum water content (OWC) that is defined as the water content when earth reaches its maximum dry density (MDD) for a given compactive effort. This has been observed on rammed earth studied in [118]. In CSRE, OWC and MDD can change with cement content as shown in **Figure 1.22** [136], as observed also in [137].

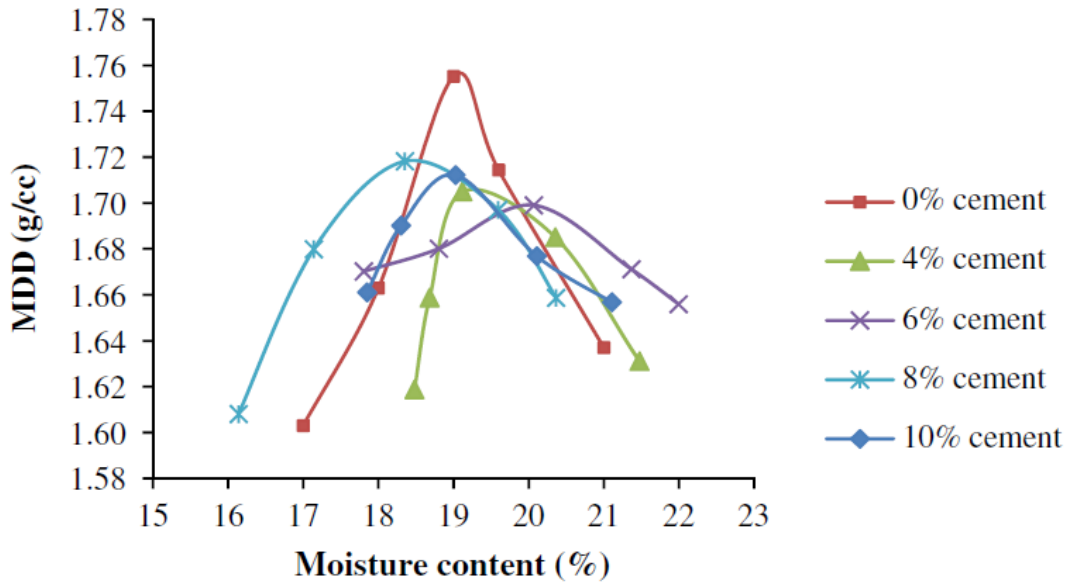


Figure 1.22 Relationship between maximum dry density and moisture content for CSRE with different cement contents [136].

As far as CSRE is concerned, the major factors that affect its compressive strength include either soil type or property, dry density, compaction water content, cement content, moisture content, compaction energy and curing condition.

Due to the diversity of natural soil component, soil type can influence the compressive strength of CSRE [132]. It's also been observed that CSRE yielded maximum compressive strength under a certain clay fraction of soil which might be attributed to the best packing density [138]. Some parameters related with soil property such as linear shrinkage, plasticity index, liquid index and particle size distribution are commonly employed to evaluate soil suitability for rammed earth [129], [133]. Particularly, it can be observed that the parameter, soil particle size distribution was used frequently in research publications [118], [119], [124], [125], [127], [137], [139]; however it should be noted that this parameter could not be used alone as a criteria [129].

In most of publications, it's reported that dry density necessarily played a crucial role to compressive strength of CSRE; the higher dry density, the higher compressive strength [136]–[138], [140]. Density increase accompanied with the increase of strength can be attributed to reduction in porosity leading to better particle contact and hence more effective cementation due to cement hydration products [138]. The compressive strength of CSRE made with soil containing 15.8% clay increased with the increase of compaction water content when water content changed near optimum water content, regardless of cement content [137]. However, a recent study on CSRE made with limestone and without clay (5% OPC by weight of limestone) revealed that lower compaction water contents caused higher compressive strength when water content changed near

optimum water content, and that compressive strength is reversely proportional with dry density [125].

Cement content has a strong influence on the compressive strength of CSRE. In general, the cement content used in CSRE is not more than 20% (by soil mass). For CSRE with compressive strength higher than 5 MPa, cement hydration might mainly contribute to the strength gain due to the bonds created by the hydrated cement particles [124]. Increasing cement content in CSRE improved compressive strength, accompanying by the growing of density [136]. Increasing of cement dosages led to more cementitious material suitable to establish water insoluble bonds with the silt and sand particles and hence resulted in higher strength for CSRE [138]. The almost linear relationship between compressive strength and cement content (up to 20%) has been observed in [118], also by other researchers [131], [138].

The increase of compaction energy (at constant OWC) enhanced compressive strength and density of CSRE [136].

The compressive strength of CSRE decreased alongside the increase of moisture content, according to a linear relationship as shown in [138], [139].

As all cementitious materials, It's also found that curing can significantly improve the compressive strength of CSRE [136], [138].

Apart from compressive strength, some other mechanical properties of CSRE are important such as tensile strength, elastic modulus, pull-out bond resistance of steel and conductivity. In fact, tensile strength and elastic modulus of CSRE are influenced by the same factors which compressive strength depends on. A almost linear relationship between tensile strength and cement content (up to 20%), has been observed in [118]. The elastic modulus of CSRE is very sensitive to dry density and cement content; higher cement content and dry density were beneficial for elastic modulus [138]. The pull-out bond resistance of steel in CSRE has been shown to be related to compressive strength, embedment length, steel type, and specimen preparation method through the investigation based on five different soil stabilised by varying cement content (2.5 ~ 10% by dry mass) [126]. Conductivity slightly decreased with the increase of cement content [118].

1.7.3.2 Durability of cement-stabilised rammed earth

Durability of rammed earth highly depends on compaction quality [128]. The strength of CSRE reflects its compaction quality, thereby compressive strength can be a good indicator of durability of CSRE. A compressive strength comparison between 32-year-old CSRE unprotected from incident rainfall and 28-day-old CSRE, which was manufactured by using the same material and nominal compaction regime, suggested that ageing caused a considerable loss of compressive strength [127]. However, compressive strength of CSRE alone is not enough as an indicator of

durability of CSRE. The durability of CSRE should be also related to its water absorption, shrinkage and erosion resistance.

Due to the fact that soil is very sensitive to water, a significant difference in terms of compressive strength of rammed earth in dry and wet conditions can be found, as shown in **Figure 1.23**. That is mainly attributed to the presence of clay that absorbs water and becomes soft. Usually, the ratio between wet strength and dry strength is used to evaluate whether it is adequate to build rammed earth wall. For instance, the ratio 0.46 ~ 0.64, depending on the severity of the rainfall, was recommended in [131] for clayey and hard laterite soil. The ratio depends upon the clay fraction of soil mix and cement content [138]. It seems the ratio of uncured CSRE (0.54 ~ 0.71) was higher than that of cured CSRE (0.30 ~ 0.49), which may be due to the hydration of unhydrated cement in uncured CSRE when it is wetted [136]. Maintaining the wet strength of CSRE at a satisfactory level would require proper soil selection, desirable compaction level and adequate stabilizer content [132].

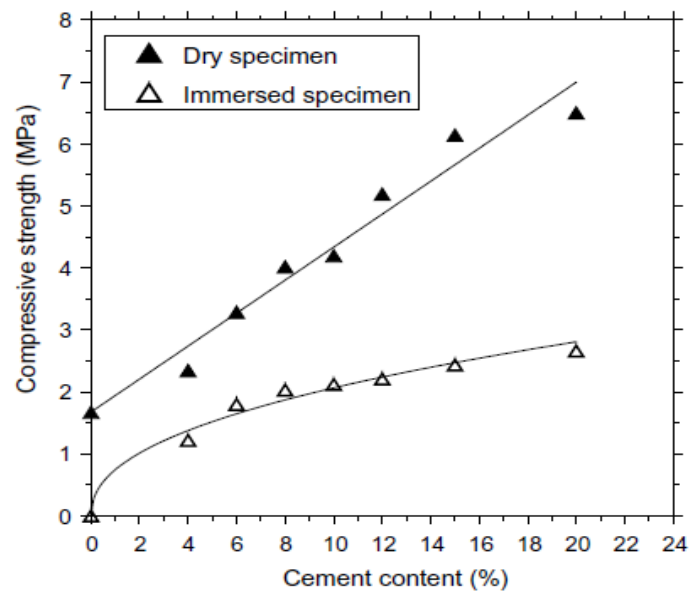


Figure 1.23 Relationship between compressive strength and cement content for CSRE under dry and immersion conditions [118].

The water absorption of CSRE decreased from 21.2% to 5.3% when the content of cement content increased from 2% to 10%, by spraying water to simulating high rainfall for one hour [132], as confirmed in reference [138]. It's also noticed that the water absorption by immersion of CSRE increased when the fraction of clay increased, which might be due to clay mineral and the porosity of CSRE [138]. The results on water absorption by capillary also showed the trend that water absorption decreased with increasing cement content in reference [118]. It's been revealed that the saturated water content (water absorption) of CSRE decreased from 21% to 9% with the increase

of its dry density from 1600 to 2000 kg/m³; that is because that lower density would have higher porosity and hence could accommodate more water under saturated condition [137].

The shrinkage of CSER increased rapidly during the first days after compaction, and then reached a stable value [118], [132]. Increasing cement content is beneficial for reducing shrinkage; **Figure 1.24** shows the effect of cement content on the development of shrinkage [118]. Drying shrinkage of CSRE is primarily governed by the plasticity index of the constituent soil, and to a lesser extent by cement content [141]. More clay usually means more shrinkage [121].

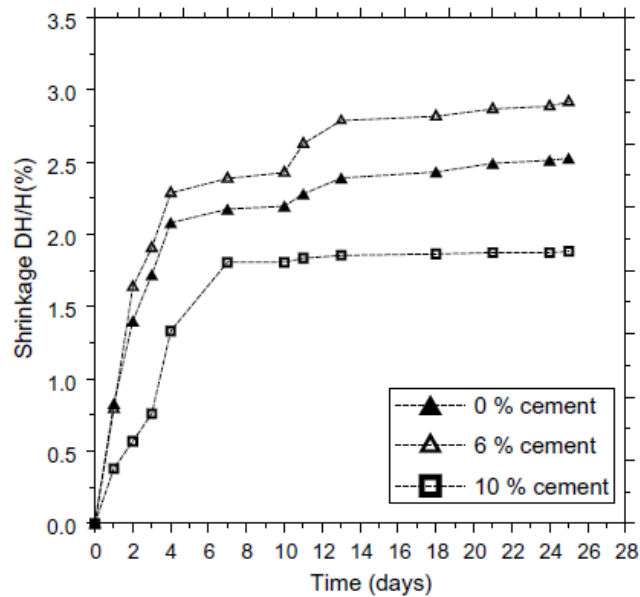


Figure 1.24 Effect of cement content on shrinkage evolution in time of CSRE [118].

Erosion of rammed earth materials is caused by the breakdown of inter-aggregate bonds (cemented or uncemented), generally provoked by moisture ingress or rain/wind pressure [127]. In order to evaluate this kind of degradation action, accelerated erosion test is often used by spraying a high pressure water [129]. The tests in reference [118] showed that for CSRE no visible damage was observed while unstabilised rammed earth was in complete disintegration. Erosion rate of CSRE decreased with increasing cement content [132].

Generally, cement-stabilised rammed earth construction is unreinforced; nevertheless, steel bar might be embedded in some special parts in order to provide seismic resistance, support over openings in wall and fix up roof structure [126]. However, the pH of natural soil is 7.73 while sand 9.05, and therefore the pH of reconstituted soils is in the range of 7.73 ~ 9.05 [137]. Anyway, the pH of rammed earth could be increased if rammed earth stabilised with cement, due to cement hydration. However, currently, no any related publication can be found. Neither any publication dealing with corrosion of steel in CSRE has been found.

Chapter 2

Experimental procedure

The use of new sustainable cementitious materials for structural concrete raises questions about the durability of reinforced concrete structures. For this reason, characterising their durability-related properties is necessary.

In this research, different types of cementitious materials were cast with water/cement (w/c) ratio from 0.47 to 0.55 by using CEM II/A-L 42.5R (Portland limestone cement), CEM I 52.5R (Portland cement) or CSA-based cements (blends of calcium sulfoaluminate (CSA) cement with ordinary cement) and by replacing ordinary cement with glass powder and adding calcium oxide (CaO) powder into CSA-based cements. Waste glass was used also in the form of expanded glass aggregate. In order to study the durability of reinforced concrete structures made with these different cementitious materials, several types of steel bars (carbon steel and galvanised steel) were also used.

This chapter describes the specimens and the laboratory tests performed for the characterisation of studied cementitious materials and for assessing their roles in relation to the corrosion protection of steel bars in different environmental conditions. Tests for studying the passivation of steel as well as the resistance to the penetration of aggressive agents such as chloride and the corrosion behaviour are described.

2.1 Materials

2.1.1 Binder type

Different types of binders were used for studied cementitious materials: CEM II/A-L 42.5R, CEM I 52.5R, CSA-based cements, glass powder and CaO powder. **Table 2.1** shows their chemical compositions. In **Table 2.2**, it has been reported the main constituents of CSA-based cements. Pure CSA cement (SR03) was constituted by 78% CSA clinker and 22% anhydrite. The main mineralogical phases of CSA clinker are ye'elimite ($C_4A_3\bar{S}$) and belite (C_2S). Two blended cements (SL05 NF and SL05) based on the combination of 30% CSA clinker, 10% anhydrite and 60% of, respectively, CEM I 52.5R cement and CEM II/A-L 42.5R cement were considered. The addition of calcium oxide (CaO) to blended CSA cement produced by Buzzi Unicem (Italy) was also considered in order to verify its role on durability properties of CSA-based concrete. Glass powder was used as mineral addition in partial replacement of ordinary cement for standard mortar with

and without expanded glass aggregates. Glass powder was obtained by crushing waste green bottles and then grinding into specific surface area of around 600 m²/kg; this specific surface area was chosen based on a previous study in [63] aimed at comparing the effects of ground glass and traditional types of pozzolanic materials on the strength and durability properties of mortars.

Table 2.1 Chemical compositions of binders.

Chemical composition	CEM II/A-L 42.5R	CEM I 52.5R	SL05 NF	SL05	SR03	Glass powder	CaO powder
CaO	62.52	64.58	53.99	53.85	43.9	11.35	100
SiO ₂	17.84	18.66	14.09	13.55	7.6	68.67	-
SO ₃	2.54	3.82	11.16	10.67	17.5	0.13	-
Al ₂ O ₃	4.16	5.19	12.70	11.25	21.7	2.73	-
MgO	1.98	1.95	1.76	1.64	2.59	1.41	-
Fe ₂ O ₃	3.09	2.05	2.51	2.96	2.07	0.66	-
TiO ₂	0.16	0.23	0.54	0.48	0.92	-	-
Na ₂ O	0.23	0.28	0.27	0.23	0.32	13.25	-
K ₂ O	0.85	1.01	0.60	0.54	0.23	1.11	-
Cl ⁻	0.058	0.02	0	0	-	-	-
M.E.*	0.02	0.02	0.09	0.05	0.18	-	-
L.o.I.**	6.57	2.19	2.29	4.78	2.97	-	-

* Minor elements.

** Loss on ignition.

Table 2.2 Constituents and ye'elimite content of CSA-based cements.

Constituents	SL05 NF	SL05	SR03
CEM II/A-L 42.5R	---	60	---
CEM I 52.5R	60	---	---
CSA clinker	30	30	78*
Anhydrite	10	10	22
Ye'elimite (C ₄ A ₃ S̄)	15.5	15.5	40.6

*Containing 3% anhydrite phase.

2.1.2 Aggregates

Limestone aggregates, consisting of 5 different fractions (filler sand, Calc 1, Calc 2, Calc 3 and Calc 4) from Zandobbio (Bergamo, Italy), were used for casting concrete. Limestone aggregates have a maximum size of 12 mm and the combination of the different fractions in order to fit Fuller's grading curve was 35% filler sand, 15% Calc 1, 15% Calc 2, 15% Calc 3, and 20% Calc 4. **Figure 2.1** shows the grading curves of limestone aggregate fractions. Standard sand was used for waste glass mortar. A commercial expanded glass with particles size in the range of 2 ~ 4 mm was used as lightweight aggregates.

For making rammed earth, a simulated soil was made by mixing Calc 2 limestone aggregates with 8 types of sand in different particle size as shown in **Figure 2.2**, produced by Sabbie Sataf (Pavia, Italy). The mix proportion of simulated soil will be reported in **Table 2.7**.

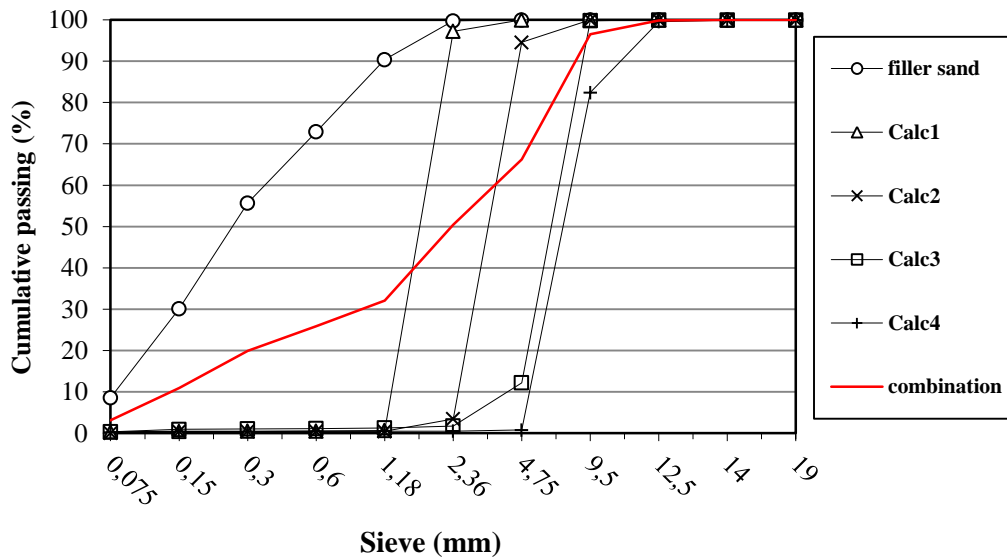


Figure 2.1 Grading curves of limestone aggregate fractions.

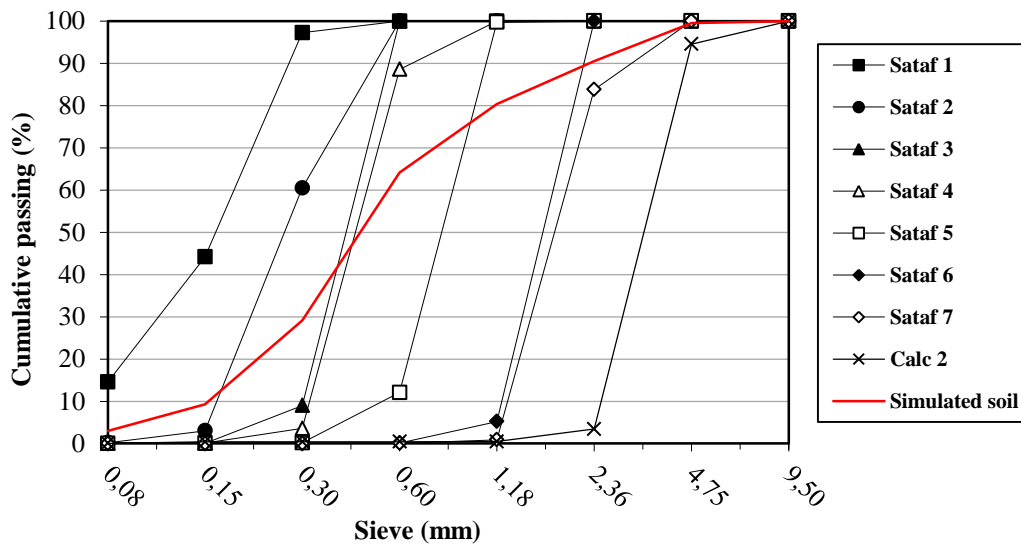


Figure 2.2 Grading curves of Sataf sand and simulated soil.

2.1.3 Reinforcements

Different steel bars were used for electrochemical tests carried out in order to evaluate their corrosion behaviour in the cementitious materials studied in this research. **Table 2.3** shows the chemical composition, mechanical property and different surface conditions of type B450C carbon steels with 18 mm and 10 mm diameter provided by SISMIC. The carbon steels were taken from both bundles of recent production and exposed outside for respectively 6 months and one year in order to obtain different pre-rusting conditions with respect the condition defined as “as-received”. Sandblasted bars were also considered for comparison purpose. Moreover, the absence of chlorides in the rust was confirmed by dissolution in nitric acid and titration.

Table 2.3 Chemical composition, mechanical properties and surface conditions of 18 mm and 10 mm diameter carbon steels.

		∅ 18 mm	∅ 10 mm
Chemical composition (wt%)	C	0.20	0.19
	Mn	0.79	0.81
	Cr	0.15	0.16
	Si	0.21	0.19
	P	0.022	0.021
	S	0.033	0.041
Mechanical properties	Yield strength f_y (MPa)	663	637
	Tensile strength f_t (MPa)	540	556
	Elongation A under maximum load (%)	11.8	8.3
Surface conditions	As-received	A1	A1
	Sandblasted	A2	A2
	Lowly rusted (6 months outdoor exposure)	B	B
	Highly rusted (1 year outdoor exposure)	C1*	C
		C2	

*Intermediately rusted.

Carbon steel bars with 16 mm diameter used for waste glass mortar and both CSA-based and reference concrete, were sandblasted prior to being placed in such cementitious materials. In addition, galvanised steel bars with 16 mm diameter were used for CSA-based concretes. Only in ordinary concrete considered as a reference in comparison with CSA-based concretes, galvanised steel bars with 10 mm diameter were used. Carbon steel bars with 10 mm diameter were sandblasted and used in cement-stabilised rammed earth.

2.2 Mix proportion

Firstly, an ordinary concrete with slump class S4 (160 ~ 210 mm) was cast with w/c ratio of 0.5 to study the passivation of carbon steel bars with different surface conditions. **Table 2.4** shows the mix design of such concrete. Two concrete mixtures, labelled as “518” and “531”, were cast to prepare reinforced specimens respectively with 18 and 10 mm bars. Such concretes were mixed with 400 kg/m³ Portland limestone cement (CEM II/A-L 42.5R), 200 kg/m³ deionised water, 1768 kg/m³ of limestone crushed aggregates and a superplasticizer admixture (Dynamon SX) in dosages equals to 3.2 and 2.96 kg/m³, respectively for “518” and “531” mixtures.

Table 2.4 Mix proportion of concrete for studying the passivation of carbon steel bars with different surface conditions (dosage in kg/m³).

Mix code	Water/cement ratio	Cement type	Cement	Aggregates	Superplasticizer
518	0.5	CEM II/A-L 42.5R	400	1768	3.2
531					2.96

The passivation of carbon steel was also studied in case of using mortar made with waste glass. **Table 2.5** shows the mix design of waste glass mortar cast with water/binder ratio of 0.5 which is typically used for preparing standard mortar. The proportion (by mass) is one part of binder

Chapter 2

Experimental procedure

(cement or cement with glass powder), 3 parts of aggregates and one half part of deionised water. In case of using expanded glass as aggregates, the volume of expanded glass was maintained the same as that of standard sand. In a subsequent part of this research, several types of concrete were cast by using CSA-based cements; for comparison, a reference concrete was also cast. The mix proportion of CSA-based concretes were defined based on the results of a previous study made by the same research group [97] within which the current experimental work was carried out. Each type of concrete was cast with two different w/c ratios (0.47 and 0.55) according also to the suggestions from project sponsor, except pure CSA concrete made with SR03 cement and cast at w/c ratio of 0.55. For the w/c ratio of 0.55, a concrete with addition of 0.4% chloride (by mass of cement) was also cast for each type of binder except for pure CSA cement SR03. An acrylic-based superplasticizer admixture (Dynamon SX, Mapei) was used for ordinary concrete and mortar whilst a special admixture (Compactcrete 39 NX, Addiment Italia) was used for CSA-based concretes. **Table 2.6** shows the mix proportion of CSA-based concretes. Calcium oxide (CaO) was added into SL05 NF cement and SL05 cement in partial replacement of cement (2.5% by mass). SL05 NF cement without the addition of CaO was also used. In order to avoid the fast hardening of CSA concrete, the mixing water (deionised water) was cooled in refrigerator ahead of casting.

Table 2.5 Mix proportion of waste glass mortar (dosage in kg/m³).

Mix code	Cement type	Water/binder ratio	Cement	Ground glass	Standard sand	Expanded glass
M134	CEM I 52.5R	0.5	517	0	1552	0
M135			362	155	1552	0
M136			362	155	0	184
M137			517	0	0	184

Table 2.6 Mix proportion of CSA-based concretes (dosage in kg/m³).

Mix code	Water/cement ratio	Binder type	Cement	Aggregates	Superplasticizer		CaCl ₂
					LAB 2766	Dynamon SX	
519	0.47	CEM II/A-L 42.5R	327	1995	0	7.98	0
520	0.55			1925		3.27	2.05
521				1925		3.27	2.05
522	0.47	SL05 NF	327	1995	-	0	0
523	0.55			1925	4.9		2.05
524				1925	3.86		2.05
525	0.47	SL05 NF+CaO*	319	1995	6.54	0	0
526	0.55			1925	4.91		2.05
527				1925	3.86		2.05
528	0.47	SL05+CaO*	319	1995	6.54	0	0
529	0.55			1925	3.60		2.05
530				1925	3.27		2.05
532	0.55	SR03	327	1925	3.27	0	0

* The quantity of added CaO powder is 8 kg/ m³.

Finally, for making cement-stabilised rammed earth, raw materials were firstly mixed together according to the mix design given in **Table 2.7** and following the mix procedures used for preparing

standard mortar; then, the mixture was transferred into metallic formwork and compacted in two layers of 50 mm by compaction system, as seen in **Figure 2.3**. The mix proportion of cement-stabilised rammed earth was recommended based on the study made in collaboration with the University of West Australia.

Table 2.7 Mix proportion of cement-stabilised rammed earth (dosage in kg/m³).

Composition		Percentage (%)		Mass	
Simulated soil	Sand	Sataf 1	20	100	348
		Sataf 2	12		209
		Sataf 3	23		400
		Sataf 4	8		139
		Sataf 5	17		296
		Sataf 6	6		104
		Sataf 7	5		87
	Coarse aggregates	Calc 2	9		157
Stabiliser	Cement	CEM II/A-L 42.5R	5*	87	
Compaction water	Water	Deionised water	8.5*	149	

* By mass of simulated soil.



Figure 2.3 Preparation of cement-stabilised rammed earth specimens.

2.3 Summary of test specimens and test types

Tests were carried out on different types of specimen. **Table 2.8 ~ 2.11** summarise all specimens used in this research, their geometry dimensions and test types to which they are dedicated. Mechanical properties, such as compressive strength and dynamic elastic modulus, besides to carbonation and chloride resistance were measured on 100 mm cube specimens. Hardened properties of mortar were evaluated on 40x40x160 mm³ prismatic specimens. Electrical resistivity of studied mixtures was measured on both 100 mm cube and 40x40x160 mm³ prism. Reinforced cylindrical specimens (with diameter of 59 or 67 mm and height of 110 mm) were prepared to study the corrosion behaviour of steel bars embedded in studied mixtures. Conversely, reinforced cubic specimens have been used only for cement-stabilised rammed earth.

Table 2.8 reports the labels and geometry dimensions of all specimens and relative tests carried out with them for studying the passivation and corrosion protection of carbon steel bars with different surface conditions embedded in ordinary concrete. **Table 2.9 ~ 2.11** summarise respectively the labels and geometry dimensions of specimens and their corresponding tests for the characterisation of durability properties of recycled waste glass mortars, CSA-based concretes and cement-stabilised rammed earth. The curing condition and environmental exposure are also indicated for all specimens.

Table 2.8 Specimens and tests carried out for studying corrosion behaviour of carbon steel bars with different surface conditions.

Specimen	Dimension	Test type	Exposure condition
518-1,518-2	100 mm cube	28-day density, compressive strength and resistivity	Moist curing
531-1,531-2		28-day density, compressive strength and resistivity	Moist curing
518-A1-2	Ø 67x110 mm cylinder (reinforced with 18 mm diameter steel)	Electrochemical test (for more details refer to section 2.4.3)	Exposure condition A*
518-A1-3, 518-A1-4			Exposure condition B**
518-A2-2			Exposure condition A*
518-A2-3, 518-A2-4			Exposure condition B**
518-B-2			Exposure condition A*
518-B-3, 518-B-4			Exposure condition B**
518-C1-2			Exposure condition A*
518-C1-3, 518-C1-4			Exposure condition B**
518-C2-2			Exposure condition A*
518-C2-3, 518-C2-4			Exposure condition B**
531-A1-1	Ø 59x110 mm cylinder (reinforced with 10 mm diameter steel)		Exposure condition A*
531-A1-2, 531-A1-3			Exposure condition B**
531-A2-1			Exposure condition A*
531-A2-2, 531-A2-3			Exposure condition B**
531-B-1			Exposure condition A*
531-B-2, 531-B-3			Exposure condition B**
531-C-1			Exposure condition A*
531-C-2, 531-C-3			Exposure condition B**

* Exposure condition A: Self-desiccation (23°C), 20°C + R.H. 80%, 20°C + immersion, 20°C + accelerated carbonation (4% CO₂, R.H. 65 ± 5% and 20 ~ 23°C).

**Exposure condition B: Self-desiccation (23°C), 20°C + R.H. 80%, 20°C + immersion, 20°C + immersion cycles in 3.5% NaCl.

Table 2.9 Samples and tests for studying waste glass mortar.

Specimen	Dimension	Test type	Exposure condition
M134~137-1	40x40x160 mm ³ prism*	7-day density, compressive strength	Moist curing
M134~137-2		28-day density, compressive strength	Moist curing
M134~137-3		3-month density, compressive strength	Moist curing
M134~137-4		6-month density, compressive strength	Moist curing
M134~137-7		Electrical resistivity test and density	Water curing
M134~137-8	25x25x285 mm ³ prism	Alkali attack test	1 M NaOH solution (20°C)
M134~137-1		ASR expansion test	1 M NaOH solution (80°C)
M134~137-2			
M134-1, M134-2	Ø 67x110 mm cylinder	Electrochemical test (for more details refer to section 2.4.3)	Self-desiccation (23°C)
M135-1, M135-2			

* Demoulded 1 day after casting.

Chapter 2
Experimental procedure

Table 2.10 Samples and tests for studying CSA-based concretes.

Specimen	Dimension	Test type	Exposure condition
519~530-1,2	100 mm cube**	density, compressive strength, ultrasonic test and SEM observations	1-day moist curing
519~530-3,4			7-day moist curing
519~530-5,6			28-day moist curing
519~530-7,8		density, compressive strength, ultrasonic test	90-day moist curing
Mix X-9,10*		Chloride penetration	7 days moist curing + immersion in 3.5% NaCl solution
Mix X-11,12,13*		Natural carbonation	7 days moist curing + outdoor sheltered exposure
Mix X-14,15,16*			28 days moist curing + outdoor sheltered exposure
Mix X-17,18*		Accelerated carbonation	28 days moist curing + 4% CO ₂ exposure
Mix X-19,20*		Water absorption	28 days moist curing
Mix X-1,2*		Ø 50x100 mm cylinder	Conductance test
Mix X-1,2,3*	40x40x160 mm ³ prism**	Resistivity test	Water curing
Mix X-1,2*	Ø 100 mm cylinder**	Capillary absorption	28 days moist curing
519,522,525,528-1,2 (alkaline, w/c=0.47)	Ø 67x110 mm cylinder (with carbon steel bar)	Electrochemical test (for more details refer to section 2.4.3)	See Table 2.12
520,523,526,529-3,4 (alkaline, w/c=0.55)			
521,524,527,530-7 (alkaline, 0.4% Cl, w/c=0.55)			
520,523,526,529-5,6 (carbonated, w/c=0.55)			
521,524,527,530-8 (carbonated, 0.4% Cl, w/c=0.55)			
532-1,2,3 (alkaline, w/c=0.55)			
519,522,525,528-Z1 (alkaline, w/c=0.47)			
520,523,526,529-Z2 (alkaline, w/c=0.55)			
521,524,527,530-Z4 (alkaline, 0.4% Cl, w/c=0.55)			
520,523,526,529-Z3 (carbonated, w/c=0.55)			
521,524,527,530-Z5 (carbonated, 0.4% Cl, w/c=0.55)			
532-Z1,Z2,Z3 (alkaline, w/c=0.55)			

* Mix X includes the mixtures 519, 520, 522, 523, 525, 526, 528 and 529.

** Demoulded 1 day after casting.

Table 2.11 Samples and tests for studying cement-stabilised rammed earth.

Specimen	Dimension	Test type	Exposure condition
RE-33	100 mm cube	Electrical resistivity; 28-day compressive strength; density	Moist curing
RE-34			
RE-81		Electrical resistivity; 28-day compressive strength; density	
RE-82			
RE-1,2,3,4	100 mm cube (reinforced by carbon steel)*	Electrochemical test (for more details refer to section 2.4.3)	Self-desiccation (23°C) + immersion (20°C)
RE-73, RE-74	100 mm cube*	Carbonation test	Laboratory condition

* Demoulded 6 days after casting.

2.4 Experimental methods

In the previous section, information such as number, geometry dimensions and exposure conditions of all tested specimens has been reported. This section describes the experimental methods used for testing all the specimens.

2.4.1 Materials characterisation methods

2.4.1.1 Visual and macroscopic observations

The surface conditions of pre-oxidised steel bars were firstly documented by visual observation and subsequently observed through a Wild M8 stereo-microscope and scanning electron microscope (SEM).

2.4.1.2 Microstructure observations

In order to investigate the microstructure of pre-oxidised steel bars, around 1 cm long portions were cut off and mounted into thermosetting acrylic resin. The exposed section of steel bar was polished and subjected to Nital attack. Metallographic sections were observed at optical microscope (OM) and SEM. **Figure 2.4** shows metallographic section prepared with four 10 mm carbon steel bars with different surface conditions.



Figure 2.4 A sample for metallographic analysis of pre-oxidised and sandblasted steel bars.

SEM used in this research is Zeiss EVO 50 EP (LaB₆ cathode electron gun) that equipped with an Oxford Inca Energy 200 Energy Dispersive Spectroscopy (EDS) with an ultra-thin window detector of 133eV resolution (at Mn).

For studying the effect of hydration process on microstructure of CSA-based concretes, a sample was collected for each type of mixture at different curing age and immediately the hydration process of sample was stopped by using acetone (C₃H₆O). All samples were conserved in laboratory till the testing date of SEM observations.

2.4.1.3 X-ray diffraction (XRD)

The crystalline compounds of corrosion products that were collected from steels with 18 mm diameter labelled as "C2" (exposed outdoor environment for 1 year), were identified by XRD diffractometer using Cu K_{α1} radiation (1.5406 Å wavelength) at a scan speed of 2°/min³.

2.4.2 Tests on mortar and concrete

2.4.2.1 Workability

The consistence of waste glass mortar was determined according to UNI EN 1015-3:2007, whilst the workability of concrete was tested according to UNI EN 12350-2:2009.

2.4.2.2 Dynamic elastic modulus

The dynamic elastic modulus of hardened concrete was determined by measuring the ultrasonic pulse velocity (UPV) according to RILEM recommendation NDT1. The measurements were carried out on 100 mm cubes before compressive test. Dynamic elastic modulus E_d (GPa) was determined according to the following formula:

$$E_d = f(\mu) \times \rho \times (v)^2 \quad (2.1)$$

where, E_d is dynamic elastic modulus, $f(\mu)$ is the function of dynamic Poisson's ratio and equal to 0.8, ρ is concrete density and v is UPV of concrete.

The ultrasonic test was conducted on two opposite faces of 100 mm cube sample by a UPV tester (UPV-E49, Controls Italy) as shown in **Figure 2.5**. Sample mass was recorded before starting this test in order to obtain the concrete density. The value of UPV can be read directly on the screen of instrument after setting the dimension parameters of sample. The measurement was performed on two opposite cube faces (excluding casting surface). Therefore, two measurements can be done on each sample. Finally, an average UPV of two cubic specimens was considered to calculate E_d .

³ The above microstructural analysis tests were done with collaboration of SAMM Laboratory (Politecnico di Milano).



Figure 2.5 Ultrasonic test setup for cubic concrete sample.

2.4.2.3 Compressive strength

The compressive test of waste glass mortar was carried out by following UNI EN 196-1:2005. The compressive strength of the different studied concrete and cement-stabilised rammed earth was determined according to UNI EN 12390-3:2009. Compressive test on mortar and concrete specimens were carried out at different time of moist curing at 20°C and 95% R.H.. Compressive tests on cube specimens were carried out with testing machine having 3000 KN maximum load at constant rate of loading of 0.5 MPa/s. Compressive tests on prismatic specimens of mortar were performed with testing machine with 250 KN maximum load.

2.4.2.4 Electrical resistivity

In order to evaluate the development in time of the microstructure of different materials studied in this research, the electrical conductance of cube and prism specimens was measured by using a COND 6 conductivity meter and two copper plates placed with wet sponges on opposite faces of the sample as shown in **Figure 2.6**. After demoulding, prismatic specimens were submerged in water and stored at curing chamber at 20°C. Conversely, cubic specimens were cured in moist condition (at 20°C and 95% R.H.). Conductance can be converted into electrical resistivity by the following equation:

$$\rho = \frac{K}{G} = \frac{S}{LG} \quad (2.2)$$

where, ρ is electrical resistivity, K is the cell constant, G is conductance, S and L are respectively section area and length through which current passes.



Figure 2.6 Conductance test on prism sample.

The electrical resistivity of concrete was also monitored under self-desiccation condition (i.e. in the absence of evaporation and water supply) on specimens embedding a probe made with mixed metal oxide (MMO) coated/activated titanium which were sealed in an isolated container. The conductance was monitored by an AMEL instruments 160 conductivity meter that was connected with a computer in order to acquire the data automatically already at the initial stage of hydration process for around 24 hours after casting. During the subsequent period, the conductance was measured with the conductivity meter. **Figure 2.7** shows the probe and setups to measure the conductance of specimens (under self-desiccation condition).



Figure 2.7 A handmade resistivity probe and conductance tests.

2.4.2.5 Capillary absorption and water absorption

The resistance of capillary absorption of concrete was determined according to UNI EN 13057:2003. The thickness of tested cylindrical specimens is around 35 mm. Specimens for capillary test were dried in oven at 40°C and subsequently they were maintained in a container for 24 hours in contact with a water level of few millimetres. Measurement of mass after 12 and 30 minutes and 1, 2, 4 and 24 hours from starting of the partial immersion were carried out for 2 replicate specimens for each type of concrete.

The water absorption test of concrete was also carried out according to UNI 7699 on cubic specimens which were firstly dried in oven at $105 \pm 5^\circ\text{C}$ till mass change less than 0.015% at an interval not less than 24 hours. Then, all cube specimens were fully immersed to regularly monitor the mass till mass change is less than 0.01% at an interval not less than 24 hours.

2.4.2.6 pH analysis

In order to evaluate the pH of pore solution of studied concrete or mortar, tests were carried out with an electrode on solution obtained from powder samples by mixing 10 grams of ground concrete or mortar (80% of particles passing through 80 μm sieve) with 10 ml of CO_2 -free deionised water after stirring for 5 minutes according to the procedure reported in reference [142]. A pH meter, produced by Crison, was used for measuring the pH of pore solution. **Figure 2.8** shows the pH test setup. Concrete samples were collected from each type of concrete after reinforced specimens (alkaline and carbonated) being splitted. In addition, reference and CSA-based mortars ($w/c = 0.5$) made with standard sand were determined pH after 1, 4, 7, 28 and 145 days curing.

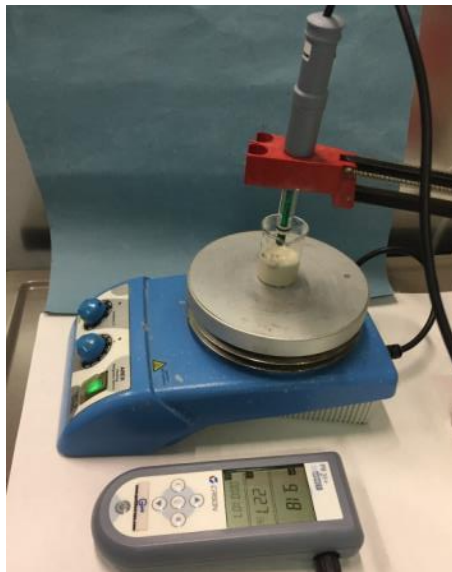


Figure 2.8 pH of concrete or mortar test setup.

2.4.2.7 Natural carbonation and accelerated carbonation

Cubic specimens for natural carbonation test were exposed in sheltered outdoor environment as shown in **Figure 2.9a**. After 90, 180 and 360 days exposure, the carbonation depth on splitted specimens was determined by using a solution of phenolphthalein and a commercial pH indicator. The average value of carbonation depth of each carbonated side was calculated.

The accelerated carbonation test was performed on cubic specimen coated on five sides by painting epoxy resin as shown in **Figure 2.9b**. CO_2 is allowed to penetrate from the uncoated face.

The coated specimens were exposed into a carbonation chamber with 4% CO₂ at 65 ± 5% R.H. and 20 ~ 23°C for around 70 days. Afterwards, each specimen was splitted and phenolphthalein was sprayed on one half. Five measurements of carbonation depth were carried out along with each carbonated side and the average value was calculated as nominal carbonation depth.

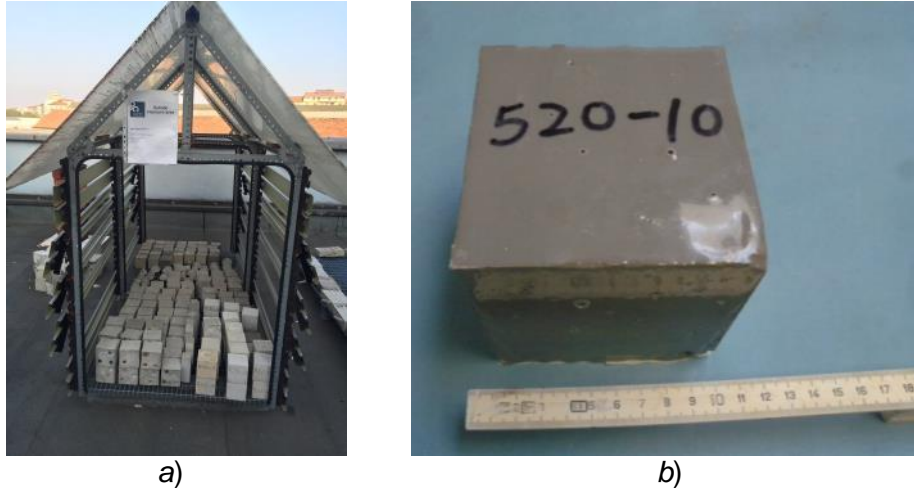


Figure 2.9 Natural carbonation site a) and specimen with uncoated bottom side b) for accelerated carbonation test.

2.4.2.8 Chloride penetration test and chloride content analysis

Also cubic specimens dedicated to evaluate chloride resistance of studied mixtures were coated with epoxy resin as shown in **Figure 2.9b**. After coating the specimens, they were fully immersed in 3.5% NaCl solution for a period of almost 7 months. Subsequently, each specimen was cored along with the direction of chloride penetration. Afterwards, each core with diameter of 25 mm was cut into six slices of 10 mm thickness, parallel to the exposed surface. The tool used for cutting cores is a water-cooled diamond saw. Each slice was ground into powder and the obtained powder sample was dried in oven at 105 ± 5°C for 24 hours in order to obtain dry mass. Around 5 grams of powder was dissolved in 25 ml nitric acid (1:1) with the addition of 50 ml deionised water. The solution was heated until boiling as shown in **Figure 2.10**. After cooling down the solution, 100 ml solution was finally prepared by supplementing deionised water. Finally, 25 ml of the prepared solution was tested with 0.01 M silver nitrate solution by potentiometric titration. The chloride content of each slice was expressed as percentage of chloride by mass of concrete. Finally, chloride coefficient was derived through fitting the curve defined by **Equation 1.4**.



Figure 2.10 Chloride content analysis for CSA-based concrete.

2.4.2.9 Alkali silica reaction and alkali attack

ASR test was carried out by conforming to ASTM C1567-13. The test duration was extended till 70 days rather than 14 days as specified.

For alkali attack test, prism specimens ($40 \times 40 \times 160 \text{ mm}^3$) were completely immersed in 1 M NaOH solution and were kept in curing chamber. The mass of specimens was monitored regularly.

2.4.3 Electrochemical tests on reinforced mortar

For electrochemical tests on reinforced specimens, the typical three-electrode electrochemical system consisting of a working electrode, a reference electrode and a counter reference, was employed.

2.4.3.1 Reinforced specimens

All steel bars for corrosion tests were cut into 100 mm long. For this experimental work rebars with different diameter (10, 16 and 18 mm) were used. The two ends of each bar were coated by a layer of styrene-butadiene-rubber (SBR) modified cement mortar that was made with 5 parts of CEM I 52.5R, 6 parts of fine limestone aggregates and 4 parts of SBR. The length of exposed area of steel embedded in concrete was 60 mm. The reference electrode was made with mixed metal oxide (MMO) coated/activated titanium wire. Additionally, the counter electrode was made with MMO activated titanium wires as well. The reference electrode, counter electrode together with working electrode (steel bar) were fixed with a PVC tube (110 mm height) used as formwork for reinforced specimens and sealed by a round PP foam support cap at one end. Reference MMO coated/activated titanium electrode was in parallel placed close to steel bar. **Figure 2.11** demonstrates the component parts of formwork for reinforced specimen.

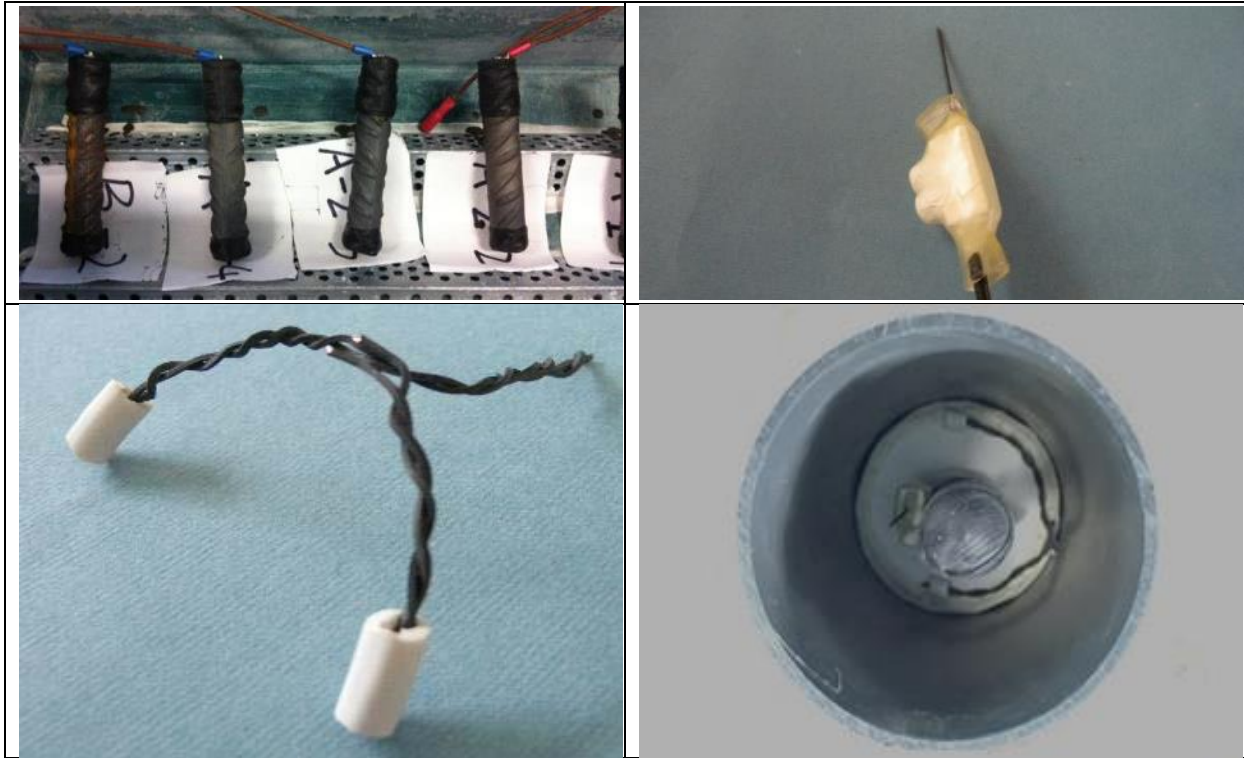


Figure 2.11 Component parts of formwork for reinforced specimen and a freshly cast specimen.

2.4.3.2 Exposure conditions

For studying the corrosion behaviour of carbon steel bars with different surface conditions embedded in ordinary concrete, the reinforced specimens were manufactured and demoulded the day after casting and immediately wrapped up with plastic films so as to avoid evaporation of water and to ensure self-desiccation condition (i.e. in the absence of evaporation and water supply). They were subsequently placed in a climatic chamber (**Figure 2.12**) with the controlled temperature (23°C). After almost two months, the plastic films was removed and the reinforced specimens were maintained in the same chamber at 20°C and 80% R.H. condition; the specimens reinforced with steel bar with 18 and 10 mm diameter were exposed in these conditions respectively for 8 months and 50 days. Finally, the reinforced specimens were immersed in tap water (20°C) for around one month. At the end of the periods of both self-desiccation and immersion conditions, anodic polarisation tests were carried out on reinforced specimens.

Subsequently, for each series of reinforced specimen (three duplicates), one was maintained in a carbonation chamber at 4% CO₂, 65 ± 5% R.H. and 20 ~ 23°C until concrete completely carbonated. Then the carbonated reinforced specimens were immersed in tap water (water level around 1 cm below the top surface of reinforced specimen) for 48 hours. The other two reinforced specimens were subjected to immersion cycles in 3.5% NaCl (solution level around 1 cm below the top surface of reinforced specimen). 1-day of immersion cycle was followed by at least 6 days of drying in laboratory condition. The test was repeated for as many cycles until the onset of steel

corrosion. Subsequently, each corroded specimen was splitted into two half parts in order to do visual examination of corrosion condition of steel bar. Afterwards, around 3 grams powder was collected by scraping broken concrete pieces close to steel surface in reinforced specimens. The chloride content of each powder sample was analysed by dissolution in nitric acid and titration.



Figure 2.12 Climatic chamber and data logger setup used for corrosion tests.

For studying waste glass mortar, the reinforced specimens were covered with plastic films immediately after casting and maintained in a climatic chamber (at 23°C) for around 70 days.

As far as CSA-based concrete is concerned, the reinforced specimens were demoulded one day after casting. Subsequently, the reinforced specimens were wrapped up with plastic films and stored in climatic chamber (at 23°C); 7 days later, some of these specimens were selected to be exposed to accelerated carbonation chamber for about 250 days in order to favor a complete carbonation. The rest of reinforced specimens were subjected to various exposure conditions with different temperature and humidity as summarised in **Table 2.12**. Finally, all the reinforced specimens were splitted in order to do the visual examination of corrosion condition.

Table 2.12 Exposure conditions of reinforced CSA-based specimens.

Exposure condition	self-desiccation 23 °C	R.H. 80%, 20°C	R.H. 95%, 20°C	R.H. 95%, 40°C	R.H. 80%, 20°C	Immersion** 20°C
Alkaline specimens*	≈ 7 month	≈ 1 month	≈ 3 months	≈ 3 months	≈ 5 months	3 days
Carbonated specimens*	---	---	≈ 3 months	≈ 3 months	≈ 5 months	3 days
SR03 alkaline specimens	≈ 3 and a half months	≈ 1 month	≈ 1 month	---	---	3 days

* SR03 alkaline specimens were not included.

** water level around 1 cm below the top surface of reinforced specimen.

For studying cement-stabilised rammed earth, reinforced specimens were made also with cement-stabilised rammed earth. They were cured for one week after casting in formwork. Subsequently, they were demoulded and sealed with plastic films immediately in order to allow self-desiccation

conditions in climatic chamber at 23°C for about 2 months. Afterwards, they were fully immersed in tap water for two days.

2.4.3.3 Corrosion tests

The corrosion potential of steel versus MMO-Ti reference electrode can be monitored either by data logger annexed with climatic chamber or by using a portable voltmeter. The potential of steel versus saturated calomel electrode (SCE) can be measured by placing SCE on the surface of reinforced specimen with a wet sponge as shown in **Figure 2.13**. Besides, the potential of MMO-Ti reference electrode versus SCE can also be measured through voltmeter manually.

In addition to corrosion potential, corrosion rate of reinforced specimens was determined by linear polarisation resistance (LPR) technique. Corrosion current density (i_{corr}) can be calculated by the following formula:

$$i_{corr} = \frac{B}{A \cdot R_p} \quad (2.3)$$

where, B is constant (26 mV for active steel and 52 mV for passive steel), A is the steel surface area exposed in concrete or mortar (m²), and R_p is polarisation resistance (Ω). In this study, B was considered equal to 26 mV.

In order to obtain the value of R_p , ±10 mV polarising voltage were imposed by potentiostatic instrument as seen in **Figure 2.13**, from anodic and cathodic directions respectively; the duration of each polarisation is 30 seconds and the current at the end of polarisation was recorded. The nominal R_p for calculating current density is the average value of R_p obtained from anodic and cathodic polarisations.



Figure 2.13 Corrosion potential and corrosion rate measurements.

The anodic polarisation test was carried out on by imposing a steel potential of + 200 mV vs SCE on steel, recording its polarisation current (i_p) in the following 24 hours by data logger. A further description of parameters chosen for the polarisation test will be presented in **Chapter 4 (Section 4.2)**.

Chapter 3

Results

This chapter describes the results of experimental study aimed at assessing the corrosion protection of steel in new sustainable cementitious materials that have been introduced in the previous chapter. The results are presented by distinguishing in following four subtopics: 1) the study of the passivation and corrosion behaviour of carbon steel in ordinary concrete, considering also the role of rust which may be formed at the production plant or at construction site; 2) the investigation on the use of recycled waste glass in mortars and its effects on durability of reinforced concrete; 3) the study of the corrosion protection of both carbon steel and galvanized steel provided by concrete made with CSA-based cements; 4) the study of passivation of carbon steel in cement-stabilised rammed earth. For each topic, the results are presented in terms of concrete characterization for durability-related properties and electrochemical tests on reinforced specimens.

3.1 Tests on carbon steel bars with different surface conditions

Firstly, carbon steels bars with different surface conditions used in this research were characterised; subsequently, the tests were carried out on ordinary concrete; finally, the passivation of steel bars was studied as a function of humidity of concrete both in free corrosion condition and under anodic polarisation. The corrosion behaviour of steel bars subjected to carbonation and chloride penetration were also studied.

3.1.1 Characterisation of carbon steel bars with different surface conditions

In order to characterise carbon steel bars with different surface conditions, firstly the appearance of the bars was documented visually and through a stereo-microscope; subsequently, the microstructure and oxides layer of metallographic sections of these steel bars were observed by optical microscope and scanning electron microscope; finally, the composition of rust layer was analysed by XRD analysis.

Figure 3.1 shows the visual comparison of the steel bars with 10 mm diameter. Steel bar labelled as “A1” (as-received) presents a dark-grey surface. Sandblasted steel bar, labelled as “A2”, shows a smooth surface but with some “dark spots” along the longitudinal rib, which might be due to production process. Pre-rusted steel bar indicated as “B” (exposed outdoors for 6 months) can be seen corrosion products mainly located between ribs. Pre-rusted steel bar labelled as “C” (exposed outdoors for 1 year) is covered completely by a layer of red-brownish rust.

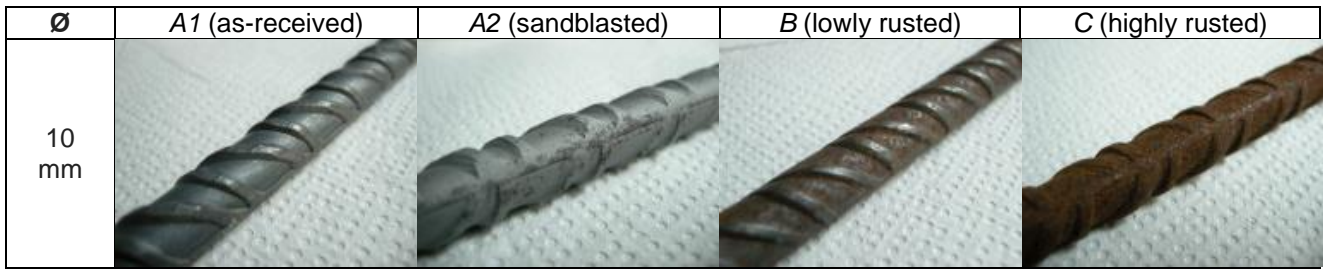


Figure 3.1 A visual comparison of the surface of 10 mm diameter steel bar.

The results of the visual observation on steel bars with 18 mm diameter are shown in **Figure 3.2**. Steel bar with mill scale and 18 mm diameter “A1” seems to have an intact surface. The surface of sandblasted steel with 18 mm diameter “A2” is smooth without defects. For steel bars with 18 mm diameter, the atmospheric exposure led to the formation of corrosion products on their surface. Based on visual observations, steel bars exposed to the atmosphere for 1 year were divided into type “C1” and type “C2” which indicated respectively as “intermediately rusted” and “highly rusted”. Steel bar with 10 mm diameter indicated as “C”, appears more rust than those labelled as “C1” and “C2”.

Figure 3.3 compares the appearance of steel bars with different surface conditions, showing typical pictures of the observations made through a stereo-microscope. It can be clearly observed that the surface of the steel bar “A1” with 10 mm diameter has some defects which are not present on comparable steel bar “A1” with 18 mm diameter. It’s confirmed again that sandblasted steel bar “A2” with 18 mm diameter has a very smooth surface whilst there are some “dark spots” on the surface of sandblasted steel bar “A2” with 10 mm diameter. All pre-rusted steel bars are covered by red-brownish rust; in particular, pre-rusted steel bar “C” with 10 mm diameter is almost fully covered with rust.

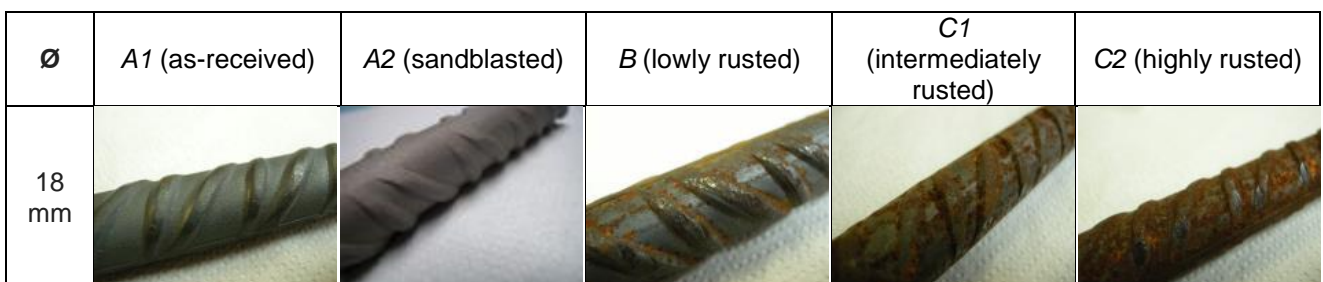


Figure 3.2 A visual comparison of the surface of 18 mm diameter steel bar.

Surface condition		$\varnothing = 10$ mm	$\varnothing = 18$ mm
A1 (as-received)			
A2 (sandblasted)			
B (lowly rusted)			
C (highly rusted)	C1 (intermediately rusted)		
	C2 (highly rusted)		

Figure 3.3 Comparison of the steel bar surface observed by stereo-microscope.

Metallographic sections of steel bars with the mill scale and different diameters (10 mm and 18 mm) are shown in **Figure 3.4**. Steel bar with 10 mm diameter presents two different zones, distinguished as inner core (zone 1) and outer layer (zone 2), showing different microstructures.

Chapter 3
Results

Steel bar with 18 mm diameter has three different zones: core zone (zone 1), middle layer (zone 2) and outer layer (zone 3). Both 10 mm and 18 mm diameter steel bars exhibit homogenous ferrite-perlite inner core (zone 1) that is a typical feature of hypo-eutectoid steel. The martensite outer layer of both 10 mm and 18 mm diameter steels is affected by thermal treatments performed during the production process. The middle layer of steel bar with 18 mm diameter is a transition layer.

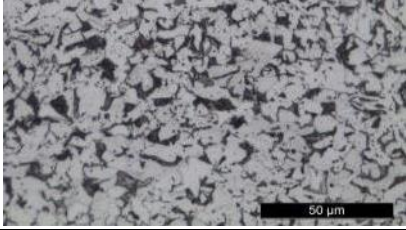
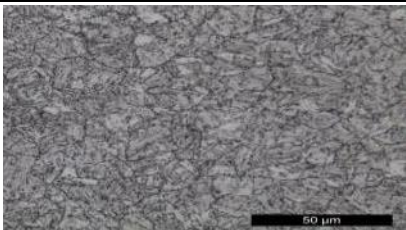
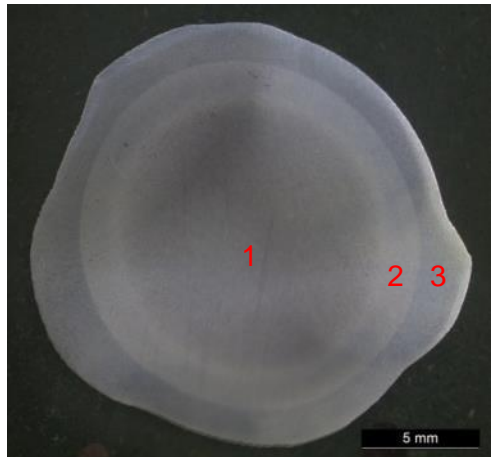
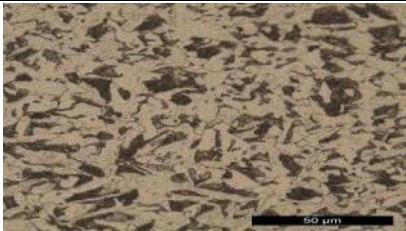
Diameter	Metallographic section	Microstructure	Note
10 mm			1.Core zone
			2.Outer layer
18 mm			1.Core zone
			2.Middle layer
			3.Outer layer

Figure 3.4 Optical microscopy images of cross sections of steel bars labelled “as-received” with mill scale and different diameters (10 mm and 18 mm).

Figure 3.5 shows the oxides present on the steel bars with different surface conditions observed by optical microscope. It can be seen that the thickness of mill scale is around dozen of microns. The thickness of rust layer due to atmospheric exposure for 6 months and 1 year reaches around

Chapter 3
Results

50 μm and 100 μm respectively; however, it's also noticed that the rust layer covering on the steel bars is uneven, as shown in **Figure 3.6**, thanks to SEM observations. In addition, for pre-rusted steel bars with 18 mm diameter indicated as “B” and “C2”, some cracks (around 100 μm long) underlying rust layers extend into steel substrate. That could be also ascribed to production process.

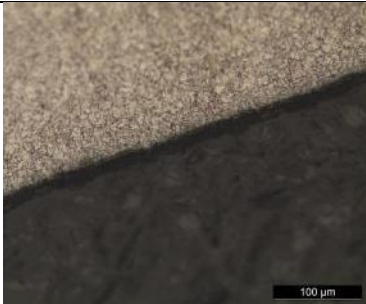
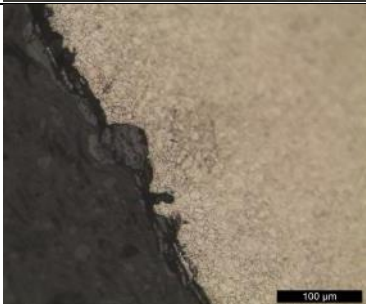
Surface condition		$\varnothing = 10 \text{ mm}$	$\varnothing = 18 \text{ mm}$
A1 (as-received)			
			
C (highly rusted)	C1 (intermediately rusted)		
	C2 (highly rusted)		

Figure 3.5 Optical microscopy images of the oxide layers of steel bars with different surface conditions. (The surface condition indicated as “C” with respect to the 10 mm diameter steel bar.)

Furthermore, the composition of rust layer has been analysed through XRD analysis, as shown in **Figure 3.7**. Mineral compounds such as goethite ($\text{FeO}(\text{OH})$), lepidocrocite ($\gamma\text{-FeO}(\text{OH})$) and magnetite (Fe_3O_4) are typical products due to atmospheric corrosion of iron.

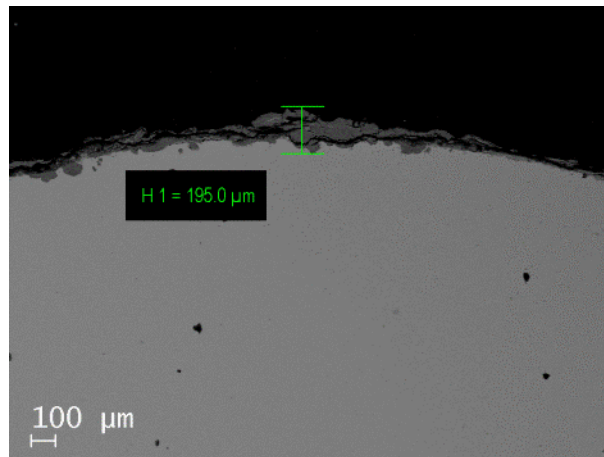


Figure 3.6 The rust layer of pre-rusted steel bar (“C1”) observed by SEM.

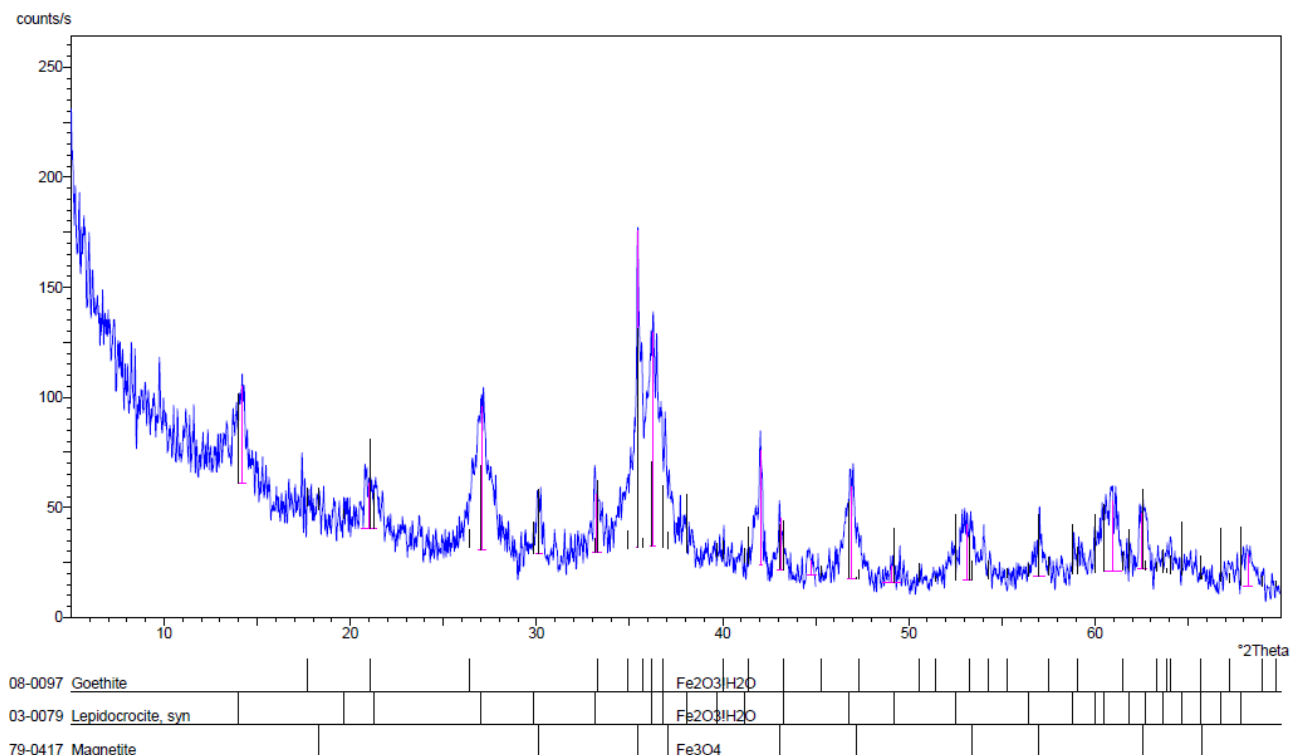


Figure 3.7 XRD analysis of the rust layer of steel bar (highly rusted) with 18 mm diameter.

3.1.2 Properties of studied concrete

Before studying the passivation and corrosion behaviour of pre-rusted steel bars in ordinary concrete, it has been necessary to test the properties of ordinary concrete that was cast in two batches to prepare reinforced specimens.

In **Table 3.1**, fresh and hardened properties of studied ordinary concrete made with Portland limestone cement are listed. The slump of both batches of concrete had exceeded the low limit (16 cm) of “S4” slump class. The compressive strength of concrete after 28 days curing reached 54 ~

58 MPa. Electrical resistivity measured at 28 days curing for both batches of concrete varied in the range of 55 ~ 60 ($\Omega \cdot m$).

Table 3.1 Properties of studied concrete (w/c = 0.5).

Property	Concrete for 18 mm diameter steel	Concrete for 10 mm diameter steel
Slump (cm)	16	22
1-day hardened density* (kg/m^3)	2417	2449
28-day compressive strength (MPa)	58	54
28-day electrical resistivity ($\Omega \cdot m$)	56	60

*After demoulding.

3.1.3 Corrosion behaviour of pre-rusted steel in concrete

In order to investigate the effect of different degrees of pre-rusting of steel bars on their passivation and on corrosion behaviour when embedded in ordinary concrete and exposed to various humidity conditions, firstly the free corrosion potential and corrosion rate of steel bars were monitored. Anodic polarisation tests were also carried out to ascertain the condition of passivation of the steel bars with different surface conditions embedded in ordinary concrete during different exposure conditions. The effects of the oxides layer of the steel bars on the corrosion induced by the subsequent penetration of carbonation and chloride were also investigated.

Free corrosion potential and corrosion rate

All reinforced specimens were subjected to self-desiccation conditions for 2 months (at 23°C) the day after casting; subsequently they were exposed to 20°C and 80% R.H. condition. Once stable condition in terms of corrosion was reached, they were immersed in tap water. It is widely recognised that if corrosion potential of steel is higher than -200 mV vs SCE and corrosion rate of steel is lower than 1 mA/m^2 (corresponding to $1.17 \text{ } \mu\text{m/year}$), steel is in passive condition.

Figure 3.8a-b show respectively corrosion potential (E_{corr} vs SCE) and corrosion rate (i_{corr}) of replicate specimens (3 for each surface condition), reinforced with 10 mm diameter steel during different exposure conditions. **Figure 3.8a** shows that the corrosion potential of all steel bars increased gradually under the self-desiccation condition and during 80% R.H. condition (20°C). The limit of -200 mV vs SCE was exceeded after few days of self-desiccation condition, reaching corrosion potential of around 50 mV vs SCE at the end of the exposure at 20°C and 80% R.H.. After immersion of reinforced specimens, their corrosion potentials quickly dropped for a stable range of -20 ~ -120 mV vs SCE, except for the specimen "A1-2" (as-received). According to **Figure 3.8b**, the corrosion rate of all steel bars decreased gradually after casting until reached stable level within few days of self-desiccation condition; most of the specimens had corrosion rates lower than 1 mA/m^2 ; only few reinforced specimens maintained corrosion rates very close to 1 mA/m^2 during

the whole exposure tests. A slight increase to values of corrosion rate of replicate specimens was observed in immersion period.

Figure 3.9 shows the results in terms of corrosion potential and corrosion rate of replicate reinforced specimens with 18 mm diameter steel. The evolution in time of corrosion potential of 18 mm steel bars, as shown in **Figure 3.9a**, is similar to that of 10 mm steel bars. Overall the specimens reinforced with 18 mm steel bars, regardless surface conditions, maintained in all humidity conditions corrosion potential higher than -200 mV vs SCE, supporting the hypothesis that also the pre-rusted steel bars with 18 mm diameter were in passive state. Although the evolution trend of corrosion rate of 18 mm steel bars embedded in concrete as function of time (**Figure 3.9b**), is similar to that of 10 mm steel bars, reaching stable state after few days of self-desiccation condition, a significant variation of values, even more than 1 mA/m², can be seen between the bars with different surface conditions. Reinforced specimens, labelled “C1” (intermediately rusted), showed the highest stable value, around 7 mA/m²; the reinforced specimens indicated as “B2” and “C2” (respectively, lowly rusted and highly rusted) had stable corrosion rates slightly higher than 1 mA/m²; reinforced specimens labelled as “A1” and “A2” (i.e. as-received and sandblasted) showed the lowest stable value, around 0.5 mA/m².

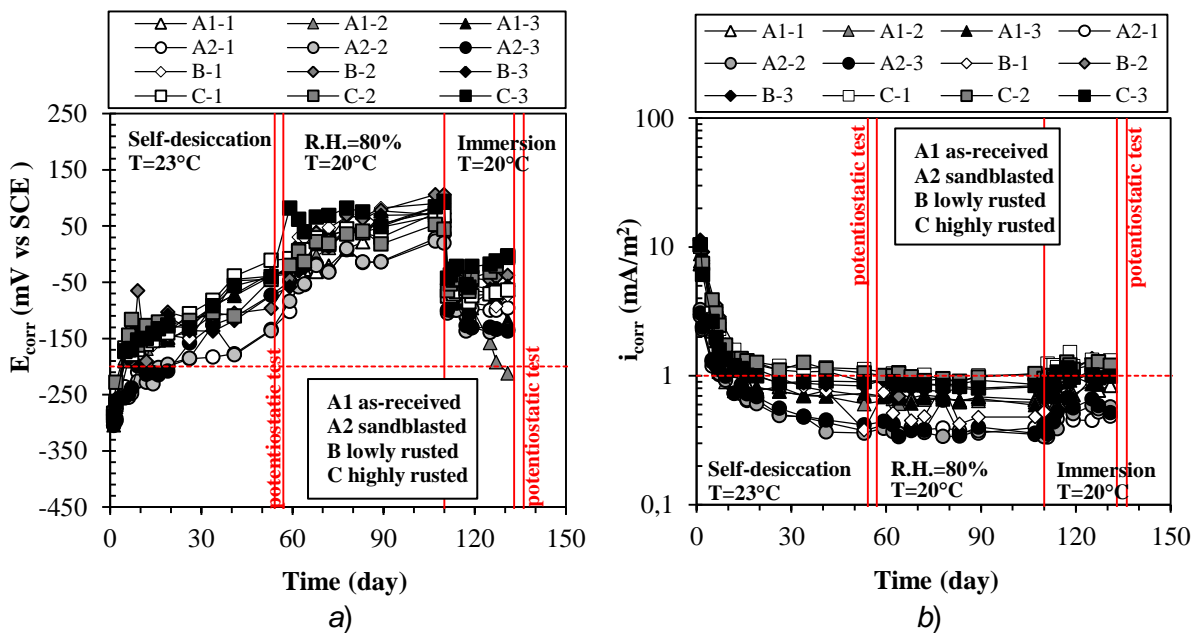


Figure 3.8 Monitoring of a) corrosion potential (E_{corr} vs SCE) and b) corrosion rate (i_{corr}) of replicate reinforced specimens with 10 mm diameter steel bars in different surface conditions during different exposure conditions.

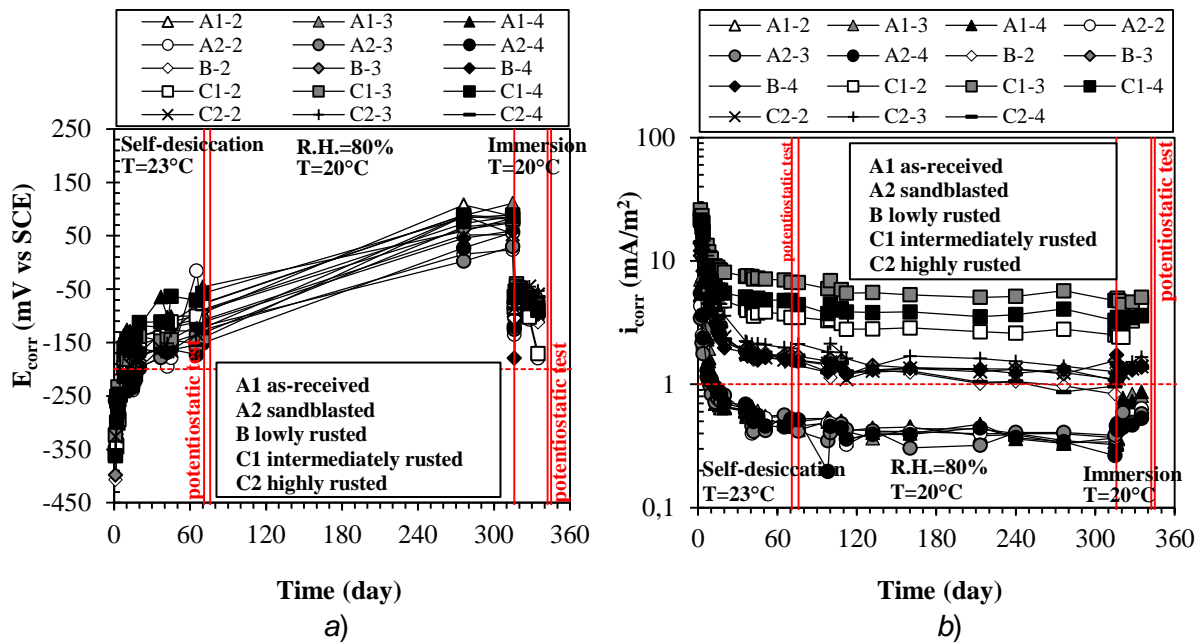


Figure 3.9 Monitoring of a) corrosion potential (E_{corr} vs SCE) and b) corrosion rate (i_{corr}) of replicate reinforced specimens with 18 mm diameter steel bars in different surface conditions during different exposure conditions.

Anodic polarisation

Anodic potentiostatic polarisation test was carried out on all reinforced specimens at the end of both self-desiccation and immersion conditions. **Figure 3.10-3.11** show respectively the results of anodic potentiostatic polarisation test on specimens reinforced with 10 mm and 18 mm steel bars. Regardless surface condition of steel bar and exposure times studied, the current density of all steel bars decreased quickly after starting the test and reached stable values during the following period; the current density of all reinforced specimens was lower than 1 mA/m² at the end of 24 hours testing.

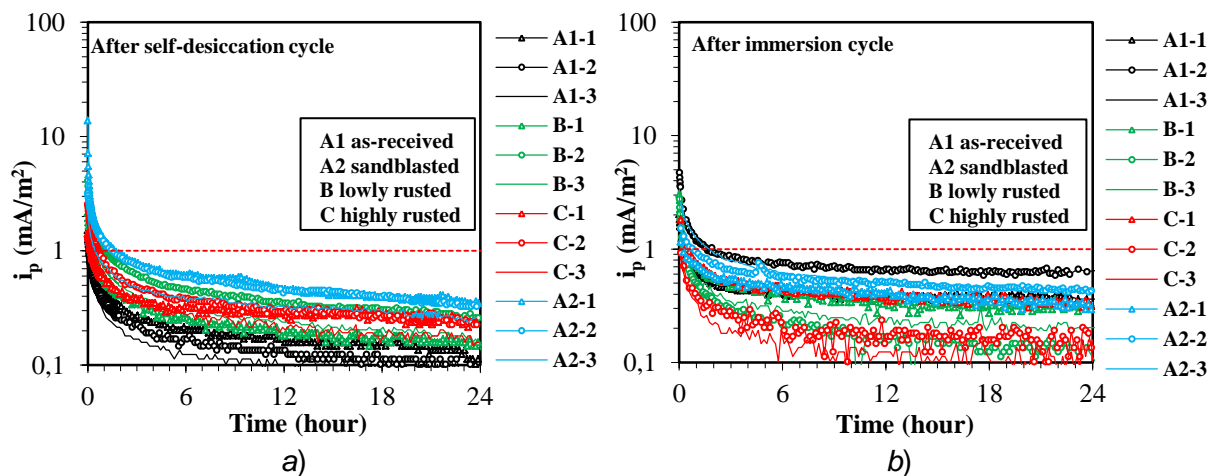


Figure 3.10 Results of the 24 hours potentiostatic polarisation at +200 mV vs SCE in terms of current density (i_p) for 10 mm steel bars with different surface conditions embedded in concrete after a) self-desiccation and b) immersion.

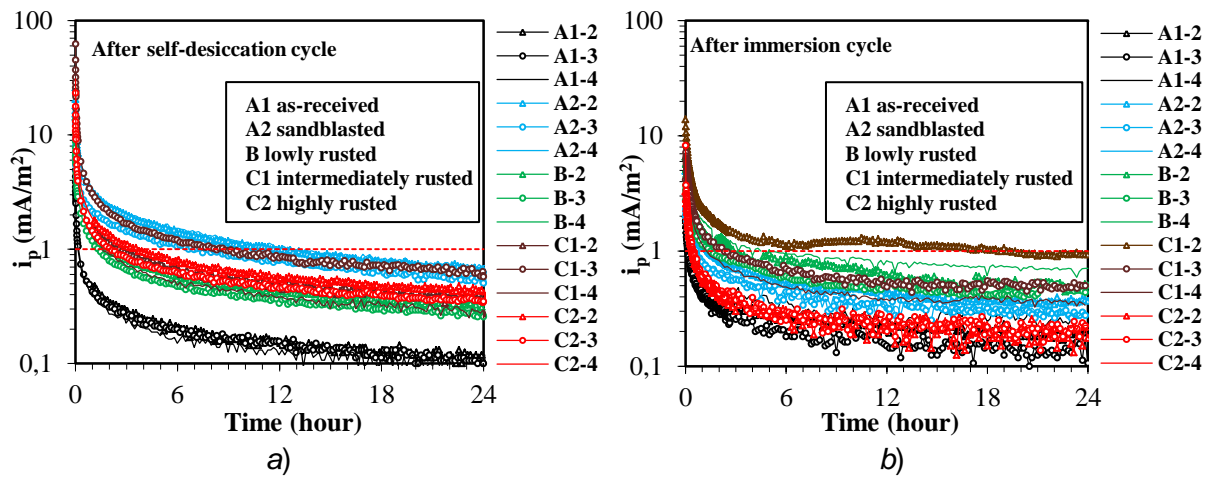


Figure 3.11 Results of the 24 hours potentiostatic polarisation at +200 mV vs SCE in terms of current density (i_p) for 18 mm steel bars with different surface conditions embedded in concrete after a) self-desiccation and b) immersion.

Carbonation-induced corrosion

In order to evaluate the effect of the pre-rusting on corrosion propagation, part of the reinforced specimens were subjected to accelerated carbonation.

Figure 3.12a-b show respectively the evolution of corrosion potential (E_{corr} vs SCE) and corrosion rate (i_{corr}) of 10 mm steel bars in carbonated concrete immersed in tap water for 48 hours and subsequent 100 hours of drying in laboratory environment. During immersion condition, the corrosion potential of all reinforced specimens decreased quickly; after 48 hours of immersion, the corrosion potential of all reinforced specimens was below -350 mV vs SCE. In particular, specimens with sandblasted steel bar reached a corrosion potential value of -600 mV vs SCE. During drying condition, the corrosion potential of all reinforced specimens increased and exceeded -200 mV vs SCE at the end of drying condition, except the specimen with sandblasted steel bar showing a potential slightly lower than -200 mV vs SCE. The corrosion rate of all reinforced specimens increased quickly in the immersion condition, reaching 5 mA/m² at the end of immersion condition regardless the surface conditions. During the subsequent 100 hours drying, corrosion rates of all steels decrease slightly, but still above 1 mA/m² until the end of drying condition.

A similar trend of corrosion potential and corrosion rate regarding 18 mm steel bars in carbonated concrete can be seen in **Figure 3.13**. However, it's also noticed that as-received steel (specimen "A1-2") seems to be still in passive condition, which was evidenced by the fact that its corrosion potential was not below -200 mV vs SCE and its corrosion rate was not above 1 mA/m² during the whole test period.

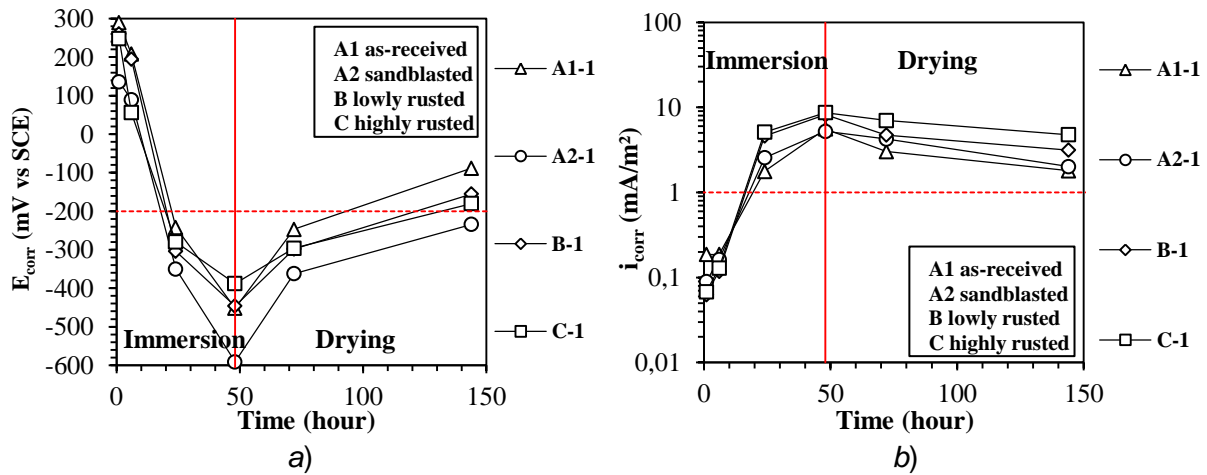


Figure 3.12 Monitoring of a) corrosion potential (E_{corr}) and b) corrosion rate (i_{corr}) of 10 mm diameter steel bars in carbonated concrete during the period of 48 hours immersion and subsequent 100 hours drying in laboratory environment.

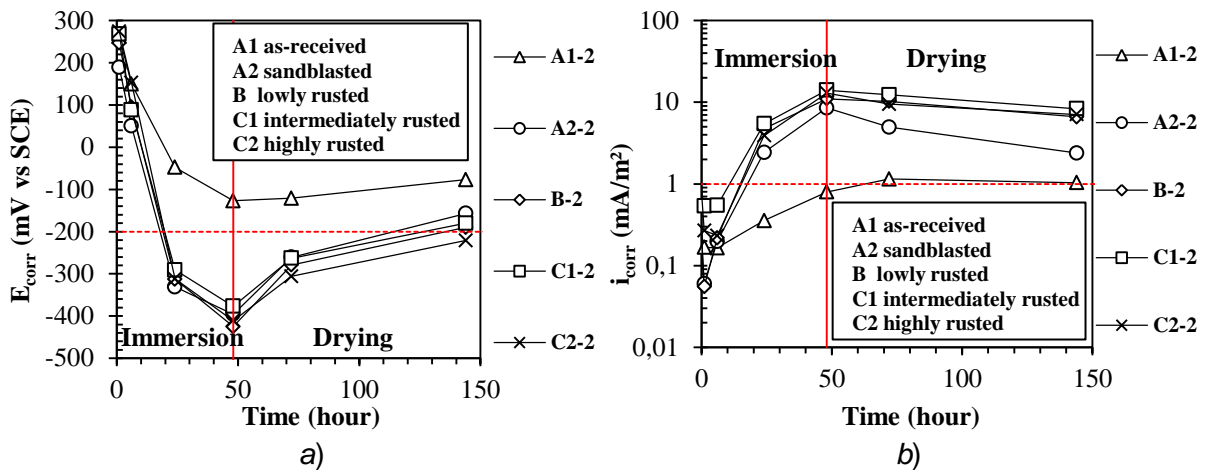


Figure 3.13 Monitoring of a) corrosion potential (E_{corr}) and b) corrosion rate (i_{corr}) of 18 mm diameter steel bars in carbonated concrete at the period of 48 hours immersion and subsequent 100 hours drying in laboratory environment.

Chloride-induced corrosion

Effects due to chloride penetration on steel bars with different surface conditions embedded in ordinary concrete was evaluated by monitoring the corrosion potential (E_{corr} vs SCE) and corrosion rate (i_{corr}) of reinforced specimens exposed to ponding cycles in 3.5% NaCl solution. The immersion phase last 1 day and the drying phase was 6 days (at least). **Figure 3.14a** and **Figure 3.15a** show respectively the evolution of corrosion potential of 10 mm and 18 mm steel bars over the whole test period. At the beginning, the corrosion potential of all steel bars was above -200 mV vs SCE. A definitive decrease of the potential at value lower than -200 mV vs SCE indicates the initiation of corrosion. Corresponding with the decrease of corrosion potential, the corrosion rate of steel bar increased immediately as it can be seen in **Figure 3.14b** and **Figure 3.15b**. It should be also stressed that the concrete cover for two types of reinforced specimens was identical (25 mm). Reinforced specimen in which the corrosion of steel has initiated as detected by the decrease of

the corrosion potential and the increase of corrosion rate, was splitted to extract steel bar and collect a piece of concrete close to steel surface in order to measure its chloride content. Comparable initiation time were observed for replicate specimens reinforced with steel bars with the same surface conditions. It can be observed that different initiation times for different surface conditions. As an example, corrosion started after around 200 days for as received steel bar with 10 mm diameter (A1) whereas the corrosion of sandblasted steel bar with 10 mm diameter (A2) occurred after more than 350 days. In **Table 3.2**, the number of ponding cycles to which each specimen was subjected before splitting and the corresponding chloride content close to steel surface that represents chloride threshold value are shown.

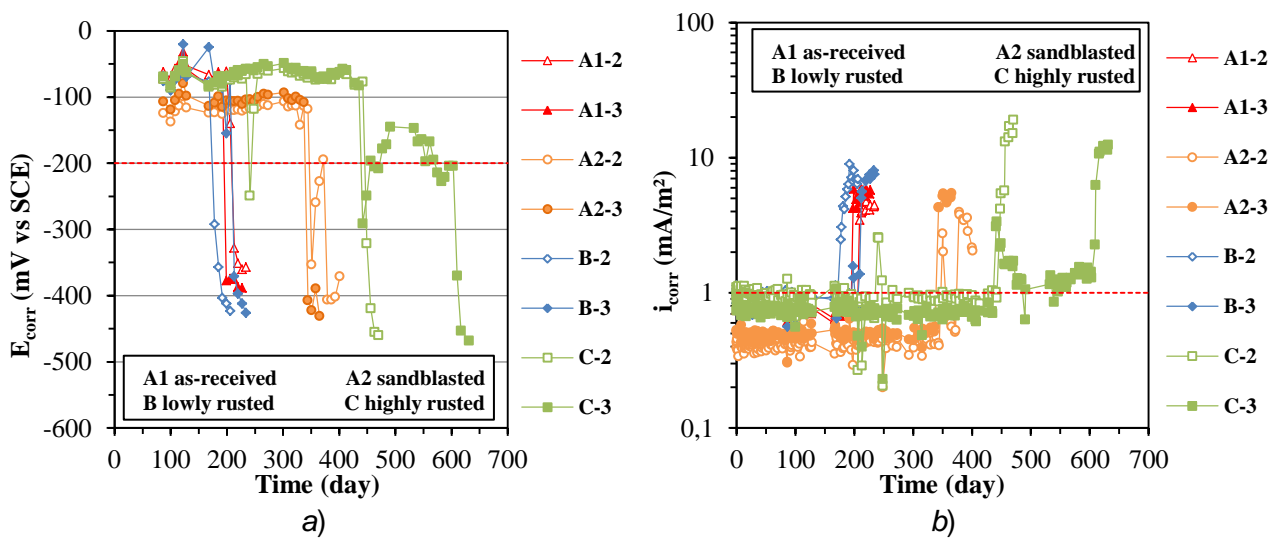


Figure 3.14 Monitoring of a) corrosion potential (E_{corr}) and b) corrosion rate (i_{corr}) of 10 mm steel bars with different surface conditions embedded in concrete under cyclic immersion in 3.5% NaCl solution.

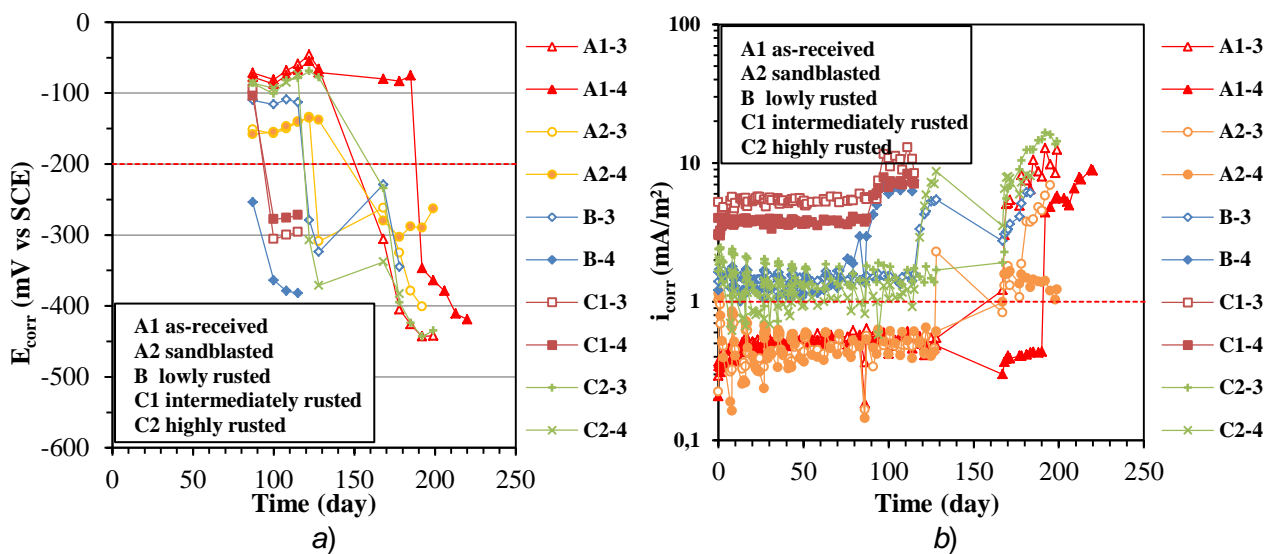


Figure 3.15 Monitoring of a) corrosion potential (E_{corr}) and b) corrosion rate (i_{corr}) of 18 mm steel bars with different surface conditions embedded in concrete under cyclic immersion in 3.5% NaCl solution.

Table 3.2 Chloride contents of concrete samples (by concrete mass) collected close to steel surface of reinforced specimens exposed to ponding cycles in 3.5% NaCl.

Surface condition	Sample	18 mm diameter steel		Sample	10 mm diameter steel	
		Chloride content (%)	Cycle		Chloride content (%)	Cycle
As-received	A1-3	0.545	22	A1-2	0.210	27
	A1-4	0.498	25	A1-3	0.188	26
Sandblasted	A2-3	0.419	21	A2-2	0.417	48
	A2-4	0.674	22	A2-3	0.466	43
Lowly rusted	B-3	0.404	19	B-2	0.338	23
	B-4	0.228	15	B-3	0.344	27
Highly rusted	C1-3*	0.256	15	C-2	0.758	57
	C1-4*	0.255	15			
	C2-3	0.645	22	C-3	0.989	75
	C2-4	0.708	19			

*Intermediately rusted.

3.2 Tests on mortar with waste glass

This section reports the results of tests carried out on mortar made with finely grounded glass powder used as mineral addition and/or with expanded glass as lightweight aggregates in total replacement of ordinary sand. Beneficial effects of glass powder on the durability of waste glass mortar have been studied in terms of compressive strength, electrical resistivity, ASR expansion and corrosion protection of steel.

3.2.1 Fresh and hardened properties of waste glass mortar

Consistence and fresh density of the studied waste glass mortar are shown in **Table 3.3**. The consistence of M134 reference mortar (made with OPC) was 134%. For mortar with a binder obtained by replacing 30% OPC with glass powder, an improvement of consistence was obtained by reached a value of 150%. However, mortar with 30% of glass powder and expanded glass in total replacement of ordinary sand showed a consistence of 139%, which was slightly higher than that of reference mortar. When only standard sand was totally substituted by expanded glass, the consistence of mortar was 131%, slightly lower than that of reference mortar. Fresh density of mortar made with 30% OPC replaced by glass powder (M135) was comparable to that of reference mortar (**Table 3.3**). As expected on lightweight cementitious materials, both mortars made with expanded glass (M136 and M137) obtained much lower fresh density (around 1200 kg/m³).

Table 3.3 Fresh properties of waste glass mortar.

Fresh property	M134*	M135*	M136*	M137*
Consistence (%)	134	150	139	131
Fresh density (kg/m ³)	2273	2244	1177	1206

*M134:OPC; M135:30% OPC replaced by glass powder; M136:30% OPC replaced by glass powder and 100% standard sand replaced by expanded glass; M137:OPC and 100% standard sand replaced by expanded glass.

Compressive strength of all types of mortar was tested at 7, 28, 90 and 180 days of moist curing. The results of the mechanical tests are shown in **Figure 3.16**. The compressive strength of reference mortar (M134) was about 53 MPa after 7 days of moist curing and increased gradually over the next 3 ~ 6 months curing up to 65 MPa. Mortar made with 30% OPC replaced by glass powder (M135) had a compressive strength value of 40 MPa after 7 days of curing; due to the pozzolanic reaction in the prolonged curing, its compressive strength increased progressively, reaching 71 MPa. Conversely, the compressive strength of lightweight mortars made with expanded glass (M136 and M137) showed no noticeable change during 6 months curing, maintaining value lower than mortar without expanded glass (around 16 MPa).

Figure 3.17 shows the evolution of electrical resistivity for all types of mortar over around 3 years water curing. The electrical resistivity of all types of mortar increased rapidly since the beginning. After around 3 months curing, the electrical resistivity of the studied mortars reached stable trend, although lower values (about $50 \Omega \cdot m$) were reached for mortars made without glass powder (M134 and M137) if compared to those with glass powder. Electrical resistivity of M135 and M136 mortars made with different aggregate but with glass powder was respectively $350 \Omega \cdot m$ and $150 \Omega \cdot m$, noticeably higher than that of M134 and M137 mortars made without glass powder.

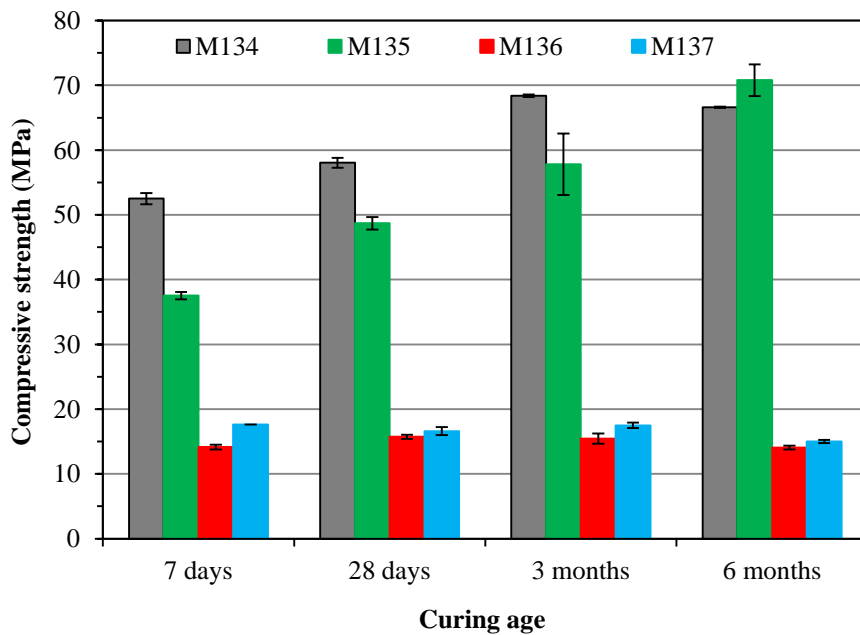


Figure 3.16 Compressive strength of recycled waste glass mortar as function of curing age. (M134:OPC; M135:30% OPC replaced by glass powder; M136:30% OPC replaced by glass powder and 100% standard sand replaced by expanded glass; M137:OPC and 100% standard sand replaced by expanded glass.)

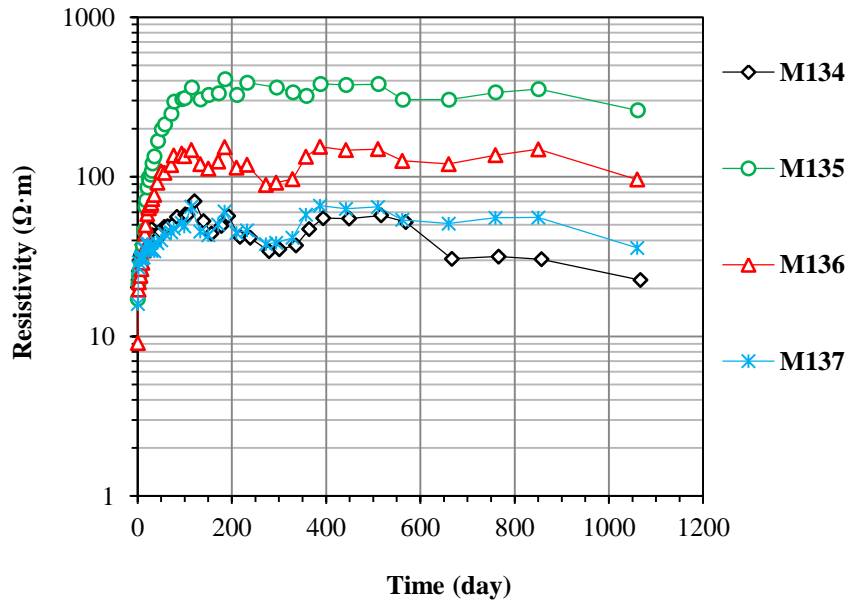


Figure 3.17 Evolution of electrical resistivity (average value of two replicate specimens) of recycled waste glass mortar under water immersion over time. (M134:OPC; M135:30% OPC replaced by glass powder; M136:30% OPC replaced by glass powder and 100% standard sand replaced by expanded glass; M137:OPC and 100% standard sand replaced by expanded glass.)

3.2.2 Durability properties of waste glass mortar

Figure 3.18 shows the evolution in time of expansion for all studied mortar in 1M NaOH solution at 80°C. Based on the results measured on the first 14 days, it is found that all types of mortar satisfied the 0.1% expansion limit specified in ASTM C1567-13, except reference mortar (M134); in particular, the mortar made with 30% OPC replaced by glass powder and 100% standard sand replaced by expanded glass (M136) showed the lowest expansion. However, based on the data measured during the whole test period (extended to 11 weeks), the expansion of reference mortar (M134) as well as mortar made with 30% OPC replaced by glass powder (M135) continuously increased, reaching after about 2 months average expansion of 0.62% and 0.38% respectively for M134 and M135 mortar respectively. Differently, the mortars made with expanded glass (M136 and M137) exhibited negligible expansion and reached expansion limit only at the end of test. Although expansion of M137 mortar was not significant, it's important to point out that this mortar showed some cracks on the surface (**Figure 3.18**) after about 30 days test.

Figure 3.19 shows the density variation measured on all types of mortar immersed in 1 M NaOH (laboratory temperature) over 3 years. Standard mortar made with ordinary sand (M134 and M135) showed very stable density (2200 ~ 2300 kg/m³) during the whole test period. Whereas the density of lightweight mortars made with expanded glass (M136 and M137) increased from 1200 kg/m³ to 1400 kg/m³ in the first year, maintaining stable value around 1500 kg/m³ in the following two years.

Moreover, for all types of mortar exposed in 1 M NaOH at laboratory temperature, no crack or noticeable expansion was observed over the test of 3 years.

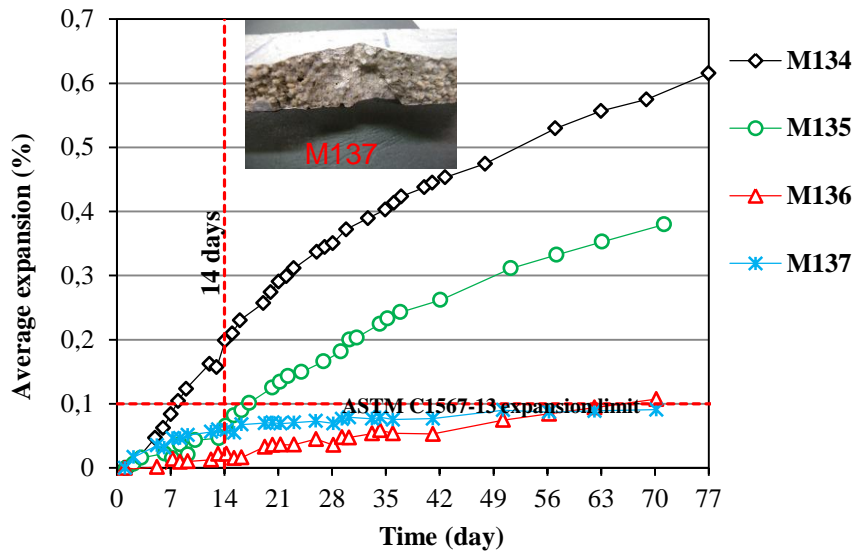


Figure 3.18 Trend of average expansion (obtained from two replicate specimens) of waste glass mortars in 1 M NaOH solution at 80°C. (M134:OPC; M135:30% OPC replaced by glass powder; M136:30% OPC replaced by glass powder and 100% standard sand replaced by expanded glass; M137:OPC and 100% standard sand replaced by expanded glass.)

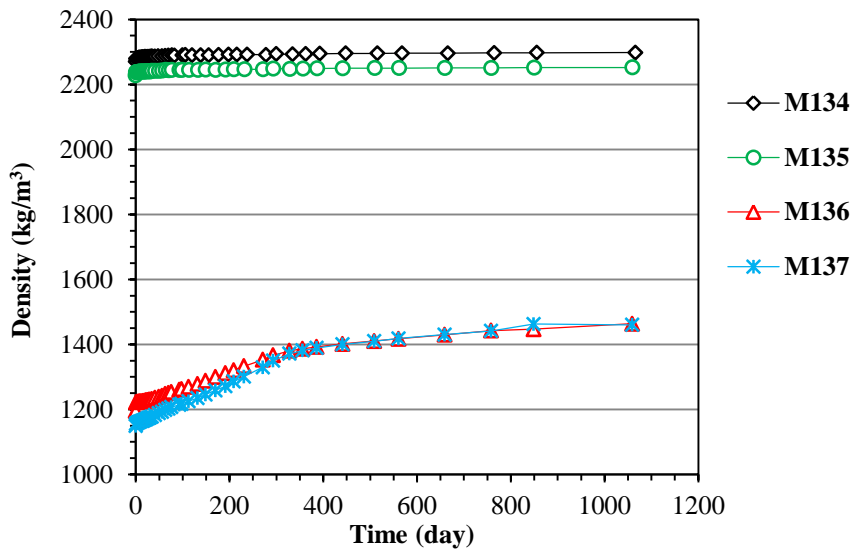


Figure 3.19 Time evolution of density of waste glass mortars immersed in 1 M NaOH solution at 20°C. (M134:OPC; M135:30% OPC replaced by glass powder; M136:30% OPC replaced by glass powder and 100% standard sand replaced by expanded glass; M137:OPC and 100% standard sand replaced by expanded glass.)

3.2.3 Corrosion behaviour of carbon steel embedded in waste glass mortar

In order to study the passivation of carbon steel bar embedded in mortar with glass powder, the corrosion potential and corrosion rate of reinforced specimens were monitored under self-desiccation condition. **Figure 3.20** shows the evolution of corrosion potential and corrosion rate of

carbon steel bars in M134 reference mortar and M135 mortar made with 30% glass powder in replacement of ordinary cement over around 70 days. Within the first week, corrosion potential of all reinforced specimens increased steeply over -200 mV vs SCE while corrosion rate decreased below 1 mA/m²; during the following period, both corrosion potential and corrosion rate maintained stable values. It can be noticed that no significant difference of corrosion potential and corrosion rate of steel was observed for reference specimens and those with glass powder. After 30 days of self-desiccation condition, the corrosion potential of steel bars in mortar with glass powder was slightly higher than that of steel bars in reference mortar; as a consequence, the corrosion rate of steel bars in mortar with glass powder was slightly lower than that of steel bars in reference mortar.

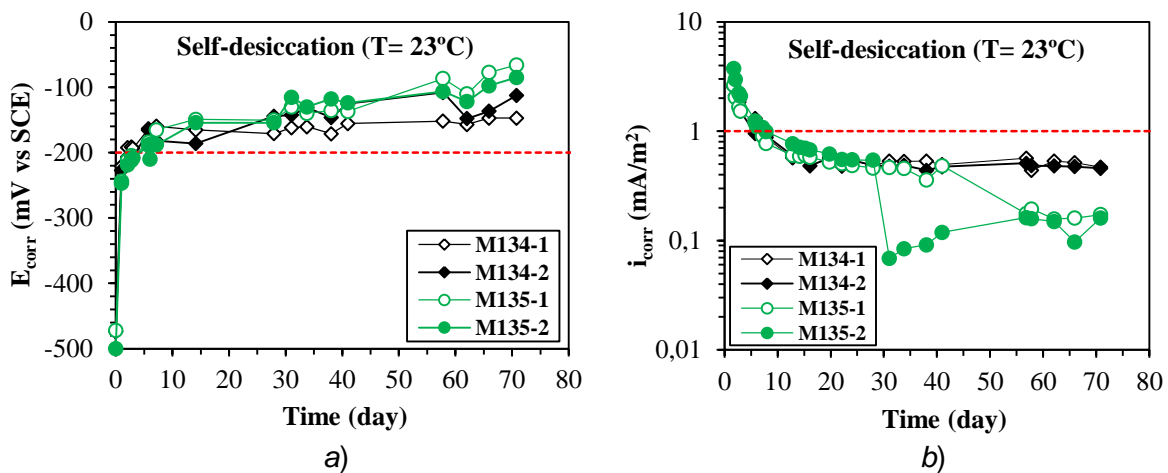


Figure 3.20 Monitoring of a) corrosion potential (E_{corr} vs SCE) and b) corrosion rate (i_{corr}) of carbon steel bars embedded in waste glass mortar and under self-desiccation condition. (M134:OPC; M135:30% OPC replaced by glass powder.)

3.3 Tests on concrete with CSA-based cements

The use of new cement such as CSA-based cement can influence the durability of reinforced concrete structures; a study on corrosion protection of steel embedded in these new binders is needed. In this section the results of experimental tests on corrosion behaviour of carbon steel and galvanised steel in concrete made with CSA-based cements are described. Firstly, the results of characterisation tests such as compressive strength, electrical resistivity, capillary absorption and water absorption, pH, resistance of carbonation and chloride penetration on CSA-based concretes are presented. Secondly, the passivation and corrosion behaviour of both carbon steel and galvanised steel embedded in CSA-based concretes are shown.

3.3.1 Properties of CSA-based concretes

Fresh and hardened properties.

Table 3.4 shows the workability and 1-day hardened density of the CSA-based concretes (including reference concrete) studied in this research. A superplasticizer admixture (**Table 2.6**)

was adopted with different dosages in each mixture in order to achieve slump class of S4 with slump varying between 16 and 21 cm. The 1-day hardened density of all mixtures (no data on mixture 524) fell into the range between 2400 and 2500 kg/m³.

Table 3.4 Workability and hardened density of CSA-based concretes.

Mix code	Slump (cm)	Hardened density* (kg/m ³)	Note
519	>21	2492	w/c=0.47,CEM II/A-L 42.5R, chloride-free
520	>21	2438	w/c=0.55,CEM II/A-L 42.5R, chloride-free
521	<21	2478	w/c=0.55,CEM II/A-L 42.5R, 0.4% chloride
522	-	2481	w/c=0.47, SL05 NF, chloride-free
523	>21	2445	w/c=0.55, SL05 NF, chloride-free
524	<21	-	w/c=0.55, SL05 NF, 0.4% chloride
525	17.5	2489	w/c=0.47, SL05 NF+CaO, chloride-free
526	19	2443	w/c=0.55, SL05 NF+CaO, chloride-free
527	20	2454	w/c=0.55, SL05 NF+CaO, 0.4% chloride
528	17	2448	w/c=0.47, SL05+CaO, chloride-free
529	18.5	2442	w/c=0.55, SL05+CaO, chloride-free
530	21	2434	w/c=0.55, SL05+CaO, 0.4% chloride
532	1	2463	w/c=0.55, SR03, chloride-free

* After demoulding (1 day).

Mechanical properties

The compressive strength and dynamic elastic modulus of CSA-based concretes were studied at different curing ages (1, 7, 28 and 90 days) in moist condition.

Figure 3.21 shows the compressive strength of reference concrete (made with CEM II/A-L 42.5R cement) and CSA-based concretes. SR03 concrete (w/c=0.55) showed a high compressive strength of 56 MPa 1 day after casting (**Figure 3.21a**). Compressive strength of concretes made by blending CSA cement with ordinary cement, namely binders labelled as SL05 NF, SL05 NF+CaO and SL05+CaO, was intermediate (from 28 MPa to 36 MPa) after 1 day of curing, between that of the pure CSA concrete (SR03) and reference concrete (26 MPa). A compressive strength comparable to that of pure CSA concrete after 1 day curing was obtained on reference concrete with the same mix proportion only after 28 days of curing. After 28 days of curing, the average compressive strength was 53 MPa for reference concrete and 58 MPa for CSA-based concrete with SL05+CaO binder, higher than those of concretes with SL05 NF with and without CaO equal to 49 MPa and 53 MPa respectively. Concrete with pure CSA cement (SR03) showed values of compressive strength after 28 days and 90 days around 70 MPa, higher than those of all other mixtures, except for concrete with SL05NF cement after 90 days of curing. Comparing **Figure 3.21b** with **Figure 3.21a**, it can be observed that chlorides added to concretes didn't induce any significant influence to compressive strength; only a slight increase of compressive strength after 7 and 28 days curing was measured on CSA-based concretes. A reduction of w/c ratio from 0.55 to 0.47 allowed to increase slightly the compressive strength measured after 28 days and 90 days of curing for CSA-based concretes as confirmed by comparing **Figure 3.21c** with **Figure 3.21a**.

According to the results shown in **Figure 3.21a-c**, the addition of CaO induced a slight decrease of compressive strength by comparing the compressive strength between concretes with SL05 NF and SL05 NF+CaO binders.

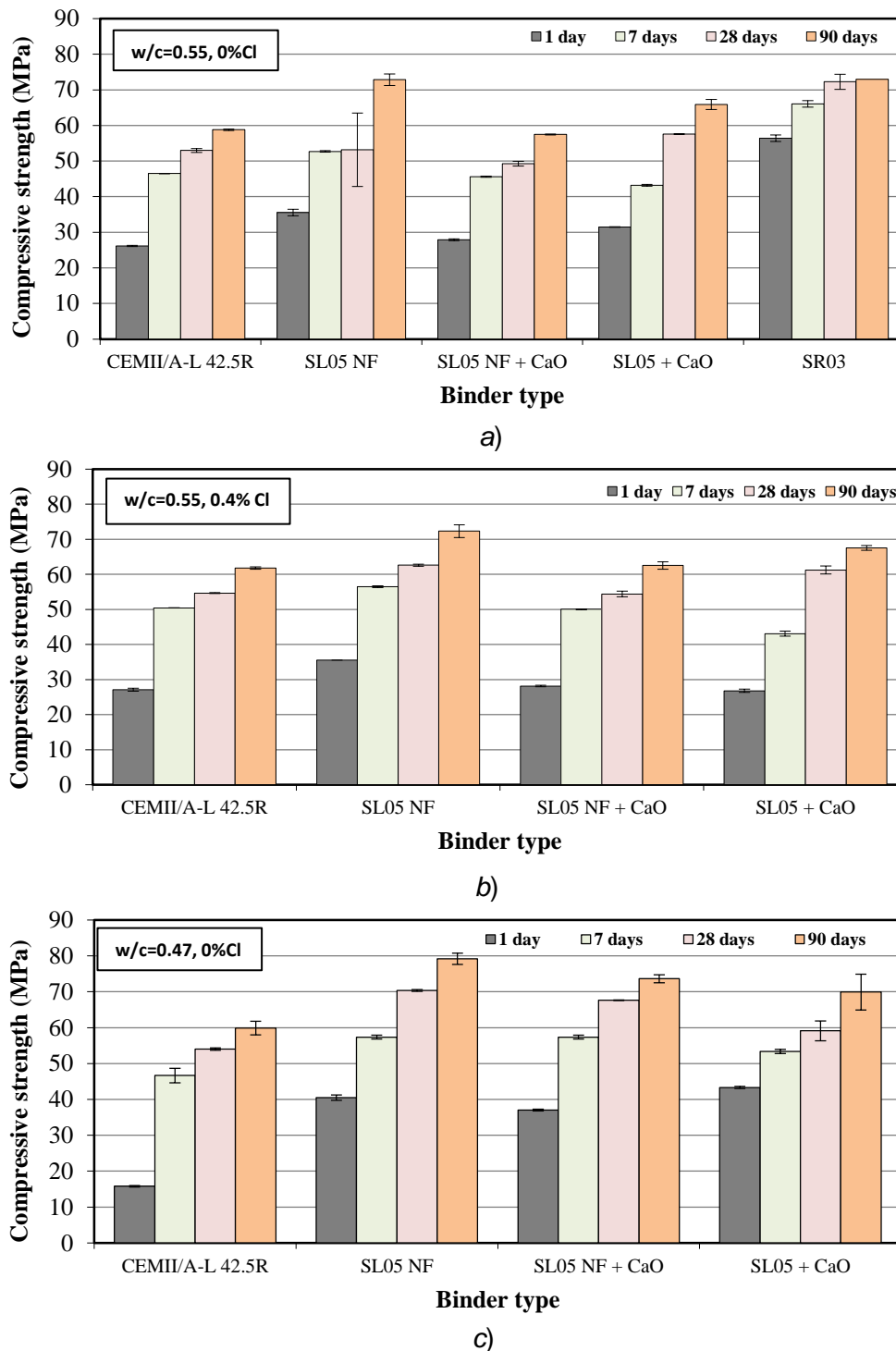


Figure 3.21 Compressive strength (average value of two replicate specimens) of reference concrete and CSA-based concretes a) $w/c=0.55$, chloride-free, b) $w/c=0.55$, 0.4% chloride and c) $w/c=0.47$, chloride-free in terms of curing age.

Figure 3.22 shows the dynamic elastic modulus of CSA-based concretes. After 1 day curing, the dynamic elastic modulus of CSA-based concretes (24~32 GPa) was slightly higher than that of reference concrete (21~25 GPa). For all mixtures, dynamic elastic modulus increased as a function of curing time.

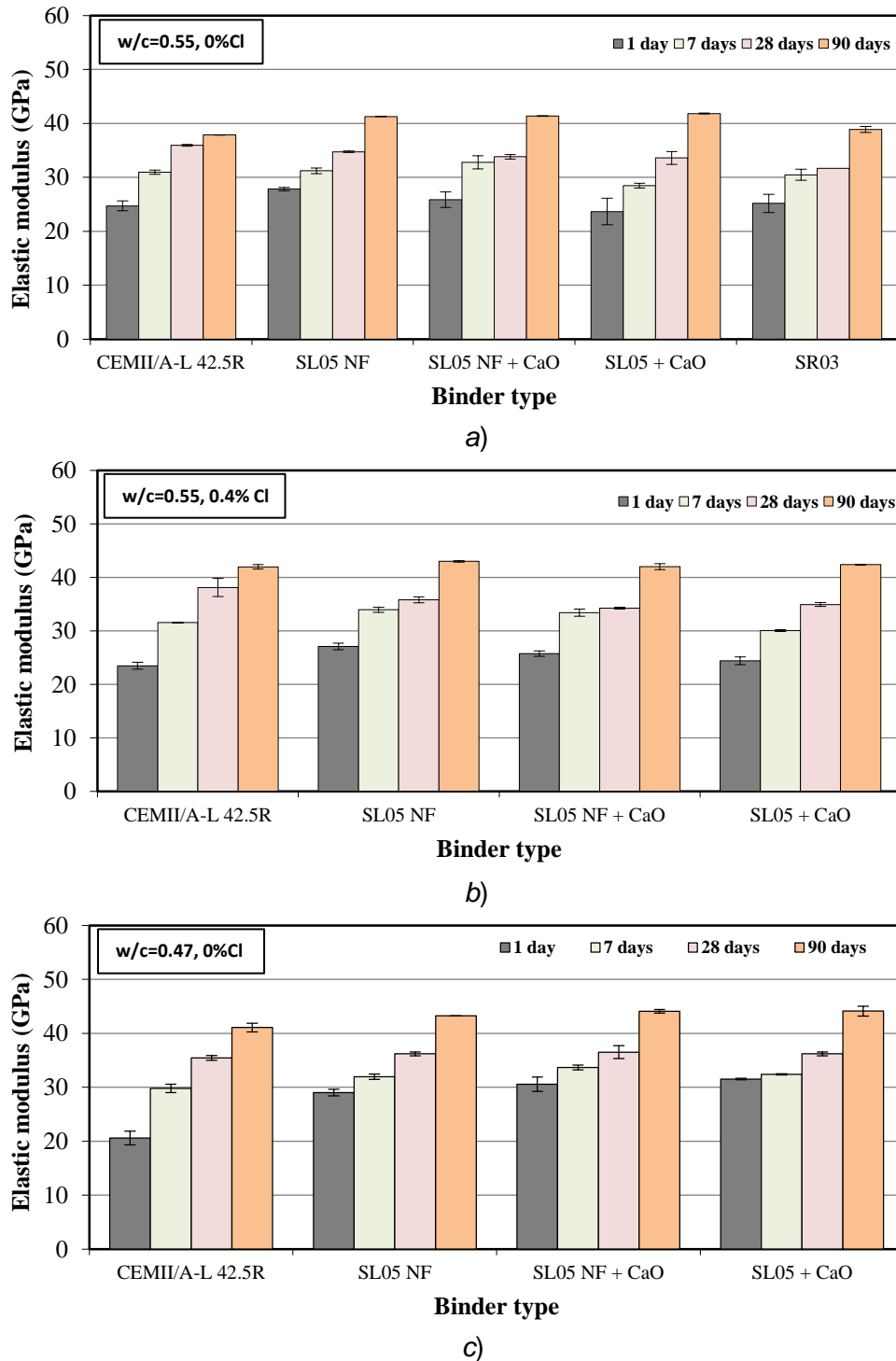


Figure 3.22 Dynamic elastic modulus (average value of two replicate specimens) of reference concrete and CSA-based concretes a) w/c=0.55, chloride-free, b) w/c=0.55, 0.4% chloride and c) w/c=0.47, chloride-free in terms of curing age.

SEM observations

SEM observation and EDS analysis of reference concrete and CSA-based concretes with w/c ratio of 0.55 without chloride added were carried out on samples collected from cube specimens cured for 1, 7 and 28 days. For reference concrete, SEM observation was only performed on sample after 28 days curing. For concrete made with pure CSA cement, SEM observation was only conducted on sample after 1 day curing. All SEM observations carried out on the studied mixtures are reported in **Appendix A**.

Figure 3.23a shows the microstructure of reference concrete after 28 days curing. It can be observed that this concrete has the typical microstructure due to the formation of hydration products of Portland limestone cement. EDS analysis (**Figure 3.23b**) shows mainly the common elements of the hydration products (calcium, oxygen and silicon in major amounts, in addition to magnesium, sulphur, aluminium and potassium).

Figure 3.24 shows the SEM images and EDS analyses of concrete made with pure CSA cement (SR03) after 1 day of moist curing. In **Figure 3.24a**, it can be seen an air-void inside the concrete sample, whilst the part surrounding it appears very compact. At higher magnification (**Figure 3.24b**), it can be observed that the inner of air-void showed with lots of fine needle-like particles with the typical morphology of ettringite; it can also be seen some cracks inside the air-void. Three EDS analyses were performed in the spots shown in **Figure 3.24a**. The EDS results (**Figure 3.24c-e**) reveal the prevalent calcium (Ca), aluminium (Al) and oxygen (O); but also the significant presence of sulphur (S) specially inside the air-void as configuration of calcium sulfoaluminate nature of the cement. Trace amounts of silicon (Si), iron (Fe), carbon (C) and magnesium (Mg) minerals was also observed. For comparison with reference concrete (**Figure 3.23a**), it can be observed that pure CSA concrete has different morphology and chemical composition (**Figure 3.24**). A more compacted microstructure for CSA concrete (**Figure 3.24b**) the day after casting was observed with respect of limestone concrete after 28 days of curing (**Figure 3.23a**).

Figure 3.25 shows the SEM images and EDS analyses of CSA-based concretes made with different sulfoaluminate cements after 1 day of curing. It can be observed that CSA-based concretes have similar morphology to pure CSA concrete one day after casting, with a lot of needle-like particles. Based on EDS results, it was found that the Al/Ca ratio of CSA-based concretes was intermediate between that of reference concrete and that of pure CSA concrete (SR03). Besides, more compacted pastes of CSA-based cements after 28 days of moist curing were observed, as shown in **Appendix A**.

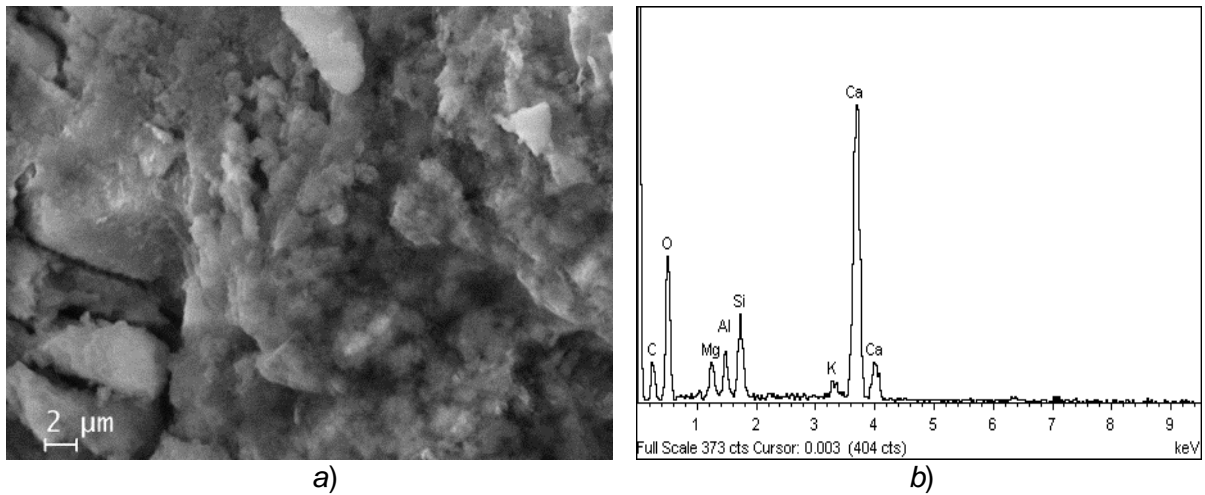


Figure 3.23 SEM image a) and EDS analysis b) of reference concrete made with CEM II/A-L 42.5R ($w/c=0.55$), after 28 days of moist curing.

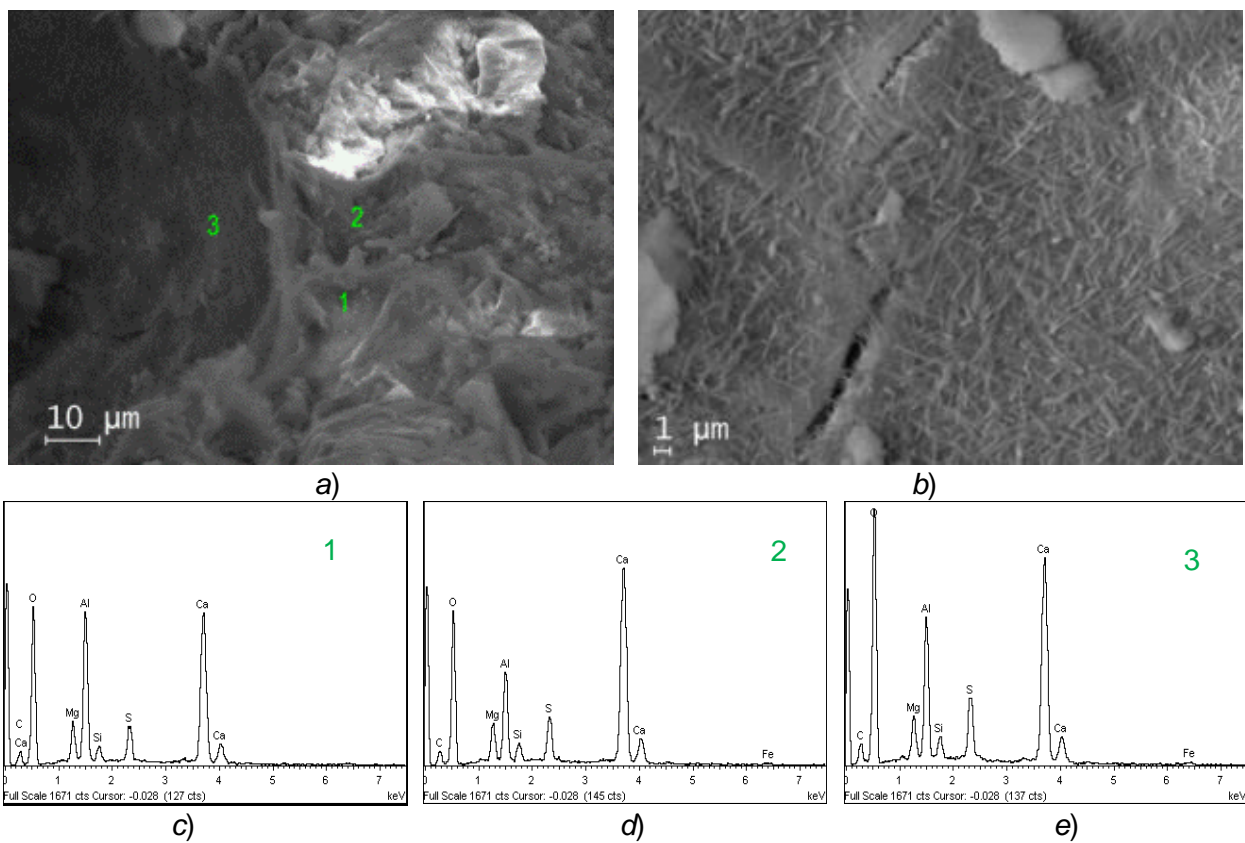


Figure 3.24 SEM images a) and b) at different magnifications and EDS analyses c), d) and e) for concrete made with SR03 binder ($w/c=0.55$), after 1 day of moist curing.

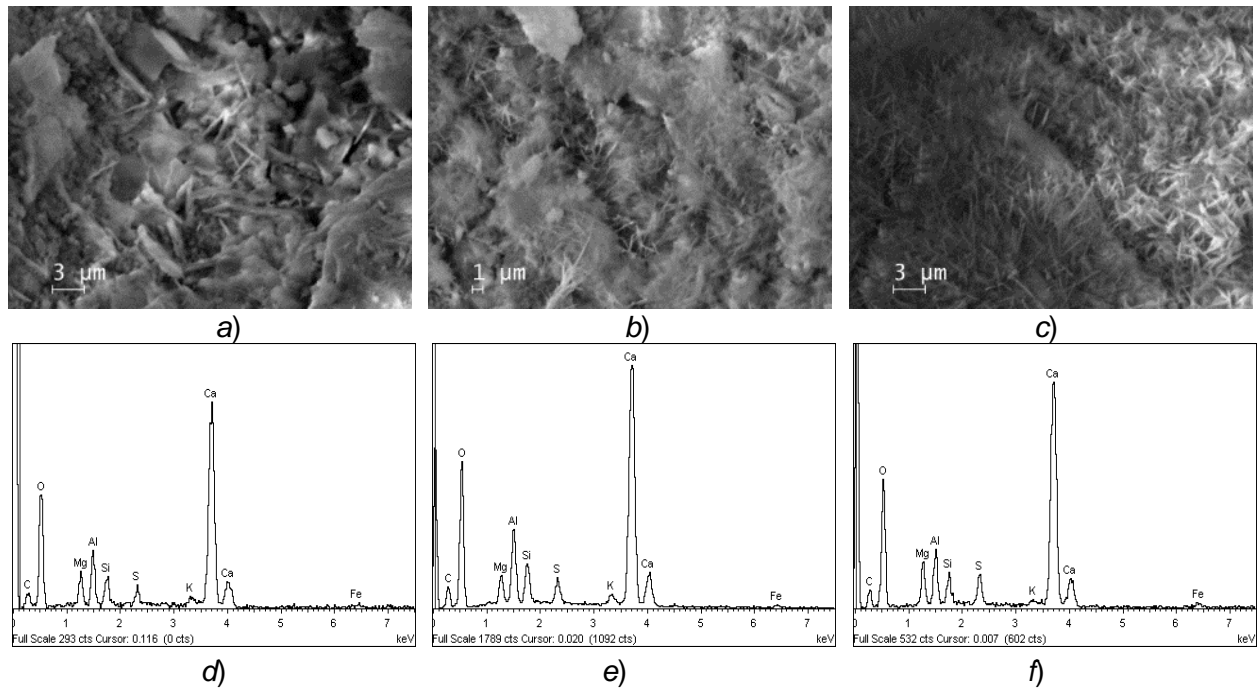


Figure 3.25 SEM images and EDS analyses of CSA-based concretes ($w/c=0.55$) made with *a)* and *d)* SL05 NF binder, *b)* and *e)* SL05 NF+CaO binder and *c)* and *f)* SL05+CaO binder, after 1 day of moist curing.

Electrical resistivity

Figure 3.26a and **Figure 3.26c** highlight the electrical conductance of reference concrete and CSA-based concretes respectively with w/c ratios of 0.47 and 0.55 under self-desiccation condition as function of time since the first hours of curing. A peak in conductance can be observed in all types of concrete during the first 24 hours. Reference concrete showed a much wider peak (around 3.5 hours) than that of CSA-based concretes which with their fast kinetics during hydration process led to a narrow peak already after 1 hour. Few days after mixing, the value of conductance of all concretes was so small that the difference between them was negligible. In order to analyse the long-term difference, the electrical conductance of all concretes was converted into electrical resistivity through **Equation 2.2**. The results obtained in terms of electrical resistivity of reference concrete and CSA-based concretes are shown in **Figure 3.26b** and **Figure 3.26d**. Reference concrete showed lower resistivity than that of CSA-based concretes; SL05NF concrete showed an intermediate trend compared to reference concrete and CSA-based concretes added with CaO. In the case of w/c ratio of 0.47, as shown in **Figure 3.26b**, SL05+CaO concrete showed the highest resistivity whereas in the case of w/c ratio of 0.55, as shown in **Figure 3.26d**, SL05 NF+CaO concrete was the best.

CSA-based concretes at both w/c ratios 0.47 and 0.55 immersed into water also exhibited much higher resistivity over time when compared to reference concrete (**Figure 3.27**). At both w/c ratios,

SL05 NF+CaO concrete showed the highest resistivity over others, reaching values until 250 $\Omega\cdot\text{m}$ and 150 $\Omega\cdot\text{m}$ respectively in case of w/c ratios of 0.47 and 0.55.

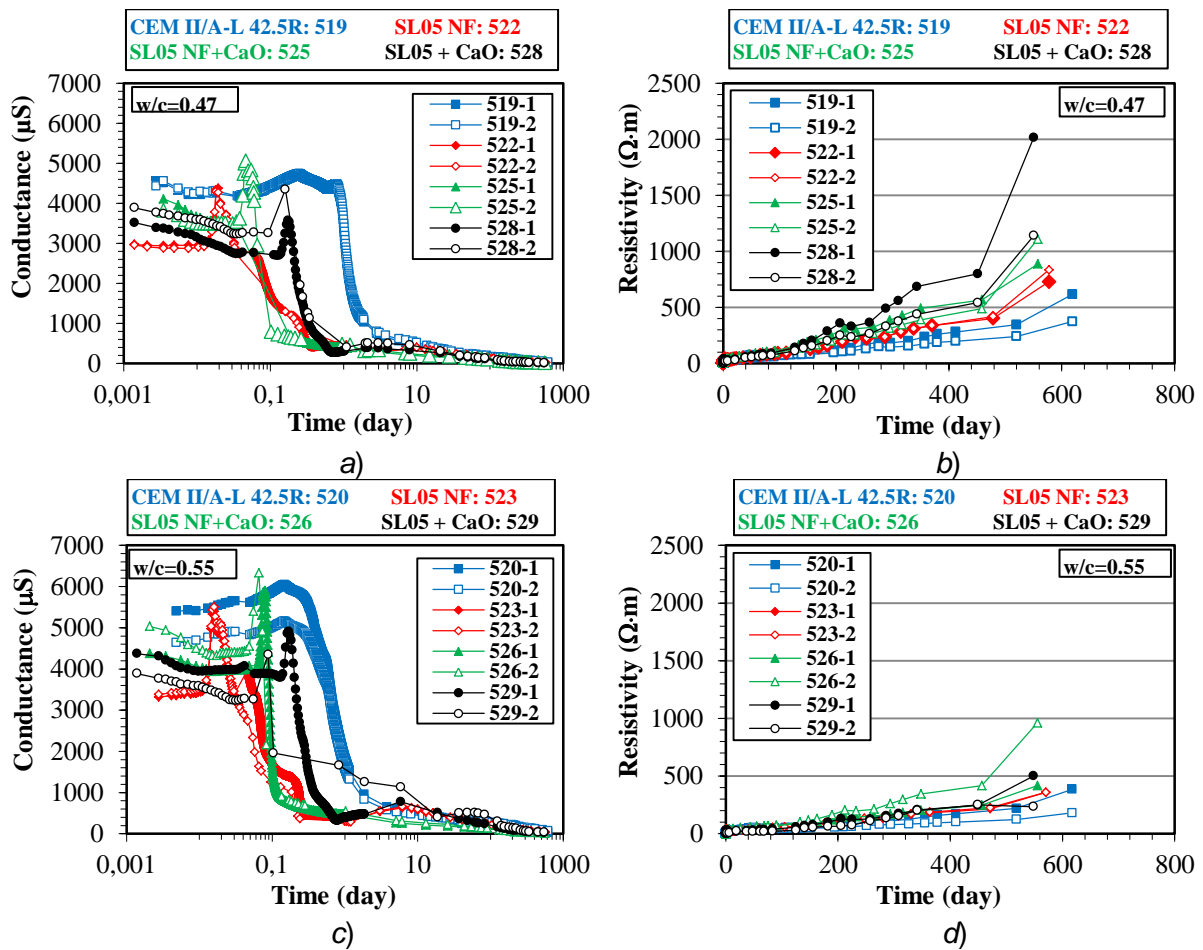


Figure 3.26 Time evolution of conductance of reference concrete and CSA-based concretes with w/c=0.47 a) and w/c=0.55 c) concretes under self-desiccation condition (at 23°C), respectively corresponding to b) and d) which represent the time evolution of inverse of concrete conductance.

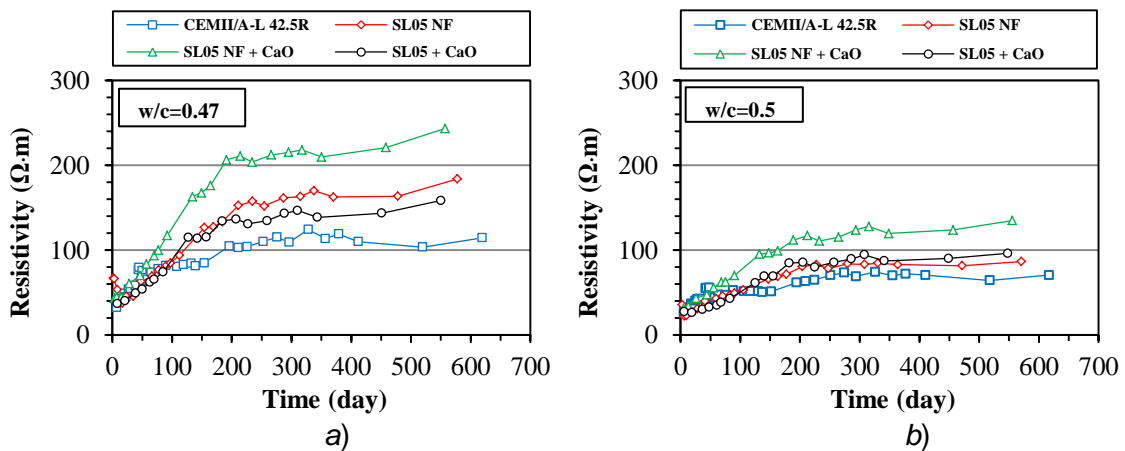


Figure 3.27 Evolution of resistivity (average value of two replicate specimens) of reference concrete and CSA-based concretes with a) w/c=0.47 and b) w/c=0.55 under water immersion condition over time.

Capillary absorption and water absorption

Capillary absorption of reference concrete and CSA-based concretes ($w/c = 0.47$ and 0.55) was monitored within 24 hours and the results are shown in **Figure 3.28**. It can be observed that the water uptake of reference concrete was higher than that of CSA-based concretes. In the case of w/c ratio of 0.47 , as shown in **Figure 3.28a**, at the end of capillary absorption test, the water uptake of reference concrete reached around 2.5 kg/m^2 , while the water uptake of CSA-based concretes ranged between 1.5 and 2 kg/m^2 . In the case of w/c equal to 0.55 (**Figure 3.28b**), the water uptake of reference concrete reached around 4 kg/m^2 at the end of capillary absorption test, while the water uptake of CSA-based concretes was about 3 kg/m^2 .

Figure 3.29 shows the water absorption of all types of concrete with w/c ratios of 0.47 and 0.55 totally immersed in water. It can be noted that CSA-based concretes absorbed slightly more water than reference concrete. The differences between CSA-based concretes were not significant.

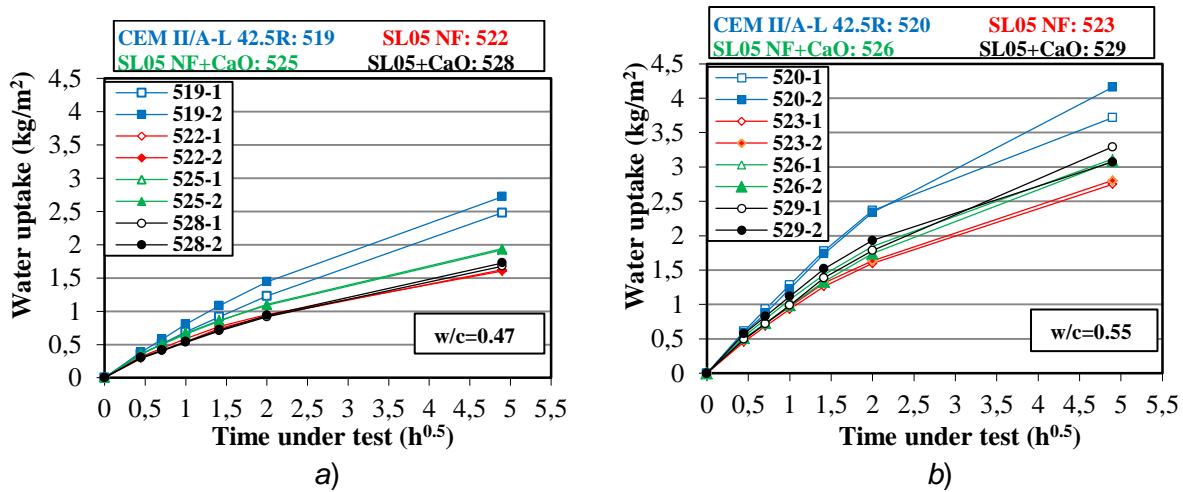


Figure 3.28 Capillary absorption of reference concrete and CSA-based concretes with a) $w/c=0.47$ and b) $w/c=0.55$.

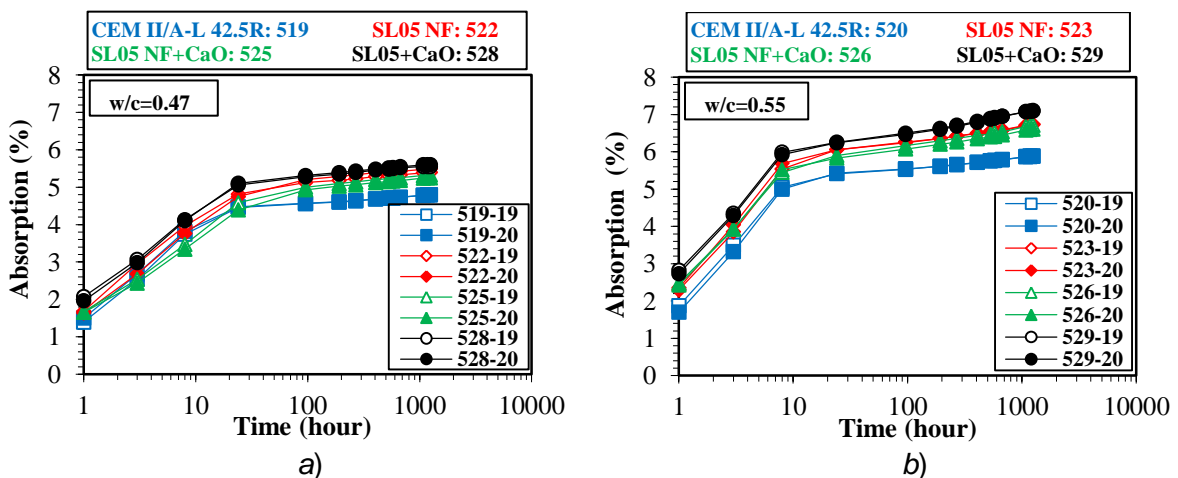


Figure 3.29 Water absorption of reference concrete and CSA-based concretes (totally immersed in tap water) with a) $w/c=0.47$ and b) $w/c=0.55$.

Penetration of carbonation

Figure 3.30 shows the carbonation depth (in natural conditions) as a function of time for all concretes studied, different binder type, w/c ratio (0.47 and 0.55) and curing time (7 days and 28 days). It can be noted that SL05+CaO concrete showed higher carbonation depth regardless of w/c ratio and curing time. In the case of w/c equal to 0.47, SL05 NF concrete performed the best carbonation resistance. Carbonation resistance of CSA-based concretes was susceptible to curing time; longer curing time was helpful to improve carbonation resistance. In the case of w/c ratio of 0.55, reference concrete performed the best carbonation resistance. Carbonation resistance of both SL05NF concrete and SL05 NF+CaO concrete was susceptible to curing time.

Table 3.5 reports the carbonation depth measured on all concretes (w/c = 0.47 and 0.55) cured for 28 days and subjected to accelerated carbonation (4.0% CO₂, 65 ± 5% R.H. and 20 ~ 23°C) for 70 days. SL05+CaO concrete showed the worst carbonation resistance, whose carbonation depth reached 21 mm at both w/c ratios (0.47 and 0.55). SL05NF concrete and reference concrete had the similar carbonation resistance and they were slightly influenced by the change of w/c.

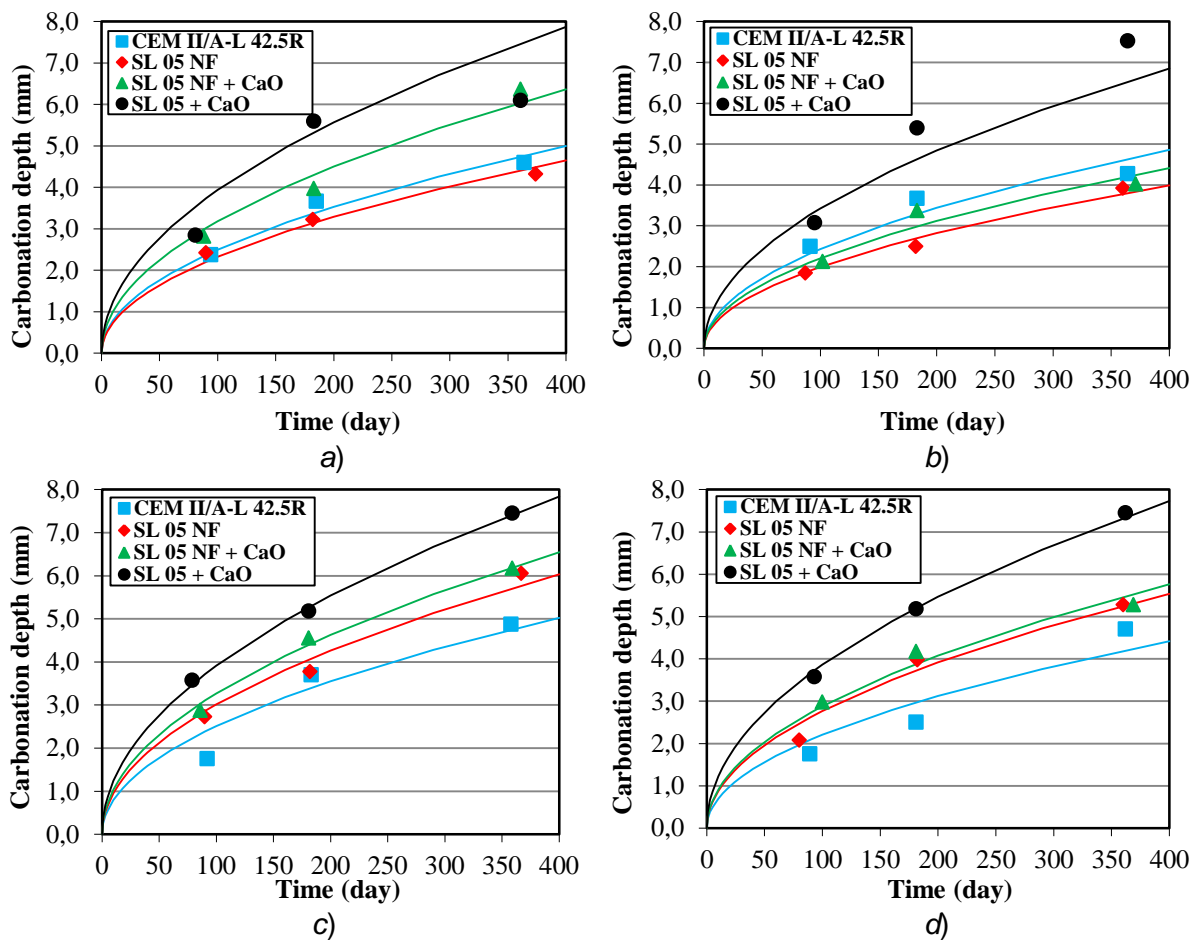


Figure 3.30 Time evolution of carbonation depth of reference concrete and CSA-based concretes a) w/c=0.47, cured for 7 days, b) w/c=0.47, cured for 28 days, c) w/c=0.55, cured for 7 days and d) w/c=0.55, cured for 28 days under outdoor exposure.

Table 3.5 Average value of carbonation depth of reference concrete and CSA-based concretes (accelerated carbonation test*).

Binder type	w/c=0.47	w/c=0.55
CEM II/A-L 42.5R	14.8	17.2
SL05 NF	15.6	17.5
SL05 NF + CaO	17.7	16.5
SL05 + CaO	20.6	20.7

* Around 70 days exposure in carbonation chamber (4% CO₂, 65 ± 5% R.H. and 20 ~ 23°C).

Chloride penetration

Figure 3.31 shows the chloride profiles carried out on all concretes studied (w/c = 0.47 and 0.55) immersed for 7 months in 3.5% NaCl solution. It can be observed that SL05+CaO concrete and reference concrete showed similar profile; the profile of SL05NF concrete was comparable with that of SL05 NF+CaO concrete. Both SL05 NF concrete and SL05 NF+CaO concrete showed better chloride penetration resistance at both w/c ratios when compared to SL05+CaO concrete and reference concrete.

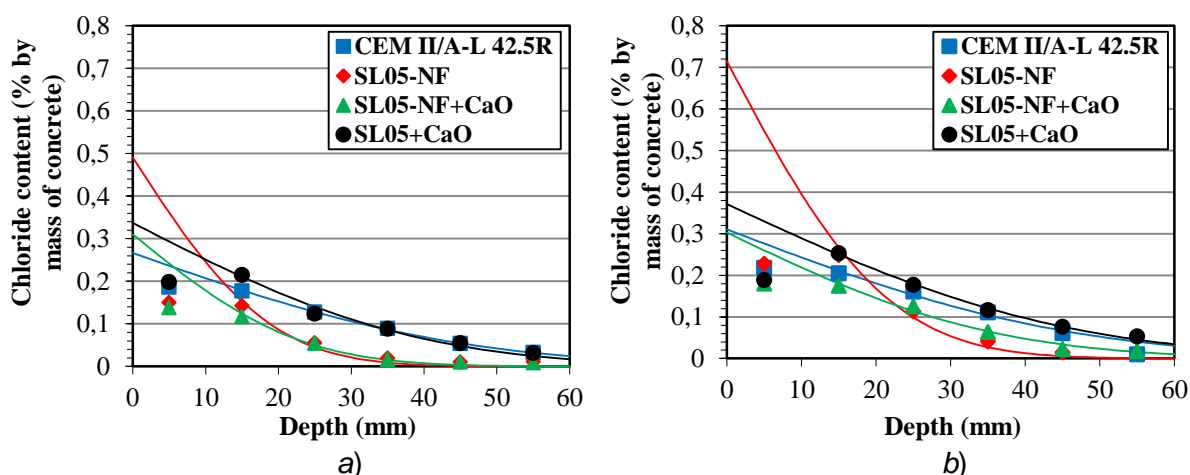


Figure 3.31 Chloride penetration profiles of reference concrete and CSA-based concretes with a) w/c=0.47 and b) w/c=0.55, after 7 months immersion in 3.5% NaCl solution.

pH measurements

At the end of electrochemical tests all reinforced specimens were splitted. The pH of concrete samples (one for each type of concrete) collected from the broken specimens was measured. In addition, the pH of reference mortar and CSA-based mortars (w/c=0.5) was tested at different curing ages. The results of pH measurements are shown in **Table 3.6** by distinguishing concrete samples (both alkaline and carbonated) and mortar samples. A pH value of about 10.9 was measured on concrete sample made with pure CSA cement (SR03); for the other types of alkaline concrete, it was around 12.5. Once carbonated, all concrete studied showed a pH value of 9.3 ~ 9.5, the typical value of carbonated concrete. **Table 3.6** shows also the results of pH measurements carried out on mortar samples in alkaline condition in order to evaluate the pH

evolution as a function of curing time. It can be noticed for all mortars, regardless of binder type, slightly higher values of pH in the first days after casting than that measured for prolonged curing. Subsequently, the pH of mortars cured for 28 days or more (145 days) reached values similar with that measured on comparable concrete samples.

Table 3.6 pH of reference concrete and CSA-based concretes and mortars.

Sample type	CEM II/A-L 42.5R	SL05 NF	SL05 NF+CaO	SL05+CaO	SR03	
Alkaline concrete (w/c=0.55)*	12.62	12.41	12.63	12.45	10.88	
Carbonated concrete (w/c=0.55)*	9.5	9.38	9.48	9.30	-	
Alkaline mortar (w/c=0.5)	1 day	12.82	12.62	12.79	12.45	11.52
	4 days	12.99	12.98	12.99	12.95	12.04
	7 days	13.05	13.02	13.07	12.97	12.07
	28 days	12.60	12.51	12.56	12.48	11.22
	145 days	12.78	12.60	12.58	12.40	11.41

*Derived from reinforced specimens after finishing all electrochemical tests.

3.3.2 Corrosion behaviour of steel embedded in CSA-based concretes

In order to investigate the passivation and corrosion behaviour of steel bars, including carbon steel and galvanised steel, embedded in CSA-based concretes and for comparison in reference concrete, electrochemical tests were carried out on both alkaline and carbonated reinforced specimens exposed to different environment conditions. The role of chloride added in mixture (0.4% by cement mass) was also considered.

3.3.2.1 Alkaline reinforced specimens

The alkaline reinforced specimens made with all types of mixture and studied with respect to two w/c ratios (0.47 and 0.55) were subjected after casting at self-desiccation condition (23°C), and subsequently were exposed into various conditions with different temperature (20°C or 40°C) and relative humidity (80% or 95%); finally, all alkaline reinforced specimens were immersed in tap water for 48 hours. The corrosion potential and corrosion rate of both carbon steel bar and galvanised steel bar embedded in these concretes were monitored during the whole test period; in addition, the potential of titanium electrode embedded in each reinforced specimen was recorded as well. For one of two w/c ratios (0.55), comparable reinforced specimens with addition of 0.4% chloride by mass of cement were also exposed for comparison at the same conditions.

Figure 3.32 shows the results of electrochemical tests on alkaline reinforced specimens made by ordinary concrete (with CEM II/A-L 42.5R cement) which was considered as reference.

Figure 3.32a shows that the corrosion potential of carbon steel bars increased gradually in self-desiccation period, reaching values above -200 mV vs SCE already few days later after casting as a confirmation of passive state; at the end of self-desiccation period, the corrosion potential of carbon steel bars ranged between 0 and 100 mV vs SCE. Subsequently, stable values of

corrosion potential were observed during exposure condition 20°C and 80% R.H.. After exposure at 20°C and 95% R.H., a decrease of corrosion potential of carbon steel bars towards -200 ~ -100 mV vs SCE was observed. Subsequently, a slight increase in corrosion potential (especially for concrete with w/c ratio of 0.55) took place when temperature was increased to 40°C. Only the corrosion potential of carbon steel bars in concrete with w/c ratio of 0.47 (specimens "519-1" and "519-2") showed a slight tendency towards a more negative potential during the exposure at 95% R.H.; anyway their corrosion potentials were maintained around -200 mV vs SCE. A confirmation of the corrosion potential measured at 20°C and 80% R.H. was obtained by repeating electrochemical tests in this condition after the exposure condition at 40°C and 95% R.H.. Even in immersion condition to which carbon steel bars embedded in ordinary concrete were exposed after the period of exposure at 20°C and 80% R.H., the corrosion potential values of all carbon steel bars were above -200 mV vs SCE. The addition of 0.4% of chloride in ordinary concrete did not affect significantly the corrosion potential of carbon steel bars; this amount of chloride did not allow corrosion initiation as confirmed in terms of corrosion potential which was above -200 mV vs SCE regardless of exposure conditions.

Galvanised steel bars showed an evolution of corrosion potential similar to that of carbon steel bars both in self-desiccation and 20°C and 80% R.H. conditions; only with a shift of around 200 mV at more negative values was observed. In the initial stage of the exposure condition at 20°C and 95% R.H., the corrosion potential of galvanised steel bars decreased quickly below -200 mV vs SCE and subsequently increased gradually during the rest of the whole test period. However, during immersion condition, galvanised steel bars showed a fall of corrosion potential, until around -650 mV vs SCE for galvanised steel bars in 0.47 w/c ratio concrete without chloride (specimen "519-Z1"), -440 and -550 mV vs SCE for galvanised steel bars in 0.55 w/c ratio concrete respectively with and without chloride (specimens "521-Z4" and "520-Z2"). In general, a corrosion potential of galvanised steel above -550 mV vs SCE was considered typical of passive condition [5].

As far as carbon steel bars are concerned, **Figure 3.32b** shows a progressive decrease of the corrosion rate during the self-desiccation condition, reaching values of 0.3 mA/m². By increasing the relative humidity and temperature, a slight increase in the corrosion rate was observed; anyway values of corrosion rate below 1 mA/m² were maintained, even in immersion condition as a confirmation of passive state. Also galvanised steel bars reached passivation condition in the self-desiccation period, showing values of corrosion rate around 0.1 mA/m². By comparing with the measurements obtained on carbon steel bars, the corrosion rate of galvanised steel bars showed different evolution in time; it started increasing during the following 20°C and 80% R.H. exposure condition and continued to increase during the subsequent 20°C and 95% R.H. exposure condition, until reached values above 1 mA/m². Corrosion rate lower than 3 mA/m² was also

maintained during the exposure at 40°C and 95% R.H.. Only a decrease in terms of corrosion rate to values below 1 mA/m² was measured in the subsequent exposure condition 20°C and 80% R.H.. It can be observed that this decrease trend corresponds to the increase trend shown in **Figure 3.32a**. In immersion condition, galvanised steel bars show higher corrosion rate (above 1 mA/m²), which corresponds to lower corrosion potentials as mention before. The addition of 0.4% of chloride in ordinary concrete didn't affect significantly the corrosion rete of steel bars, which is in agreement with its effect on the corrosion potential of steel bars.

Also the potential of MMO activated titanium electrode (MMO-Ti) embedded in all mixtures made with ordinary cement (different for w/c ratio and chlorides content) was measured. The potential of this kind of electrode is known to be pH-dependent and sensitive to the changes of temperature and oxygen concentration. The potential of titanium electrodes in ordinary concrete (**Figure 3.32c**) showed some fluctuations during the whole exposure cycle, which is mainly due to the variations in humidity and the amount of oxygen availability close to titanium electrode embedded in concrete. At the beginning of self-desiccation period, the potential of almost all electrodes progressively increased between -100 and 0 mV vs SCE. Despite the variation of potential values, a steady trend of potential increase was observed during the rest of self-desiccation period and the subsequent 20°C and 80% R.H. exposure period. In the subsequent exposure conditions (at 20/40°C, 95% R.H., and 20°C and 80% R.H.), no significant change of potential was noticed.

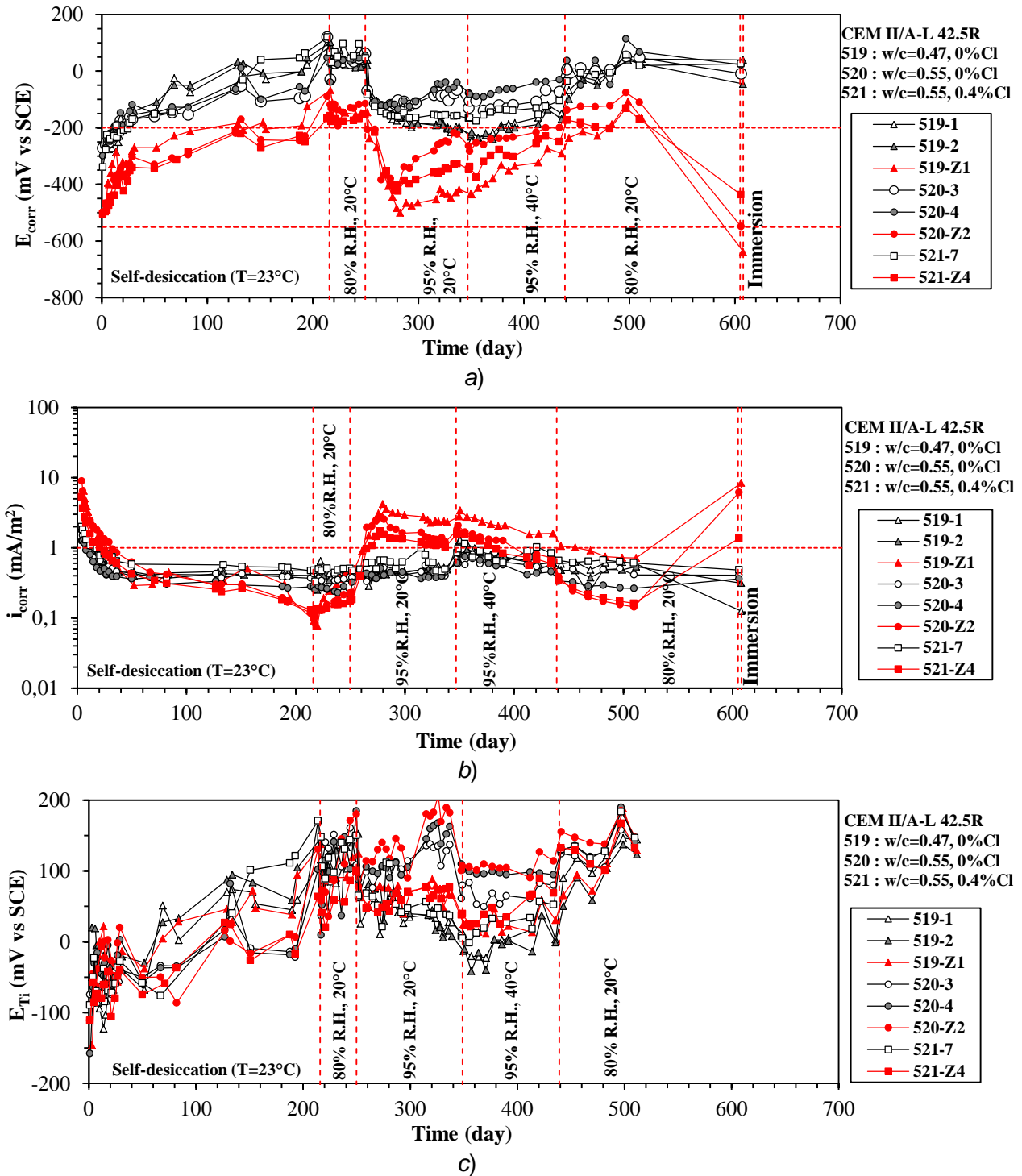


Figure 3.32 Monitoring of a) corrosion potential (E_{corr} vs SCE), b) corrosion rate (i_{corr}) and c) potential of titanium electrode (E_{Ti} vs SCE) of reinforced specimens made with ordinary cement (CEM II/A-L 42.5R) during exposure conditions at different relative humidity (R.H.) and temperature. (Reinforced specimens with carbon and galvanised steels are indicated respectively with black and red symbols)

Figure 3.33 shows the results of electrochemical tests on alkaline reinforced specimens made by SL05 NF cement.

The corrosion potential of carbon steel bars (**Figure 3.33a**) increased gradually in self-desiccation period and reached -200 mV vs SCE few days after casting; at the end of self-desiccation period, the potential of carbon steel bars in SL05 NF concretes reached 0 mV vs SCE. These potential were almost maintained in the subsequent exposure conditions. However, during the exposure at 40°C and 95% R.H., the corrosion potential of carbon steel bars in 0.55 w/c ratio concrete without chloride (specimens “523-3” and “523-4”) reached values slightly lower than -200 mV vs SCE. Then the potential of carbon steel bars started increasing slowly in the rest of this period. In the repeated exposure condition at 20°C and 80% R.H., the potential of carbon steel bars increased slowly to values around 0 mV vs SCE which were maintained their potentials also in immersion condition. The corrosion potential of galvanised steel bars (**Figure 3.33a**) showed very low values ranging between -800 and -700 mV vs SCE after casting.

In comparable mixtures, the corrosion potential of galvanised steel bars increased gradually in self-desiccation period, reaching around -400 mV vs SCE at the end of self-desiccation period. Some fluctuations of corrosion potential were showed during the subsequent exposure condition at 20°C and 80% R.H., although corrosion potential was maintained above -400 mV vs SCE. After exposure to 20°C and 95% R.H., the corrosion potential of galvanised steel bars decreased progressively at values around -700 mV vs SCE in 20 days. Subsequently, the corrosion potential of galvanised steel bars increased slowly in the rest of the whole test period and reached -550 mV vs SCE at the beginning of repeated condition at 20°C and 80% R.H.. In immersion condition, the corrosion potential of galvanised steel bars maintained their potential values slightly higher than -550 mV vs SCE. The addition of 0.4% of chloride in SL05 NF concretes didn't affect significantly the corrosion potential of both carbon steel bars and galvanised steel bars.

Figure 3.33b shows that the corrosion rate of carbon steel bars in SL05 NF concrete was slightly higher than 1 mA/m² after casting. During the self-desiccation period, few days after casting, the corrosion rate of carbon steel bars reached a stable value around 0.5 mA/m² that lasted throughout the rest of the whole exposure period, even in immersion condition. Galvanised steel bars showed high corrosion rate (around 10 mA/m²) after casting and subsequently, decreased quickly, showing as low as the corrosion rate of carbon steel bars at the later stage of self-desiccation period. The low corrosion rate state was maintained during the following exposure condition at 20°C and 80% R.H.. After exposure to 20°C and 95% R.H., the corrosion rate of galvanised steel bars increased progressively within 20 days till around 3.5 mA/m² and maintained in the rest of this cycle. Next, the corrosion rate of galvanised steel bars decreased gradually and again became lower than 1 mA/m²

in the following exposure condition at 40°C and 95% R.H. and the repeated condition at 20°C and 80% R.H., even in immersion condition.

The potentials of titanium electrodes in SL05 NF concretes (**Figure 3.33c**) increased slightly at the beginning of self-desiccation period and subsequently in the rest of self-desiccation period maintained stable values in the range between -100 and 0 mV vs SCE. Then the potential of almost all electrodes increased slightly during the subsequent exposure condition at 20°C and 80% R.H., but with pronounced fluctuation. In the following exposure condition at 20°C and 95% R.H., the potential of all electrodes showed a tendency of increase at the beginning, but subsequently the potential of two electrodes embedded in 0.47 w/c ratio concrete without chloride (specimens "522-1" and "522-2") fell down to around -100 mV vs SCE; in the rest of this exposure period, the potential of all electrodes maintained their own potentials. In the following exposure condition at 40°C and 95% R.H., the potential of those two electrodes in specimens "522-1" and "522-2" increased whereas the potential of the other electrodes decreased; therefore potentials of all electrodes converged in the range between -50 and 50 mV vs SCE. Finally, in the repeated exposure condition at 20°C and 80% R.H., the potential of electrodes increased slightly, reaching 0 mV vs SCE.

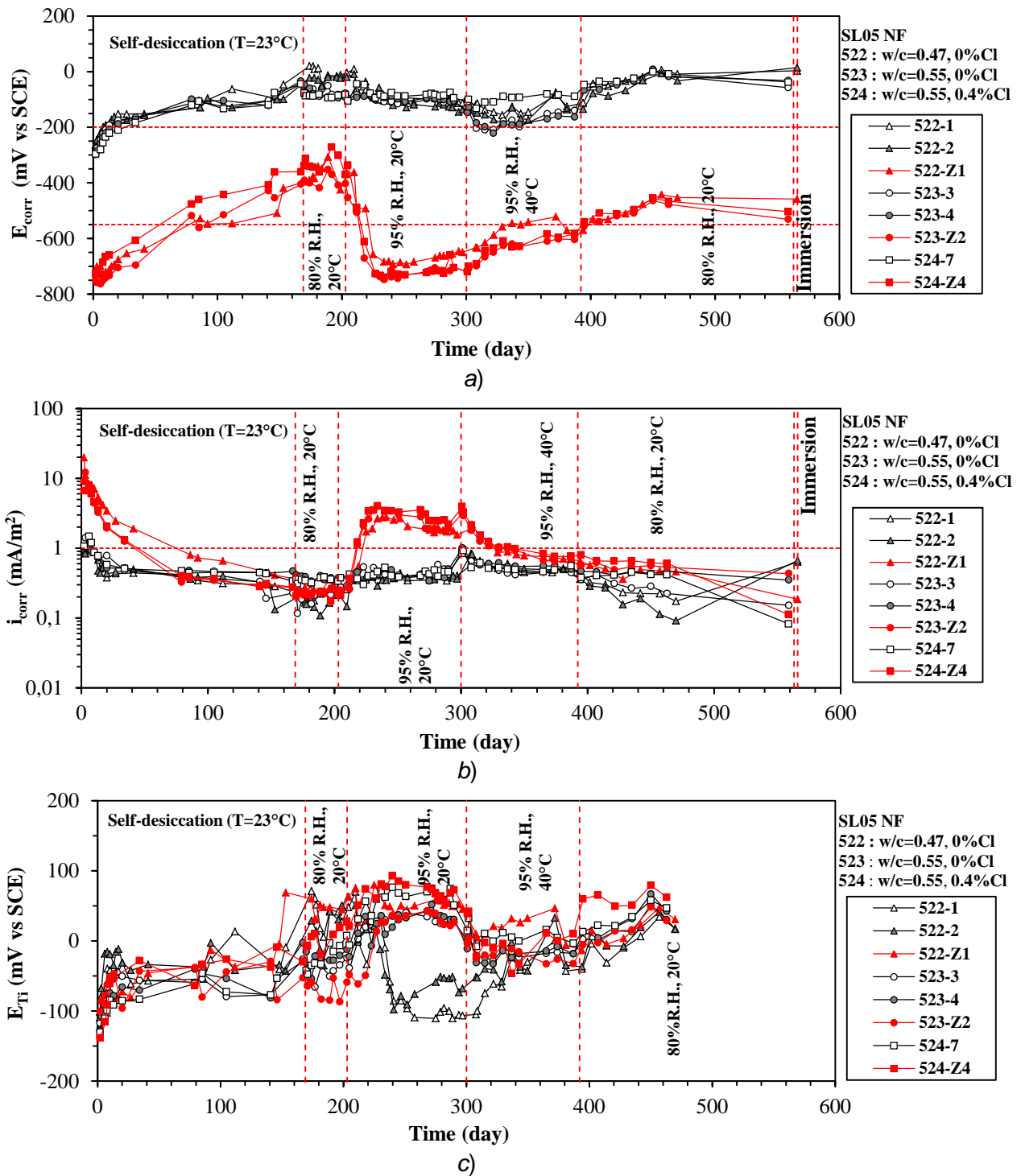


Figure 3.33 Monitoring of a) corrosion potential (E_{corr} vs SCE), b) corrosion rate (i_{corr}) and c) potential of titanium electrode (E_{Ti} vs SCE) of reinforced specimens made with SL05 NF binder during exposure conditions at different relative humidity (R.H.) and temperature. (Reinforced specimens with carbon and galvanised steels are indicated respectively with black and red symbols)

Figure 3.34 shows the results of electrochemical tests on alkaline reinforced specimens made by SL05 NF cement with the addition of CaO.

The evolution in time of corrosion potential of both carbon steel and galvanised steel bars (**Figure 3.34a**) embedded in SL05 NF+CaO concretes was very similar to that shown in **Figure 3.33a**, except that galvanised steel bars embedded in concrete with w/c ratio of 0.55 (specimens “526-Z2” and “527-Z4”) showed a significant fell of potential, being around -700 mV vs SCE in immersion condition.

Figure 3.34b shows the evolution in time of corrosion rate of both carbon steel bars and galvanised steel bars, which is very similar to the trend shown in **Figure 3.33b** (i.e. in SL05 NF mixtures); only the corrosion rates of galvanised steel bars in 0.55 w/c ratio concrete with and without chloride (specimens “526-Z2” and “527-Z4”) in immersion condition reached values of around 2 mA/m²; slightly higher than that measured in SL05 NF mixtures. The corrosion rate of galvanised steel bars in specimens “526-Z2” and “527-Z4” was higher than 2 mA/m², in fact, which corresponds to corrosion potential values lower than -550 mV vs SCE as shown in **Figure 3.34a**.

The trend of potential of titanium electrodes embedded in SL05 NF+CaO concretes (**Figure 3.34c**) was similar to the trend shown in **Figure 3.33c**; except that the potential of these two electrodes embedded in 0.47 w/c ratio concrete without chloride (specimens “525-1” and “525-2”) did not show different trend with that of the other electrodes during the 20°C and 95% R.H. exposure condition.

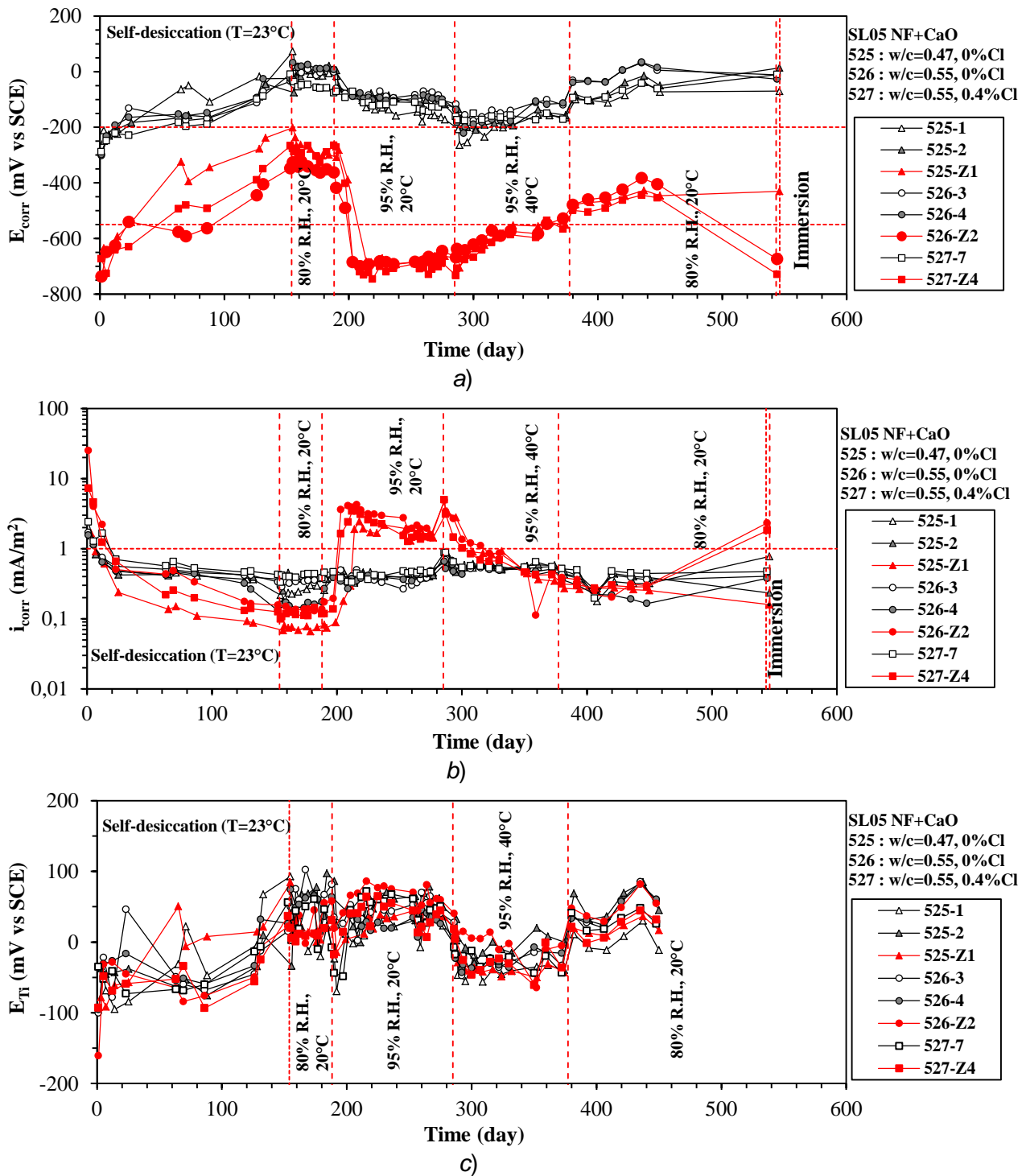


Figure 3.34 Monitoring of a) corrosion potential (E_{corr} vs SCE), b) corrosion rate (i_{corr}) and c) potential of titanium electrode (E_{Ti} vs SCE) of reinforced specimens made with SL05 NF+CaO binder during exposure conditions at different relative humidity (R.H.) and temperature. (Reinforced specimens with carbon and galvanised steels are indicated respectively with black and red symbols)

Figure 3.35 shows the results of electrochemical tests on alkaline reinforced specimens made by SL05 cement with the addition of CaO.

It can be noticed that the evolution in time of corrosion potential of carbon steel bars in SL05+CaO concretes (**Figure 3.35a**) was very similar with the evolution in time of corrosion potential of carbon steel bars in SL05 NF+CaO concretes (**Figure 3.34a**). Likewise, the potential of galvanised steel bars in SL05+CaO concretes showed the similar trend as in reference ordinary concrete, except that the potential value of reinforced specimen “530-Z4” was around -350 mV vs SCE in immersion condition .

The evolution in time of corrosion rate of both carbon steel bars and galvanised steel bars (**Figure 3.35b**) is very similar with that in **Figure 3.34b** (i. e. in SL05 NF+CaO mixtures); only the corrosion rate of galvanised steel bar in reinforced specimen “530-Z4” increased up to around 5 mA/m² in the beginning of exposure condition at 40°C and 95% R.H.; the corrosion rate of all steel bars were below 1 mA/m² in immersion condition.

Figure 3.35c shows the potential of titanium electrodes embedded in SL05+CaO concretes. It can be noticed that the trend of potential of titanium electrodes embedded in SL05+CaO concretes was similar to the potential of titanium electrodes embedded in SL05 NF+CaO concretes (**Figure 3.34c**).

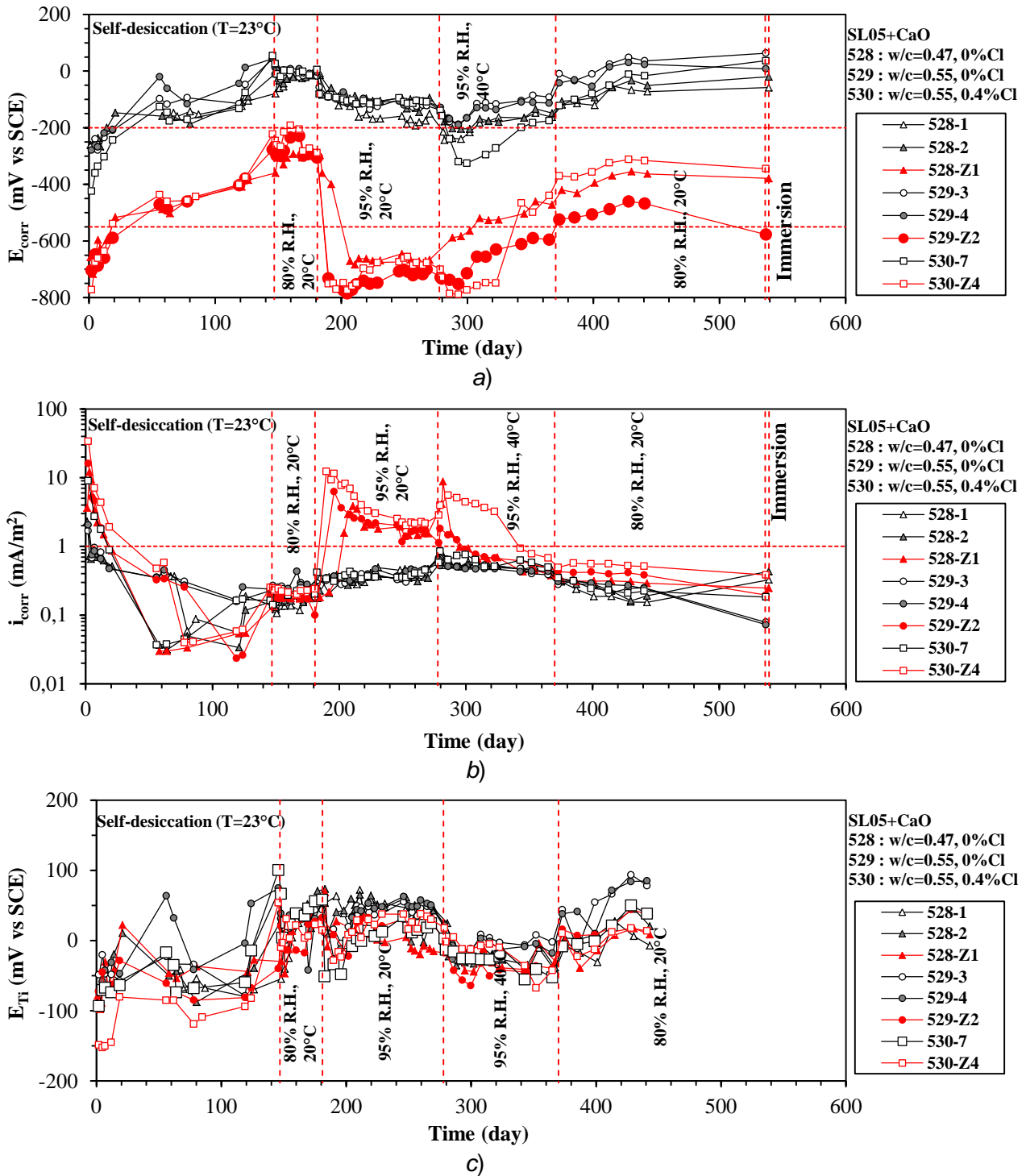


Figure 3.35 Monitoring of a) corrosion potential (E_{corr} vs SCE), b) corrosion rate (i_{corr}) and c) potential of titanium electrode (E_{Ti} vs SCE) of reinforced specimens made with SL05+CaO binder during exposure conditions at different relative humidity (R.H.) and temperature. (Reinforced specimens with carbon and galvanised steels are indicated respectively with black and red symbols)

Figure 3.36 shows the results of electrochemical tests on alkaline reinforced specimens made with SR03 cement (pure CSA).

The corrosion potential of carbon steel bars in SR03 concretes (**Figure 3.36a**) was around -200 mV vs SCE after casting and increased slowly, reaching the value around -130 mV vs SCE at the end of self-desiccation period. Subsequently, a very stable potential was observed during the subsequent exposure conditions at 20°C (80% and 95% R.H.). In immersion condition, the corrosion potential of all carbon steel bars fell down to around -450 mV vs SCE. Galvanised steel bars showed a trend similar to corrosion potential of carbon steel bars but with a reduction of around 400 mV in terms of potential during the whole exposure cycle, except that the reinforced specimen “532-Z4” with respect to galvanised steel bar showed a fall of potential (around 100 mV) during the exposure condition at 20°C and 95% R.H..

Figure 3.36b shows the corrosion rate of carbon steel bars which was slightly higher than 1 mA/m² after casting and subsequently decreased. Until the middle of self-desiccation period, when the corrosion rate of carbon steel bars increased again and reached close to 1 mA/m² at the end of self-desiccation period. Subsequently, the stable corrosion rates (slightly lower than 1 mA/m²) were maintained during the following exposure condition at 20°C and 80% R.H., but a slight decrease was observed in the subsequent exposure condition at 20°C and 95% R.H.. In immersion condition, the corrosion rate of carbon steel bars was slightly lower than 1 mA/m². Galvanised steel bars showed high corrosion rate (around 6 mA/m²) after casting and decreased quickly during the self-desiccation period, being around 0.1 mA/m² at the end of self-desiccation period. The low corrosion rate state was maintained during the following exposure condition at 20°C and 80% R.H.. In the subsequent exposure condition at 20°C and 95% R.H., the corrosion rate of galvanised steel bars increased gradually, but did not reach 1 mA/m². In immersion condition, the corrosion rates of galvanised steel bars was slightly higher than 1 mA/m².

The potential of titanium electrodes embedded in SR03 concretes (**Figure 3.36c**) ranged between -100 and -50 mV vs SCE after casting and soon reached around -50 mV vs SCE. Subsequently, the potential of all electrodes maintained also in the subsequent exposure condition at 20°C and 80% R.H.. The potential of all electrodes increased up to around 0 mV vs SCE in exposure condition at 20°C and 95% R.H..

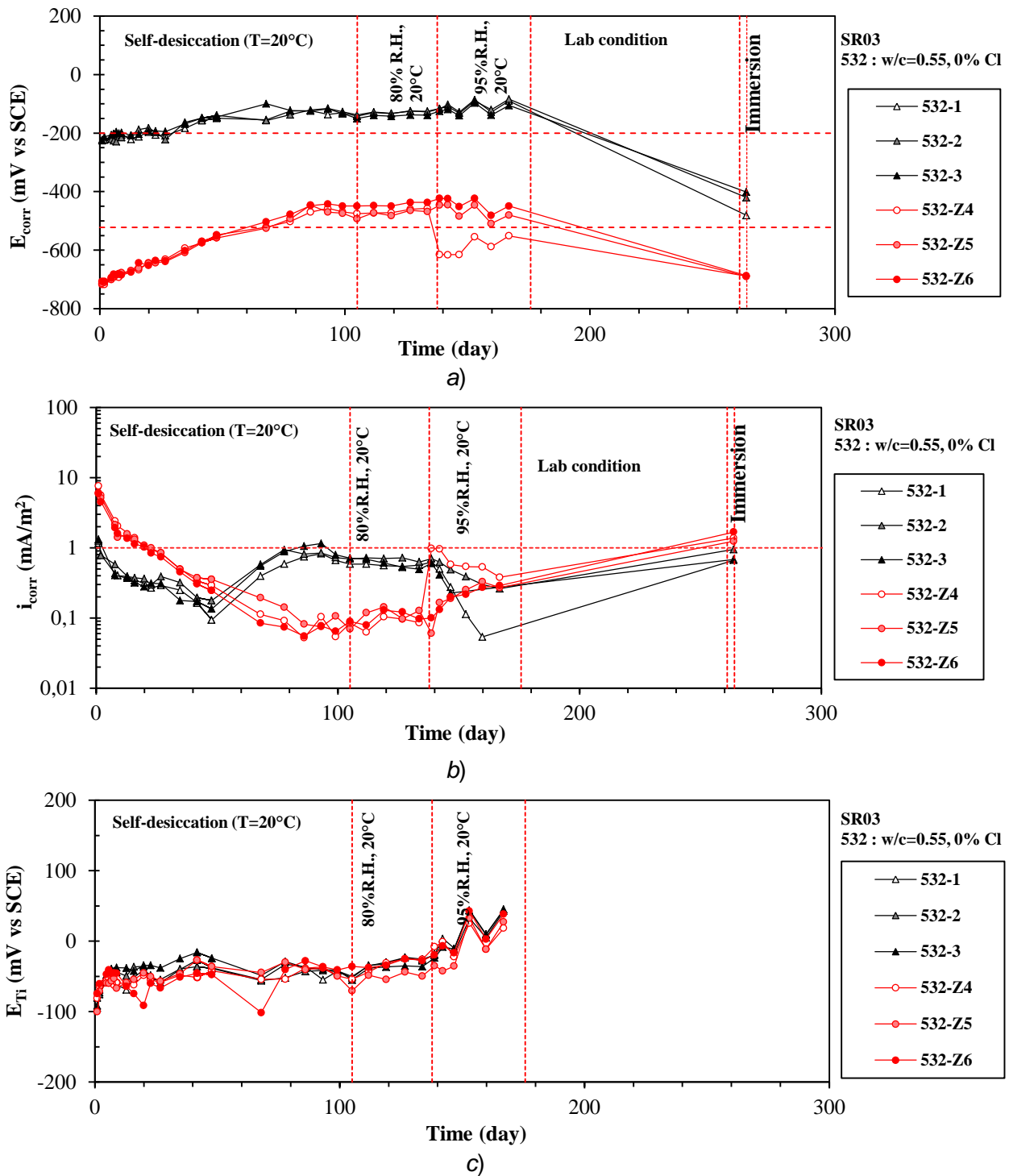


Figure 3.36 Monitoring of a) corrosion potential (E_{corr} vs SCE), b) corrosion rate (i_{corr}) and c) potential of titanium electrode (E_{Ti} vs SCE) of replicate reinforced specimens made with SR03 binder during exposure conditions at different relative humidity (R.H.) and temperature. (Reinforced specimens with carbon and galvanised steels are indicated respectively with black and red symbols)

3.3.2.2 Carbonated reinforced specimens

As far as this research is concerned, corrosion tests were also carried out on reinforced specimens subjected to accelerated carbonation for around 70 days after 7 days curing. In order to study the corrosion behaviour of both carbon steel and galvanised steel in carbonated CSA-based concretes ($w/c=0.55$) without or with chloride, the carbonated reinforced specimens were exposed to the same exposure conditions considered for comparable specimens in alkaline state. The corrosion potential and corrosion rate of both carbon steel and galvanised steel embedded in carbonated CSA-based concrete were monitored during the whole test period; in addition, the potential of titanium electrode embedded in carbonated CSA-based concrete was recorded as well.

Figure 3.37 shows the results of electrochemical tests on carbonated reinforced reference concrete made with ordinary cement (CEM II/A-L 42.5R).

As shown in **Figure 3.37a**, after 7 days curing, the corrosion potential of carbon steel bars (E_{corr} (vs SCE)) were around -280 mV vs SCE; after subsequent 70 days accelerated carbonation, the potential of carbon steel bars increased up to around 30 mV vs SCE, except for the specimen "521-8" (with 0.4% Cl) which showed a slight drop of corrosion potential (around 100 mV). If carbonation front has reached the steel bar and corrosion has initiated, the propagation stage of corrosion begins. Since the propagation time depends on the moisture content of concrete, all reinforced specimens were exposed to different humidity conditions. At the beginning of exposure to 20°C and 95% R.H., the corrosion potential of carbon steel bars quickly decreased to around -600 mV vs SCE by maintaining steady corrosion potential during the rest of this exposure condition and the subsequent condition at 40°C and 95% R.H.. In the following 20°C and 80% R.H. exposure condition, the corrosion potential of carbon steel bars increased gradually by reaching the limit of -200 mV vs SCE except for specimen "521-8" (with 0.4% Cl). In immersion condition, the corrosion potential of carbon steel bars in concrete without and with chloride (specimens "520-5", "520-6" and "521-8") were around -600 mV vs SCE.

Embedded in the same concrete, galvanised steel bars showed values of corrosion potential around -500 ~ -600 mV vs SCE and around 0 mV vs SCE respectively, before and after accelerated carbonation. At the beginning of 20°C and 95% R.H. exposure condition, the corrosion potential of galvanised steel bars steeply decreased to around -480 mV vs SCE in concrete without chloride (specimen "520-Z3") and to around -900 mV vs SCE in concrete with chloride (specimen "521-Z5"), and then maintained comparable lower potential during the rest of this exposure condition. The corrosion potential of the two galvanised steel bars increased gradually during the subsequent conditions at 40°C and 95% R.H. and at 20°C and 80% R.H., attaining -166 mV vs SCE for the former (specimen "520-Z3") and -529 mV vs SCE for the latter (specimen "521-Z5") at

the end of 20°C and 80% R.H. exposure condition. In immersion condition, their potential values reached around -800 mV vs SCE.

In terms of corrosion rate (i_{corr}), it can be observed (**Figure 3.37b**) that, after 7 days curing, the corrosion rate of carbon steel bars ranged between 1 and 2 mA/m²; after 70 days of accelerated carbonation, all reinforced specimens were exposed at 20°C and 95%R.H., as a consequence, the corrosion rate of carbon steel bars reached stable values of 4 and 20 mA/m² respectively in free-chloride concrete and in concrete with 0.4% of chloride. Comparable values of corrosion rate was maintained when temperature was increased from 20°C to 40°C (95% R.H.). It can be observed that the corrosion rate decreased below 1 mA/m² as the temperature and humidity decreased to 20°C and 80% R.H. except for carbon steel embedded in concrete with 0.4% of chloride (2~3 mA/m²). In immersion condition, the corrosion rate of specimens “520-5” and “520-6” (without chloride) were around 15 mA/m², whereas for carbon steel embedded in concrete with chloride, corrosion rate reached value around 30 mA/m².

After 7 days curing, the corrosion rate of galvanised steel bars were around 2 mA/m²; after subsequent 70 days accelerated carbonation, the corrosion rate of galvanised steel bars decreased below 1 mA/m². Galvanised steel bar embedded in free-chloride carbonated concrete showed, when exposed at 20°C and 95% R.H., corrosion rate of 0.4 ~ 0.5 mA/m², lower than that of carbon steel in the same mixture and exposure condition. When temperature was increased from 20°C to 40°C, galvanised steel bar reached in steady condition with comparable values in terms of corrosion rate. Galvanised steel bar exposed at 20°C and 80% R.H. showed a further decreasing of corrosion rate until value of 0.04 mA/m² whereas in immersion condition, corrosion rate reached around 10 mA/m². Galvanised steel bar embedded in concrete with 0.4% of chloride (specimen “521-Z5”), maintained value higher than 1 mA/m² in all exposure conditions.

Figure 3.37c shows that potential of titanium electrodes ranged between -150 and 0 mV vs SCE, typical of alkaline condition in the first 7 days after curing. Due to accelerated carbonation, the potential of titanium electrodes which is known to be pH-dependent, increased up to 250 ~ 300 mV vs SCE, as confirmed by all specimens made with CEM II/A-L 42.5R cement. Since this electrode is also sensitive to the changes of temperature and oxygen concentration, its potential decreased to 0 ~ 100 mV vs SCE and 200 mV vs SCE when specimens were exposed at 95% R.H. and 80% R.H. respectively.

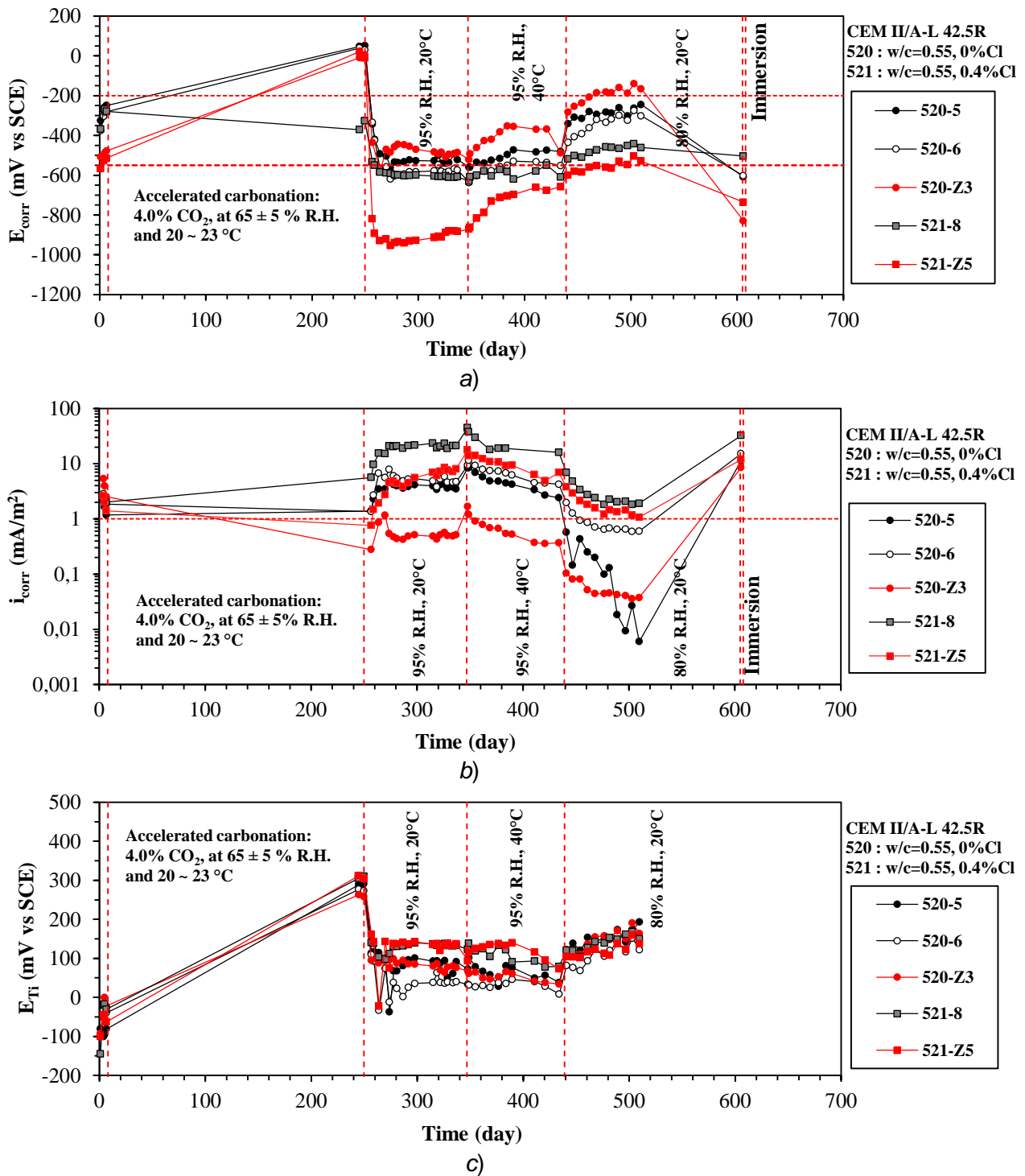


Figure 3.37 Monitoring of a) corrosion potential (E_{corr} vs SCE), b) corrosion rate (i_{corr}) and c) potential of titanium electrode (E_{Ti} vs SCE) of carbonated reinforced specimens made with ordinary cement (CEM II/A-L 42.5R) during exposure conditions at different relative humidity (R.H.) and temperature. (Reinforced specimens with carbon and galvanised steels are indicated respectively with black and red symbols)

Figure 3.38 shows the results of electrochemical tests on carbonated reinforced SL05 NF concrete made with SL05 NF cement.

The corrosion potential of carbon steel bars embedded in carbonated SL05 NF concrete (**Figure 3.38a**) is similar to that of carbon steel bars shown in **Figure 3.37a**. However, it's noticed that the potential of carbon steel bars in free-chloride SL05 NF concrete (specimens "523-5" and "523-6") was steady and close to -200 mV vs SCE during 20°C and 80% R.H. exposure condition whereas in ordinary concrete reached values below -200 mV vs SCE. Corrosion potential of galvanised steel bars in SL05 NF concrete increased from -700 mV vs SCE to -550 mV vs SCE and -400 mV vs SCE respectively, depending on whether chlorides were added or not after 70 days accelerated carbonation. It can be noticed that, galvanised steel bars in SL05 NF concrete reached corrosion potential lower than that in ordinary concrete. During the exposure to 95% R.H. (at 20°C and 40°C) and immersion condition, galvanised steel bar embedded in concrete with 0.4% of chloride (specimen "524-Z5") showed corrosion potential of -900 ~ -1000 mV vs SCE. Galvanised steel bar embedded in concrete without chloride (specimen "523-Z3") showed in dry condition (80% R.H.) higher corrosion potential (up to -400 mV vs SCE) than measured in the same mixture with 0.4% of chloride.

In terms of corrosion rate (i_{corr}), **Figure 3.38b** shows both carbon steel bars and galvanised steel bars embedded in carbonated SL05 NF concretes (with or without chlorides) exposed to 95% R.H. (at 20°C and 40°C) and immersion conditions values above 1 mA/m² (up to 70 ~ 90 mA/m² in presence of chloride). When reinforced specimens were exposed to 20°C and 80% R.H., corrosion rate of carbon steel bars and galvanised steel bars decreased below 1 mA/m², except embedded in mixtures with chlorides.

After exposure to accelerated carbonation process, the corrosion potential of titanium electrodes embedded in carbonated SL05 NF concrete (**Figure 3.38c**) showed a certain variability with values ranged between 250 and 500 mV vs SCE. After subsequent exposure at 95% R.H. (at 20°C and 40°C), the corrosion potential of titanium electrodes decreased to values comparable with those measure in ordinary concrete. A slight increase of corrosion potential was measure at 20°C and 80% R.H..

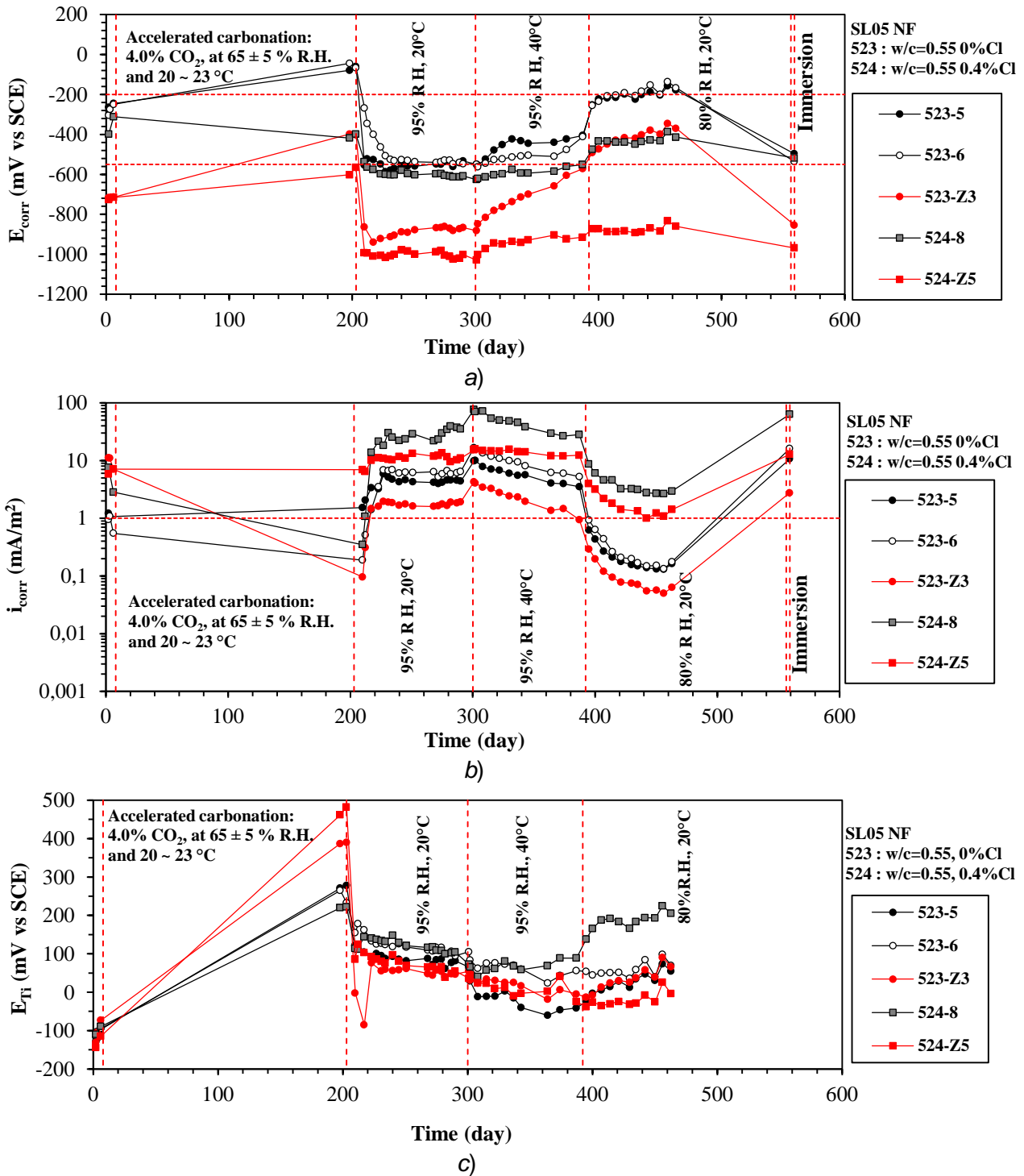


Figure 3.38 Monitoring of a) corrosion potential (E_{corr} vs SCE), b) corrosion rate (i_{corr}) and c) potential of titanium electrode (E_{Ti} vs SCE) of carbonated reinforced specimens made with SL05 NF binder during exposure conditions at different relative humidity (R.H.) and temperature. (Reinforced specimens with carbon and galvanised steels are indicated respectively with black and red symbols)

Figure 3.39 shows the results of electrochemical tests on carbonated reinforced SL05 NF+CaO concrete made by SL05 NF cement with the addition of CaO.

The corrosion potential of carbon steel bars in carbonated SL05 NF+CaO concrete (**Figure 3.39a**) showed the similar trend as in carbonated SL05 NF concrete. However, it's noticed that the corrosion potential of carbon steel bar in carbonated SL05 NF+CaO concrete with 0.4% of chloride (specimen "527-8") reached -222 mV vs SCE after 70 days accelerated carbonation. The corrosion potential of galvanised steel bar in carbonated SL05 NF+CaO concrete without chloride (specimen "527-Z3") showed the similar trend as in carbonated SL05 NF concrete without chloride, reaching around -200 mV vs SCE at 20°C and 95% R.H. exposure condition. But the corrosion potential of galvanised steel bar in carbonated SL05 NF+CaO concrete with 0.4% of chloride (specimen "527-Z5") increased when exposed to 95% R.H. (at 20°C and 40°C) and maintained a stable value of around -550 mV vs SCE at 20°C and 95% R.H. exposure condition. In immersion condition, the corrosion potential values of galvanised steel bars in carbonated SL05 NF+CaO concretes were below -800 mV vs SCE.

It's interesting to notice that the difference in terms of corrosion rate between carbon steel bars and galvanised steel bars in carbonated SL05 NF+CaO concretes without chloride (**Figure 3.39b**) is not significant, also in carbonated SL05 NF+CaO concretes with 0.4% of chloride in all exposure conditions. When exposed to 95% R.H. (at 20°C and 40°C), the corrosion rate of all reinforced specimens were higher than 1 mA/m², while if exposed to the exposure condition at 20°C and 80% R.H. it was lower than 1 mA/m². It's necessary to point out that the corrosion rate of steels in concrete chloride was lower than that of steels in concrete with 0.4% of chloride.

Figure 3.39c shows the potential of titanium electrodes in carbonated SL05 NF+CaO concrete, demonstrating a similar trend as shown in carbonated ordinary concrete.

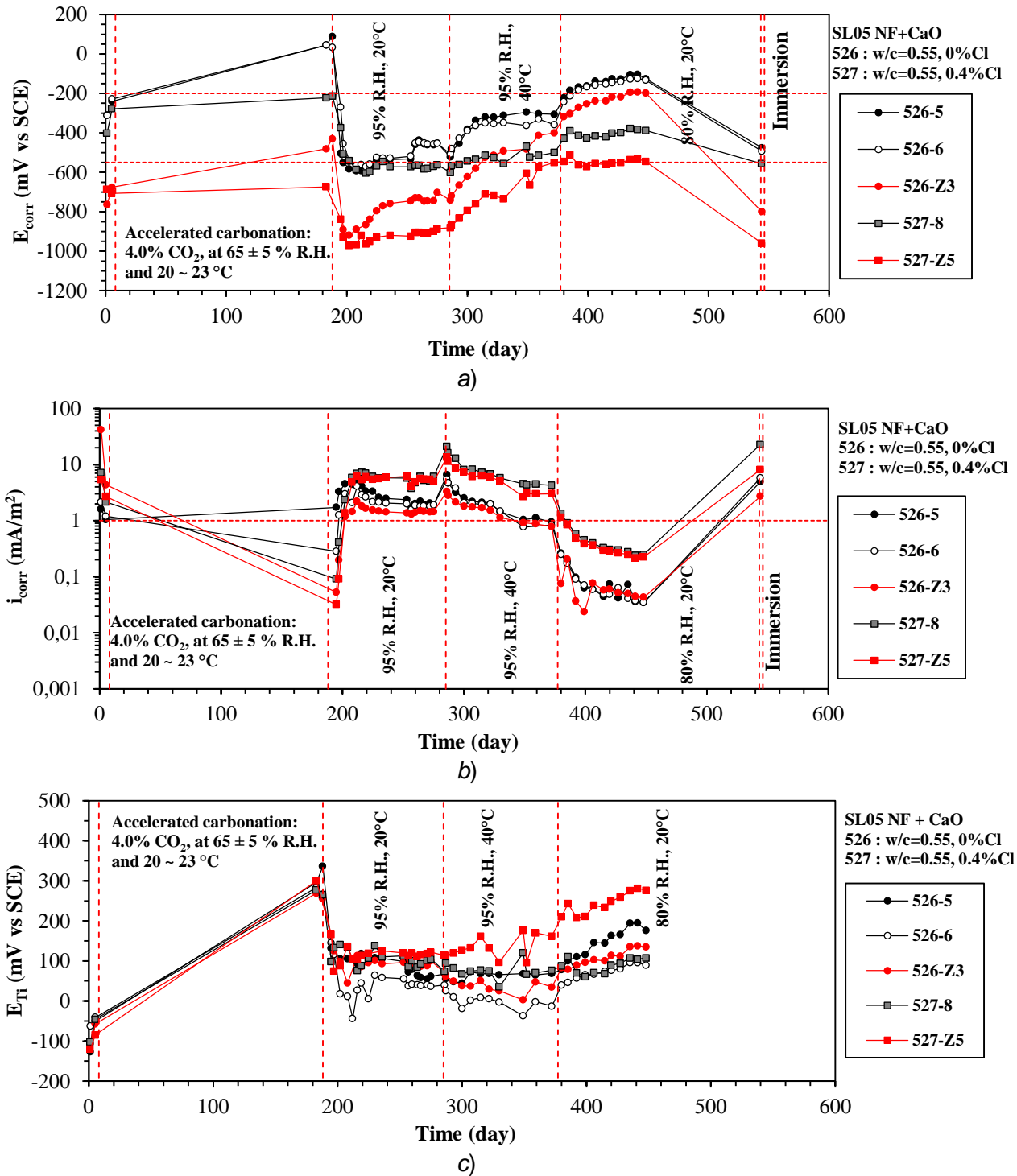


Figure 3.40 shows the results of electrochemical tests on carbonated reinforced SL05 concrete made by SL05 cement with the addition of CaO.

The evolution in time of corrosion potential of carbon steel bars in carbonated SL05+CaO concrete (**Figure 3.40a**) is similar to that in carbonated ordinary concrete (**Figure 3.37a**). The corrosion potential values of galvanised steel bars in carbonated SL05+CaO concrete, after 70 days accelerated carbonation were not higher than -550 mV vs SCE, but reached values around -1000 mV vs SCE when exposed to 20°C and 95% R.H.. Their corrosion potential gradually increased at 95% R.H. condition (at 20°C and 40°C). The corrosion potential of galvanised steel bar in carbonated SL05+CaO concrete without chloride (specimen “529-Z3”) reached around -200 mV vs SCE at the 20°C and 80 % R.H. exposure condition. Whereas the corrosion potential of galvanised steel bar in carbonated SL05 NF+CaO concrete with 0.4% of chloride (specimen “530-Z5”) maintained a stable value of around -700 mV vs SCE at 20°C and 80% R.H. exposure condition. In immersion condition, the corrosion potential values of galvanised steel bars in carbonated SL05+CaO concretes were below -800 mV vs SCE.

In terms of corrosion rate (i_{corr}), as shown in **Figure 3.40b**, both carbon steel bars and galvanised steel bars in carbonated SL05+CaO concrete showed similar trend as in ordinary concrete. However, it's observed that the corrosion rate of all reinforced specimens were higher than 1 mA/m² at 95% R.H. condition (at 20°C and 40°C), but the corrosion rate of all reinforced specimens were lower than 1 mA/m² or close to 1 mA/m² when exposed to 20°C and 80% R.H. exposure condition. It's noticed that the corrosion rates of both carbon steel and galvanised steel bars increased in concrete with 0.4% of chloride. Interesting, galvanised steel bars shower slightly lower corrosion rate values than carbon steel bars in concrete without and with chloride.

The corrosion potential of titanium electrodes in carbonated SL05 concrete (**Figure 3.40c**) showed no significant difference with that in carbonated ordinary concrete.

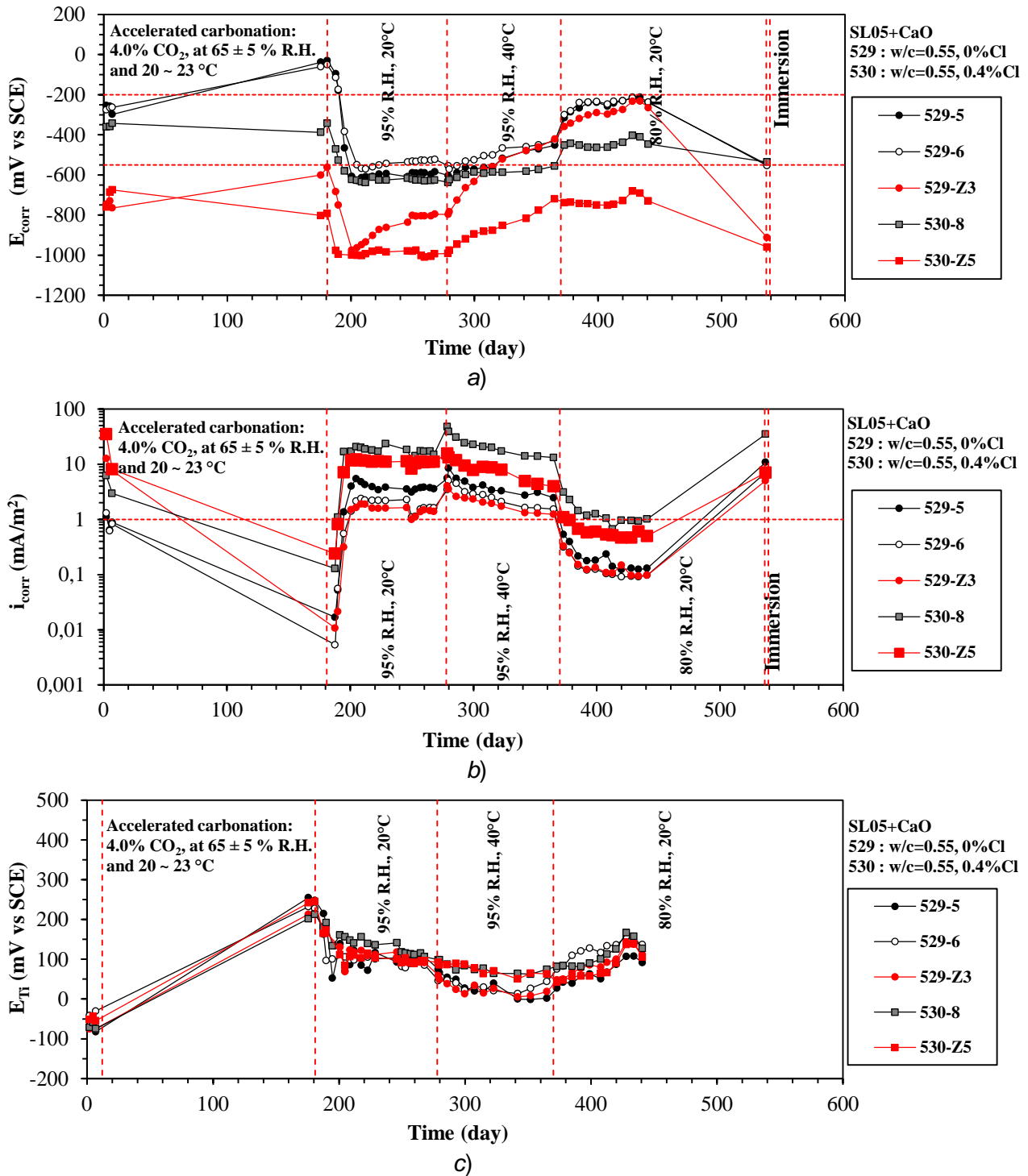


Figure 3.40 Monitoring of a) corrosion potential (E_{corr} vs SCE), b) corrosion rate (i_{corr}) and c) potential of titanium electrode (E_{Ti} vs SCE) of carbonated reinforced specimens made with SL05+CaO binder during exposure conditions at different relative humidity (R.H.) and temperature. (Reinforced specimens with carbon and galvanized steels are indicated respectively with black and red symbols)

3.4 Tests on cement-stabilised rammed earth

To study the corrosion protection of carbon steel in cement-stabilised rammed earth (CSRE), the results obtained by several tests including density, electrical resistivity, compressive strength and carbonation resistance, were described in this section. Moreover, the results obtained in terms of the corrosion potential and corrosion rate of carbon steel bar embedded in CSRE under self-desiccation and immersion conditions are also described.

3.4.1 Properties of cement-stabilised rammed earth

In **Table 3.7**, the properties of CSRE are shown. Density of replicate CSRE specimens, measured after demoulding (1 day after casting), was around 1950 kg/m³. As expected, after curing, the density of CSRE slightly decreased. The compressive strength of all CSRE specimens after 28 days curing ranged from 3.38 MPa to 4.08 MPa. It can be noticed that the electrical resistivity of CSRE in moist condition increased with time; however, the electrical resistivity of all CSRE specimens at 28 days curing age was not more than 20 Ω·m; lower than that of ordinary concrete. The carbonation depth reached 40 mm just after 47 days exposure in laboratory condition.

Table 3.7 Properties of cement-stabilised rammed earth studied.

Sample	Density (kg/m ³)				Electrical resistivity (Ω·m)			Compressive strength (MPa)	Exposure time (days)	Carbonation depth (mm)
	1 day*	14 days	22 days	28 days	14 days	22 days	28 days	28 days		
RE-81	1946	1935	1919	1910	5.58	8.69	8.88	3.38	7	3.3
RE-82	1975	1949	1932	1920	7.38	11.99	15.64	4.08	22	16.5
RE-33	1927	1913	1894	1872	5.76	11.14	19.51	3.44	47	40
RE-34	1962	1938	1929	1912	6.11	10.63	13.89	3.58	-	-

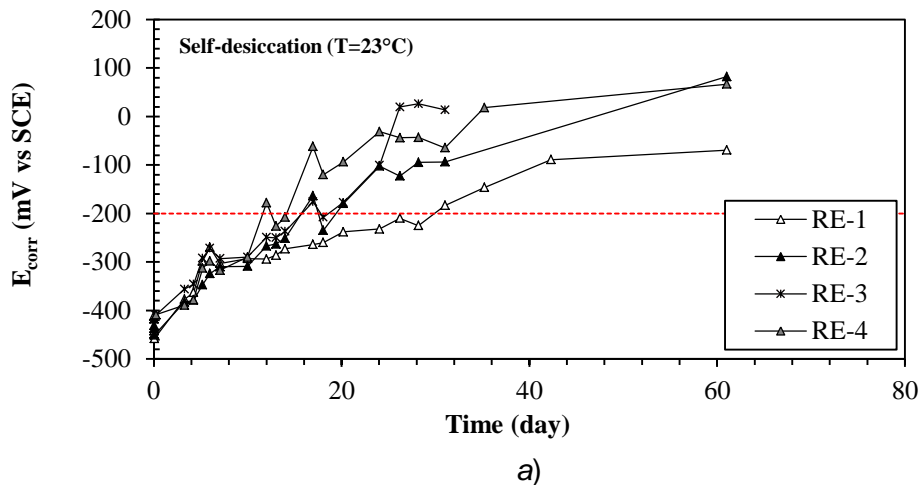
* After demoulding.

3.4.2 Corrosion behaviour of carbon steel embedded in cement-stabilised rammed earth

The corrosion potential and corrosion rate of CSRE specimens reinforced with carbon steel bars were monitored under self-desiccation condition. **Figure 3.41** shows the evolution of corrosion potential (E_{corr} vs SCE), potential of titanium electrode (E_{Ti} vs SCE) and corrosion rate (i_{corr}) over around 60 days in self-desiccation condition. The corrosion potential of carbon steel bars increased progressively, until reached stable values around 0 mV vs SCE for specimens “RE-2”, “RE-3” and “RE-4”; differently, carbon steel bar embedded in “RE-1” specimen showed a maximum corrosion potential (-100 mV vs SCE) lower than other reinforced specimens. All reinforced specimens reached the corrosion limit of -200 mV vs SCE within 15 ~ 20 days, except for “RE-1” specimen that spent about one month to reach passive condition. A confirmation of passive condition of

carbon steel bars embedded in CSRE was found on the base of corrosion rate measurements (**Figure 3.41b**). Although few days after casting, reinforced specimens showed corrosion rate of around $6 \sim 9 \text{ mA/m}^2$; this corrosion parameter decreased with time in self-desiccation condition to values ranged between 0.02 and 0.1 mA/m^2 at 7 days after casting; during the following period, the corrosion rate of steel bars in CSRE show a quick decrease; at 24 days, the corrosion rate of steel bars in all specimens were lower than 1 mA/m^2 . The potential of titanium electrode depends on pH-dependent of solution and oxygen availability. So a certain variability of the measurements of the potential of titanium electrodes (**Figure 3.41c**) should be attributed to their different sensitivity at oxygen available if differently compacted. A slight difference in terms of compaction effort should be hypothesized for these reinforced specimens. The potentials of titanium electrodes showed a trend of quick increase except that specimen "RE-1" showed a slow increase.

After around 60 days of self-desiccation, all the reinforced CSRE specimens were fully immersed in tap water for 48 hours. During the first hours of the immersion phase, corrosion rates of carbon steel bars in CSRE were dispersed (**Figure 3.42**); only the corrosion rate of carbon steel bar in specimen "RE-4" was lower than 1 mA/m^2 , whereas the corrosion rate of steel bars in the specimens "RE-1" and "RE-3" were around 3.5 mA/m^2 . At the end of immersion test, the corrosion rate of carbon steel bars in all specimens converged to around 2 mA/m^2 . Corrosion potential of carbon steel bar in specimen "RE-4" was higher than -200 mV vs SCE at the beginning of immersion; however, at the end of immersion test, only the corrosion potential of steel bar in specimen "RE-1" was more than -200 mV vs SCE , attaining around -160 mV vs SCE .



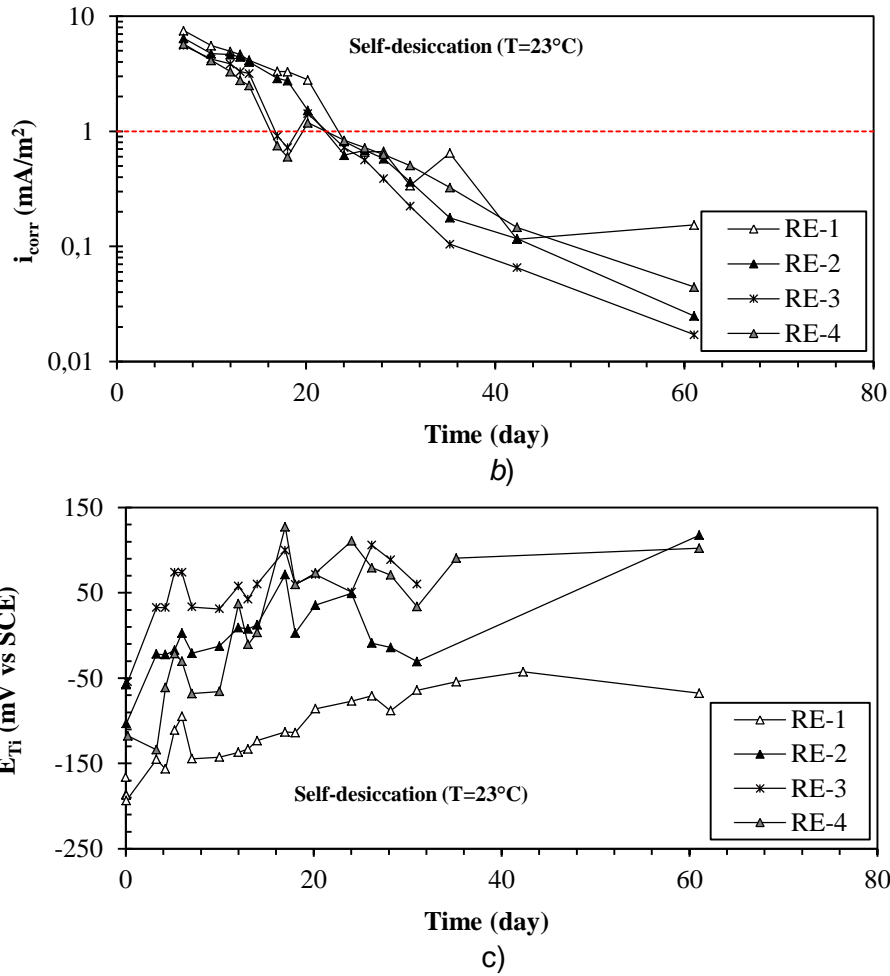


Figure 3.41 Monitoring of a) corrosion potential (E_{corr} vs SCE), b) corrosion rate (i_{corr}), and c) potential of titanium electrode (E_{Ti} vs SCE) as function of time for reinforced cement-stabilised rammed earth under self-desiccation condition.

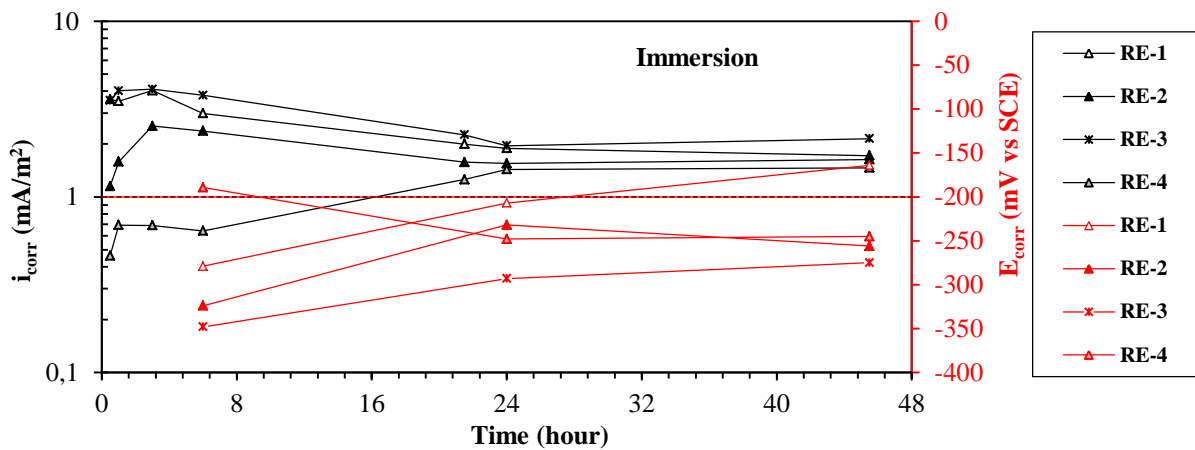


Figure 3.42 Monitoring of corrosion potential (E_{corr} vs SCE, red symbols) and corrosion rate (i_{corr} , black symbols) as function of time for reinforced rammed earth specimens during the period of 48 hours immersion.

Chapter 4 Discussion

Corrosion protection of steel in new sustainable cementitious materials depends on the capacity of these new materials to passivate steel and it has the utmost importance for the potential durability of reinforced concrete structures made with these new sustainable cementitious materials. If steel embedded in these new materials reaches passive state, the corrosion rate of steel is negligible due to the formed passive film on steel surface. In highly alkaline environment provided by ordinary concrete, steel is covered with a protective oxide film (passive layer) so that under ideal conditions the corrosion rate is typically less than 1 mA/m^2 (i.e. $1 \text{ }\mu\text{m/year}$ for steel). Conversely, the complex and variable nature of new sustainable cementitious materials could affect the passivation and corrosion of steel embedded in them; in particular, the pH of pore solution around the steel bar but also the physical and chemical properties of these new sustainable cementitious materials could influence the corrosion behaviour of reinforcement. Key factors affecting the depassivation and corrosion of steel in new sustainable cementitious materials include also the surface properties and the chemical composition of the steel. However, carbonation and chlorides penetration can lead to the depassivation of steel embedded in sustainable cementitious materials. Once it happens, the corrosion behaviour of active steel embedded in sustainable cementitious materials under different relative humidity and temperature or chloride environment is needed to be investigated in order to provide information about the propagation stage of steel corrosion.

This chapter is dedicated to discuss the results that have been presented and described in the previous chapter in terms of corrosion protection of steel in new sustainable cementitious materials. Firstly, the results of alkalinity tests carried out on new sustainable concrete studied in this research and the results in terms of characterisation of carbon steel bars with different surface conditions are discussed. Secondly, the passivation of carbon steel bars with different surface conditions embedded in ordinary concrete is evaluated. Moreover, the passivation of carbon steel embedded in new sustainable cementitious materials is discussed. The effect of carbonation and chlorides on the corrosion behaviour of carbon steel bars with different surface conditions embedded and of carbon steel in CSA-based concretes when exposed to different environments is also discussed. Finally, use of corrosion-resistant rebars (such as galvanised steel) embedded in CSA-based concretes has been discussed.

4.1 The factors influencing passivation of steel

The factors influencing the passivation of steel in new sustainable cementitious materials could include the pH of the solution contained in the pores of new sustainable cementitious materials, and the presence of surface layers on steel (such as the mill scale due to manufacturing process, or trace of rust covered by atmospheric exposure or a zinc coating produced by galvanising process). Depletion of oxygen, carbonation of concrete cover and chlorides penetration have to be considered since they might also cause modifications to chemical composition of concrete. In particular, carbonation decreases the alkalinity of concrete cover and fails passive film of steel. Chloride ions can also break down passive film of steel when its concentration close to steel surface reaches a certain amount. When the alkalinity of new sustainable cementitious materials is not enough to passivate carbon steel, it might be necessary to use corrosion-resistant steel such as galvanised steel. In this section, the alkalinity of sustainable concretes made with the new sustainable cementitious materials studied in the framework of this thesis and the characterisation of carbon steel bars with different surface conditions are discussed, in order to help understand the passivation of carbon steel in these new sustainable cementitious materials.

4.1.1 pH of new cementitious materials

In order to investigate on the actual pH of the pore solution of the different sustainable cementitious materials studied in this research, pH measurements were carried out. As far as the results obtained in this research and reported in other research, **Figure 4.1** shows the pH of reference concrete made with CEM II/A-L 42.5R cement and CSA-based concretes cast with w/c ratio of 0.55. For comparison, also the pH of a waste glass powder mortar and cement-stabilised rammed earth comparable with those studied in this research, is reported. Clearly, it can be seen that the pH of reference concrete and CSA-based concretes is close to 12.6 except pure CSA concrete made with SR03 cement (slightly lower than 11), whereas glass powder mortar has a pH value slightly higher than 13 and the pH of cement-stabilised rammed earth (made with crushed limestone) is around 12. As expected, pure CSA concrete has a low pH due to the fact that its main phase hydration product is ettringite that cannot provide high concentrations of alkali ions (Na and K) and calcium ion (Ca) compared to the blending cements based on the combination of 30% pure CSA clinker, 10% anhydrite and 60% of respectively CEM I 52.5R (SL05 NF) and CEM II/A-L 42.5R (SL05). However, blending with ordinary cement can modify its phase assemblage and therefore increase its pH comparable with that of reference concrete. The high pH of mortar made with glass powder might be due to the release of alkali from glass powder. Apparently, the pH value of around 12 of cement-stabilised rammed earth should be ascribed to the hydration of the cement used as stabiliser.

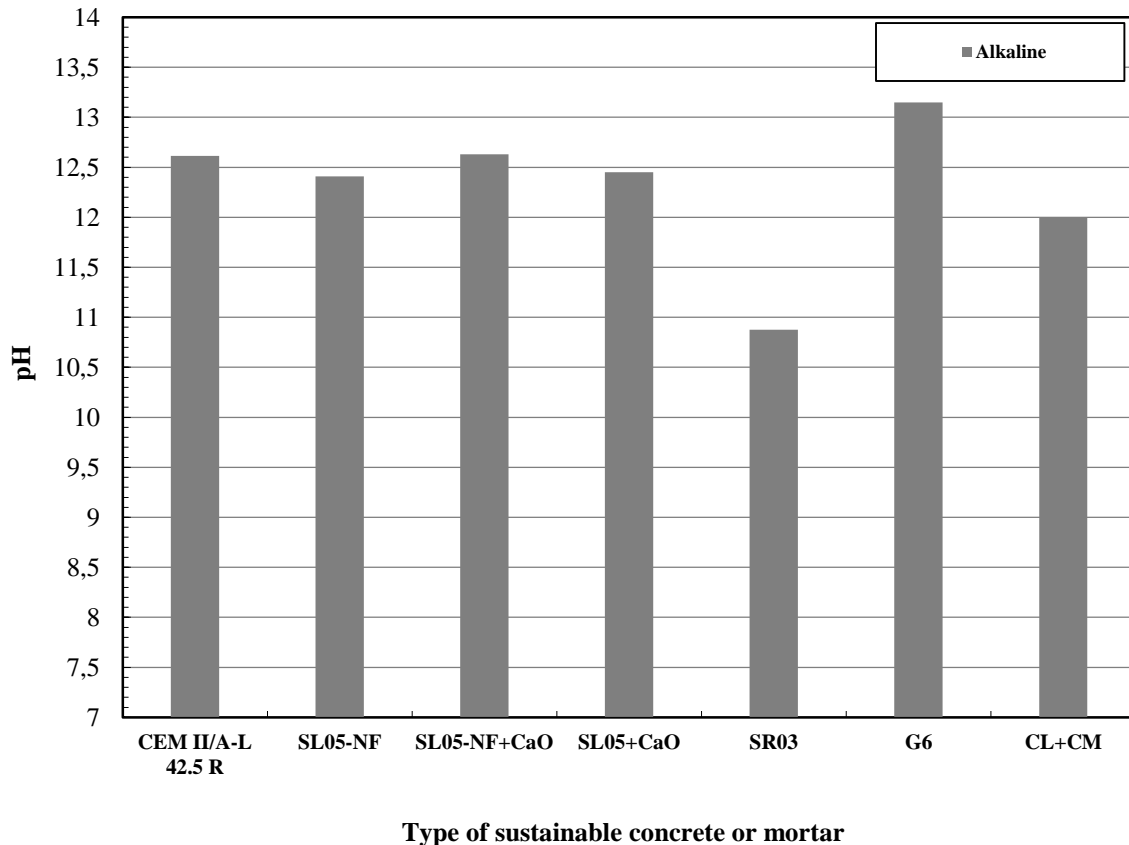


Figure 4.1 pH of alkaline reference concrete (CEM II/A-L 42.5R) and CSA-based concretes (SL05 NF, SL05 NF+CaO, SL05+CaO and SR03) cast in this research and the pH of glass mortar (G6) and cement-stabilised rammed earth (CL+CM) measured in other research. (Glass mortar studied in this research is comparable with “G6” mortar in terms of type of mineral addition and mix proportions used in [63], pH data provided by mCD lab; pH data of cement-stabilised rammed earth from [143], CL= crushed limestone, CM=cement.)

Furthermore, **Figure 4.2** shows the evolution of pH of a reference mortar and CSA-based mortars ($w/c=0.5$) as a function of the curing up to 145 days. It can be observed that each type of mortar reaches their highest pH value within 4 ~ 7 days after casting, subsequently decreases between 7 days and 28 days, and maintains a stable value beyond 28 days. In fact, the trend of pH evolution of all types of mortar reflects the process of cement hydration and the release of ions from the binder to the solution. The pH of blended CSA-based mortars (made with ordinary cements), including SL05 NF, SL05 NF+CaO and SL05+CaO, have not shown significant difference with that of reference concrete regardless curing age. This might be due to the fact that a high amount of ordinary cement was used. During all curing age, the pH of pure CSA mortar (SR03) is lower than that of other mortars as observed before. However, the results of pH measured on pure CSA mortar are not in agreement with the results reported in [108], [115]; this could be due to the scattering of composition of CSA cements as highlighted also from literature survey.

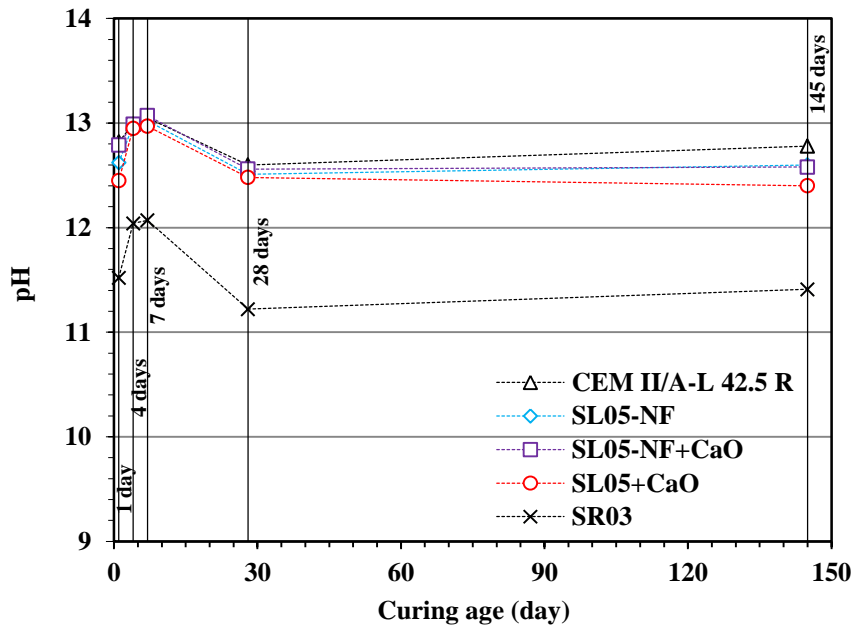


Figure 4.2 pH of reference mortar and CSA-based mortars (w/c=0.5) at different curing ages.

4.1.2 Steel surface condition

It's well known that steel passivation could be influenced from the surface conditions. For this reason, different surface conditions of rebars have been also considered in this research. In particular, carbon steel rebars manufactured at the same plant and characterised by different degree of pre-rusting caused by outdoor exposure up to 1 year have been considered. Typically reinforcing bars are used in the as-received condition after manufacturing at the production plant and thus rebars coated with only a layer of mill scale have been also taken into account. For comparison purpose, comparable sandblasted bars were also studied.

As an example, **Figure 4.3** compares the appearance of 18 mm diameter steel bars with different surface conditions by visual observations and the analysis of surface oxides with scanning electron microscope. The mill scale, which is on the surface of as-received steel, appears dark-grey and compact. Actually, it is not always adhered with steel substrate and has some cracks. Therefore, it's not a uniform protective layer. As a consequence of atmospheric corrosion, red-brown oxides were formed on the surface of steel bar; these corrosion products had a porous morphology when compared with the mill scale. The thickness of the oxide layers was estimated on metallographic section of each type of steel bar. **Figure 4.4** shows the trend of the average thickness of the oxide layers and its range of variation in terms of exposure time. The thickness of the mill scale of both 10 and 18 mm diameter steel bars ranged between 5 and 20 μm . After 1 year of atmospheric exposure, the average thickness of oxide layers of both 10 and 18 mm diameter steel bars was around 100 μm (with a maximum value for 18 mm steel bar up to 190 μm). As far as the mineralogical composition of the oxides is concerned, XRD analysis detected typical products due

to atmospheric corrosion of iron such as lepidocrocite ($\gamma\text{-FeO(OH)}$) and goethite (FeO(OH)). The detected magnetite is likely due to the remaining mill scale that may have not been completely replaced by rust.

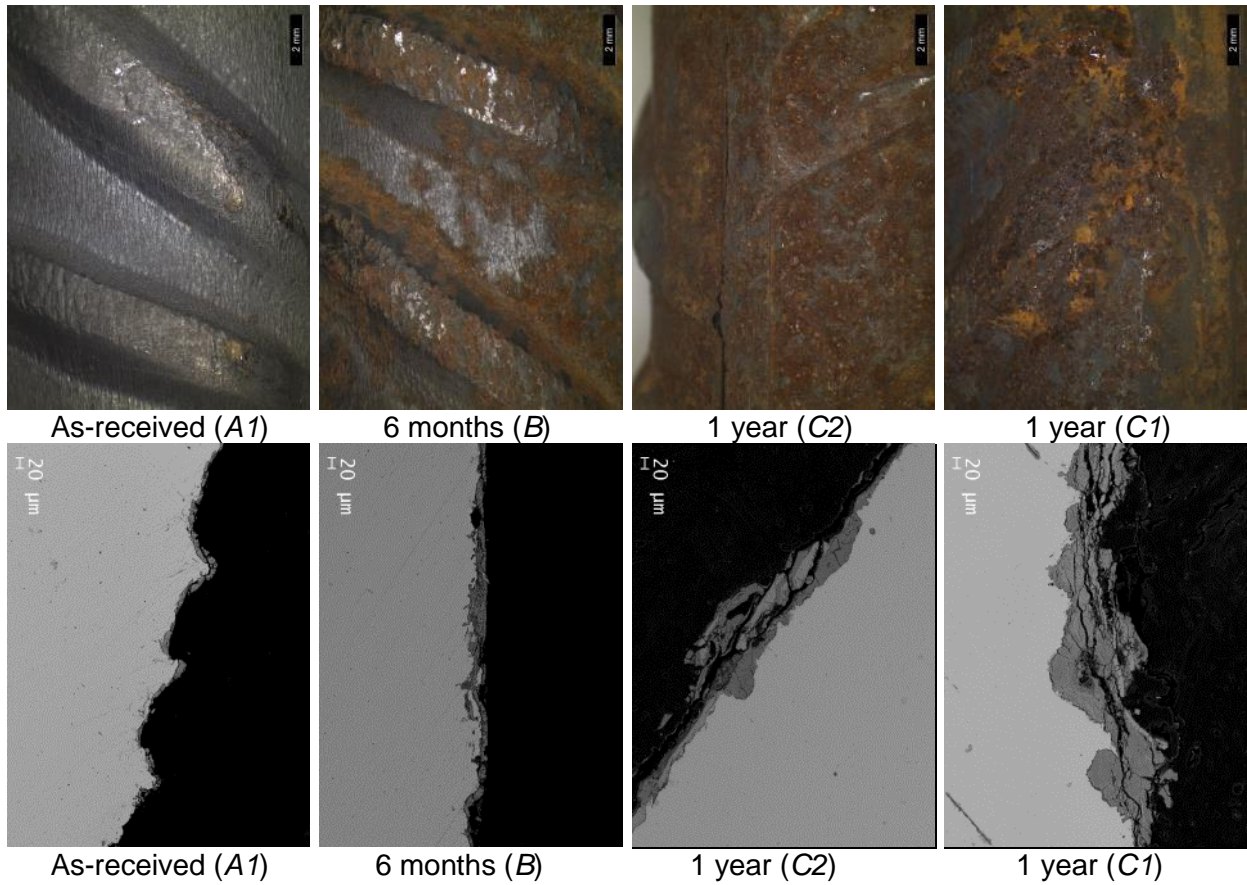


Figure 4.3 Comparison of the visual appearance of surface condition and oxide layers of steel bars with 18 mm diameter.

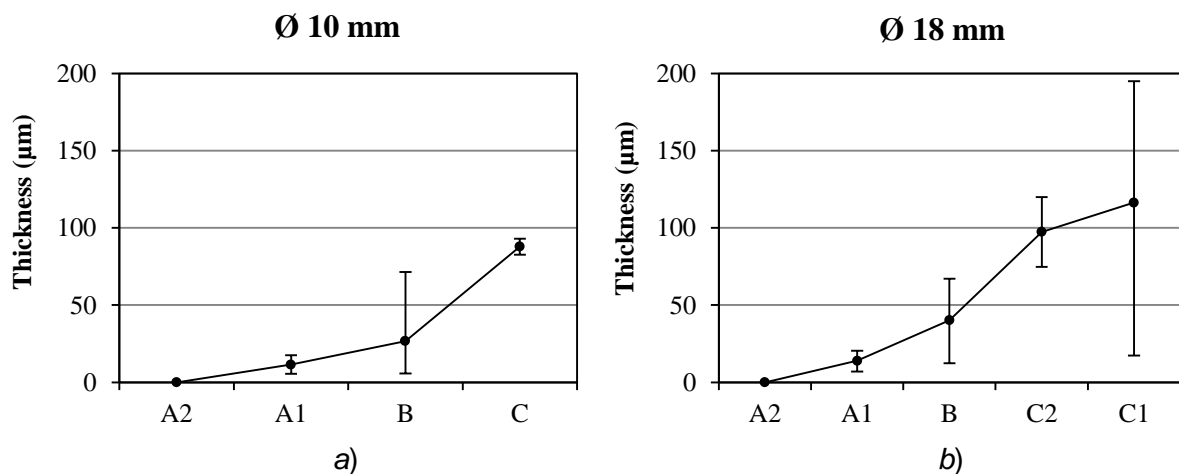


Figure 4.4 Thickness of oxide layers present on steel bars with different diameters a) 10 mm and b) 18 mm exposed to several conditions. (A2:sandblasted; A1:as-received; B:exposed for 6 months; C, C1 and C2:exposed for 1 year)

4.2 Passivation of carbon steel in alkaline ordinary concrete

In order to detect possible critical conditions for passivation due to steel surface, corrosion tests were carried out in concrete and the behaviour of steel was studied in relation of concrete moisture.

In general, the passivation of carbon steel bar embedded in ordinary concrete can be characterised by corrosion potential higher than -200 mV vs SCE and corrosion rate value lower than 1 mA/m^2 , which indicates the formation of stable passive film on steel surface.

The influence of steel surface condition on passivation of steel in ordinary concrete was investigated under three different relative humidity conditions; namely self-desiccation (at 23°C), 80% R.H. (at 20°C) and immersion (at 20°C). In particular, reinforced specimens were maintained in self-desiccation conditions for 2 months; subsequently they were exposed to a relative humidity of 80% for other two months; finally, they were immersed in tap water for a period of one month. **Figure 4.5** summarises the corrosion potential and corrosion rate measured on all types of steel embedded in a typical structure concrete at the end of each condition. The corrosion rate was monitored with the polarisation resistance method. The results clearly reveal that the corrosion potential value of steel depends on the relative humidity of concrete, showing positive values (0 ~ 90 mV vs SCE) in 80% R.H. condition but negative ones (-150 ~ -100 mV vs SCE) in self-desiccation and immersion conditions. It can be observed that almost all the negative values were above -200 mV vs SCE, which indicates that all steel bars are in passive state. The negative potential of steel should be attributed to the fact that oxygen is less available to the surface of steel under high humidity conditions. According to **Figure 4.5b**, it can be observed that the corrosion rate of all 10 mm diameter steel bars was very low, showing no sign of corrosion, regardless with exposure condition. The corrosion rate of 18 mm steel bars without rust (i. e. as-received and sandblasted) was below 1 mA/m^2 in all exposure conditions; in contrast, all the pre-rusted 18 mm diameter steel bars showed corrosion rate higher than 1 mA/m^2 (in particular, specimens reinforced with bars in C1 condition). However, it can be observed that the humidity to which the specimens were exposed did not have any significant effect. These results support the hypothesis that also steel bars with pre-rusting are in passive conditions.

In order to confirm the condition of passivation of steel, the further anodic polarisation test was carried out on reinforced specimens at the end of both self-desiccation and immersion conditions by means of imposing a potential of +200 mV vs SCE on steel embedded in ordinary concrete. At the potential of +200 mV vs SCE, if the steel is passive, the measured steady polarisation current density (i_{pol}) that is required to maintain the imposed potential would be negligible; otherwise, the steady value of i_{pol} would be significant. The corresponding principle is depicted in **Figure 4.6**.

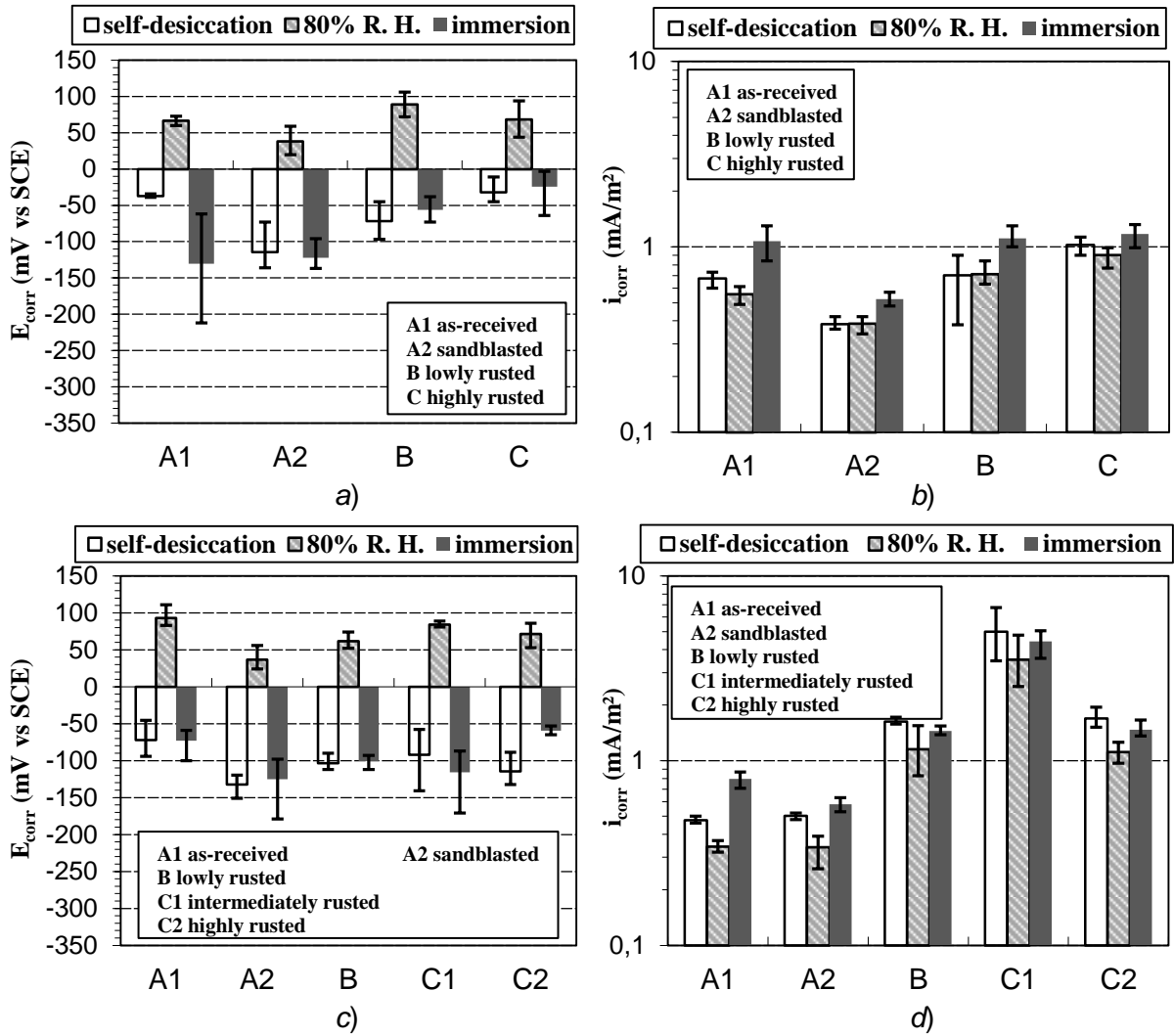


Figure 4.5 Corrosion potential (E_{corr} vs SCE) and corrosion rate (i_{corr}) of steel bars with different surface conditions and different diameters: a) and b) for 10 mm and c) and d) in case of 18 mm embedded in ordinary concrete measured at the end of each exposure condition (self-desiccation, 23°C, 80% R.H., 20°C and immersion, 20°C).

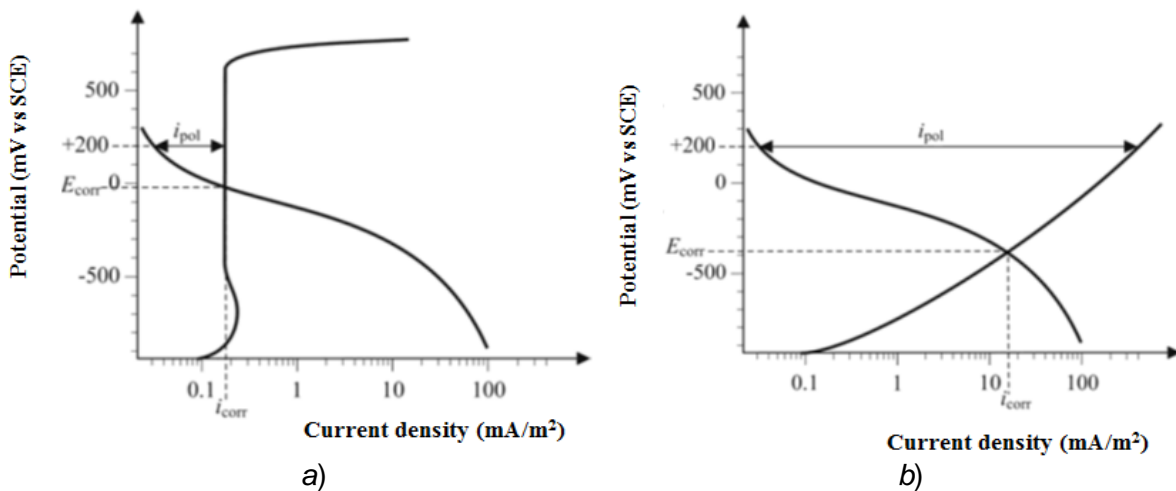


Figure 4.6 Scheme of the polarisation current (i_{pol}) of passive a) and active b) steel at +200 mV vs SCE.

Figure 4.7 and **Figure 4.8** show respectively, after self-desiccation and immersion conditions, the corrosion potential of each type of steel bar in terms of its corrosion rate before and at the end (24 hours) of anodic polarisation test. Corrosion rate (i_{corr}) measured before starting potentiostatic polarisation test (i.e. in free corrosion conditions) was obtained with the polarisation resistance method by applying a potentiostatic variation of respectively +10 mV and -10 mV versus the free corrosion potential. Conversely, during the potentiostatic polarisation test, a steel potential of +200 mV vs SCE was imposed to the steel and the current density require to maintain this potential (i_{pol}) was monitored. At this value of potential, in case the rebars were not passive, a substantial increase in the corrosion rate is expected, which can be detected by a significant increase of polarisation current density (i_{pol}). **Figure 4.7-4.8** show that at the end of all potentiostatic tests the polarisation current density (corresponding to a corrosion potential of +200 mv vs SCE) had negligible values (lower than 1 mA/m²) for all types of surface conditions. The contradictory results obtained in terms of corrosion rate between anodic polarisation test and polarisation resistance test could be explained by the hypothesis that polarisation resistance technique may overestimate the actual corrosion rate due to the presence of rust oxide at the interface of steel/concrete that may cause non-ideal capacitive effect. The hypothesis is also supported by [26] in which the authors found that, when the rusting degree of steel is high, the corrosion rate measured by electrochemical test is higher than that obtained by gravimetric loss. In fact, the corrosion rate (i_{pol}) and corrosion potential measured at the end of potentiostatic polarisation tests showed in all humidity conditions (after self-desiccation and immersion) a comparable corrosion behaviour with negligible corrosion rate between the sandblasted bars and the bars with mill scale and with different degrees of pre-rusting, confirming that the pre-rust present on the surface of the steel was not detrimental to the passivation of the rebars in the concrete.

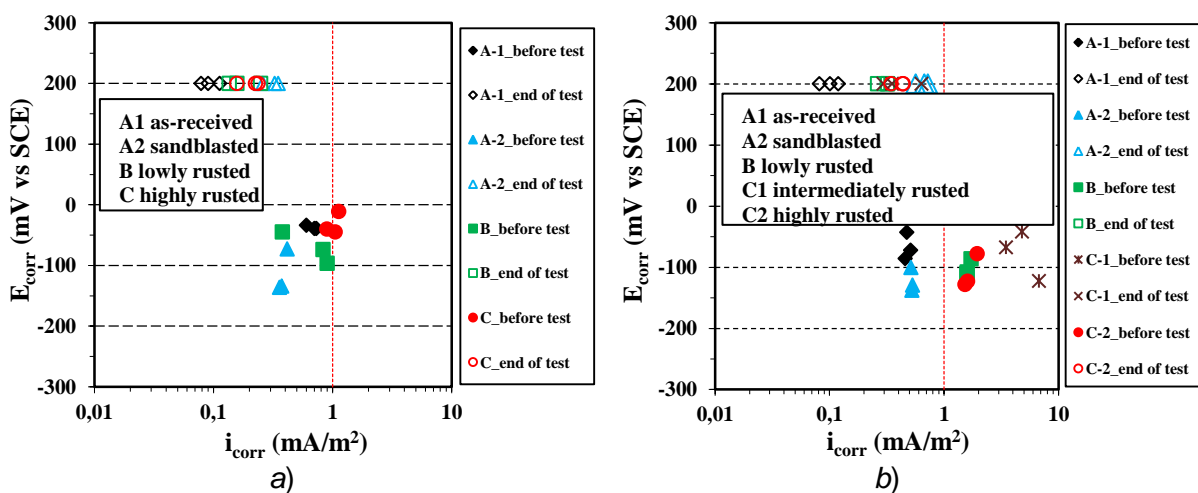


Figure 4.7 Corrosion potential (E_{corr} vs SCE) as function of corrosion rate (i_{corr}) measured on a) 10 mm and b) 18 mm diameter steel bars with different surface conditions embedded in ordinary concrete, before and at the end of anodic polarisation test carried out at the end of self-desiccation condition.

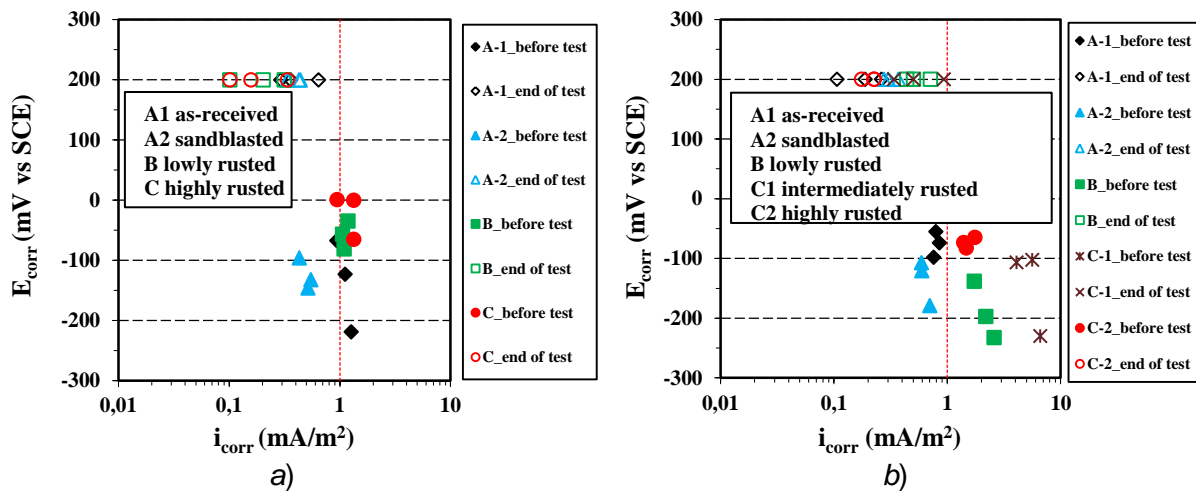


Figure 4.8 Corrosion potential (E_{corr} vs SCE) as function of corrosion rate (i_{corr}) measured on a) 10 mm and b) 18 mm diameter steel bars with different surface conditions embedded in ordinary concrete, before and at the end of anodic polarisation test carried out at the end of immersion condition.

4.3 Passivation of carbon steel in sustainable cementitious materials

The effects on passivation of carbon steel in concrete may be even more serious when binders alternative to ordinary Portland cement (OPC) are considered, due to the different nature of hydration products and composition of the pore solution.

In this section, the passivation of carbon steel embedded in the different sustainable cementitious materials studied in this research is discussed. Before discussing the passivation of steel, the main properties of these sustainable cementitious materials (i. e. glass powder mortar, CSA-based concretes and cement-stabilised rammed earth) are illustrated.

4.3.1 Properties of sustainable cementitious materials

4.3.1.1 Properties of waste glass mortar

The use of waste glass in construction materials appears among the most sustainable options considering that glass has a chemical composition compatible with that of sand and cement and its use could reduce in turn the environmental cost of concrete. The effects of the combined use of waste glass as a potential replacement of cement and/or expanded aggregates on durability and performance of the mortars studied in this thesis work are discussed in this section. Different mortars with w/c ratio equal to 0.5 and mix proportion of 1:3:0.5, respectively of binder (CEM II/A-L 42.5R cement, also in partially replacement with recycled glass powder), aggregates (standard sand or expanded glass) and water, were performed. **Table 4.1** summarises the properties of waste glass mortar studied.

Table 4.1 Summary of properties of waste glass mortar (according to average value of two or three replicated specimens).

Mortar	Waste glass (%)		Consistence (%)	Fresh density (kg/m ³)	Compressive strength (MPa)				Electrical resistivity (Ω·m)			ASR expansion (%)	
	Glass powder	Expanded glass			7 days	28 days	90 days	180 days	28 days	100 days	500 days	14 days	70 days
M134	-	-	134	2273	53	58	68	67	45	58	57	0.20	0.57
M135	30	-	150	2244	38	49	58	71	103	310	380	0.07	0.38
M136	30	100	139	1177	14	16	15	14	67	135	149	0.02	0.11
M137	-	100	131	1206	18	17	17	15	36	49	64	0.06	0.09

Consistence and fresh density

A waste glass powder with specific surface of 600 m²/kg was considered in this research. Mortars were made also with a commercial expanded glass aggregates with particle size in the range of 2 ~ 4 mm. Consistence results, as shown in **Table 4.1**, showed that fine glass powder was beneficial for improving the consistence of mortar, whereas coarse expanded glass slightly decreased the consistence of mortar. Glass powder particles can fill the interstices between cement particles and lead to more water to be released, which facilitates the lowering of the friction between particles [73]. Besides, the low water absorption and smooth surface of glass powder may contribute to improve the consistence of mortar. However, expanded glass particles can increase the friction between particles due to its coarse surface with negative effects on consistence. Also the high water absorption of expanded glass aggregates due to high porosity can cause the fluidity loss of fresh mortar made with them. The mortar made with glass powder in partial replacement of OPC showed comparable fresh density with reference mortar made with CEM I 52.5R cement. Conversely, mortars with expanded glass aggregates led to decrease the density to around 1200 kg/m³.

Compressive strength

Owing to the occurrence of pozzolanic reaction of glass powder at later age, the compressive strength of normal mortar made with glass powder (71 MPa) was higher than that of reference mortar (67 MPa) after 6 months curing, as confirmed from the results reported in [50], [71]. In contrast, lightweight mortar made with expanded glass (M137) showed a compressive strength of 15 ~ 18 MPa and no enhancement of strength during the curing process, which should be attributed to the high porosity and low resistance of expanded glass particles [69]. The lightweight mortar made with glass powder (M136) showed a compressive strength of 14 ~ 16 MPa, comparable with that of lightweight mortar without glass powder (M137).

Electrical resistivity

To evaluate changes in the capillary porosity during hydration process of the different glass mortar studied in this research, electrical resistivity was measured on water curing specimens. Specimens of reference mortar (M134) together with that of mortar with comparable cement and expanded

glass in replacement of standard sand soon reached stable values around $50 \Omega \cdot \text{m}$, showing no significant increase during 500 days curing, as shown in **Table 4.1**. Conversely, mortars with glass powder reached values of $135 \Omega \cdot \text{m}$ and $310 \Omega \cdot \text{m}$, respectively if made with expanded glass and standard sand, after 100 days water curing. These high electrical resistivity values of mortars with glass powder can be attributed to the well-known effect of pore refinement brought about by the pozzolanic reaction [72]. Also, a minor effect due to reduction in ionic content in the pore solution induced by pozzolanic reaction can be considered.

ASR expansion

Based on the obtained results of ASR expansion of waste glass mortars, both glass powder and expanded glass are useful for suppressing effectively ASR expansion. In fact, lightweight mortars made with expanded glass aggregates (M136 and M137, **Table 4.1**) showed a negligible expansion (lower than 0.1%), even after 70 days of exposure in 1 M NaOH solution. Conversely, reference mortar without waste glass (M134) showed a sharp increase of ASR expansion, as summarised in **Table 4.1**, reaching 0.2% and 0.57% after 14 and 70 days test respectively.

The phenomenon that fine glass powder is helpful to reduce ASR expansion has been reported by many researchers [50], [55], [65], [71], [76], [144]. A common explanation refers to the pozzolanic reaction of fine glass powder in cementitious materials, allowing the dissolved reactive silica and alkali in glass powder to be largely consumed to form C-S-H gel before ASR reaction initiation [145]. Whereas the excellent ability of expanded glass particles to suppress ASR expansion, as also reported in [80], [146], should attribute to the porous structure of expanded glass that is able to accommodate the large amount of ASR gel produced [68]. The cracks occurred on the surface of mortars made with expanded glass (M136 and M137) might be due to the reason that the space inside expanded glass particles was not enough to accommodate the progressively produced ASR gel, as seen in **Figure 4.9**, and that the tensile strength of expanded glass was too low to resist cracking stress.



Figure 4.9 Cracked surface of expanded glass mortar (specimen M137) subjected to ASR test. M137:100% standard sand replaced by expanded glass.

4.3.1.2 Properties of CSA-based concrete

Also the interest on innovative binders based on calcium sulfoaluminate (CSA) cement has increased mainly in relation to sustainability issues. In this research, different CSA-based cements (shown in **Section 2.1**) have been considered and their role on concrete performance was studied.

Workability and hardened density of CSA-based concrete

The low workability (1 cm) of pure CSA concrete (SR03) was the result of the quick formation of ettringite that can typically occur within 15 ~ 20 mins after casting [104]. Differently, for all other concrete obtained by blending sulfoaluminate cement with ordinary cement or with the addition of CaO, a comparable workability of consistence class S4 (16 ~ 21 cm) was measured. The hardened density of CSA-based concretes was not different with that of ordinary concrete.

Mechanical properties of CSA-based concrete

The compressive strength of reference concrete (made with CEM II/A-L 42.5R cement) and CSA-based concretes at different curing ages (1, 7, 28 and 90 days) was listed in **Table 4.2**.

By comparing mixtures made with w/c ratio equal to 0.55, it can be observed that concrete with pure CSA cement (SR03) showed highest compressive strength already after 1 day of curing (56 MPa), as shown in **Table 4.2**; this mechanical performance has to be attributed to different hydration products, mainly ettringite, formed at the early age. Although, blended CSA concretes achieved compressive strength (28 ~ 35 MPa, at 1 day) lower than that of pure CSA concrete; their performance were higher if compared with ordinary concrete. The addition of CaO slightly reduced the compressive strength of CSA-based concretes when comparing the compressive strength between SL05 NF and SL05 NF+CaO CSA-based concretes, which could be due to the reason that the increased quantity of lime, especially free lime, may influence the hydration of ye'elimite [106]. The difference of dynamic elastic modulus between CSA-based concretes and reference concrete was not so significant as that measured in terms of compressive strength.

Table 4.2 Compressive strength of CSA-based concretes (according to average value of two replicated specimens).

Binder type	R _{c,1} (MPa)		R _{c,7} (MPa)		R _{c,28} (MPa)		R _{c,90} (MPa)	
	0.47	0.55	0.47	0.55	0.47	0.55	0.47	0.55
CEM II/A-L 42.5R	15.8	26.2	46.7	46.5	54	53	59.9	58.8
SL05 NF	40.5	35.6	57.4	52.7	70.4	53.1	79.2	72.9
SL05 NF+CaO	37	27.9	57.4	45.6	67.6	49.3	73.6	57.5
SL05+CaO	43	31.5	53.4	43.2	59.1	57.6	69.9	65.9
SR03	-	56.4	-	66	-	72.3	-	72.9

Electrical resistivity

Figure 4.10a-b shows the electrical resistivity of the different concrete (w/c = 0.47 and 0.55) as a function of time (28 days, 90 days and 1 year) after mixing on specimens in water curing. CSA-

based concretes with w/c ratio of 0.55 showed no significant difference in terms of electrical resistivity if compared with reference concrete after 28 and 90 days of water curing. However, after a prolonged curing up to 1 year, CSA-based concretes showed higher electrical resistivity than reference concrete ($71 \Omega \cdot m$); especially CSA-based concrete made with SL05 NF cement and the addition of CaO reached about $210 \Omega \cdot m$. This could be attributed to the denser microstructure of CSA concrete [104]. In general, higher electrical resistivity values were founded with decreasing of w/c ratio (**Figure 4.10b**). Adding CaO can noticeably enhance electrical resistivity, due to its influence on hydration process as confirmed by monitoring the conductance of specimens under self-desiccation conditions since the first minutes after casting (**Figure 3.26**). During the first hours of hydration process, a peak of conductance can be observed in all concrete. This is due to the initial increase in the conductance as a result of ions from the binder to the solution, followed by decrease caused by the development of hydration products. The addition of CaO slightly delayed the appearance of peak of conductance and resulted in higher conductance, which could be because that CaO may influence the hydration of ye'elinite [106].

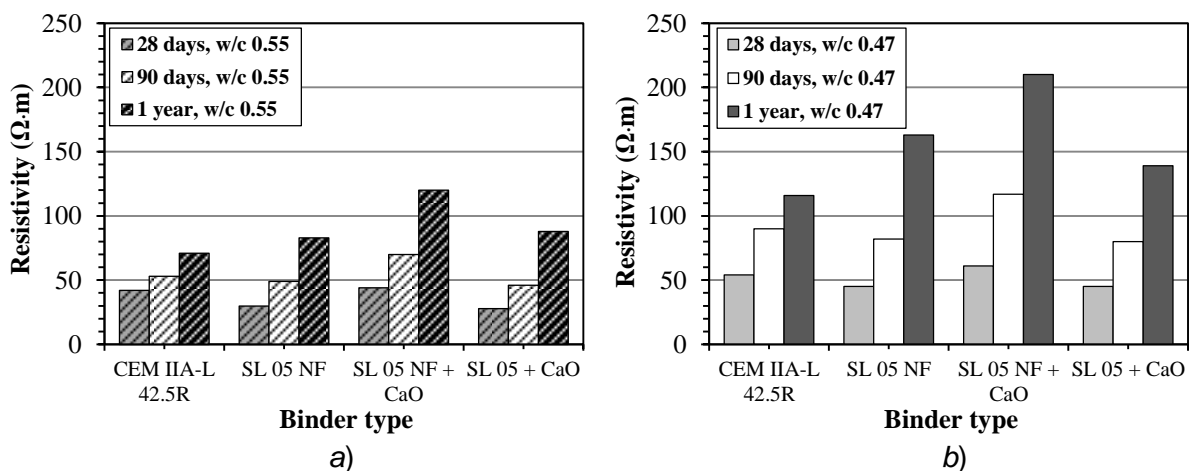


Figure 4.10 Electrical resistivity (average value of two or three replicate specimens) of reference concrete and CSA-based concretes made with w/c ratios of a) 0.55 and b) 0.47 after 28 days, 90 days and 1 year of water curing.

Capillary absorption and water absorption

The sorption coefficient S ($kg/(m^2 \cdot h^{0.5})$) of capillary absorption was calculated for all CSA-based concretes and reference concrete studied in this research.

Figure 4.11 shows the average sorption coefficient of each type of concrete made with two w/c ratios (0.47 and 0.55). At both w/c ratios (0.47 and 0.55), reference concrete showed the highest sorption coefficient (0.62 and $1.13 kg/(m^2 \cdot h^{0.5})$), confirming again that CSA-based concretes developed denser microstructure than ordinary concrete. The addition of CaO slightly increased sorption coefficient of CSA-based concrete.

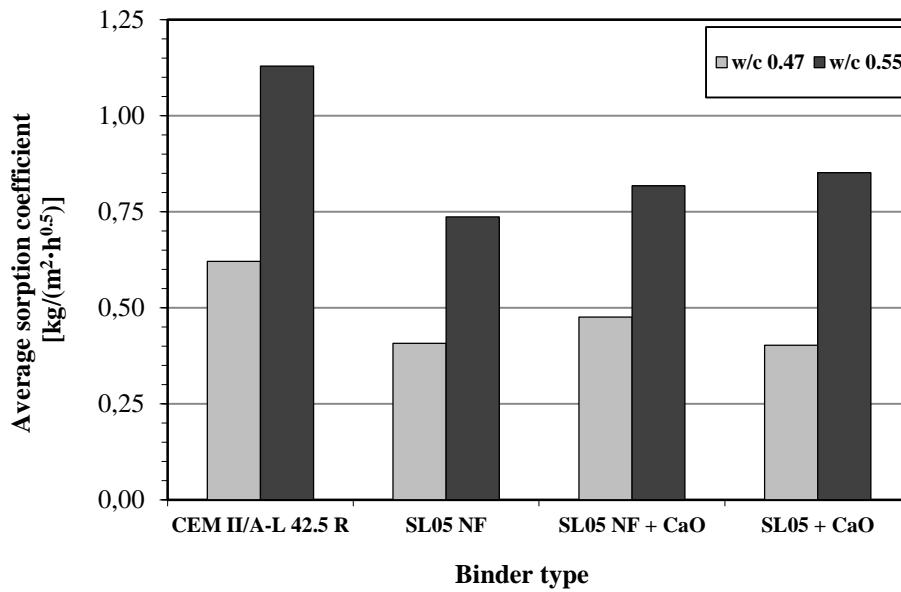


Figure 4.11 Sorption coefficient (average value of two replicate specimens) of reference concrete and CSA-based concretes made with 0.47 and 0.55 w/c ratios.

The water absorption test at atmospheric pressure can reflect the open porosity of concrete. **Figure 4.12** shows the total water uptake of reference concrete (4.8% and 5.9% respectively for w/c ratios of 0.47 and 0.55) and CSA-based concretes at the end of test. CSA-based concretes showed only a slightly higher open porosity than reference concrete. The addition of CaO had no influence on the open porosity of concrete. Considering the fact that “SL05” cement was the blend of limestone cement (CEM II/A-L 42.5R) with CSA clinker (30%), it might be deduced that CSA clinker leads to higher open porosity of concrete.

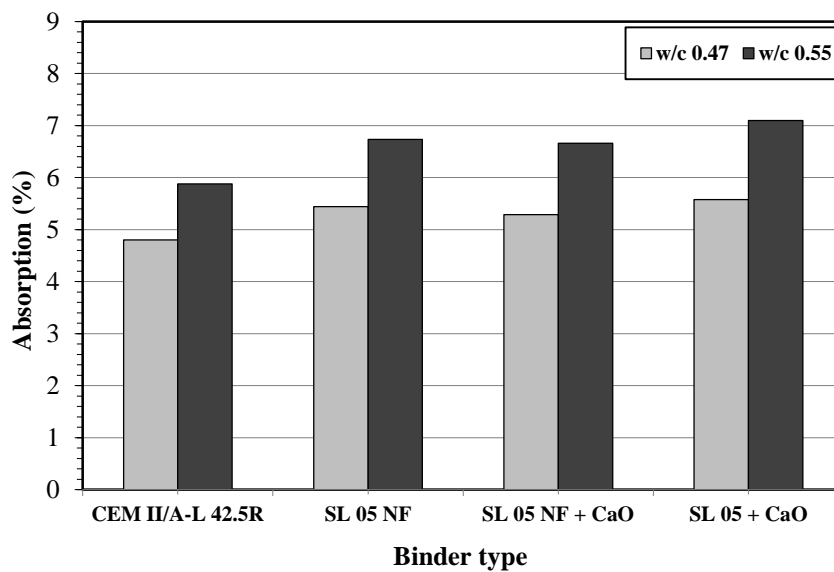


Figure 4.12 Absorption (average value of two replicate specimens) of reference concrete and CSA-based concretes made with 0.47 and 0.55 w/c ratios under fully immersion for 52 days.

Carbonation resistance

In relation to service life of reinforced structures, the concrete resistance to the penetration of carbonation should be assessed (both in accelerated and natural carbonation).

Figure 4.13 compares the carbonation coefficients of reference concrete and CSA-based concretes subjected to accelerated carbonation (4% CO₂, 65 ± 5% R.H. and 20°C). CSA-based concretes made with “SL05 NF” and “SL05 NF+CaO” binders showed the comparable carbonation resistance with reference concrete regardless of w/c ratio, ranging between 33 and 40 mm/year^{0.5}. However, CSA-based concrete made with “SL05+CaO” binder had weaker carbonation resistance (47 mm/year^{0.5}) than reference concrete. Considering the fact that “SL05” cement is the blend of limestone cement (CEM II/A-L 42.5R) with CSA clinker, this result confirms that CSA clinker has weaker carbonation resistance when compared to ordinary concrete, as has been reported in [97], [103], [111]. This is because ettringite is susceptible to carbonation [103]–[105].

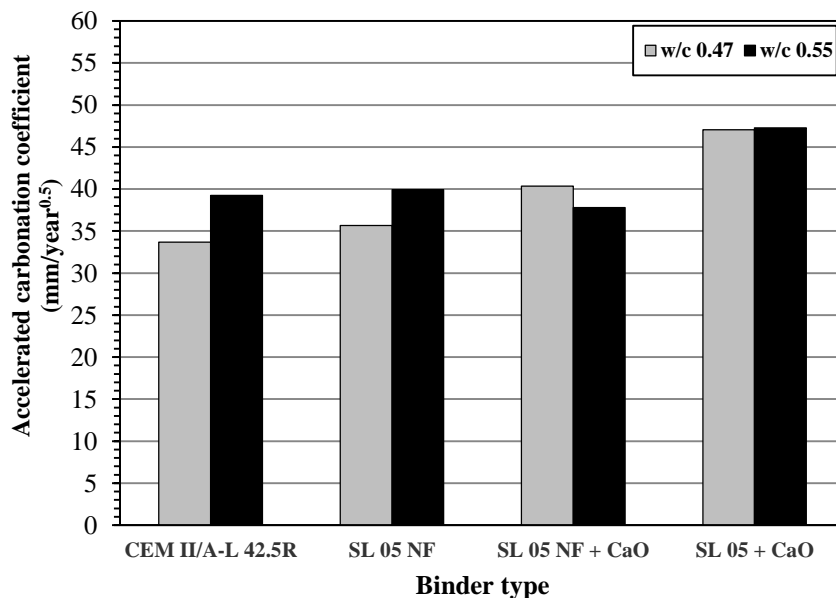


Figure 4.13 Accelerated carbonation coefficient (average value of two replicate specimens) of reference concrete and CSA-based concretes (cured 28 days) made with different w/c ratios (0.47 and 0.55) after around 70 days accelerated carbonation (4% CO₂, 65 ± 5% R.H. and 20°C).

Figure 4.14 shows the carbonation coefficients of reference concrete and CSA-based concretes cured for different time (7 and 28 days) under natural carbonation. It seems that curing time has no significant influence on carbonation resistance of both reference concrete and CSA-based concretes. CSA-based concrete made with “SL05+CaO” binder had the worst carbonation resistance (around 7 mm/year^{0.5}). Whereas CSA-based concretes made with “SL05 NF” and “SL05 NF+CaO” binders did not show significant carbonation resistance when compared to reference concrete (around 4.5 mm/year^{0.5}).

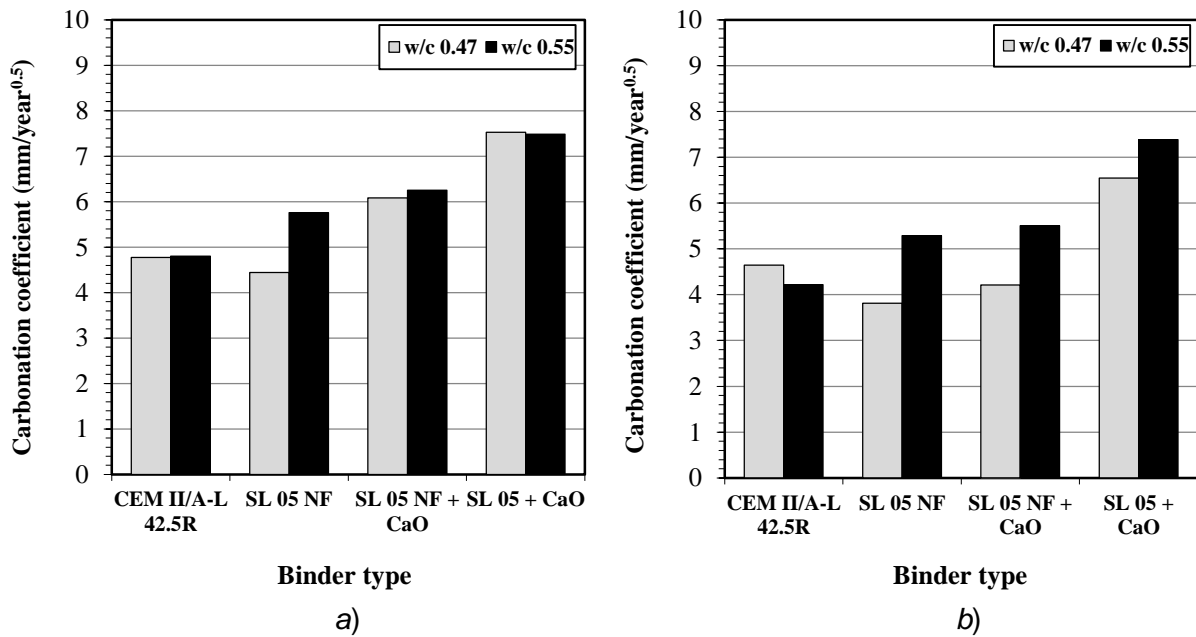
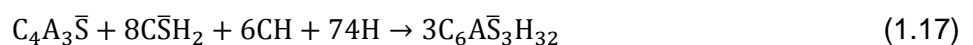


Figure 4.14 Carbonation coefficient of reference concrete and CSA-based concretes made with different w/c ratios (0.47 and 0.55) a) cured 7 days, and b) cured 28 days, after 1 year outdoor exposure.

Chloride penetration resistance

Also, the resistance to chlorides penetration of CSA-based concretes was studied.

Figure 4.15 shows the chloride diffusion coefficients of reference concrete and CSA-based concretes with different w/c ratios (0.47 and 0.55) measured after immersion for 7 months in 3.5% NaCl solution. CSA-based concretes showed the better resistance to chloride penetration when compared to reference concrete, which is in agreement with the results reported in [113]. In particular, the lowest diffusion coefficients were measured for concrete made with SL05 NF cement and with w/c ratios of 0.47 and 0.55, respectively equal to 6 and $8 \times 10^{-12} \text{ m}^2/\text{s}$. concretes with blended CSA cements (such as SL05 NF and SL05) and an addition of CaO showed an intermediate behaviour in terms of resistance to chloride penetration between ordinary concrete and concrete with SL05 NF cement. Addition of CaO contributed to increase the diffusion coefficient of blended CSA concrete. Moreover, the role of w/c ratio was more evident in concrete made with addition of CaO. High AFm/AFt ratio (AFm:monosulphate ($\text{C}_6\text{A}\bar{\text{S}}_3\text{H}_{12}$), AFt:ettringite ($\text{C}_6\text{A}\bar{\text{S}}_3\text{H}_{32}$)) is helpful for enhancing the chloride penetration resistance of CSA-based concretes, owing to the chloride binding ability of AFm [109]. The presence of CaO can help form more AFt according to **Reaction 1.17**, therefore, decreases the AFm/AFt ratio.



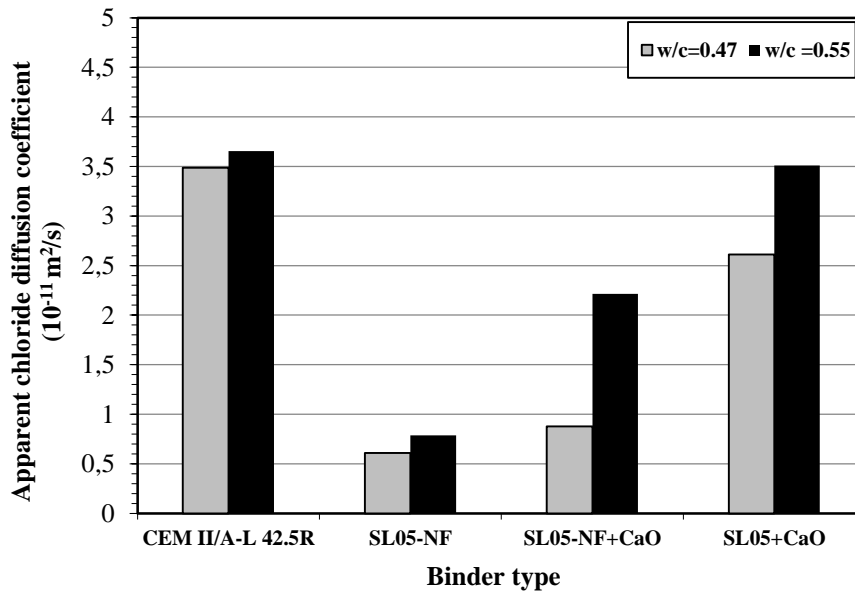


Figure 4.15 Apparent chloride diffusion coefficient of reference concrete and CSA-based concretes made with different w/c ratios immersed in 3.5% NaCl solution for 7 months.

4.3.1.3 Properties of cement-stabilised rammed earth

Rammed earth has been used for thousands of year also in many historic building placed around the world but in recent decades it has stimulated many interests due to increasing environmental concerns. While the technique has changed little since its origin, it's now common practise to stabilise rammed earth with small quantities of cement, making it a sustainable cementitious materials. Steel reinforcement embedded in cement-stabilised rammed earth (CSRE) is a further example of adaptation of this traditional technique. The main properties of the CSRE studied in this research has discussed in order to evaluate its protection capacity to the embedded steel.

The composition of cement-stabilised rammed earth (CSRE) studied in this research was designed in order to obtain a target dry density of 1827 kg/m^3 . This low density measured for CSRE studied in this research (below 2000 kg/m^3) is reasonable in relation to the modest dosage of cement and to high w/c ratio which have been considered. The compressive strength of CSRE highly depends on the cement dosages as well [118]. Higher cement dosage can result in more cementitious materials available to form water insoluble bond with sand particles and enhance the strength of CSRE [138]. Due to the low cement dosage (5% by soil mass) considered in this research, the compressive strength of CSRE ranged between 3 and 4 MPa. The electrical resistivity measured for ordinary concrete was around $60 \Omega \cdot \text{m}$ after 28 days curing (**Table 3.1**), whereas the electrical resistivity of CSRE was below $20 \Omega \cdot \text{m}$ at the same curing time (**Table 3.7**). The low electrical resistivity of CSRE suggests that CSRE may have a porous microstructure, considering the low cement dosage in CSRE that means no enough cement paste is available to fill sufficiently the void between sand particles or bond sand particles. Due to the high porosity of CSRE, the reaction of

carbonation in CSRE exposed in atmosphere took place quickly with time. In fact, carbonation depths of about 3 mm, 17 mm and 40 mm were measured respectively after 1 day, 3 weeks and 7 weeks of exposure in the laboratory. The relationship between carbonation depth and exposure time is described by linear trend.

4.3.2 Effect of glass powder on corrosion protection of carbon steel

The corrosion behaviour of embedded steel bars was studied in order to investigate whether steel bar can passivate in waste glass mortar similarly as in ordinary mortar. For this purpose, the corrosion conditions of steel bars embedded both in glass and standard mortar were monitored during self-desiccation conditions by measuring the corrosion potential (**Figure 3.41a**) and corrosion rate (**Figure 3.41b**). The passivation state was reached for negligible corrosion rate below 1 mA/m^2 . The time need to embedded steel to reach this passivation condition was evaluated starting from the casting of reinforced specimens and it was defined as passivation time.

Figure 4.16a-b respectively show the passivation time and steady corrosion rate of carbon steels embedded in reference mortar and glass powder mortar under self-desiccation condition. After 6 ~ 7 days, the carbon steel bars embedded in both reference mortar and glass powder mortar reached the passive state. The passivation of carbon steel in mortar could be affected by such factors as pH, electrical resistivity and capillary porosity of concrete which are influenced by the hydration process of cement [147]. As shown in **Figure 4.1**, pH of glass mortar reached 13. Moreover, it's all known that the pozzolanic reaction can help refine the microstructure of concrete or mortar, which benefits for capillary porosity [148] and electrical resistivity [63], [72] of concrete or mortar. Therefore, using glass powder in mortar is beneficial for the passivation of steel. As a consequence, the steady corrosion rate of carbon steels embedded in glass powder mortar (0.17 mA/m^2) was even lower than that in reference mortar (0.47 mA/m^2).

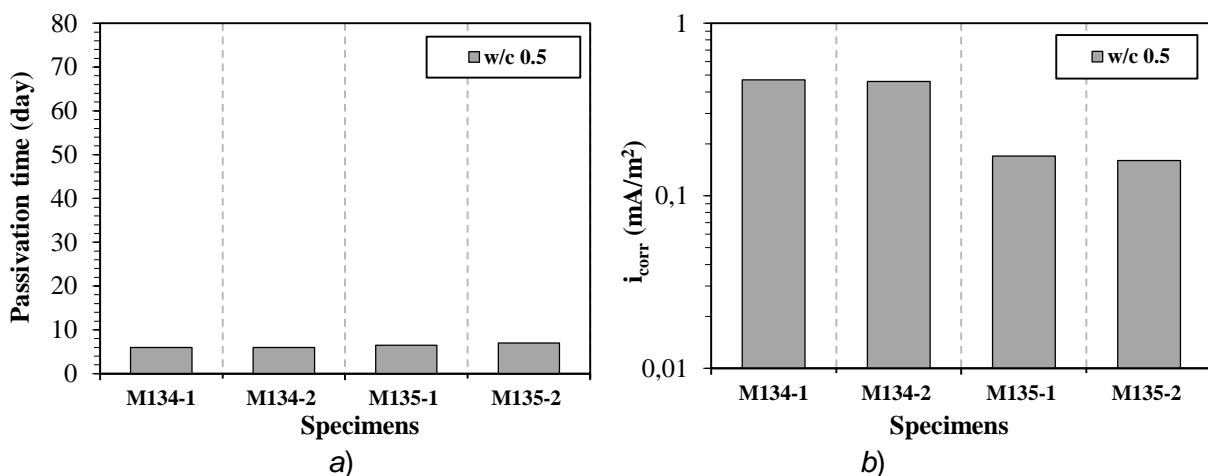


Figure 4.16 Comparison of a) passivation time and b) steady corrosion rate (i_{corr}) of carbon steels embedded in reference mortar and glass powder mortar made with 0.5 w/c ratio under self-desiccation condition. (M134:OPC; M135:30% OPC replaced by glass powder.)

4.3.3 Effect of CSA-based cement on corrosion protection of carbon steel

4.3.3.1 Passivation of carbon steel and galvanised steel in CSA-based concrete

Figure 4.17a-b compares respectively the passivation time and steady corrosion rate of carbon steel in various CSA-based concretes with different w/c ratio (with or without 0.4% chloride) under self-desiccation condition. It can be seen that the carbon steel bars embedded in CSA-based concretes without chloride showed shorter passivation time of few days when compared to that of carbon steel in reference concrete without chloride ranged between 7 and 10 days. This might be attributed to the fast kinetics of hydration of CSA clinker and to its denser microstructure at the identical w/c. As a confirmation of the passive state, steel embedded in CSA-based concrete reached low values of corrosion rate ranged between 0.3 and 0.5 mA/m² except for in concrete made with pure CSA cement SR03 (0.9 mA/m², **Figure 4.17b**). However, it's necessary to point out that pure CSA concrete was able to passivate carbon steel even if its pH was lower than those of blended CSA-based concretes as shown in **Figure 4.1**. The alkalinity of pure CSA concrete was enough to guarantee the passivity of carbon steel. Moreover, when carbon steel bars were embedded into concretes with 0.4% chloride, the passivation time of carbon steel was delayed, especially for CSA-based concretes with CaO addition. Anyway, it's clearly seen that the corrosion rate of carbon steel bars embedded in CSA-based concretes with 0.4% chloride was comparable to that in concrete without chlorides.

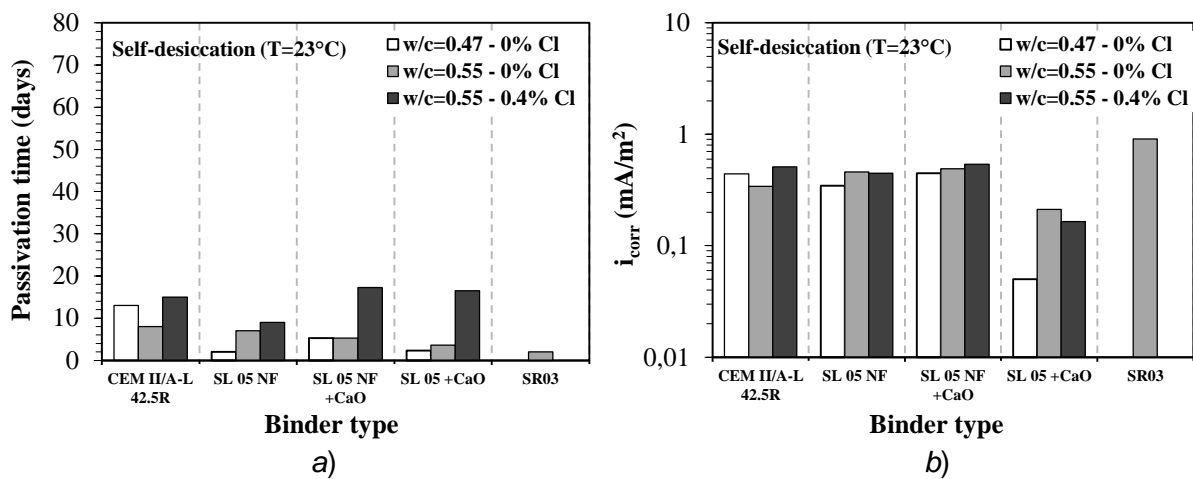


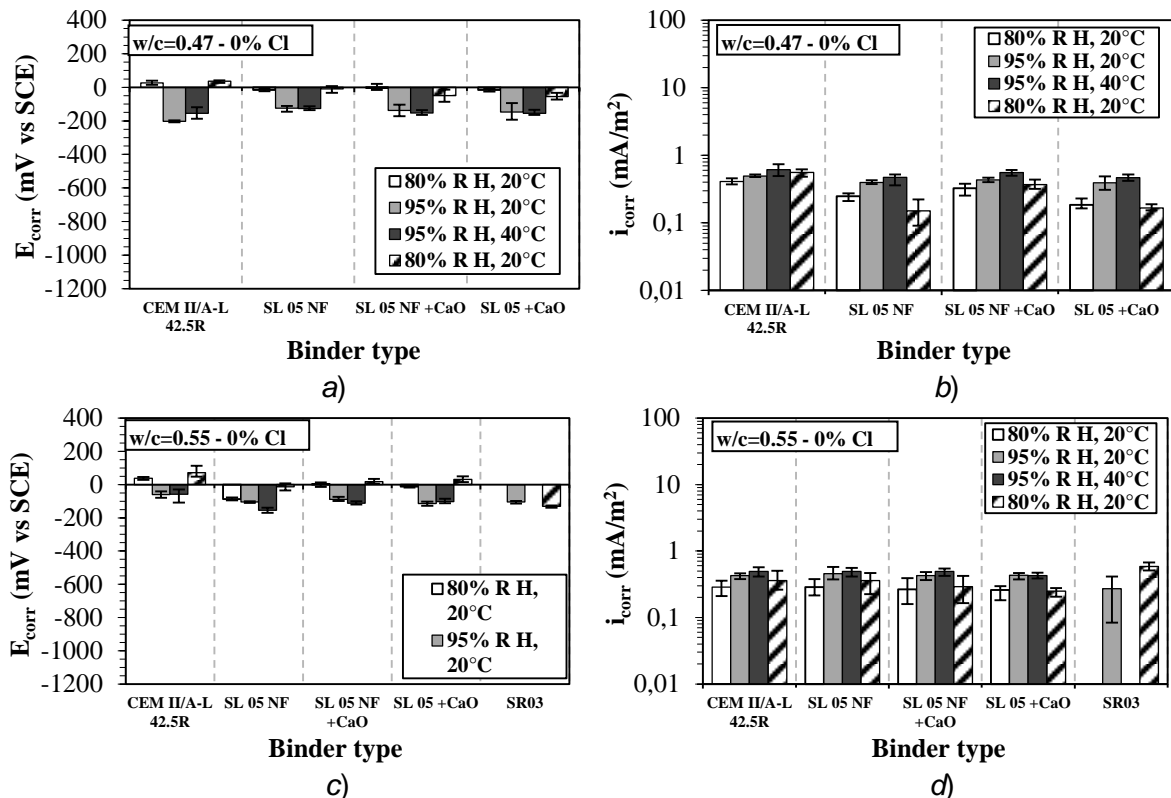
Figure 4.17 Comparison of a) passivation time and b) steady corrosion rate (i_{corr}) of carbon steels embedded in alkaline reference concrete and CSA-based concretes made with different w/c ratios and chloride content under self-desiccation condition.

4.3.3.2 Effect of exposure condition

In order to study the effect of exposure condition on the stability of passivation of carbon steel embedded in CSA-based concretes, reinforced specimens were subjected after self-desiccation

condition to several exposure conditions with different temperature (20°C or 40°C) and relative humidity (80% or 95%).

Figure 4.18 compares the average values of corrosion potential and corrosion rate of carbon steel bars embedded in reference concrete and CSA-based concretes with different w/c ratio (with or without 0.4% chloride), measured in different exposure conditions. The average value was calculated considering only steady values after the transients due to changes in temperature or relative humidity. Regardless w/c ratio and the presence or not of 0.4% chloride, corrosion potential of carbon steel bar embedded in all types of concrete, including pure CSA concrete (SR03), was above -200 mV vs SCE under all exposure conditions. Particularly, when the relative humidity was 80%, the corrosion potential of carbon steel bars maintained in the proximity of 0 mV vs SCE, which might be attributed to the fact that at lower relative humidity, the oxygen was more available in the steel/concrete interface. According to the results of corrosion potential, all carbon steel bars were in passive state. It was in line with the fact that the corrosion rate of carbon steel bar embedded in all types of concrete was lower than 1 mA/m² under all exposure conditions, showing the typical values of the conditions of passivity. Therefore, it was certain that the passivated carbon steel bar embedded in CSA-based concretes maintained its passivation state under all exposed conditions, even in 95% relative humidity and 40°C. Although the pH of pure CSA concrete was not more than 11, as shown in **Figure 4.1**, the low corrosion rate (< 1 mA/m²) of carbon steel in pure CSA concrete, even in 95% R.H., may thank to the higher electrical resistivity of pure CSA concrete [97].



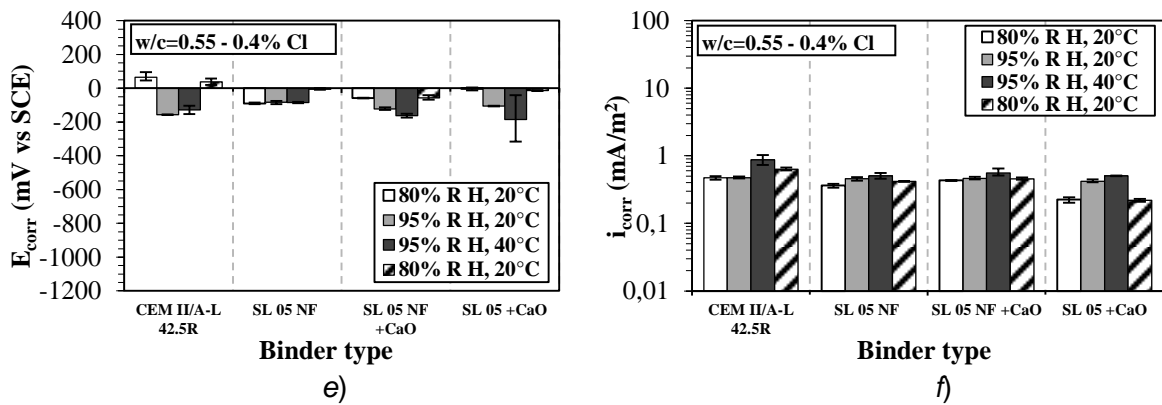


Figure 4.18 Comparison of a), c) and e) corrosion potential (E_{corr} vs SCE) and b), d) and f) corrosion rate (i_{corr}) of carbon steel bars embedded in reference concrete and CSA-based concretes made with different w/c ratio and chloride content measured at the end of each exposure condition.

4.3.4 Effect of cement-stabilised rammed earth on corrosion protection of carbon steel

Figure 4.19a-b show respectively the passivation time and steady corrosion rate of carbon steel bars embedded in cement-stabilised rammed earth (CSRE) specimens (5% cement by soil mass) under self-desiccation condition. All the reinforced rammed earth specimens reached the passive state in 22 ~ 24 days. This could be due to the low cement dosage in CSRE which cannot provide adequate alkalinity to passivate carbon steel quickly. At the end of self-desiccation condition, all carbon steel bars showed corrosion rate below 0.2 mA/m². However, considering the fact that the carbonation depth of CSRE was 40 mm after 47 days of exposure in laboratory condition, it's reasonable to infer that CSRE might rapidly fail to offer corrosion protection to embedded steel due to the fast alkalinity loss caused by carbonation. This hypothesis was confirmed by the low corrosion potential (below -200 mV vs SCE) and slightly high corrosion rate (around 2 mA/m²) of carbon steel bars measured at the end of 48 hours immersion test carried out after 100 days from the manufacture of reinforced specimens, as shown in Figure 4.20.

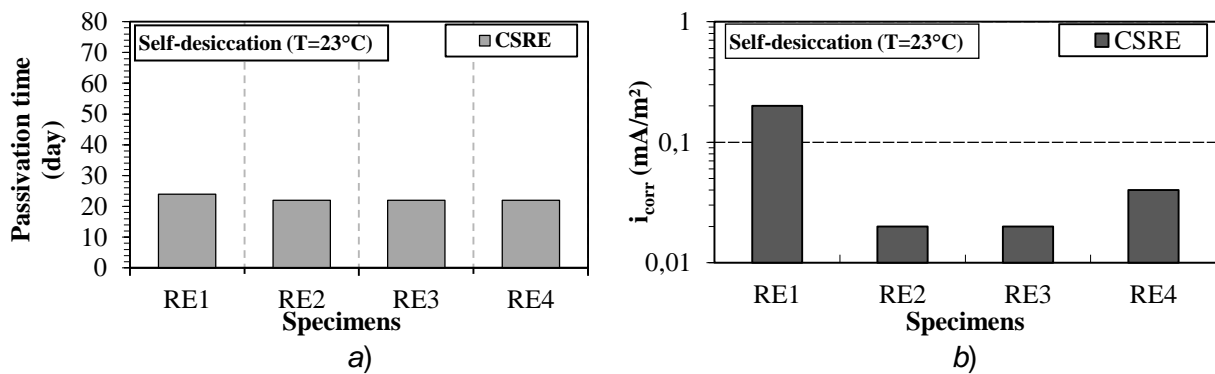


Figure 4.19 Comparison of a) passivation time and b) steady corrosion rate (i_{corr}) of carbon steel bars embedded in cement-stabilised rammed earth specimens (5% cement by soil mass) under self-desiccation condition.

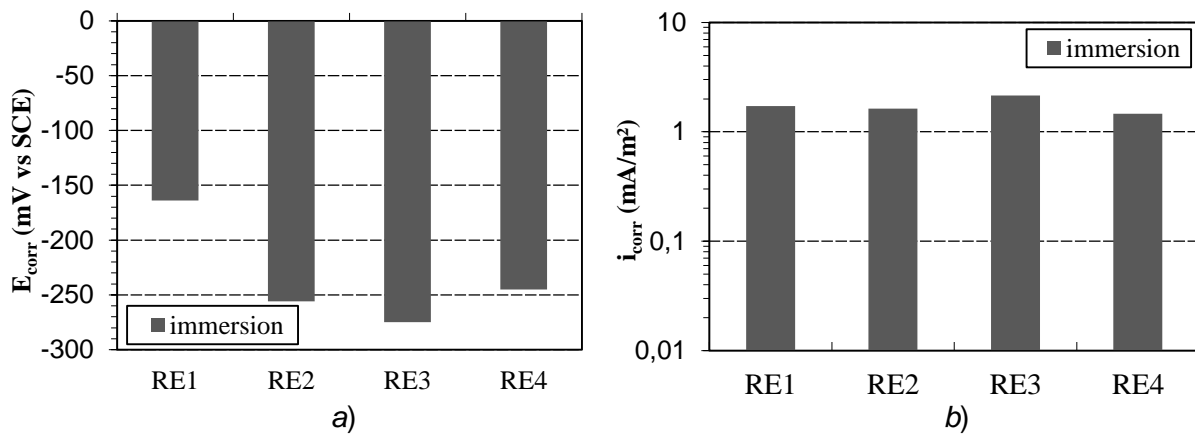


Figure 4.20 Comparison of a) corrosion potential (E_{corr} vs SCE) and b) corrosion rate (i_{corr}) of carbon steel bars embedded in cement-stabilised rammed earth specimens (5% cement by soil mass) at the end of immersion test (48 hours).

4.4 Corrosion behaviour of pre-rusted steel in ordinary concrete

Based on the previous results (**Section 4.2**), the rust present on the surface of carbon steel bars was not detrimental to the passivation of rebars in the ordinary concrete. However, it's necessary to know if rust oxide layers on steel surface can influence the duration of initiation or propagation of corrosion induced by carbonation or chloride penetration. In this section, the corrosion behaviour of pre-rusted steel in carbonated ordinary concrete and in ordinary concrete subjected to chloride penetration are discussed.

4.4.1 In carbonated ordinary concrete

Figure 4.21 shows the corrosion potential and corrosion rate measured on carbonated specimens reinforced with steel bars with different surface conditions at the end of 48 hour of immersion tests. In order to carbonate the reinforced specimens, the reinforced specimens were exposed to accelerated carbonation (4% CO₂, 65 ± 5% R.H. and 20°C). It can be observed that the corrosion potential values of both 10 mm and 18 mm diameter steel bars with different surface conditions in carbonated ordinary concrete were very low (below -400 mV vs SCE) except for 18 mm diameter as-received bar (A1) (**Figure 4.21**). The low corrosion potential of steel bars should be ascribed to the alkalinity loss of concrete contact with steel bars due to carbonation. Accordingly, the high corrosion rate (ranging between 5 and 9 mA/m² for 10 mm steel bars and around 10 mA/m² for 18mm steel bars) of reinforced specimens confirmed that all steel bars in carbonated concrete were depassivated except 18 mm diameter as-received bar (A1) which had not been depassivated yet, showing only a corrosion rate of 0.8 mA/m². It can be noticed that no significant difference of corrosion potential and corrosion rate can be found between all these active steel bars even if they present different surface conditions. Therefore, pre-rusting of steel bar did not lead to more serious corrosion in carbonated ordinary concrete than “as-received” steel bar or sandblasted bar.

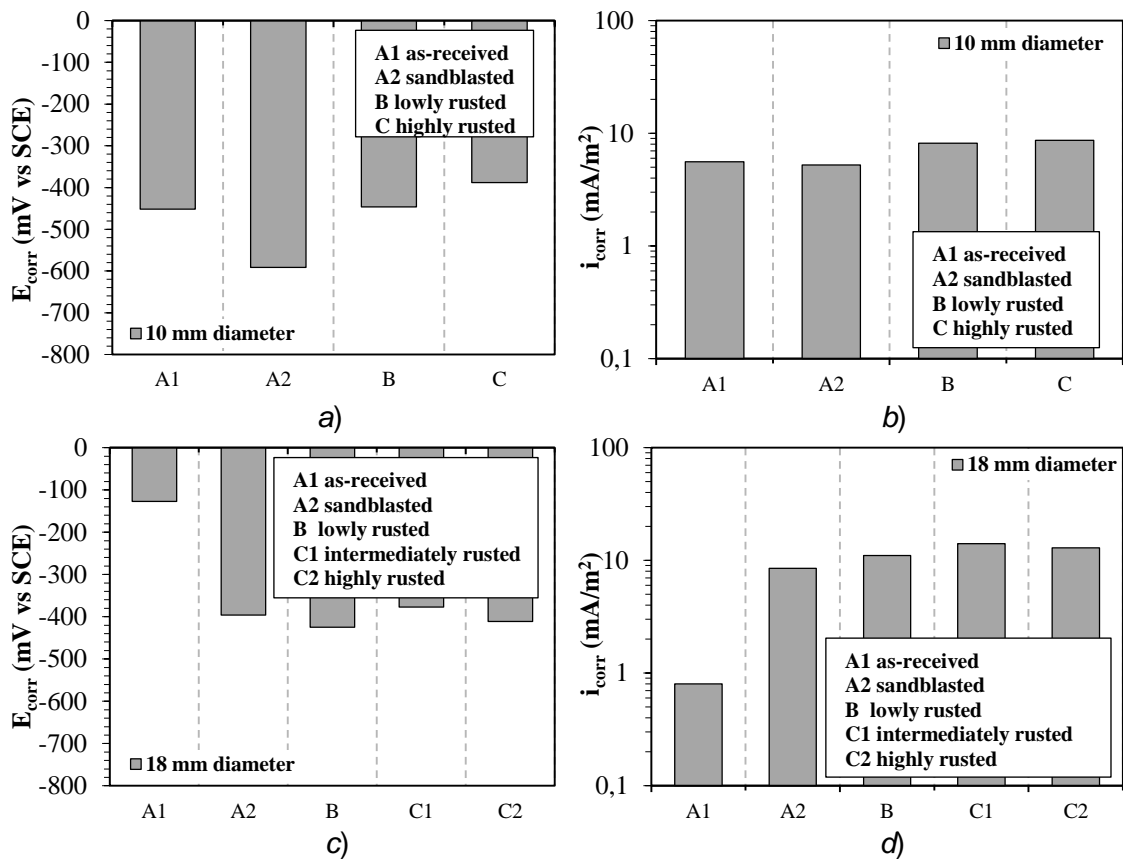


Figure 4.21 Corrosion potential (E_{corr} vs SCE) and corrosion rate (i_{corr}) of steel bars with different surface conditions and different diameters: a) and b) 10 mm and c) and d) 18 mm embedded in carbonated ordinary concrete measured at the end of immersion test (48 hours).

4.4.2 In ordinary concrete subjected to chloride penetration

Figure 4.22 shows the chloride threshold values of steel bars with different surface conditions embedded in ordinary concrete in terms of their corresponding number of ponding cycles. All the reinforced specimens were immersed in 3.5% NaCl solution for 1 day and dried in laboratory for at least 6 days in each cycle. In case of specimens reinforced with 10 mm steel bars, as shown in **Figure 4.22a**, the chloride threshold value is sequenced by A1 (as-received) < B (exposed 6 months) < A2 (sandblasted) < C (exposed 1 year). Particularly, the highly rusted bars have significantly higher chloride threshold value than other steel bars with different surface conditions. The result is in agreement with the finding in [12] that sandblasting can increase chloride threshold value of steel; the authors attributed it to the bare surface of sandblasted steel favouring the formation of a fresh and dense passive film. The results proved also the observation that rust layer can help increase chloride threshold value as reported in [16], [29]. **Figure 4.23** shows the surface condition of steel bars (10 mm diameter) with different initial surface conditions removed from splitted reinforced specimens. It can be clearly seen that each steel has a pitting spot which is typical pitting corrosion induced by chloride. It's necessary to point out that pre-rusted bar labelled as "B" has similar surface condition like as-received bar, showing no visible rust on surface except

pitting spot. However, it seems there still remained a red-brown rust layer on the “C” steel except pitting spot. Thus, the high chloride threshold value of “C” steel might be attributed to the weak physical barrier of rust layer between steel and cement hydrates [28].

Reinforced specimens with 18 mm sandblasted steel bars “A2” and lowly rusted steel bars “B” showed some variations of chloride content, as shown in **Figure 4.22b**. For this reason, the order of chloride threshold value of 18 mm steel bars is not very clear. However, the chloride threshold value of 18 mm as-received steel bars (around 0.5%) was much higher than that of 10 mm as-received steel bars (around 0.2%). This might be due to the defects of mill scale present on 10 mm as-received steels (**Figure 3.3**). Both lowly rusted steel bars “B” and intermediately rusted steel bars “C1” showed lower chloride threshold value when compared to as-received steel bars. Highly rusted steel bars “C2” had the highest chloride threshold value. **Figure 4.24a-b** compares the surface condition of steel bar “B-3” before casting and after splitting. The surface of bar “B-3” is apparently not covered by rust layer (pitting spot on the other side). However, it seems the initial rust layer still remained on the surface of bar “C2-3”, as shown in **Figure 4.24d**. Again, the high chloride threshold value of “C2” steel (highly rusted) might be attributed to the weak physical barrier of the remained rust layer. Most of steel bars just showed on single pitting spot as shown in **Figure 4.24d**. However, it’s been noticed that pre-rusted bar “C1-3” showed also a series of small corrosion spots along with its longitudinal rib, as shown in **Figure 4.24c**.

In addition, It’s also observed in **Figure 4.22** that the corrosion of 18 mm diameter steel bars initiated after all 10 mm diameter steel bars had shown clear sign of corrosion initiation, although the concrete cover of specimens reinforced with both 10 mm steel bars and 18 mm steel bars was 25 mm. The reason behind this is not clear, it might be due to different dimension of specimen; but this is out of the scope of this research. It’s necessary to point out that the number of exposure cycle did not seem to be correlated with the chloride threshold values. It should be borne in mind that that the occurrence of pitting corrosion is stochastic [9].

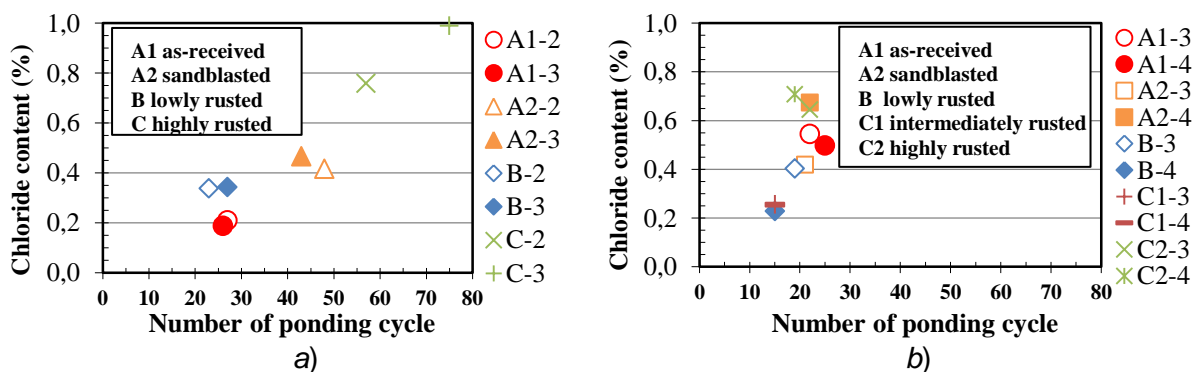


Figure 4.22 Chloride contents (by concrete mass) needed for corrosion initiation measured on concrete samples collected close to steel surface of reinforced specimens with a) 10 mm steel bars and b) 18 mm steel bars with different surface conditions as a function of number of ponding cycles.



Figure 4.23 The surface condition of 10 mm diameter steel bars with different initial surface conditions removed from the splitted reinforced specimen. (A1:as-received; A2:sandblasted; B:exposed for 6 months; C:exposed for 1 year)



Figure 4.24 Surface condition of steel bars with 18 mm diameter labelled “B-3” a) before casting and b) after splitting (pitting spot on the other side), c) “C1-3” and d) “C2-3”. (B:exposed for 6 months; C1 and C2:exposed for 1 year)

4.5 Corrosion behaviour of carbon steel in carbonated CSA-based concretes

Once the concrete cover of reinforced specimen is entirely carbonated (and hence steel is depassivated), the propagation stage of steel corrosion begins. In order to evaluate the corrosion behaviour of the steel in the different types of concrete during the propagation stage, reinforced specimens made with CSA-based concretes were exposed to the same cycles of relative humidity and temperature described for the alkaline reinforced specimens. In fact, the corrosion behaviour of steel in carbonated concrete strongly depends on relative humidity as illustrated in **Figure 4.25**. When the moisture content in concrete is less than 80%, the effect of ohmic drop must be taken into account [5]. In this section, the corrosion behaviour of carbon steel in carbonated CSA-based concretes subjected to exposure conditions with different temperature (20°C or 40°C) and relative humidity (80% or 95%) are discussed.

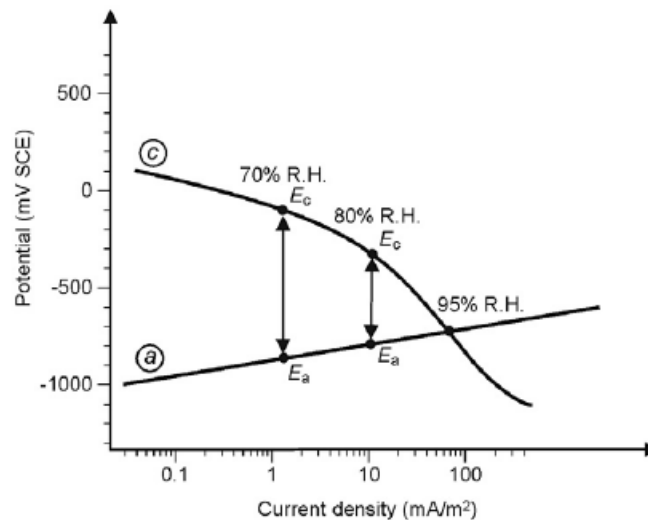


Figure 4.25 Schematic representation of the corrosion conditions of steel in carbonated concrete under environments with different humidity [5]. (Ⓐ symbol represents anodic curve, Ⓒ symbol represents cathodic curve.)

Figure 4.26 shows the average values of corrosion potential and corrosion rate of carbon steel embedded in carbonated CSA-based concretes ($w/c=0.55$) made with different binders, without and with chloride (0.4%), measured in different exposure conditions. The average value was calculated considering only steady values after the transients due to changes in temperature or relative humidity. Due to the alkalinity loss caused by carbonation, thus the corrosion potential of carbon steels in carbonated CSA-based concrete is much lower than that of carbon steels in alkaline concrete. In the condition of 95% relative humidity (at both 20°C and 40°C), regardless the presence of 0.4% chloride, the corrosion potential of carbon steel bars in carbonated CSA-based concrete was lower than -200 mV vs SCE whereas their corrosion rate values were higher than 1

mA/m^2 , confirming that all carbon steel bars were in active state. It can be observed that the addition of CaO can slightly decrease the corrosion rate of carbon steel, accompanied with the slight increase of corrosion potential of carbon steel, which should be ascribed to the increase of electrical resistivity of concrete. Without the addition of CaO, the corrosion potential and corrosion rate of steel bar embedded in CSA-based concrete was comparable with that in reference concrete. Under 20°C and 80% R.H. exposure condition, the corrosion potential of carbon steels in CSA-based concretes without chloride was above -200 mV vs SCE, accompanied with corrosion rate lower than 1 mA/m^2 . This should be attributed to the effect of ohmic resistive control, as shown in **Figure 4.25**. However, by adding 0.4% chloride, the corrosion potential of carbon steel decreased while the corrosion rate of carbon steel increased. Again, the addition of CaO can decrease the corrosion rate of carbon steel and increase the corrosion potential of carbon steel slightly.

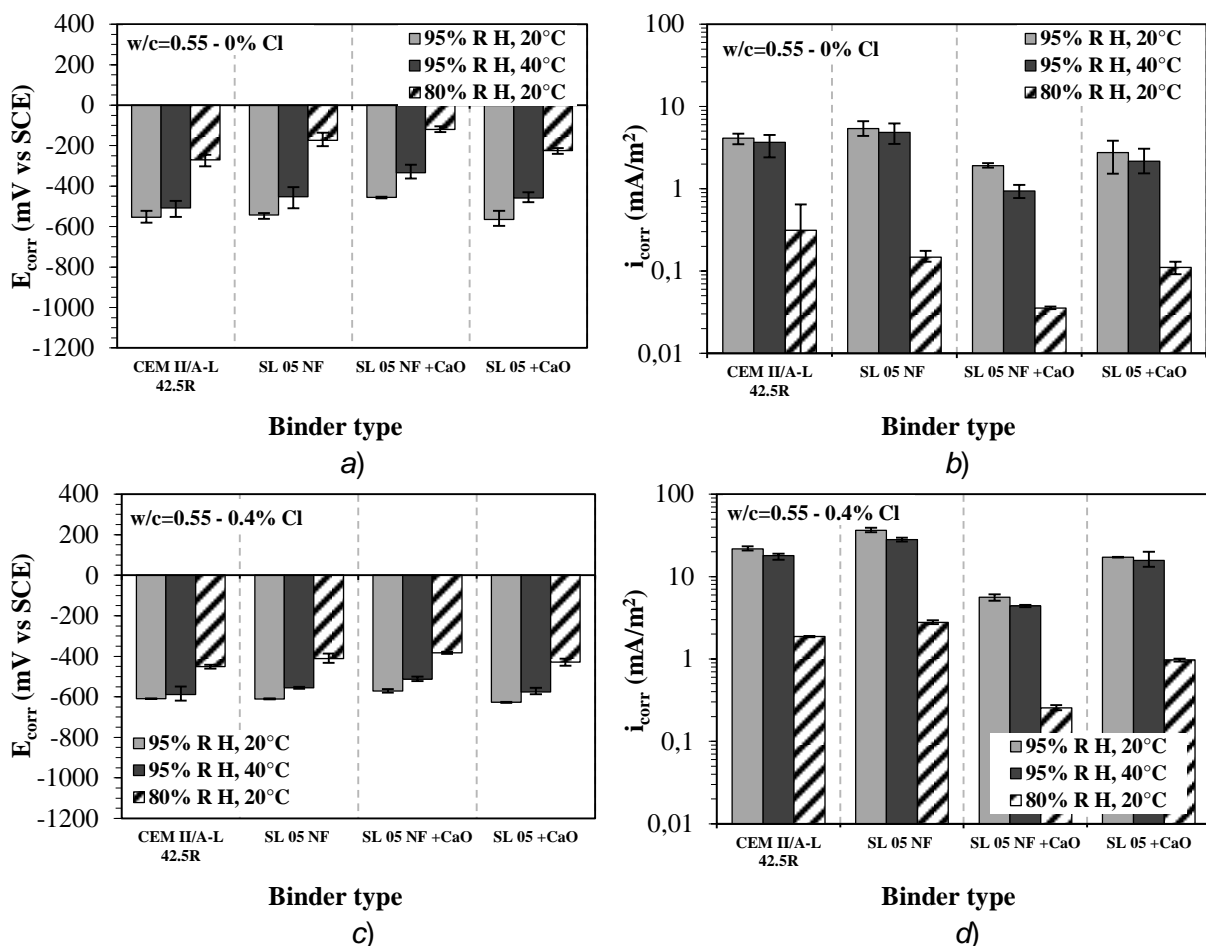


Figure 4.26 Comparison of a) and c) corrosion potential (E_{corr} vs SCE) and b) and d) corrosion rate (i_{corr}) of carbon steel bars embedded in carbonated reference concrete and CSA-based concretes ($w/c=0.55$) without and with chloride measured at the end of each exposure condition.

The corrosion condition of carbon steel was verified by visual examination after splitting all the reinforced specimens at the end of electrochemical tests. As an example, **Figure 4.27** shows the surface condition of carbon steel embedded in 0.55 w/c ratio carbonated CSA-based concrete made by SL05 NF binder without and with chloride after splitting reinforced specimens. It can be seen that the surface of carbon steel bars shows the typical general corrosion induced by carbonation. The carbon steel bars embedded in other type of concrete showed the similar appearance.



Figure 4.27 The surface condition of carbon steel in 0.55 w/c ratio carbonated CSA-based concrete a) without chloride and b) with 0.4% chloride made with SL05 NF cement.

In order to check if all types of carbonated concrete were carbonated completely, the pH of pore solution was estimated on powder samples of carbonated concrete close to steel surface after splitting reinforced specimens. **Figure 4.28** shows the pH of carbonated concrete pore solution was approximately around 9.3 without significant difference between the different types of concrete. Clearly, it can be seen that all types of concrete are carbonated completely.

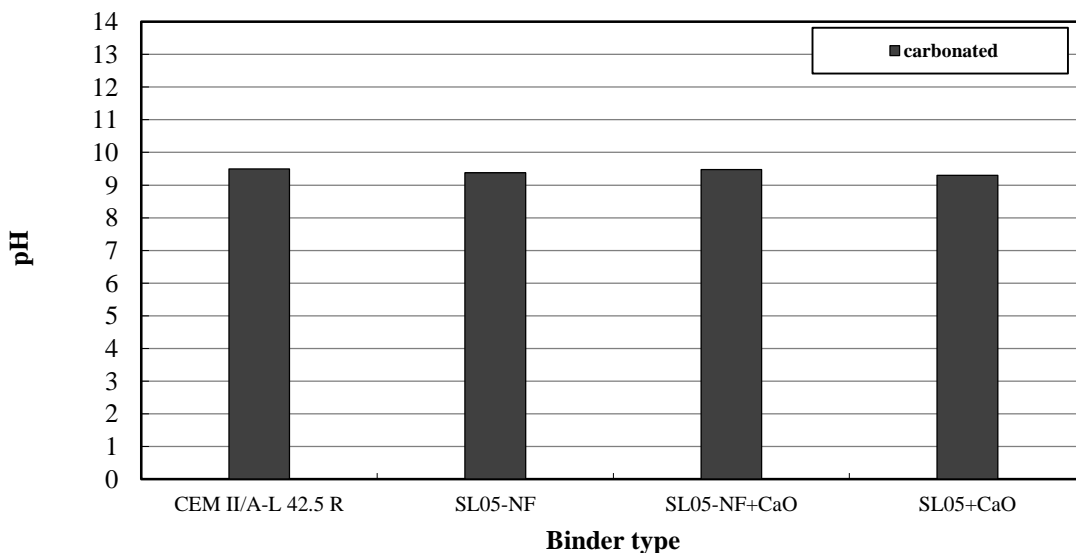


Figure 4.28 pH of carbonated reference concrete and CSA-based concretes (w/c=0.55) made with different binders (free-chloride) measured at the end of electrochemical tests.

4.6 Passivation of galvanised steel in CSA-based concretes and its corrosion behaviour in carbonated CSA-based concretes

If the alkalinity of CSA-based concrete is not enough to passivate carbon steel, it could be used an alternative type of reinforcement, i. e. galvanised steel which is a type of corrosion-resistant steel. Moreover, if galvanised steel can have low corrosion rate when embedded in carbonated CSA-based concretes, it can help prolong the propagation time of steel corrosion. In this section, the passivation of galvanised steel in CSA-based concretes and its corrosion behaviour in carbonated CSA-based concretes are discussed.

4.6.1 Passivation of galvanised steel in CSA-based concrete

Figure 4.29a-b compare the passivation time and steady corrosion rate of galvanised steel in various CSA-based concretes with different w/c ratios (with or without 0.4% chloride) under self-desiccation condition. Galvanised steels in all types of concrete took longer (more than 2 weeks in general) to reach passivation state if compared with carbon steel discussed before. Especially, the galvanised steel bars in CSA-based concrete made with SL05 NF binder took much longer to be passivated when compared with the galvanised steel bars in reference concrete. This behaviour could be attributed to the dissolving of zinc layer at high pH caused by cement hydration. Higher passivation time for galvanised steel bars reflects the difficulty of zinc with respect to carbon steel to reach passivity in highly alkaline concrete solution. Although more time was required, passivation occurred also with galvanised reinforcement as confirmed in terms of negligible corrosion rate (**Figure 4.29b**) comparable to that obtained for carbon steel bars. However, the addition of CaO showed a significant benefit to the passivation of galvanised steel, which might be ascribed to the reason that the formation of passive film on galvanised steel depends on also the concentration of calcium ions in concrete, as indicated in **Reaction 1.5** [36], [37].



It can be observed that the corrosion rate of galvanised steel in CSA-based concrete was comparable to that of galvanised steel in reference concrete (0.2 mA/m^2). Especially, galvanised steel in CSA-based concrete made with SL05+CaO binder showed slightly lower corrosion rate. It can be also seen that the corrosion rate of galvanised steel in pure CSA concrete (SR03) was slightly lower than in other concretes. This could be due to the low pH of pure CSA concrete, as shown in **Figure 4.1**, which decreases the corrosion rate of zinc layer of galvanised steel.

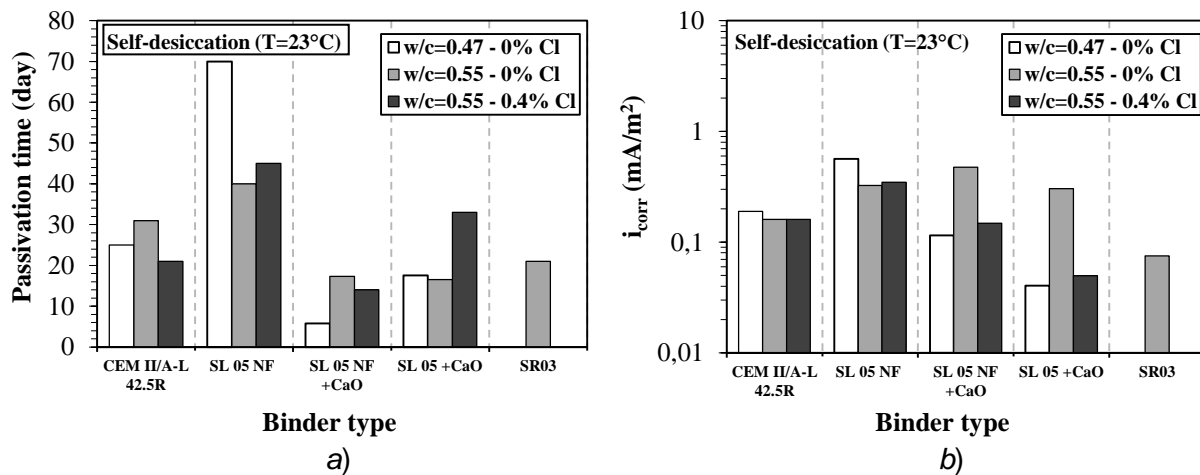


Figure 4.29 Comparison of a) passivation time and b) steady corrosion rate (i_{corr}) of galvanised steel embedded in alkaline reference concrete and CSA-based concretes with different w/c ratios and chloride content under self-desiccation condition.

4.6.2 Effect of exposure conditions

In order to study the effect of exposure condition on the stability of passivation of galvanised steel embedded in CSA-based concretes, reinforced specimens were subjected to exposure conditions with different temperature (20°C or 40°C) and relative humidity (80% or 95%) after self-desiccation condition.

Figure 4.30 shows the average values of corrosion potential and corrosion rate of galvanised steel bars embedded in reference concrete and CSA-based concretes with different w/c ratios (with or without 0.4% chloride), measured in different exposure conditions. The average value was calculated considering only steady values after the transients due to changes in temperature or relative humidity. When compared to carbon steel as discussed before, the corrosion potential values of galvanised steels were much lower (in general below -400 mV vs SCE). The low potential values are due to the presence of zinc layer on steel surface [149]. It's clearly seen that in 95% relative humidity and 20°C condition, the corrosion potential of galvanised steels was lowest (< -650 mV vs SCE), accompanied with the highest corrosion rate (1~2 mA/m²), as shown in **Figure 4.30a-b**. However, when temperature increased to 40°C, the corrosion potential of galvanised steel bars increased slightly and corrosion rate of galvanised steel bars was slightly lower than 1 mA/m². The corrosion of galvanised steel embedded in concrete is due to the dissolving of zinc layer at high pH caused by cement hydration. It's not clear whether the alleviation of corrosion of galvanised steel at 40°C is related to the rate of dissolving of zinc layer. Under 80% relative humidity and 20°C condition, galvanised steels in all types of concrete showed corrosion potential greater than -550 mV vs SCE and corrosion rate less than 1 mA/m². This might be related to the effect of ohmic resistive control. It's also noticed that the corrosion degree of galvanised steel bars in reference concrete is lower than that in CSA-based concretes. The effect of the addition of CaO

and 0.4% chloride is not significant. In general, the corrosion rate is significantly increased in all specimens due to exposure to high humidity (95%, 20°C) while no significant increasing has been observed when temperature was increased to 40°C at the same relative humidity. It has been observed some difficulties during the monitoring of corrosion potential (E_{corr} vs SCE) and corrosion rate (i_{corr}) (Figure 3.34-35) to obtain constant values for each type of exposure; this should be due to the considerable transformations of the composition of the protective layer of the galvanised reinforcement which could require also long time.

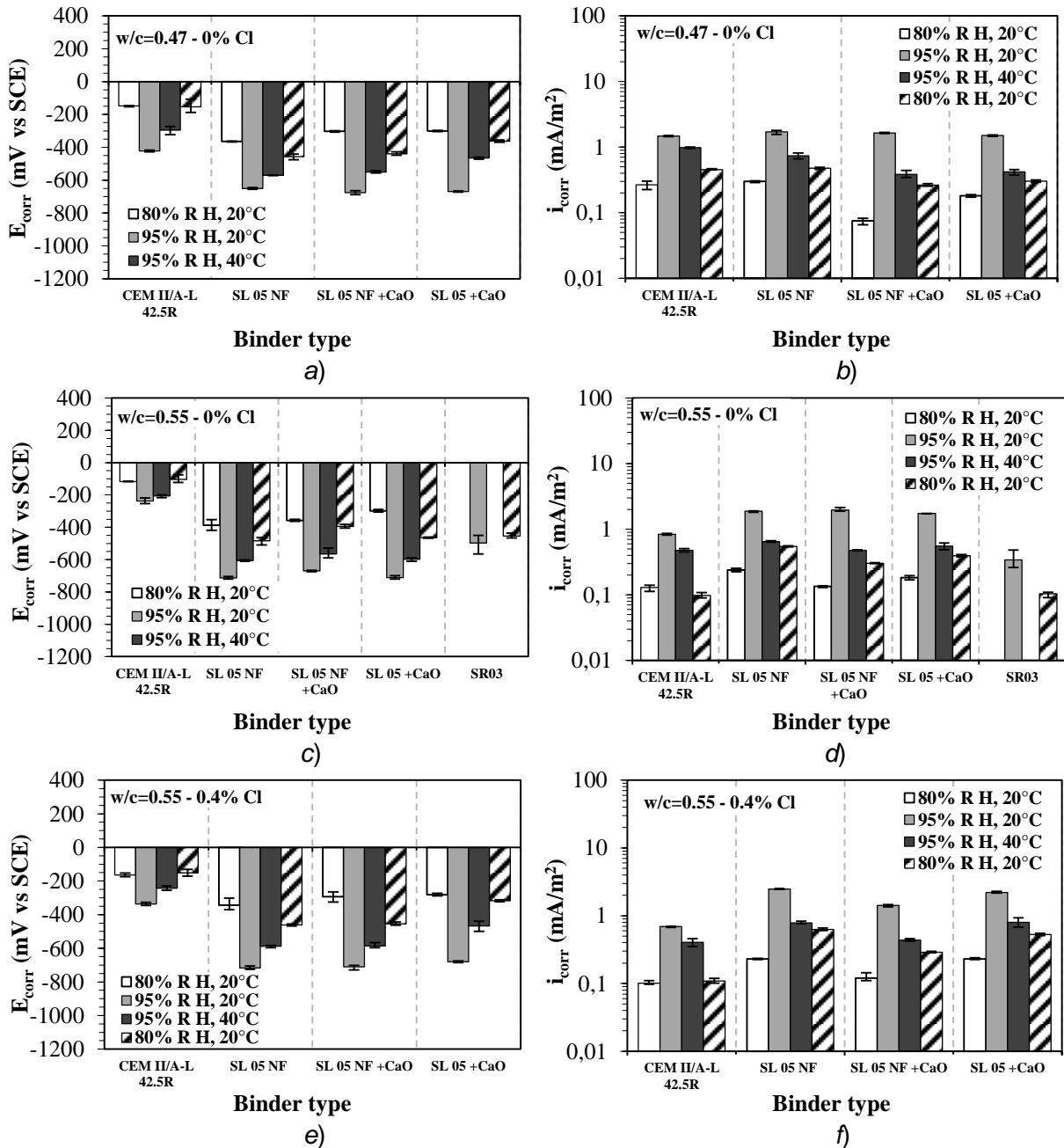


Figure 4.30 Comparison of a), c) and e) corrosion potential (E_{corr} vs SCE) and b), d) and f) corrosion rate (i_{corr}) of galvanised steel bars embedded in alkaline reference concrete and CSA-based concretes made with different w/c ratios and chloride content measured at the end of each exposure condition.

4.6.3 Corrosion behaviour of galvanised steel in carbonated CSA-based concrete

Figure 4.31 shows the mean values of corrosion potential and corrosion rate of galvanised steel embedded in carbonated reference concrete and CSA-based concrete ($w/c=0.55$) made with different binders without and with chloride (0.4%), measured in different exposure conditions. The average value was calculated considering only steady values after the transients due to changes in temperature or relative humidity. Regardless of w/c ratio and the presence or absence of 0.4% chloride, the corrosion rate of galvanised steel bars in carbonated CSA-based concrete was significantly lower than that of carbon steel in carbonated CSA-based concrete. This should be ascribed to the phenomenon that galvanised steel can maintain in passive state even when the concrete is carbonated [37], [40]. The 95% relative humidity (20°C and 40°C) and the presence of 0.4% chloride had a significant effect on the corrosion of galvanised steel bars in all types of carbonated concrete. The presence of 0.4% chloride can significantly increase the corrosion rate of galvanised steel bars in carbonated concrete. Although, it's reported that the chloride threshold of galvanised steel is much higher than carbon steel [42], [49], it is noticeably decreased in carbonated concrete [40]. Again, the addition of CaO cannot benefit to the corrosion of galvanised steel in carbonated CSA-based concrete.

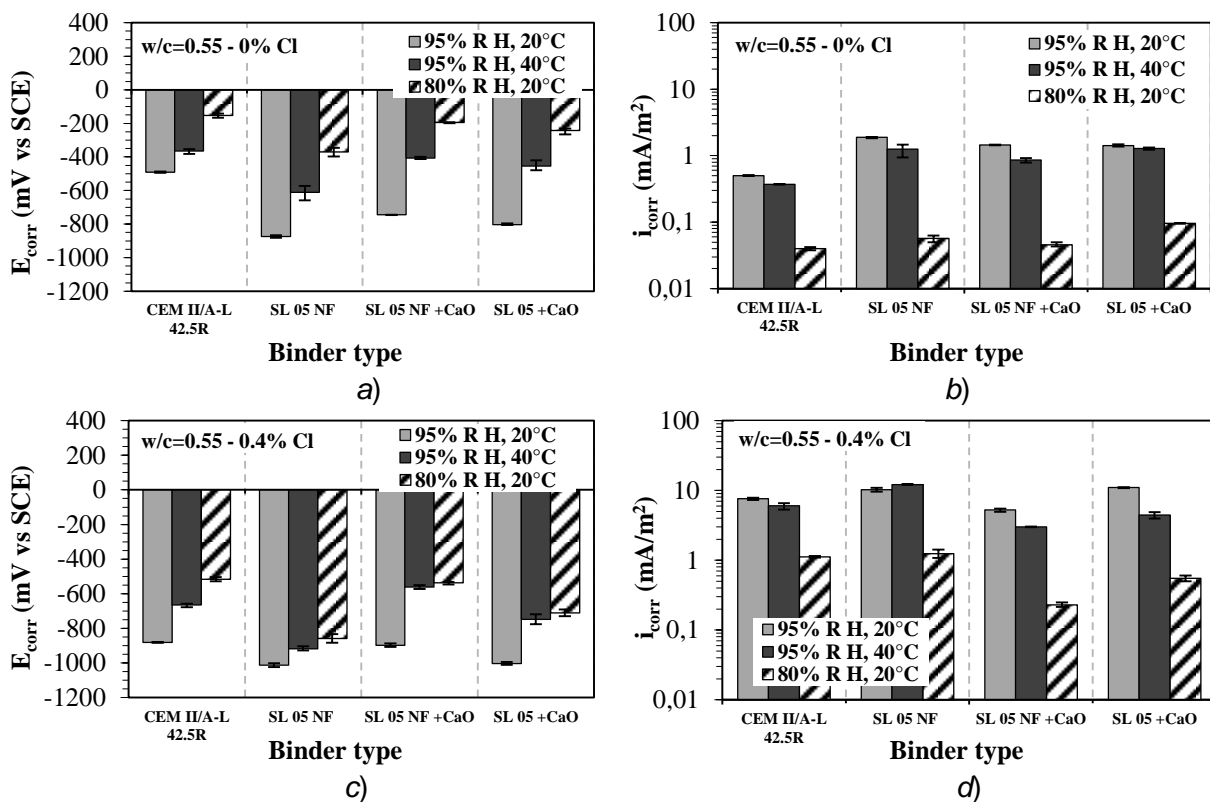


Figure 4.31 Comparison of a) and c) corrosion potential (E_{corr} vs SCE) and b) and d) corrosion rate (i_{corr}) of galvanised steel bars embedded in carbonated reference concrete and CSA-based concretes ($w/c=0.55$) without and with chloride at the end of each exposure cycle.

Conclusions and future work

The corrosion protection of steel embedded in new sustainable cementitious materials, such as waste glass mortar (made with glass powder and expanded glass), calcium sulfoaluminate-based concretes and cement-stabilised rammed earth, was studied. The pH of pore solution of these new sustainable cementitious materials around the steel rebar but also their physical and chemical properties have been considered in order to evaluate the passivation and the corrosion behaviour of steel embedded in them. Moreover, the effect of carbonation and chloride penetration on the corrosion behaviour of steel rebar in new sustainable cementitious materials has been studied.

The experimental tests have confirmed that alkaline chloride-free ordinary concrete made with limestone Portland cement (CEM II/A-L 42.5R cement) could passivate carbon steel bars in not more than 3 ~ 7 days by reaching corrosion rate less than 1 mA/m^2 . The ability of steel to reach passive conditions was studied also in presence of oxide layers such as rust, caused by atmosphere exposure, and the mill scale due to manufacture process on steel surface.

Characterization of rust layer of steel bars suggested that the rust layer formed on steel surface has a porous morphology and it is not a uniform protective layer; its average thickness increased when exposure time increased, reaching around $100 \text{ }\mu\text{m}$ after 1 year outdoor exposure. Moreover, the dark-gray mill scale on newly manufactured rebars, although it appeared compact at the naked eye, it was indeed not always adhering to the steel and it was considerably cracked.

Anyway, the results of corrosion tests revealed that the rust layer and the mill scale on the surface of carbon steel bars are acceptable and not detrimental to the passivation of steel in ordinary concrete (made with CEM II/A-L 42.5R cement); pre-rusted steel bars (both 10 and 18 mm diameter) reached passivation state in ordinary concrete, showing stable passivation in all humidity conditions (self-desiccation, 80% R.H. and immersion). The corrosion behaviour of pre-rusted steel bars with 10 and 18 mm diameter embedded in carbonated ordinary concrete did not show significant difference than that of steel rebars in “as-received” and sandblasted bars, both considered for comparison purpose. Also the role of chloride penetration on the stability of passive state of pre-rusted steel have considered. Based on the experimental results, the highly rusted steel bars (exposed for 1 year) showed the highest chloride threshold values regardless of steel diameter. However, lowly rusted steel bars (exposed for 6 months) showed slightly lower chloride threshold values when compared to sandblasted steel bars.

The durability-related properties of concrete or mortar performed with these studied new binders, have been studied. Based on the experiment results, glass powder improved the workability of mortar, while expanded glass led to a slight decrease. In the early age (7 days), replacing OPC

with 30% glass powder, the compressive strength of mortar with standard sand decreased around 15 MPa; however, glass powder mortar reached a slightly higher strength (71 MPa) after 6 months curing if compared to reference OPC mortar, due to its delayed pozzolanic reaction. Mortars containing expanded glass showed a noticeable strength loss when compared with reference mortar, and maintained their compressive strength around 16 MPa without any strength increase during 6 months curing.

Glass powder, due to the pozzolanic reaction, noticeably increased the electrical resistivity of mortar with standard sand, reaching stable value around 350 $\Omega\cdot\text{m}$. Electrical resistivity of expanded glass mortar without glass powder was slightly lower than that of reference mortar (around 50 $\Omega\cdot\text{m}$) while for the mortar with glass powder and expanded glass electrical resistivity of around 150 $\Omega\cdot\text{m}$ was reached. Glass powder, thanks to the pozzolanic reaction, increased also the resistance to alkaline-silica reaction (ASR) expansion. Lightweight mortars with expanded glass (density about 1300 kg/m^3) demonstrated extremely good resistance to ASR expansion during accelerated tests. However, the expanded glass mortars made without and with glass powder showed crack on the surface respectively at about 30 days and 70 days of accelerated ASR tests as a confirmation their susceptibility to ASR.

In alternative to supplementary cementitious materials (SCMs) such as glass powder, it could use new type of cement such as calcium sulfoaluminate (CSA). Both pure CSA cement (composed by 78% CSA clinker) and blended CSA-based cements (consisting of 30% CSA clinker and 60% ordinary cement) have been studied. Based on experimental results, CSA-based concretes ($w/c = 0.47$ and 0.55) showed higher compressive strength both at early and later age when compared to reference concrete made with Portland limestone cement (CEM II/A-L 42.5R); in particular, a compressive strength of 56 MPa was reached by pure CSA concrete ($w/c = 0.55$) already 1 day after casting, confirming that their high performance of strength at early age was due to the rapid formation of ettringite. The presence of 0.4% chloride (by cement mass) added into the mixtures didn't induce any significant influence to compressive strength. The addition of 2.5% CaO powder (by cement mass) slightly decreased the compressive strength of CSA-based concrete.

In initial stage, i.e. in the first 24 hours after casting, the conductance of CSA-based concretes (both 0.47 and 0.55 w/c ratios) varied drastically; in particular, CSA-based concretes showed sharp peaks just after few hours due to the quick release of ions produced by the hydration of cement. The peaks appeared at the very early stage revealed the faster reaction kinetics of CSA clinker and explained the high early strength of CSA-based concretes.

CSA-based concretes ($w/c = 0.47$ and 0.55) immersed into water have exhibited much higher electrical resistivity in time when compared to reference concrete. The addition of 2.5% CaO in CSA-based concretes enhanced its electrical resistivity noticeably.

Both in natural and accelerated carbonation test, SL05 NF concretes (with and without CaO) made by blending 30% CSA clinker with 60% of CEM I 52.5R showed a similar carbonation resistance to reference concrete made with CEM II/A-L 42.5R cement; SL05 concrete (with CaO) made by blending 30% CSA clinker, with 60% of CEM II/A-L 42.5R performed lower carbonation resistance. In case of natural carbonation, the carbonation coefficients of SL05 NF concretes (with and without CaO) and SL05 concrete (with CaO) were around 4.5 and 7 mm/year^{0.5} respectively. Under the condition of accelerated carbonation, the carbonation coefficients of SL05 NF concretes (with and without CaO) ranged between 35 and 40 mm/year^{0.5} while for SL05 concrete (with CaO) the carbonation coefficient reached 47 mm/year^{0.5}.

CSA-based concretes at both 0.47 and 0.55 w/c ratios showed lower capillary absorption. Low w/c ratio of 0.47 noticeably decreased the capillary absorption of concretes.

The chloride resistance of CSA-based concretes outperformed that of reference concrete. Especially, SL05 NF concrete showed the lowest chloride diffusion coefficient (around 7×10^{-12} m²/s). The addition of 2.5% CaO (by cement mass) increased the chloride diffusion coefficient. CSA-based concretes SL05 NF and SL05 with CaO were susceptible to the change of w/c ratio; increasing w/c ratio from 0.47 to 0.55 significant increased their chloride diffusion coefficients.

Cement-stabilised rammed earth is a further example of sustainable cementitious materials to be used as construction materials even it's necessary to consider some differences with respect ordinary concrete or other new cementitious materials. Based on experimental results, cement-stabilised rammed earth with 5% ordinary cement (by mass of soil) showed a dry density around 1900 kg/m³ and modest compressive strength around 4 MPa after 28 days moist curing. Electrical resistivity of cement-stabilised rammed earth just reached values around 20 Ω•m after 28 days moist curing. Due to the high porosity of cement-stabilised rammed earth, the carbonation reaction took place quickly with time. As a consequence, the carbonation resistance of cement-stabilised rammed earth was very low, based on the fact that carbonation depth reached 40 mm just after 47 days exposure in laboratory condition.

The results from pH tests showed that blended CSA-based mortars (w/c=0.5) had values of pH similar to that reference concrete made with Portland limestone cement (CEM II/A-L 42.5R), ranging between 12.5 and 13. The pH of pure CSA mortar was between 11.2 and 12.

The corrosion behavior of steel embedded in these new sustainable cementitious materials was studied in order to investigate whether steel can reach stable passive conditions regardless from the difference in terms of alkalinity. Based on corrosion tests of steel bars embedded in these new sustainable cementitious materials under self-desiccation condition (23°C), the main findings are:

The results of corrosion tests on carbon steel bars embedded in reference mortar made with CEM I 52.5R cement and glass powder mortar (replacing 30% OPC) indicated that the passivity of carbon steel bar embedded in glass powder mortar was similar as in reference mortar. The passivity conditions of carbon steel bars embedded in glass powder and reference mortars was achieved around 7 ~ 8 days after casting, when their corrosion potential reached values above -200 mV vs SCE and their corrosion rate had values below 1 mA/m².

The passivation of both galvanised and carbon steel bars is guaranteed in CSA-based concretes, even in pure CSA concrete. The average passivation time of carbon steel bars in CSA-based concretes was less than one week after casting, slightly shorter than that of reference concrete regardless of w/c ratio and the addition of CaO. The presence of 0.4% chloride (by cement mass) delayed more than one week the passivation of carbon steel bars in CSA-based concretes with the addition of 2.5% CaO (by cement mass). Longer time was required for the passivation of galvanised steel bars in CSA-based concretes and reference concrete. The average passivation time of galvanised steel bars in CSA-based concretes with CaO was slightly faster than that in reference concrete, less than 17 days regardless of w/c ratio. Nevertheless, SL05 NF CSA-based concrete (without CaO) took more than 40 days in case of w/c ratio of 0.55 and around 70 days in case of w/c ratio of 0.47 to passivate galvanised steel bar respectively.

The presence of 0.4% chloride was observed no effect to the passivation time of galvanised steel, except in SL05 CSA-based concrete (with CaO). The corrosion rate values measured on carbon steel bars in all studied alkaline concrete in alkaline condition were negligible (0.2 ~ 0.7 mA/m²) in all exposure conditions with different relative humidity (80% or 95%) and temperature (20°C or 40°C), confirming the stability of the passive film. Galvanised steel bars in all studied alkaline concrete showed passivity condition regardless of exposure condition as well; only slightly higher values (around 1mA/m²) were observed at higher relative humidity (95%).

Carbon steel bars embedded in cement-stabilised rammed earth made with 5% ordinary cement (by mass of soil) can be passivated within around 3 weeks; however, the carbon steel bars became active after around 2 months exposure in laboratory condition due to the fast carbonation of rammed earth specimens; however, the corrosion rate of carbon steel bars maintained at low level if the specimens were not wetted.

For the study of the corrosion behaviour of carbon steel and galvanised steel in carbonated CSA-based concretes subjected to exposure conditions with different relative humidity (80% and 95%) and temperature (20°C and 40°C), the major conclusions can be draw below:

Carbon steel bars embedded in carbonated CSA-based concretes (w/c=0.55) without chloride showed corrosion rate around 7 mA/m² when exposed to 95% R.H. (20 and 40°C), negligible corrosion rate was observed in 80% R.H. and 20°C exposure condition. Differently, galvanised

steel bars in carbonated concrete showed corrosion rate around 1 mA/m^2 at exposure conditions with high humidity (95%) but below 0.1 mA/m^2 at condition of 80% R.H..

In presence of 0.4% chloride (by cement mass), the corrosion rate of both carbon steel and galvanised steel in all studied carbonated concretes increased. In particular, carbon steel bars embedded in carbonated concrete made with SL05 NF CSA-based cement reached corrosion rate up to 40 mA/m^2 by increasing the relative humidity and temperature until 95% R.H. and 40°C ; in comparison, galvanised steel bars in the same conditions had lower corrosion rate around 10 mA/m^2 . The addition of 2.5% CaO (by cement mass) in CSA-based concretes can improve the corrosion protection of active steel in carbonated CSA-based concretes (absence and presence of chloride), but unfortunately, it cannot prevent the carbonation of blended CSA-based concretes.

Overall, the results presented in this thesis show that there is a great potential for the use of the studied cementitious materials since able to guarantee passivation of steel rebars.

Anyway, as shown based on the obtained results, the corrosion protection of steel embedded in cementitious materials highly depends on the pH of pore solution and the composition and microstructure of such cementitious materials. In fact, their pore microstructure can strongly influence durability-related properties. Moreover, the chemical composition and mix proportion of these new sustainable cementitious studied by different researchers in literature can be a lot of different, particularly for CSA-based cements and cement-stabilised rammed earth (also due to the combined use of supplementary mineral addition such as fly ash and ground blast furnace slag). Anyway, the literature papers dealing with the durability of the new sustainable cementitious materials studied in this research are scarce, not to mention the corrosion protection of steel bars embedded in them.

Owing to inherent relationships among constituents, microstructure and properties of new cementitious materials, more efforts are needed to reveal microstructural features of hardened cement paste.

Consequently, a possible future work could include more detailed microstructural observations on CSA-based concretes, waste glass mortar and cement-stabilised rammed earth by using SEM or other microstructural techniques. It should be useful to determine the pore size distribution and possible pH variation occurring during the hydration process of studied cementitious materials.

List of References

- [1] J. S. Damtoft, J. Lukasik, D. Herfort, D. Sorrentino, and E. M. Gartner, "Sustainable development and climate change initiatives," *Cem. Concr. Res.*, vol. 38, no. 2, pp. 115–127, 2008.
- [2] L. Barcelo, J. Kline, G. Walenta, and E. Gartner, "Cement and carbon emissions," *Mater. Struct.*, vol. 47, no. 6, pp. 1055–1065, 2014.
- [3] PBL Netherlands Environmental Assessment Agency and Joint Research Centre, "Trends in Global CO2 Emissions 2016 Report," pp. 1–86, 2016.
- [4] C. Shi, A. F. Jiménez, and A. Palomo, "New cements for the 21st century: The pursuit of an alternative to Portland cement," *Cem. Concr. Res.*, vol. 41, no. 7, pp. 750–763, 2011.
- [5] L. Bertolini, B. Elsener, P. Pedferri, E. Redaelli, and R. B. Polder, *Corrosion of Steel in Concrete: Prevention, Diagnosis, Repair*. John Wiley & Sons, 2013.
- [6] C. L. Page and M. M. Page, *Durability of Concrete and Cement Composites*. Elsevier Science, 2007.
- [7] L. Wei, M. Hervé, and P. Edouard, "Use of different rapid mixing devices for controlling the properties of magnetite nanoparticles produced by precipitation," *J. Cryst. Growth*, vol. 342, no. 1, pp. 21–27, 2012.
- [8] M. Thiery, G. Villain, P. Dangla, and G. Platret, "Investigation of the carbonation front shape on cementitious materials: Effects of the chemical kinetics," *Cem. Concr. Res.*, vol. 37, no. 7, pp. 1047–1058, 2007.
- [9] L. Bertolini, "Steel corrosion and service life of reinforced concrete structures," *Struct. Infrastruct. Eng.*, vol. 4, no. 2, pp. 123–137, 2008.
- [10] H. Böhni, *Corrosion in Reinforced Concrete Structures*. Elsevier Science, 2005.
- [11] C. Alonso, C. Andrade, M. Castellote, and P. Castro, "Chloride threshold values to depassivate reinforcing bars embedded in a standardized OPC mortar," *Cem. Concr. Res.*, vol. 30, no. 7, pp. 1047–1055, 2000.
- [12] L. Li and A. A. Sagues, "Chloride corrosion threshold of reinforcing steel in alkaline solutions-Open-circuit immersion tests," *Corroison*, vol. 57, no. 1, pp. 19–28, 2001.
- [13] P. Pedferri, "Cathodic protection and cathodic prevention," *Constr. Build. Mater.*, vol. 10, no. 5 SPEC. ISS., pp. 391–402, 1996.
- [14] C. Alonso, M. Castellote, and C. Andrade, "Chloride threshold dependence of pitting potential of reinforcements," *Electrochim. Acta*, vol. 47, no. 21, pp. 3469–3481, 2002.
- [15] E. Zitrou, J. Nikolaou, P. E. Tsakiridis, and G. D. Papadimitriou, "Atmospheric corrosion of steel reinforcing bars produced by various manufacturing processes," *Constr. Build. Mater.*, vol. 21, no. 6, pp. 1161–1169, 2007.
- [16] T. Mehmood, S. N. Ahsan, and M. S. Al-Mughaidi, "Atmospheric Rusting of Rebars and its

- effect on reinforced concrete corrosion,” *Corrosion*, p. 633/1-12, 1998.
- [17] S. J. Oh, D. C. Cook, and H. E. Townsend, “Atmospheric corrosion of different steels in marine, rural and industrial environments,” *Corros. Sci.*, vol. 41, no. 9, pp. 1687–1702, 1999.
- [18] D. de la Fuente, I. Diaz, J. Simancas, B. Chico, and M. Morcillo, “Long-term atmospheric corrosion of mild steel,” *Corros. Sci.*, vol. 53, no. 2, pp. 604–617, 2011.
- [19] E. L. Kemp, F. S. Brezny, and J. A. Unterspan, “Effect of Rust and Scale on the Bond Characteristics of Deformed Reinforcing Bars,” *ACI J.*, vol. 65, no. 9, September, pp. 743–756, 1968.
- [20] H. Bensabra and N. Azzouz, “Study of Rust Effect on the Corrosion Behavior of Reinforcement Steel Using Impedance Spectroscopy,” *Metall. Mater. Trans. A*, vol. 44, no. 13, pp. 5703–5710, 2013.
- [21] H. Tamura, “The role of rusts in corrosion and corrosion protection of iron and steel,” *Corros. Sci.*, vol. 50, no. 7, pp. 1872–1883, 2008.
- [22] E. Proverbio and R. Cigna, “Influence of rebar surface condition on polarisation resistance measurement in concrete structures,” in *Materials science forum*, 1995, pp. 877–882.
- [23] J. Avila-Mendoza, J. M. Flores, and U. C. Castillo, “Effect of superficial oxides on corrosion of steel reinforcement embedded in concrete,” *Corros. Eng.*, vol. 50, no. 11, pp. 879–885, 1994.
- [24] J. A. Gonzalez, E. Ramirez, A. Bautista, and S. Feliu, “The behaviour of Pre-rusted Steel in Concrete,” *Cem. Concr. Res.*, vol. 26, no. 3, pp. 501–511, 1996.
- [25] J. M. Miranda, E. Otero, J. A. Gonzalez, and L. S. Hernandez, “Behaviour of corroded steel in a $\text{Ca}(\text{OH})_2$ -saturated solution and in cement mortar. Possibility of rehabilitation,” *Mater. Constr.*, vol. 57, no. 285, pp. 5–16, 2007.
- [26] J. A. Gonzalez, J. M. Miranda, E. Otero, and S. Feliu, “Effect of electrochemically reactive rust layers on the corrosion of steel in a $\text{Ca}(\text{OH})_2$ solution,” *Corros. Sci.*, vol. 49, no. 2, pp. 436–448, 2007.
- [27] P. Novak, R. Mala, and L. Joska, “Influence of pre-rusting on steel corrosion in concrete,” *Cem. Concr. Res.*, vol. 31, no. 4, pp. 589–593, 2001.
- [28] T. Mohammed and H. Hamada, “Corrosion of steel bars in concrete with various steel surface conditions,” *ACI Mater. J.*, vol. 103, no. 103, pp. 233–242, 2006.
- [29] C. M. Hansson and B. Sørensen, “The threshold concentration of chloride in concrete for the initiation of reinforcement corrosion,” in *Corrosion rates of steel in concrete, ASTM STP 1065*, 1990, pp. 3–16.
- [30] U. M. Angst and B. Elsener, “Forecasting chloride-induced reinforcement corrosion in concrete-effect of realistic reinforcement steel surface conditions,” in *4th International Conference on Concrete Repair, Rehabilitation and Retrofitting*, 2016, pp. 177–184.
- [31] N. Gowripalan and H. Mohamed, “Chloride-ion induced corrosion of galvanized and ordinary steel reinforcement in high-performance concrete,” *Cem. Concr. Res.*, vol. 28, no. 8, pp. 1119–1131, 1998.

- [32] E. Sistonen, A. Cwirzen, and J. Puttonen, "Corrosion mechanism of hot-dip galvanised reinforcement bar in cracked concrete," *Corros. Sci.*, vol. 50, no. 12, pp. 3416–3428, 2008.
- [33] F. Delaunois, F. Tosar, and V. Vitry, "Corrosion behaviour and biocorrosion of galvanized steel water distribution systems," *Bioelectrochemistry*, vol. 97, pp. 110–119, 2014.
- [34] P. Pokorný, P. Tej, and M. Kouřil, "Evaluation of the impact of corrosion of hot-dip galvanized reinforcement on bond strength with concrete – A review," *Constr. Build. Mater.*, vol. 132, pp. 271–298, 2017.
- [35] D. Talbot and J. Talbot, *Corrosion Science and Technology*. CRC-Press, 1998.
- [36] F. Tittarelli and T. Bellezze, "Investigation of the major reduction reaction occurring during the passivation of galvanized steel rebars," *Corros. Sci.*, vol. 52, no. 3, pp. 978–983, 2010.
- [37] T. Bellezze, G. Roventi, E. Barbaresi, N. Ruffini, and R. Fratesi, "Effect of concrete carbonation process on the passivating products of galvanized steel reinforcements," *Mater. Corros.*, vol. 62, no. 2, pp. 155–160, 2011.
- [38] F. Belaïd, G. Arliguie, and R. François, "Porous structure of the ITZ around galvanized and ordinary steel reinforcements," *Cem. Concr. Res.*, vol. 31, no. 11, pp. 1561–1566, 2001.
- [39] A. Macías and C. Andrade, "Corrosion Rate of Galvanized Steel Immersed in Saturated Solutions of $\text{Ca}(\text{OH})_2$ in the pH Range 12-13.8," *Br. Corros. J.*, vol. 18, no. 2, pp. 82–87, 1983.
- [40] G. Roventi, T. Bellezze, G. Giuliani, and C. Conti, "Corrosion resistance of galvanized steel reinforcements in carbonated concrete: Effect of wet-dry cycles in tap water and in chloride solution on the passivating layer," *Cem. Concr. Res.*, vol. 65, pp. 76–84, 2014.
- [41] R. Vera, R. Venegas, and A. Carvajal, "Performance of Carbon Steel and Galvanized Steel in Reinforced Concrete Structures after Accelerated Carbonation," *Int. J. Electrochem. Sci.*, vol. 7, pp. 10722–10734, 2012.
- [42] S. R. Yeomans, "Performance of black, galvanized, and epoxy-coated reinforcing steels in chloride-contaminated concrete," *Corrosion*, vol. 50, no. 1, pp. 72–81, 1994.
- [43] B. S. Haran, B. N. Popov, M. F. Petrou, and R. E. White, "Studies on galvanized carbon steel in $\text{Ca}(\text{OH})_2$ solutions," *ACI Struct. J.*, vol. 97, no. 4, pp. 425–431, 2000.
- [44] B. S. Hamad and J. A. Mike, "Bond strength of hot-dip galvanized reinforcement in normal strength concrete structures," *Constr. Build. Mater.*, vol. 19, no. 4, pp. 275–283, 2005.
- [45] A. Hegyi, C. Dico, H. Constantinescu, and C. Baera, "Influence of Hot-dip Galvanizing of Reinforcement on the Kinetics and Thermodynamics of Corrosion Process in Concrete," *Procedia Eng.*, vol. 181, pp. 226–233, 2017.
- [46] F. J. Luna Molina, M. C. Alonso Alonso, E. Hernández Montes, and C. López Hombrados, "Galvanized Steel in Concrete: More Durable Structures Maintaining the Bond Length," *J. Mater. Civ. Eng.*, vol. 29, no. 8, 2017.
- [47] T. Bellezze, R. Fratesi, G. A. Plizzari, F. Tittarelli, and V. B. Bianche, "Corrosion of Steel and Galvanized Steel Reinforcing Bars in Concrete Simulating Field Conditions," in *European Corrosion Congress*, 2001, no. October 2001, pp. 1–9.

- [48] J. O. Rivera-Corral, G. Fajardo, G. Arliguie, R. Orozco-Cruz, F. Deby, and P. Valdez, "Corrosion behavior of steel reinforcement bars embedded in concrete exposed to chlorides: Effect of surface finish," *Constr. Build. Mater.*, vol. 147, pp. 815–826, 2017.
- [49] L. Maldonado, "Chloride threshold for corrosion of galvanized reinforcement in concrete exposed in the Mexican Caribbean," *Mater. Corros.*, vol. 60, no. 7, pp. 536–539, 2009.
- [50] Y. Shao, T. Lefort, S. Moras, and D. Rodriguez, "Studies on concrete containing ground waste glass," *Cem. Concr. Res.*, vol. 30, no. 1, pp. 91–100, 2000.
- [51] C. Meyer, "The greening of the concrete industry," *Cem. Concr. Compos.*, vol. 31, no. 8, pp. 601–605, 2009.
- [52] L. M. Federico and S. E. Chidiac, "Waste glass as a supplementary cementitious material in concrete - Critical review of treatment methods," *Cem. Concr. Compos.*, vol. 31, no. 8, pp. 606–610, 2009.
- [53] W. Jin, C. Meyer, and S. Baxter, "'Glasscrete'-concrete with glass aggregate," *ACI Materials Journal*, vol. 97, no. 2, pp. 208–213, 2000.
- [54] H. Zhu, W. Chen, W. Zhou, and E. A. Byars, "Expansion behaviour of glass aggregates in different testing for alkali-silica reactivity," *Mater. Struct.*, vol. 42, no. 4, pp. 485–494, 2009.
- [55] A. Sacconi and M. C. Bignozzi, "ASR expansion behavior of recycled glass fine aggregates in concrete," *Cem. Concr. Res.*, vol. 40, no. 4, pp. 531–536, 2010.
- [56] H. Du and K. H. Tan, "Use of waste glass as sand in mortar: Part II - Alkali-silica reaction and mitigation methods," *Cem. Concr. Compos.*, vol. 35, no. 1, pp. 109–117, 2013.
- [57] F. Rajabipour, H. Maraghechi, and G. Fischer, "Investigating the Alkali-Silica Reaction of Recycled Glass Aggregates in Concrete Materials," *J. Mater. Civ. Eng.*, vol. 22, no. 12, pp. 1201–1208, 2010.
- [58] R. Idir, M. Cyr, and A. Tagnit-Hamou, "Pozzolanic properties of fine and coarse color-mixed glass cullet," *Cem. Concr. Compos.*, vol. 33, no. 1, pp. 19–29, 2011.
- [59] S. B. Park, B. C. Lee, and J. H. Kim, "Studies on mechanical properties of concrete containing waste glass aggregate," *Cem. Concr. Res.*, vol. 34, no. 12, pp. 2181–2189, 2004.
- [60] Z. Z. Ismail and E. A. AL-Hashmi, "Recycling of waste glass as a partial replacement for fine aggregate in concrete," *Waste Manag.*, vol. 29, no. 2, pp. 655–659, 2009.
- [61] H. Maraghechi, S. M. H. Shafaatian, G. Fischer, and F. Rajabipour, "The role of residual cracks on alkali silica reactivity of recycled glass aggregates," *Cem. Concr. Compos.*, vol. 34, no. 1, pp. 41–47, 2012.
- [62] İ. B. Topçu and M. Canbaz, "Properties of concrete containing waste glass," *Cem. Concr. Res.*, vol. 34, no. 2, pp. 267–274, 2004.
- [63] M. Carsana, M. Frassoni, and L. Bertolini, "Comparison of ground waste glass with other supplementary cementitious materials," *Cem. Concr. Compos.*, vol. 45, pp. 39–45, 2014.
- [64] D. T. Dyer and K. R. Dhir, "Chemical reactions of glass cullet used as cement component," *J. Mater. Civ. Eng.*, vol. 13, no. 6, pp. 412–417, 2001.

- [65] A. M. Matos and J. Sousa-Coutinho, "Durability of mortar using waste glass powder as cement replacement," *Constr. Build. Mater.*, vol. 36, pp. 205–215, 2012.
- [66] M. Kamali and A. Ghahremaninezhad, "Effect of glass powders on the mechanical and durability properties of cementitious materials," *Constr. Build. Mater.*, vol. 98, pp. 407–416, 2015.
- [67] R. Nemes and Z. Józsa, "Strength of Lightweight Glass Aggregate Concrete," *J. Mater. Civ. Eng.*, vol. 18, no. October, pp. 710–714, 2006.
- [68] V. Ducman, A. Mladenovič, and J. S. Šuput, "Lightweight aggregate based on waste glass and its alkali-silica reactivity," *Cem. Concr. Res.*, vol. 32, no. 2, pp. 223–226, 2002.
- [69] M. Limbachiya, M. S. Meddah, and S. Fotiadou, "Performance of granulated foam glass concrete," *Constr. Build. Mater.*, vol. 28, no. 1, pp. 759–768, 2012.
- [70] A. A. Aliabdo, A. E. M. Abd Elmoaty, and A. Y. Aboshama, "Utilization of waste glass powder in the production of cement and concrete," *Constr. Build. Mater.*, vol. 124, pp. 866–877, 2016.
- [71] C. Shi, Y. Wu, C. Riefler, and H. Wang, "Characteristics and pozzolanic reactivity of glass powders," *Cem. Concr. Res.*, vol. 35, no. 5, pp. 987–993, 2005.
- [72] L. Bertolini, M. Carsana, M. Frassoni, and M. Gelli, "Pozzolanic additions for durability of concrete structures," *ICE*, pp. 283–291, 2011.
- [73] J. X. Lu, Z. H. Duan, and C. S. Poon, "Fresh properties of cement pastes or mortars incorporating waste glass powder and cullet," *Constr. Build. Mater.*, vol. 131, pp. 793–799, 2017.
- [74] J. Kim, C. Yi, and G. Zi, "Waste glass sludge as a partial cement replacement in mortar," *Constr. Build. Mater.*, vol. 75, pp. 242–246, 2015.
- [75] B. Taha and G. Nounu, "Properties of concrete contains mixed colour waste recycled glass as sand and cement replacement," *Constr. Build. Mater.*, vol. 22, no. 5, pp. 713–720, 2008.
- [76] L. A. Pereira-De-Oliveira, J. P. Castro-Gomes, and P. M. S. Santos, "The potential pozzolanic activity of glass and red-clay ceramic waste as cement mortars components," *Constr. Build. Mater.*, vol. 31, pp. 197–203, 2012.
- [77] A. Shayan and A. Xu, "Value-added utilisation of waste glass in concrete," *Cem. Concr. Res.*, vol. 34, no. 1, pp. 81–89, 2004.
- [78] R. Idir, M. Cyr, and A. Tagnit-Hamou, "Use of fine glass as ASR inhibitor in glass aggregate mortars," *Constr. Build. Mater.*, vol. 24, no. 7, pp. 1309–1312, 2010.
- [79] G. Bumanis, D. Bajare, J. Locs, and A. Korjakins, "Alkali-silica reactivity of foam glass granules in structure of lightweight concrete," *Constr. Build. Mater.*, vol. 47, pp. 274–281, 2013.
- [80] A. Mladenovič, J. S. Šuput, V. Ducman, and A. S. Škapin, "Alkali-silica reactivity of some frequently used lightweight aggregates," *Cem. Concr. Res.*, vol. 34, no. 10, pp. 1809–1816, 2004.
- [81] M. L. Torres and P. A. García-Ruiz, "Lightweight pozzolanic materials used in mortars:

- Evaluation of their influence on density, mechanical strength and water absorption,” *Cem. Concr. Compos.*, vol. 31, no. 2, pp. 114–119, 2009.
- [82] O. Fenyvesi, “Affect of lightweight aggregate to early age cracking in concrete,” *Period. Polytech. Civ. Eng.*, vol. 55, no. 1, pp. 63–71, 2011.
- [83] L. Zhang, “Development of the use of sulfo and ferroaluminate cements in China,” *Adv. Cem. Res.*, vol. 11, no. 15–21, 1999.
- [84] S. W. Tang, H. G. Zhu, Z. J. Li, E. Chen, and H. Y. Shao, “Hydration stage identification and phase transformation of calcium sulfoaluminate cement at early age,” *Constr. Build. Mater.*, vol. 75, pp. 11–18, 2015.
- [85] V. Kasselouri, P. Tsakiridis, C. Malami, B. Georgali, and C. Alexandridou, “A study on the hydration products of a non-expansive sulfoaluminate cement,” *Cem. Concr. Res.*, vol. 25, no. 8, pp. 1726–1736, 1995.
- [86] I. Janotka, “An experimental study on the upgrade of sulfoaluminate-belite cement system by blending with portland cement,” *Adv. Cem. Res.*, vol. 11, no. 135–41, 1999.
- [87] D. Kalogridis, G. C. Kostogloudis, C. Ftikos, and C. Malami, “Quantitative study of the influence of non-expansive sulfoaluminate cement on the corrosion of steel reinforcement,” *Cem. Concr. Res.*, vol. 30, no. 11, pp. 1731–1740, 2000.
- [88] V. Živica, “Properties of blended sulfoaluminate belite cement,” *Constr. Build. Mater.*, vol. 14, no. 8, pp. 433–437, 2000.
- [89] I. Janotka, L. Krajči, A. Ray, and S. C. Mojumdar, “The hydration phase and pore structure formation in the blends of sulfoaluminate-belite cement with Portland cement,” *Cem. Concr. Res.*, vol. 33, no. 4, pp. 489–497, 2003.
- [90] J. Péra and J. Ambroise, “New applications of calcium sulfoaluminate cement,” *Cem. Concr. Res.*, vol. 34, no. 4, pp. 671–676, 2004.
- [91] Q. Zhou, N. B. Milestone, and M. Hayes, “An alternative to Portland Cement for waste encapsulation-The calcium sulfoaluminate cement system,” *J. Hazard. Mater.*, vol. 136, no. 1 SPEC. ISS., pp. 120–129, 2006.
- [92] C. Cau Dit Coumes, S. Courtois, S. Peysson, J. Ambroise, and J. Pera, “Calcium sulfoaluminate cement blended with OPC: A potential binder to encapsulate low-level radioactive slurries of complex chemistry,” *Cem. Concr. Res.*, vol. 39, no. 9, pp. 740–747, 2009.
- [93] L. Pelletier, F. Winnefeld, and B. Lothenbach, “The ternary system Portland cement-calcium sulphoaluminate clinker-anhydrite: Hydration mechanism and mortar properties,” *Cem. Concr. Compos.*, vol. 32, no. 7, pp. 497–507, 2010.
- [94] L. Pelletier-Chaignat, F. Winnefeld, B. Lothenbach, G. Le Saout, C. J. Muller, and C. Famy, “Influence of the calcium sulphate source on the hydration mechanism of Portland cement-calcium sulphoaluminate clinker-calcium sulphate binders,” *Cem. Concr. Compos.*, vol. 33, no. 5, pp. 551–561, 2011.
- [95] I. A. Chen, C. W. Hargis, and M. C. G. Juenger, “Understanding expansion in calcium sulfoaluminate-belite cements,” *Cem. Concr. Res.*, vol. 42, no. 1, pp. 51–60, 2012.

- [96] D. Gastaldi, F. Canonico, L. Capelli, E. Boccaleri, M. Milanese, L. Palin, G. Croce, F. Marone, K. Mader, and M. Stampanoni, "In situ tomographic investigation on the early hydration behaviors of cementing systems," *Constr. Build. Mater.*, vol. 29, pp. 284–290, 2012.
- [97] M. Carsana, M. Bianchi, F. Canonico, L. Buzzi, L. Capelli, and L. Bertolini, "Corrosion behaviour of steel embedded in calcium sulphoaluminate-cement concrete," *14th Int. Congr. Chem. Cem.*, 2015.
- [98] L. H. J. Martin, F. Winnefeld, C. J. Muller, and B. Lothenbach, "Contribution of limestone to the hydration of calcium sulfoaluminate cement," *Cem. Concr. Compos.*, vol. 62, pp. 204–211, 2015.
- [99] G. Paul, E. Boccaleri, L. Buzzi, F. Canonico, and D. Gastaldi, "Friedel's salt formation in sulfoaluminate cements: A combined XRD and ²⁷Al MAS NMR study," *Cem. Concr. Res.*, vol. 67, pp. 93–102, 2015.
- [100] S. Allevi, M. Marchi, F. Scotti, S. Bertini, and C. Cosentino, "Hydration of calcium sulphoaluminate clinker with additions of different calcium sulphate sources," *Mater. Struct.*, vol. 49, no. 1–2, pp. 453–466, 2016.
- [101] D. Gastaldi, G. Paul, L. Marchese, S. Irico, E. Boccaleri, S. Mutke, L. Buzzi, and F. Canonico, "Hydration products in sulfoaluminate cements: Evaluation of amorphous phases by XRD/solid-state NMR," *Cem. Concr. Res.*, vol. 90, pp. 162–173, 2016.
- [102] G. Bernardo, A. Telesca, and G. L. Valenti, "A porosimetric study of calcium sulfoaluminate cement pastes cured at early ages," *Cem. Concr. Res.*, vol. 36, no. 6, pp. 1042–1047, 2006.
- [103] K. Quillin, "Performance of belite-sulfoaluminate cements," *Cem. Concr. Res.*, vol. 31, no. 9, pp. 1341–1349, 2001.
- [104] F. P. Glasser and L. Zhang, "High-performance cement matrices based on calcium sulfoaluminate-belite compositions," *Cem. Concr. Res.*, vol. 31, no. 12, pp. 1881–1886, 2001.
- [105] M. A. G. Aranda and A. G. la Torre, *Eco-efficient concrete: 18. Sulfoaluminate cement*. Elsevier Science, 2013.
- [106] R. Trauchessec, J. M. Mechling, A. Lecomte, A. Roux, and B. Le Rolland, "Hydration of ordinary Portland cement and calcium sulfoaluminate cement blends," *Cem. Concr. Compos.*, vol. 56, pp. 106–114, 2015.
- [107] D. Gastaldi, F. Canonico, and E. Boccaleri, "Ettringite and calcium sulfoaluminate cement: Investigation of water content by near-infrared spectroscopy," *J. Mater. Sci.*, vol. 44, no. 21, pp. 5788–5794, 2009.
- [108] F. Winnefeld and B. Lothenbach, "Hydration of calcium sulfoaluminate cements - Experimental findings and thermodynamic modelling," *Cem. Concr. Res.*, vol. 40, no. 8, pp. 1239–1247, 2010.
- [109] G. Jen, N. Stompinis, and R. Jones, "Chloride ingress in a belite-calcium sulfoaluminate cement matrix," *Cem. Concr. Res.*, vol. 98, pp. 130–135, 2017.
- [110] S. Ioannou, L. Reig, K. Paine, and K. Quillin, "Properties of a ternary calcium sulfoaluminate-calcium sulfate-fly ash cement," *Cem. Concr. Res.*, vol. 56, pp. 75–83, 2014.

- [111] C. W. Hargis, B. Lothenbach, C. J. Muller, and F. Winnefeld, "Carbonation of calcium sulfoaluminate mortars," *Cem. Concr. Compos.*, vol. 80, pp. 123–134, 2017.
- [112] M. C. G. Juenger, F. Winnefeld, J. L. Provis, and J. H. Ideker, "Advances in alternative cementitious binders," *Cem. Concr. Res.*, vol. 41, no. 12, pp. 1232–1243, 2011.
- [113] J. Zhao, G. Cai, D. Gao, and S. Zhao, "Influences of freeze-thaw cycle and curing time on chloride ion penetration resistance of Sulphoaluminate cement concrete," *Constr. Build. Mater.*, vol. 53, pp. 305–311, 2014.
- [114] C. W. Hargis, A. P. Kirchheim, P. J. M. Monteiro, and E. M. Gartner, "Early age hydration of calcium sulfoaluminate (synthetic ye'elimite, C_4A_3S) in the presence of gypsum and varying amounts of calcium hydroxide," *Cem. Concr. Res.*, vol. 48, pp. 105–115, 2013.
- [115] F. P. Glasser, "Pore solution composition of calcium sulfoaluminate cement," *Adv. Cem. Res.*, vol. 11, no. 1, pp. 23–26, 1999.
- [116] J. Beretka, M. Marroccoli, N. Sherman, and G. L. Valenti, "The influence of C_4A_3S content and W/S ratio on the performance of calcium sulfoaluminate-based cements," *Cem. Concr. Res.*, vol. 26, no. 11, pp. 1673–1681, 1996.
- [117] L. Zhang and F. P. Glasser, "Investigation of the microstructure and carbonation of CSA-based concretes removed from service," *Cem. Concr. Res.*, vol. 35, no. 12, pp. 2252–2260, 2005.
- [118] R. Bahar, M. Benazzoug, and S. Kenai, "Performance of compacted cement-stabilised soil," *Cem. Concr. Compos.*, vol. 26, no. 7, pp. 811–820, 2004.
- [119] M. Hall and Y. Djerbib, "Rammed earth sample production: context, recommendations and consistency," *Constr. Build. Mater.*, vol. 18, no. 4, pp. 281–286, 2004.
- [120] P. Jaquin, "Influence of Arabic and Chinese rammed earth techniques in the himalayan region," *Sustainability*, vol. 4, no. 10, pp. 2650–2660, 2012.
- [121] Q. B. Bui, J. C. Morel, B. V. Venkatarama Reddy, and W. Ghayad, "Durability of rammed earth walls exposed for 20 years to natural weathering," *Build. Environ.*, vol. 44, no. 5, pp. 912–919, 2009.
- [122] P. A. Jaquin, C. E. Augarde, D. Gallipoli, and D. G. Toll, "The strength of unstabilised rammed earth materials," *Géotechnique*, vol. 59, no. 5, pp. 487–490, 2009.
- [123] V. Maniatidis and P. Walker, "Structural Capacity of Rammed Earth in Compression," *J. Mater. Civ. Eng.*, vol. 20, no. 3, pp. 230–238, 2008.
- [124] D. Ciancio and J. Gibbings, "Experimental investigation on the compressive strength of cored and molded cement-stabilized rammed earth samples," *Constr. Build. Mater.*, vol. 28, no. 1, pp. 294–304, 2012.
- [125] C. T. S. Beckett and D. Ciancio, "Effect of compaction water content on the strength of cement-stabilized rammed earth materials," *Can. Geotech. J.*, vol. 51, no. February, pp. 583–590, 2014.
- [126] P. J. Walker and S. Dobson, "Pullout tests on deformed and plain rebars in cement-stabilized rammed earth," *J. Mater. Civ. Eng.*, vol. 13, no. 4, pp. 291–297, 2001.

- [127] C. T. S. Beckett and D. Ciancio, "Durability of cement-stabilised rammed earth: a case study in Western Australia," *Aust. J. Civ. Eng.*, vol. 14, no. 1, pp. 54–62, 2016.
- [128] A. Arrigoni, C. Beckett, D. Ciancio, and G. Dotelli, "Life cycle analysis of environmental impact vs. durability of stabilised rammed earth," *Constr. Build. Mater.*, vol. 142, pp. 128–136, 2017.
- [129] D. Ciancio, P. Jaquin, and P. Walker, "Advances on the assessment of soil suitability for rammed earth," *Constr. Build. Mater.*, vol. 42, no. 1, pp. 40–47, 2013.
- [130] B. V. Venkatarama Reddy and P. Prasanna Kumar, "Embodied energy in cement stabilised rammed earth walls," *Energy Build.*, vol. 42, no. 3, pp. 380–385, 2010.
- [131] C. Jayasinghe and N. Kamaladasa, "Compressive strength characteristics of cement stabilized rammed earth walls," *Constr. Build. Mater.*, vol. 21, no. 11, pp. 1971–1976, 2007.
- [132] K. K. G. K. D. Kariyawasam and C. Jayasinghe, "Cement stabilized rammed earth as a sustainable construction material," *Constr. Build. Mater.*, vol. 105, pp. 519–527, 2016.
- [133] S. Burroughs, "Soil Property Criteria for Rammed Earth Stabilization," *J. Mater. Civ. Eng.*, vol. 20, no. 3, pp. 264–273, 2008.
- [134] D. Ciancio, C. T. S. Beckett, and J. A. H. Carraro, "Optimum lime content identification for lime-stabilised rammed earth," *Constr. Build. Mater.*, vol. 53, no. 1, pp. 59–65, 2014.
- [135] Q. B. Bui, J. C. Morel, S. Hans, and P. Walker, "Effect of moisture content on the mechanical characteristics of rammed earth," *Constr. Build. Mater.*, vol. 54, pp. 163–169, 2014.
- [136] D. D. Tripura and K. D. Singh, "Characteristic Properties of Cement-Stabilized Rammed Earth Blocks," *J. Mater. Civ. Eng.*, vol. 27, no. 7, p. 4014214, 2015.
- [137] B. V. Venkatarama Reddy and P. Prasanna Kumar, "Cement stabilised rammed earth. Part A: compaction characteristics and physical properties of compacted cement stabilised soils," *Mater. Struct.*, vol. 44, no. 3, pp. 681–693, 2011.
- [138] B. V. Venkatarama Reddy and P. Prasanna Kumar, "Cement stabilised rammed earth. Part B: compressive strength and stress–strain characteristics," *Mater. Struct.*, vol. 44, no. 3, pp. 695–707, 2011.
- [139] B. V. Venkatarama Reddy, V. Suresh, and K. S. Nanjunda Rao, "Characteristic Compressive Strength of Cement-Stabilized Rammed Earth," *J. Mater. Civ. Eng.*, vol. 29, no. 2, p. 4016203, 2017.
- [140] D. Ciancio and S. Robinson, "Use of the Strut-and-Tie Model in the Analysis of Reinforced Cement-Stabilized Rammed Earth Lintels," *J. Mater. Civ. Eng.*, vol. 23, no. 5, pp. 587–596, 2011.
- [141] P. J. Walker, "Strength, durability and shrinkage characteristics of cement stabilised soil blocks," *Cem. Concr. Compos.*, vol. 17, no. 4, pp. 301–310, 1995.
- [142] M. C. Alonso, G. C. J. L., C. Walker, M. Naito, S. Pettersson, I. Puigdomenech, M. A. Cuñado, M. Vuorio, H. Weber, H. Ueda, and K. Fujisaki, "Development of an accurate pH measurement methodology for the pore fluids of low pH cementitious materials," 2012.

- [143] E. Luciano and G. Orfeo, "Corrosion of carbon steel embedded in rammed earth," Politecnico di Milano, 2016.
- [144] D. Serpa, A. Santos Silva, J. De Brito, J. Pontes, and D. Soares, "ASR of mortars containing glass," *Constr. Build. Mater.*, vol. 47, pp. 489–495, 2013.
- [145] B. Taha and G. Nounu, "Using lithium nitrate and pozzolanic glass powder in concrete as ASR suppressors," *Cem. Concr. Compos.*, vol. 30, no. 6, pp. 497–505, 2008.
- [146] M. Carsana and L. Bertolini, "Durability of Lightweight Concrete with Expanded Glass and Silica Fume," *ACI Mater. J.*, vol. 114, no. 2, pp. 207–213, 2017.
- [147] A. Poursaee and C. M. Hansson, "Reinforcing steel passivation in mortar and pore solution," *Cem. Concr. Res.*, vol. 37, no. 7, pp. 1127–1133, 2007.
- [148] S. K. Kim, S. T. Kang, J. K. Kim, and I. Y. Jang, "Effects of particle size and cement replacement of LCD glass powder in concrete," *Adv. Mater. Sci. Eng.*, vol. 2017, no. 1, 2017.
- [149] M. Carsana, F. Tittarelli, and L. Bertolini, "Use of no-fines concrete as a building material: Strength, durability properties and corrosion protection of embedded steel," *Cem. Concr. Res.*, vol. 48, pp. 64–73, 2013.

List of Test Standards

UNI EN 1015-3:2007

Methods of test for mortar for masonry - Part 3: Determination of consistence of fresh mortar (by flow table)

UNI EN 12350-2:2009

Testing fresh concrete - Part 2: Slump-test

RILEM RECOMMENDATION NDT1

Testing of concrete by the ultrasonic pulse method

UNI EN 196-1:2005

Methods of testing cement - Part 1: Determination of strength

UNI EN 12390-3:2009

Testing hardened concrete - Part 3: Compressive strength of test specimens

UNI EN 12390-2:2009

Testing hardened concrete - Part 2: Making and curing specimens for strength tests

UNI EN 13057:2003

Products and systems for the protection and repair of concrete structures - Test methods - Determination of resistance of capillary absorption

UNI 7699:2005

Calcestruzzo. Determinazione dell'assorbimento di acqua alla pressione atmosferica

(Testing Hardened Concrete - Determination of Water Absorption at Atmospheric Pressure)

ASTM C1567-13

Standard Test Method for Determining the Potential Alkali-Silica Reactivity of Combinations of Cementitious Materials and Aggregate (Accelerated Mortar-Bar Method)

Appendix A

Microstructure observations of reference concrete and CSA-based concretes

A.1 Concrete with CEM II/A-L 42.5R

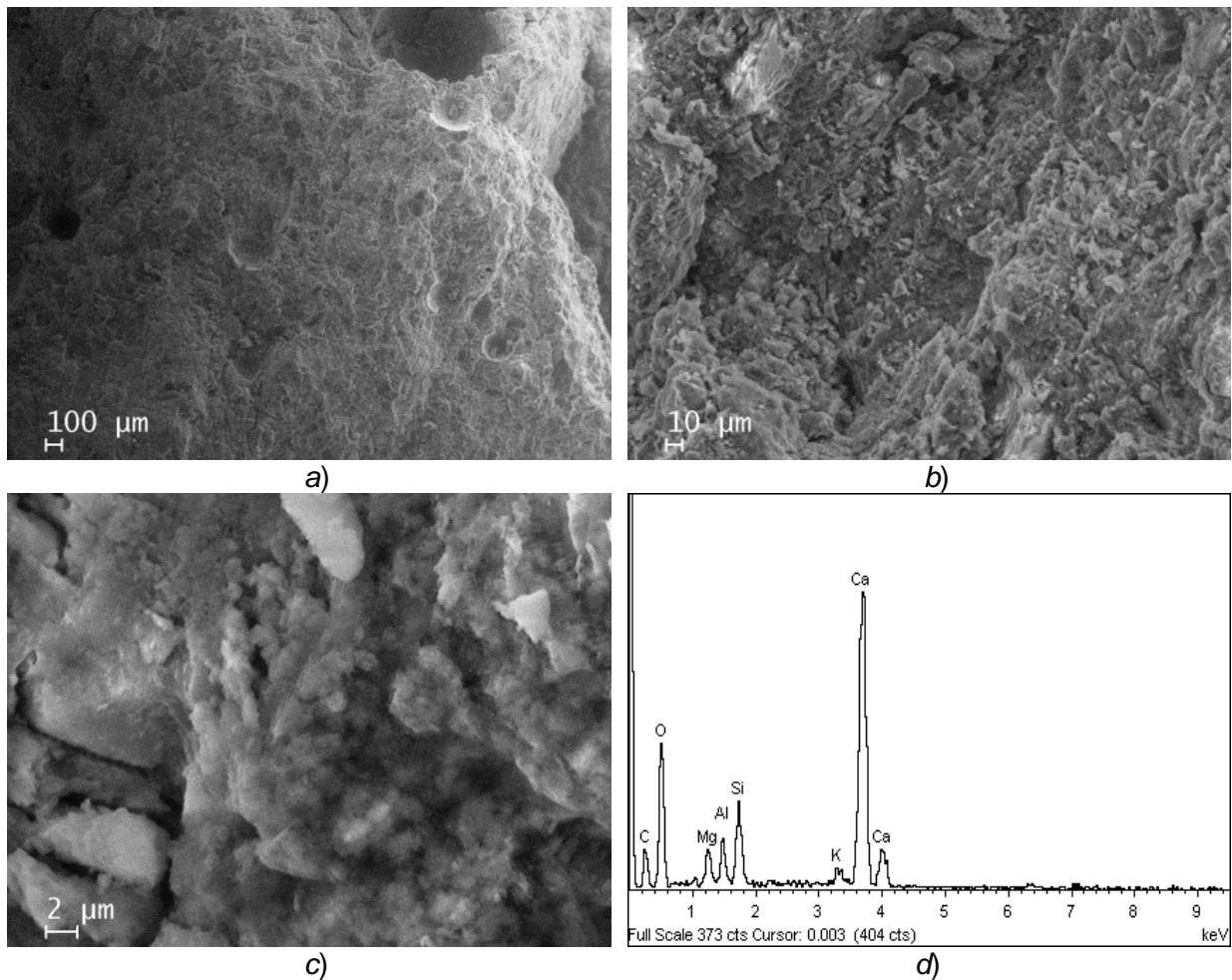


Figure A.1 SEM images at different magnifications a), b) and c) and EDS analysis d) of concrete made with CEM II/A-L 42.5R (w/c=0.55) after 28 days of moist curing.

A.2 Concrete with SL05 NF binder

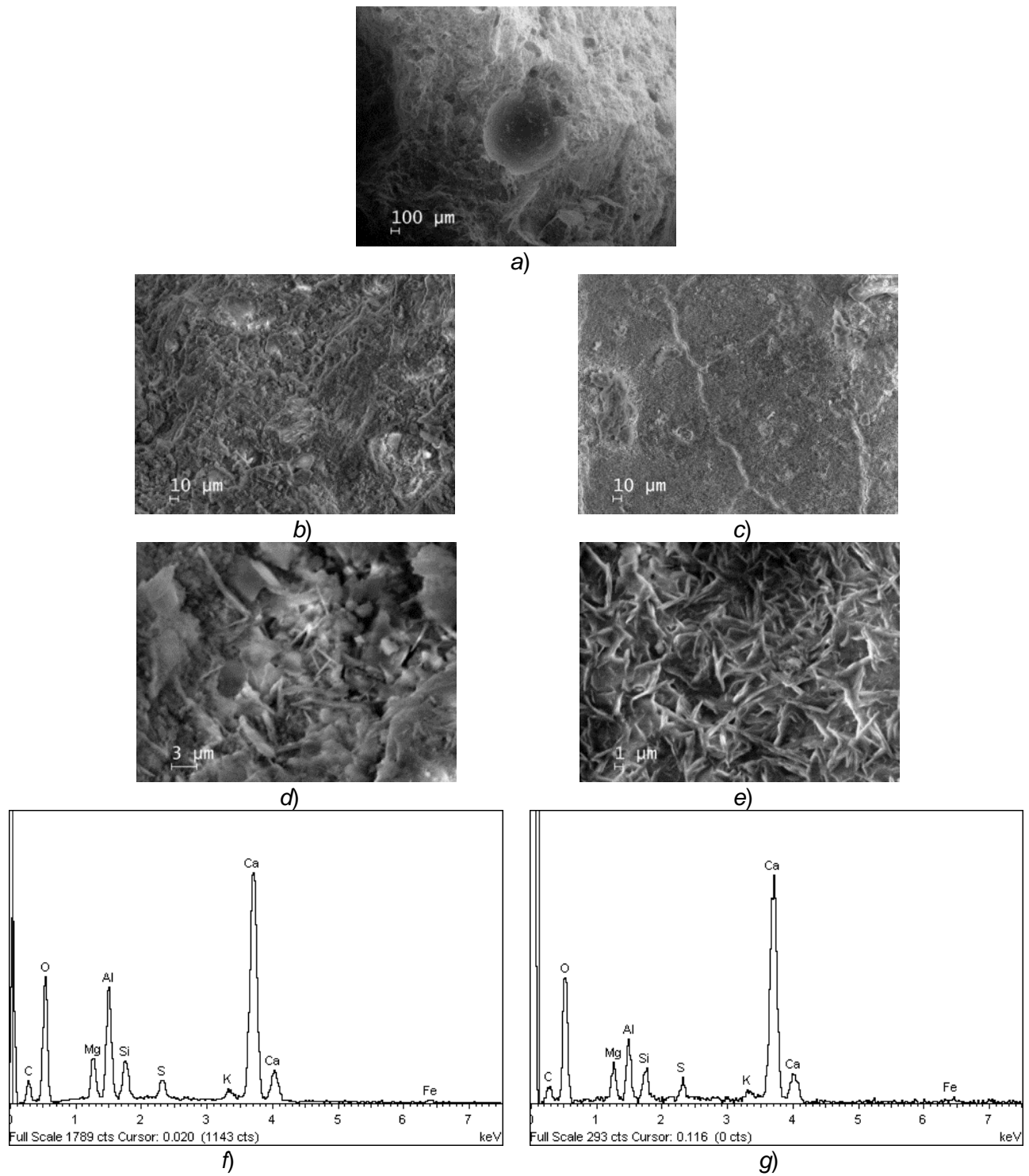


Figure A.2 SEM images at different magnifications *a)*, *b)*, *c)*, *d)*, *e)* and *f)* and EDS analyses *g)* and *h)* of concrete made with SL05 NF binder ($w/c=0.55$) after 1 day of moist curing.

Appendix A

Microstructure observations of reference concrete and CSA-based concretes

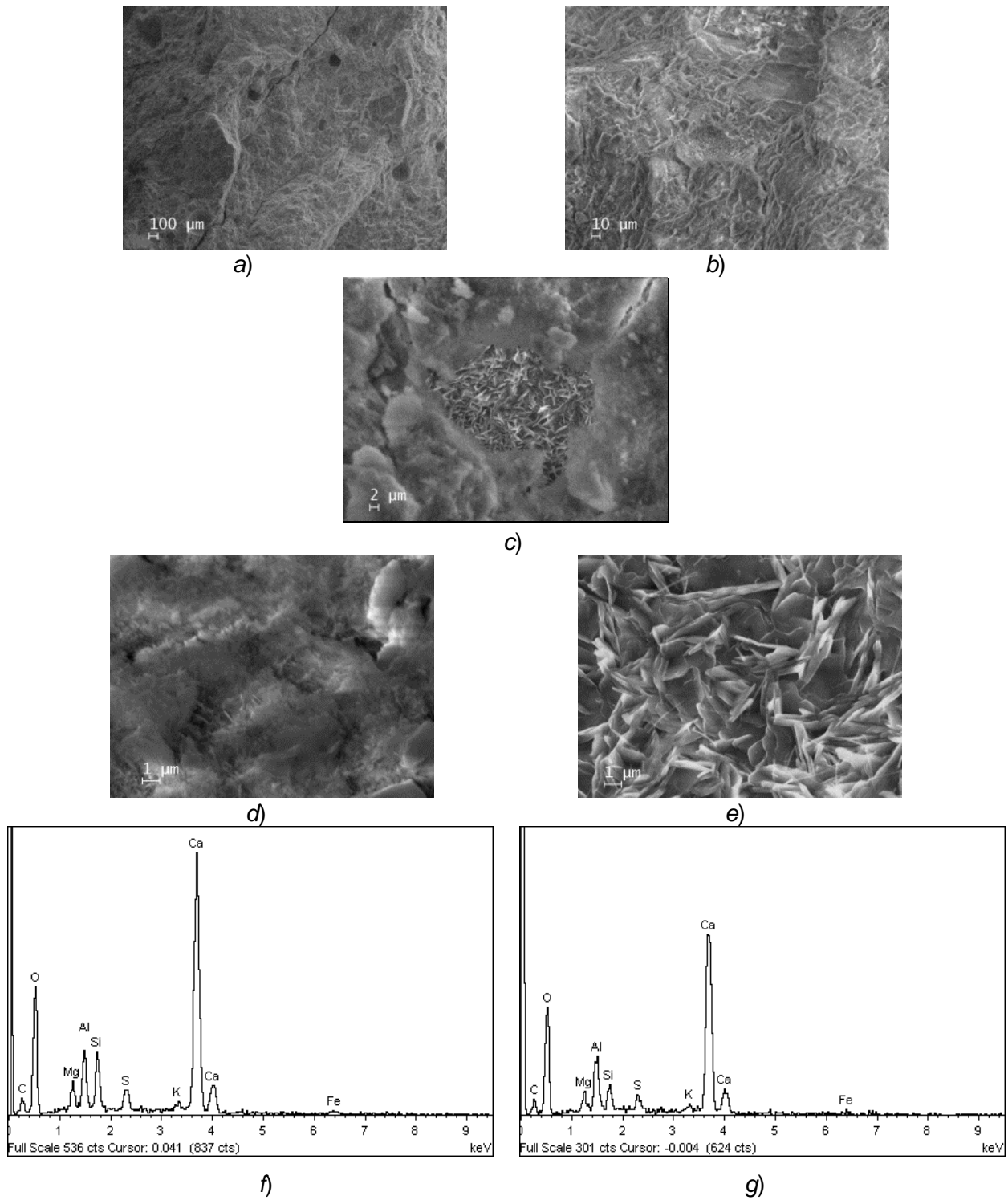


Figure A.3 SEM images at different magnifications *a)*, *b)*, *c)*, *d)* and *e)* and EDS analyses *f)* and *g)* of concrete made with SL05 NF binder ($w/c=0.55$) after 7 days of moist curing.

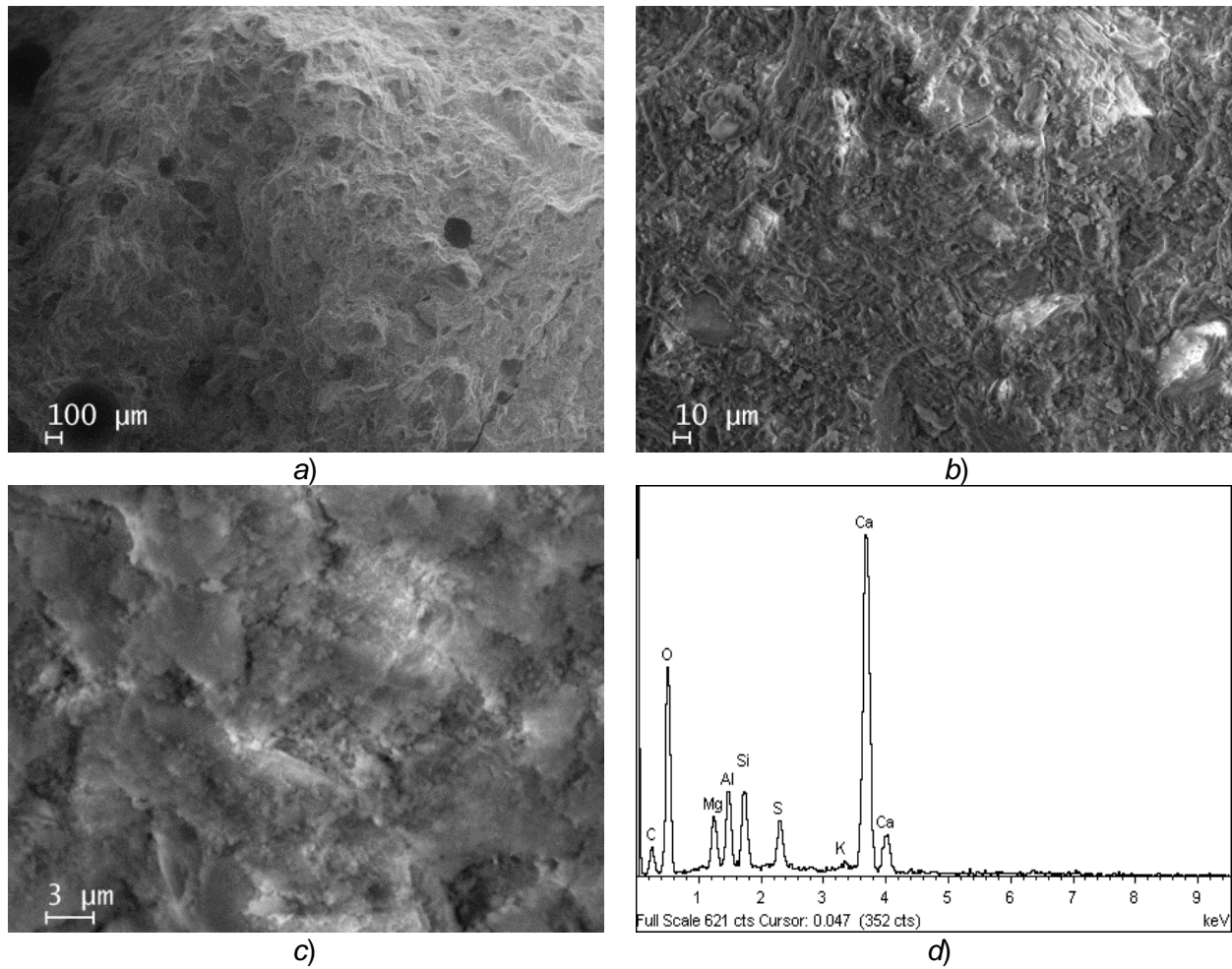


Figure A.4 SEM images at different magnifications *a)*, *b)* and *c)* and EDS analysis *d)* of concrete made with SL05 NF binder ($w/c=0.55$) after 28 days of moist curing.

A.3 Concrete with SL05 NF+CaO binder

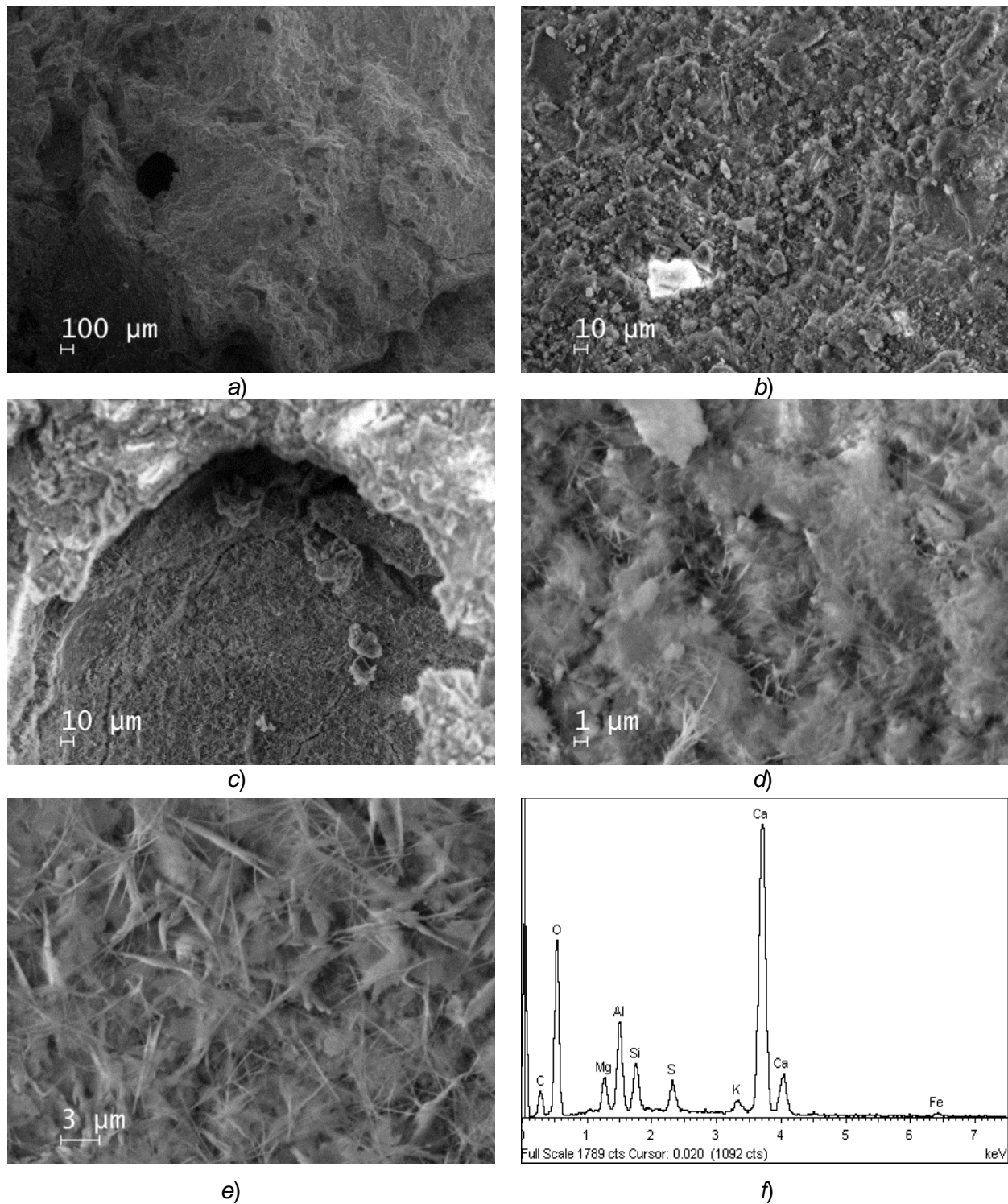


Figure A.5 SEM images at different magnifications *a)*, *b)*, *c)*, *d)* and *e)* and EDS analysis *f)* of concrete made with SL05 NF+CaO binder (w/c=0.55) after 1 day of moist curing.

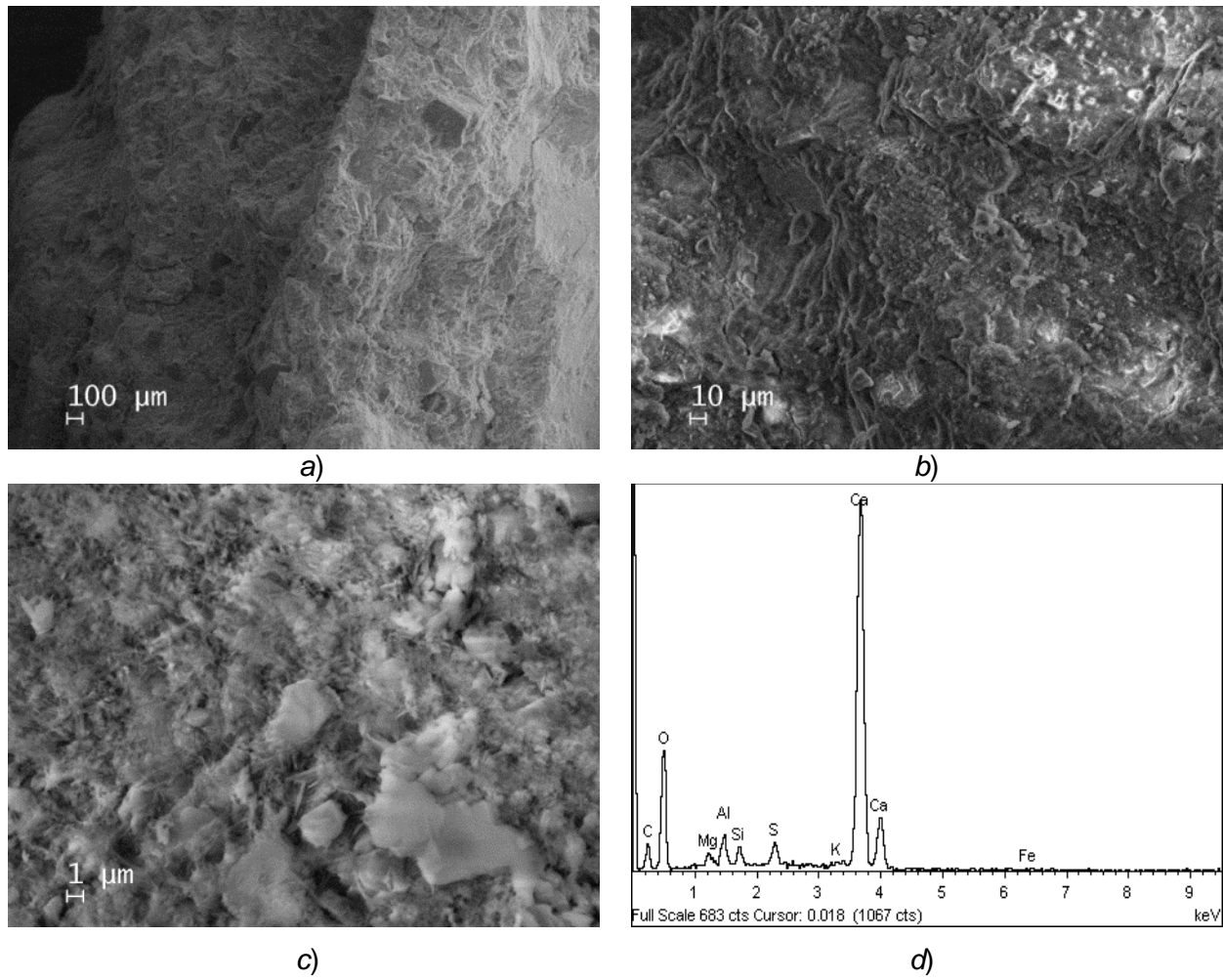


Figure A.6 SEM images at different magnifications a), b) and c) and EDS analysis d) of concrete made with SL05 NF+CaO binder ($w/c=0.55$) after 7 days of moist curing.

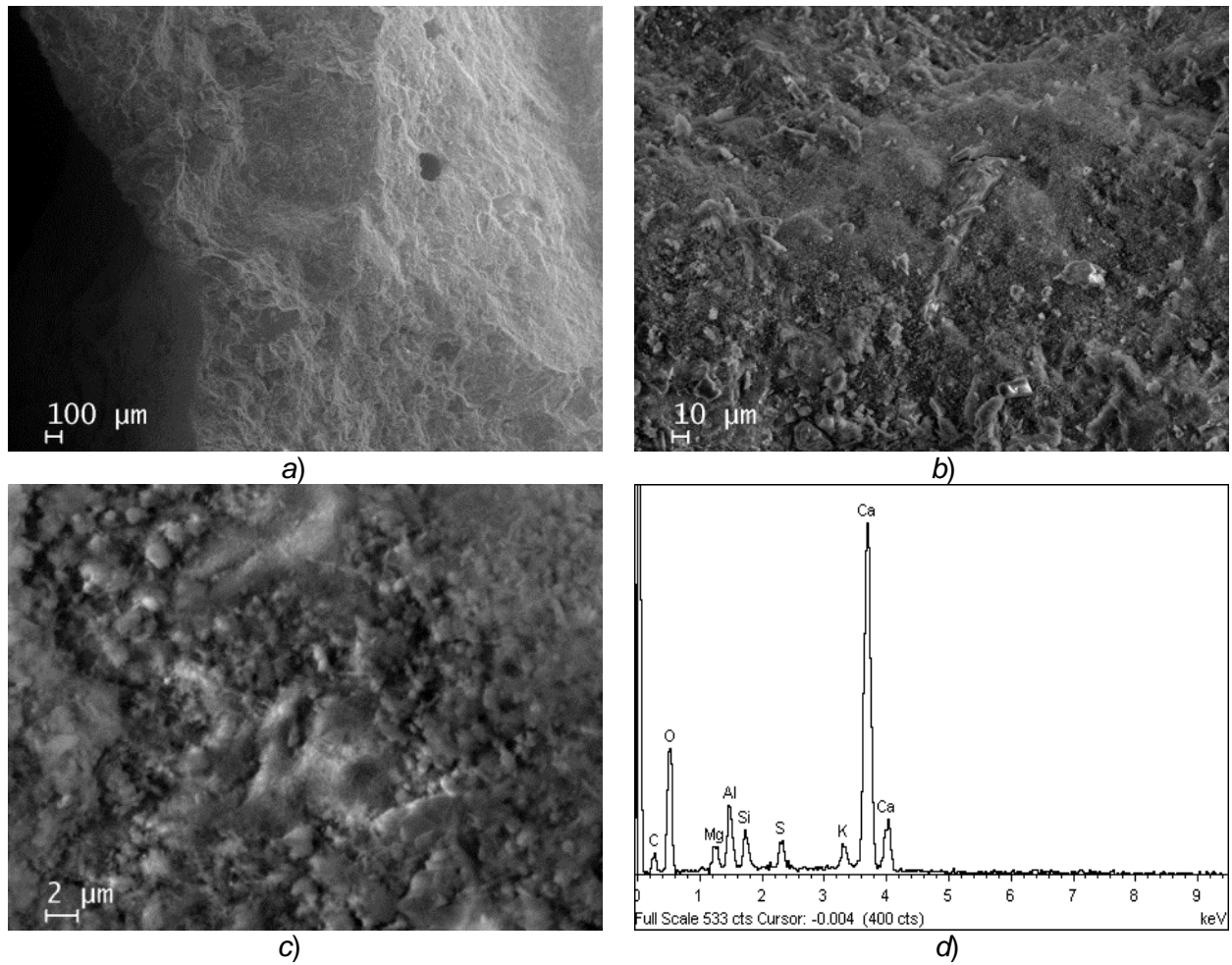


Figure A.7 SEM images at different magnifications a), b) and c) and EDS analysis d) of concrete made with SL05 NF+CaO binder ($w/c=0.55$) after 28 days of moist curing.

A.4 Concrete with SL05+CaO binder

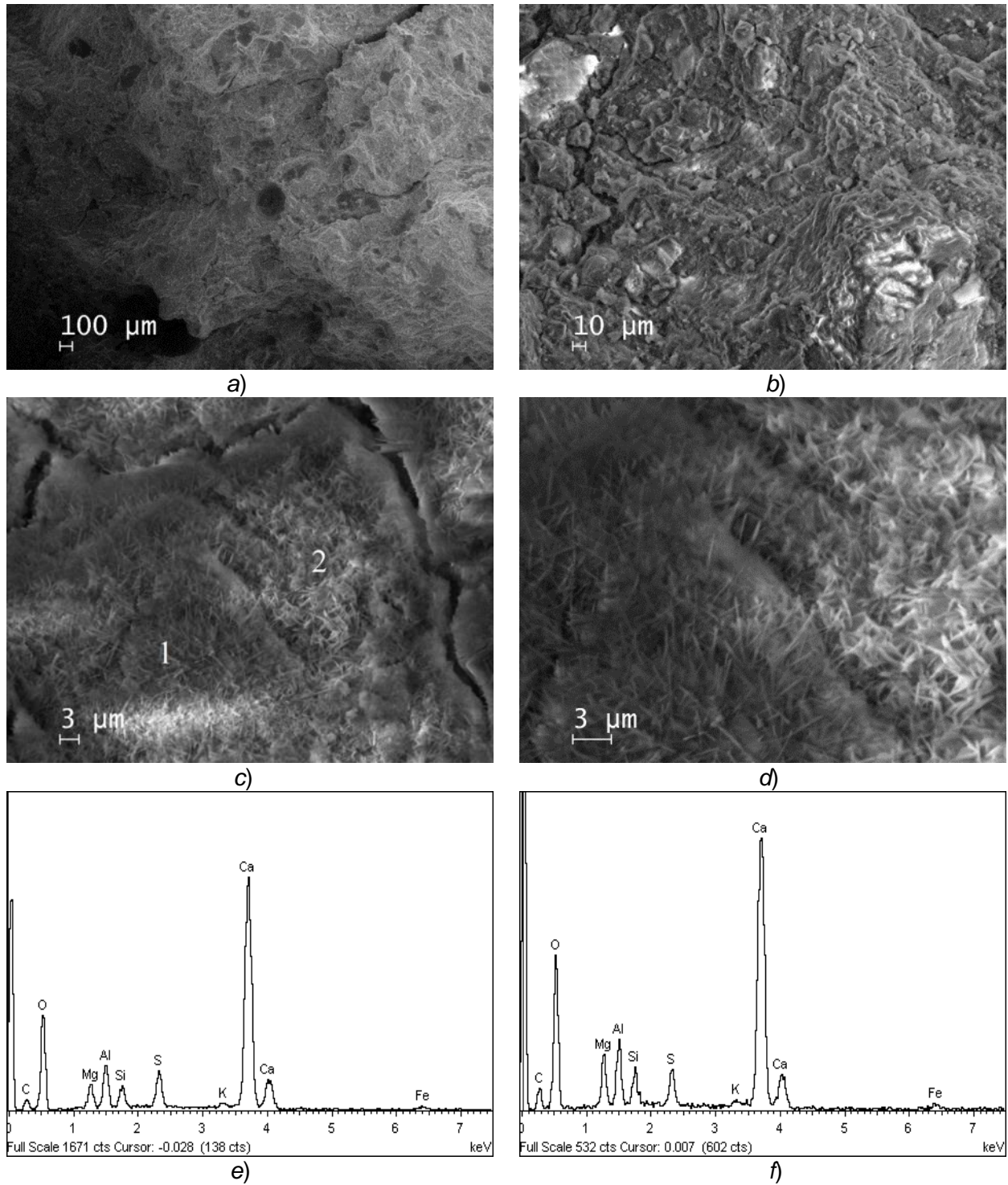


Figure A.8 SEM images at different magnifications *a)*, *b)*, *c)* and *d)* and EDS analyses *e)* and *f)* of concrete made with SL05+CaO binder ($w/c=0.55$) after 1 day of moist curing.

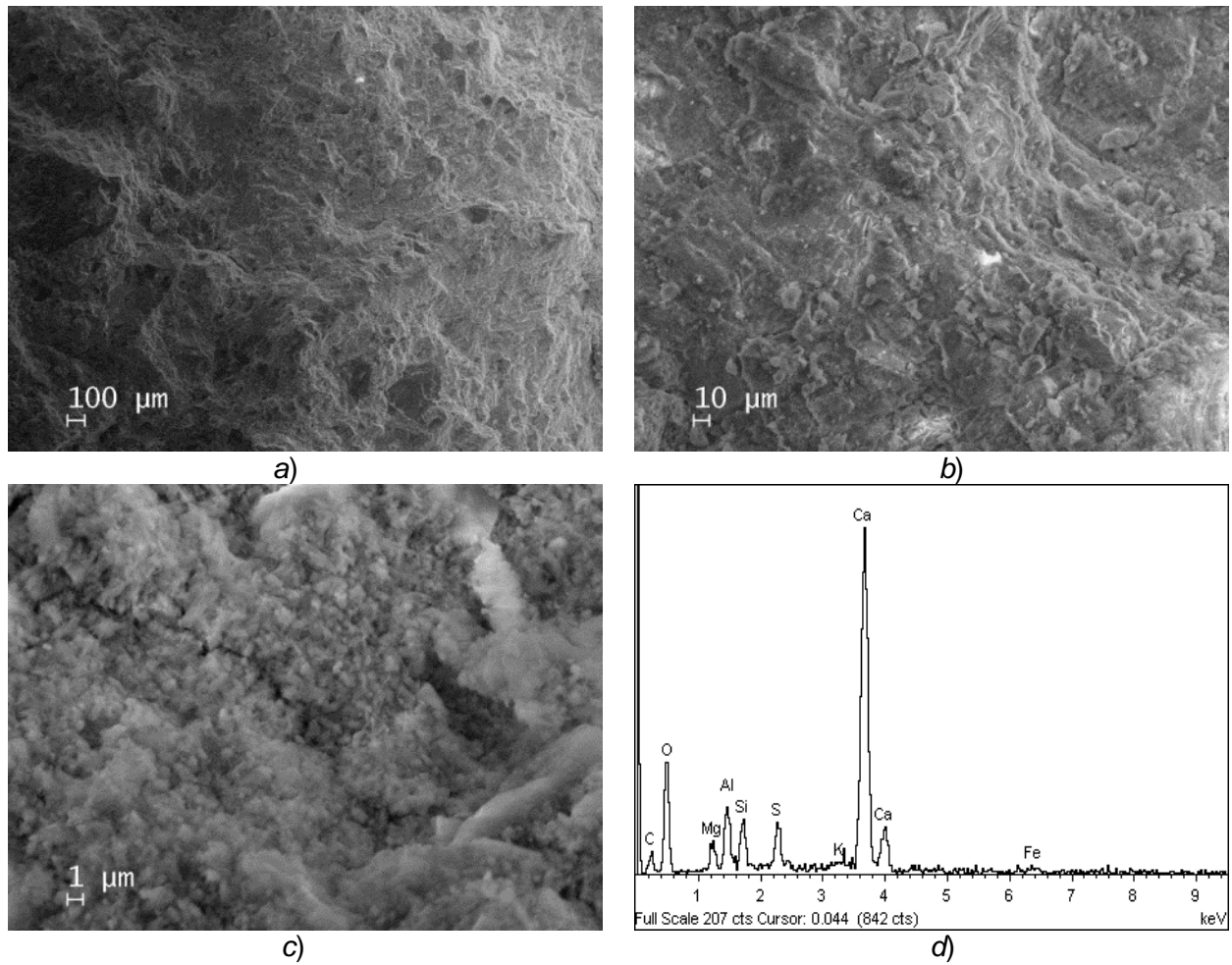


Figure A.9 SEM images at different magnifications a), b) and c) and EDS analysis d) of concrete made with SL05+CaO binder ($w/c=0.55$) after 7 days of moist curing.

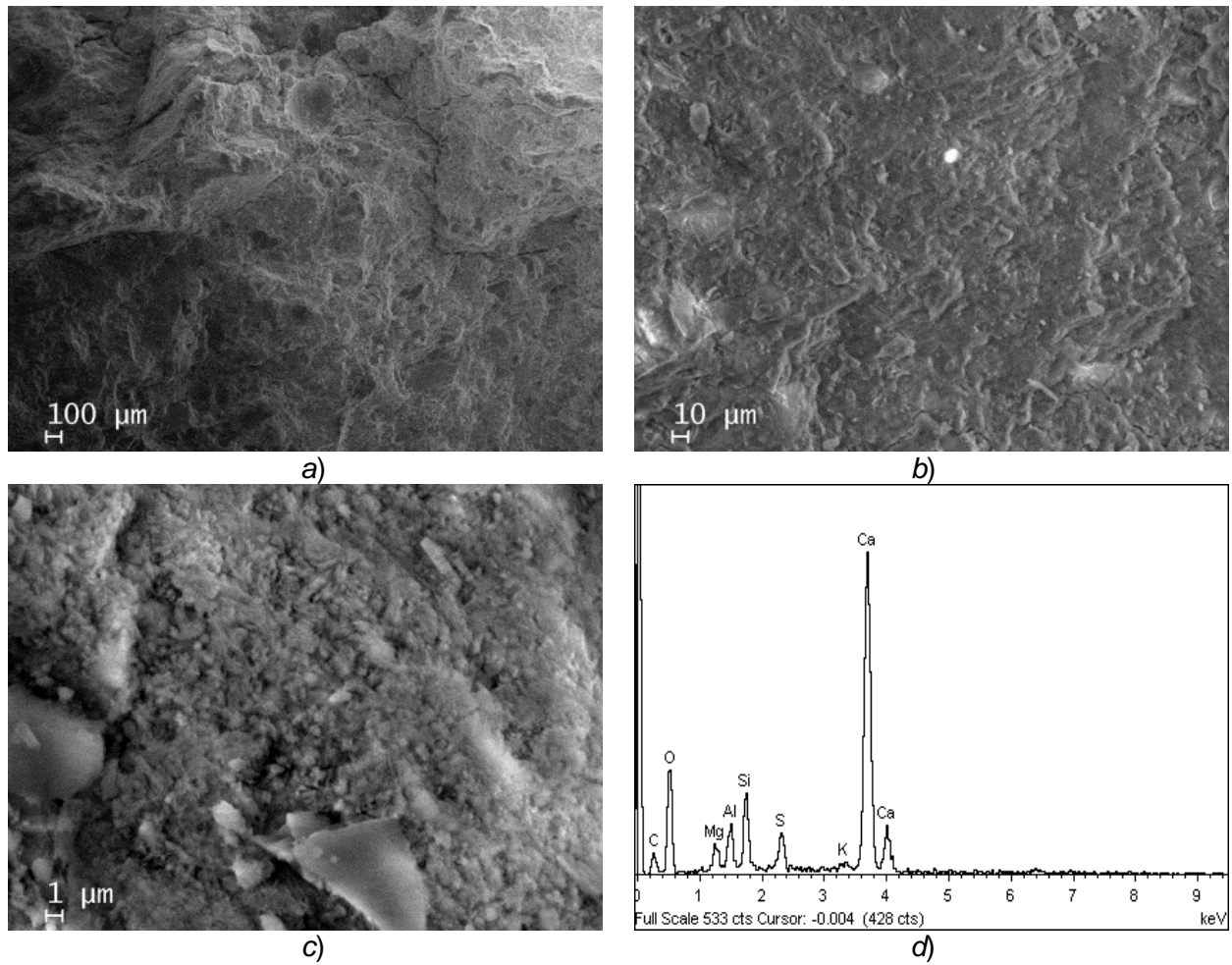


Figure A.10 SEM images at different magnifications *a)*, *b)* and *c)* and EDS analysis *d)* of concrete made with SL05+CaO binder ($w/c=0.55$) after 28 days of moist curing.

A.5 Concrete with SR03 binder

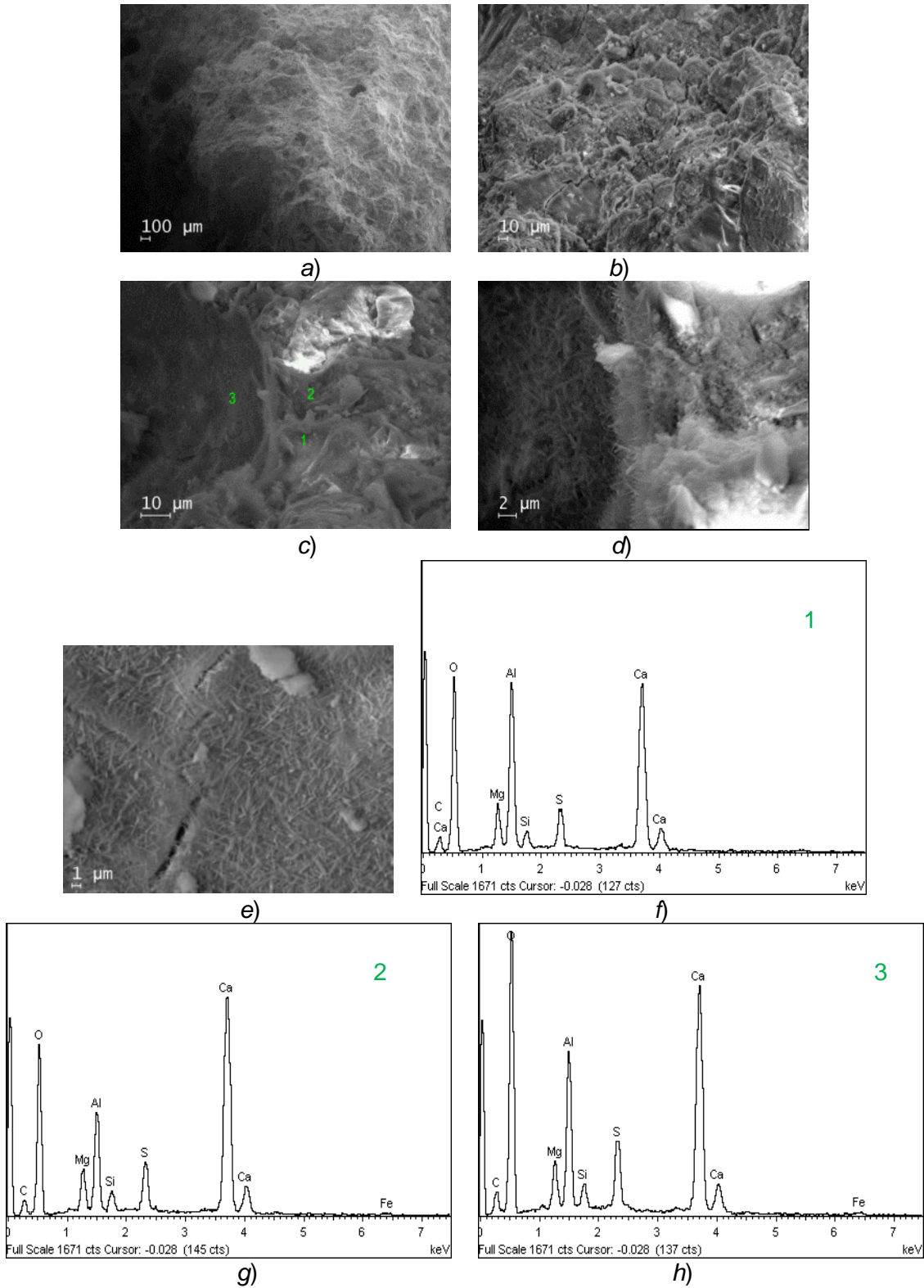


Figure A.11 SEM images at different magnifications *a)*, *b)*, *c)*, *d)* and *e)* and EDS analyses *f)*, *g)* and *h)* of concrete made with SR03 binder (w/c=0.55) after 1 day of moist curing.

Acknowledgements

First of all, I would like to acknowledge China Scholarship Council (CSC) for providing me the financial support to study abroad. Secondly, I have to thank profoundly my parents, for their unconditional love and spiritual support. Thirdly, my deepest appreciation goes to my tutor Prof. Luca Bertolini and my supervisor Dr. Maddalena Carsana. Without their patience, support and guidance over the past four years, it's impossible to finish this thesis work. They led me into the field of steel corrosion step by step. I am fortunate to have them to teach me during my doctoral study. I would like to thank the coordinator Prof. Chiara Castiglioni as well, for her kindly help throughout my study life.

In carrying out the experimental work, I have been greatly assisted by the graduate students, Chiara Cattaneo, Michele Ferrari, Silvia Guerra, Emanuele Lucianò and Grazia Orfeo. Their help is gratefully acknowledged

And, I also would like to thank my colleagues in our group: Matteo Gastaldi, Elena Redaelli, Federica Lollini and our former technician Franco Traisci. I am thankful for their help over the past four years.

Finally, I am grateful to my colleagues and friends Forood Torabian Isfahani and Marco Messina for their help and company and to my good friends, for their support and encouragements.

Specially, I dedicate this thesis to my tutor Prof. Luca Bertolini who has passed away in February, 2017.